Integration, Evaluation and Modeling of Thermal Comfort in Energy Efficiency Measures: Comparing Electric Heating Systems

by

Jérémie LÉGER

THESIS PRESENTED TO ÉCOLE DE TECHNOLOGIE SUPÉRIEURE
IN PARTIAL FULFILLMENT FOR THE DEGREE OF
DOCTOR OF PHILOSOPHY
Ph.D.

MONTREAL, AUGUST 21, 2019

ÉCOLE DE TECHNOLOGIE SUPÉRIEURE
UNIVERSITÉ DU QUÉBEC

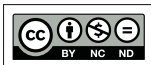

BOARD OF EXAMINERS

THIS THESIS HAS BEEN EVALUATED

BY THE FOLLOWING BOARD OF EXAMINERS

Prof. Daniel R. Rousse, Thesis Supervisor
Département génie mécanique, École de technologie supérieure, Université du Québec

Prof. Danielle Monfet, President of the Board of Examiners
Département génie mécanique, École de technologie supérieure, Université du Québec

Prof. Francois Morency, Member of the jury
Département génie mécanique, École de technologie supérieure, Université du Québec

Prof. Geoffrey Promis, External Independent Examiner
Laboratoire des Technologies Innovantes (LTI - EA 3899), Université de Picardie Jules Verne

THIS THESIS WAS PRESENTED AND DEFENDED

IN THE PRESENCE OF A BOARD OF EXAMINERS AND THE PUBLIC

ON JULY 10, 2019

AT ÉCOLE DE TECHNOLOGIE SUPÉRIEURE

ACKNOWLEDGEMENTS

I would like to thank my parents, fiancée, and friends who have supported me during the course of this project; the t3e group directed by Prof. Daniel Rousse that have given me valuable advice throughout my thesis work and have welcomed me into their group with open arms. I thank the Natural Sciences and Engineering Council of Canada (NSERC) for the funding they have provided me through a PGS-D scholarship. Lastly, I would like to acknowledge Convectair who has not only provided me with extra funding, but also allowed me to perform my experimental investigation at their location and on their cost.

Intégration, évaluation et modélisation du confort thermique dans des mesures d'efficacité énergétiques : comparer des systèmes de chauffage électriques

Jérémie LÉGER

RÉSUMÉ

Les systèmes de chauffage électriques n'ont pas tous une même performance. En effet, un simple changement de la distribution de chaleur peut engendrer une réduction de la consommation énergétique tout en maintenant le confort thermique. Dans le cadre de cette thèse, la distribution de chaleur optimale ainsi que la distribution de chaleur de certains systèmes de chauffage électriques sont étudiées et comparées. La première partie de ce travail consiste en la conception, la construction, la programmation du contrôle et la validation d'une chambre bi-climatique. Cet outil expérimental est essentiel pour comparer des systèmes de chauffage électriques à confort thermique égal. Par la suite, une nouvelle méthode numérique d'investigation de la distribution de chaleur optimale est présentée. Dans cette méthode, le concept du chauffage virtuel est introduit. Les chauffages virtuels sont un ensemble de deux systèmes de chauffage: le premier maximise la perte de chaleur d'une pièce tout en maintenant le confort thermique à l'intérieur de celle-ci; tandis que le deuxième minimise la perte de chaleur en maintenant lui aussi le même confort thermique. En utilisant la consommation énergétique des chauffages virtuels, trois nouveaux indices de performance sont introduits. Le premier mesure l'efficacité d'une distribution de chaleur. Le deuxième mesure la sensibilité de la consommation énergétique d'une pièce à la distribution de chaleur. Le troisième mesure l'écart entre le meilleur système de chauffage et un vrai système de chauffage. La consommation énergétique minimale peut aussi être utilisée comme une mesure de la performance énergétique d'une pièce. La distribution de chaleur maximale est utile pour indiquer la distribution de chaleur à éviter. En approfondissant l'investigation sur la distribution de chaleur, la chambre bi-climatique est utilisée pour étudier la distribution de température et la consommation énergétique de trois systèmes de chauffage électriques. Les résultats expérimentaux montrent que les systèmes de chauffage électriques ne distribuent pas tous la chaleur d'une même façon, et de ce fait, ne consomment pas tous la même quantité d'énergie pour atteindre le même confort thermique. Le convecteur testé a la meilleure performance énergétique quand on le compare à la plinthe électrique et au système de chauffage radiant de cette expérience. Les résultats sur la distribution de chaleur sont aussi comparés avec ceux des chauffages virtuels. Les deux méthodes montrent que chauffer les fenêtres n'est pas efficace. Cette comparaison sert aussi à valider en partie la méthode utilisée pour déterminer les chauffages virtuels. Entre autre, la méthode pour déterminer les chauffages virtuels fût aussi validée par: une comparaison de valeurs tabulées aux valeurs calculées pour le confort thermique; et une comparaison de solutions simplifiées calculées à la main aux valeurs calculées par le programme. Dans une dernière étape, les chauffages virtuels sont utilisés pour investiguer comment la distribution de chaleur optimale est influencée par la géométrie et l'isolation d'une pièce. Chaque paramètre investigué est varié individuellement pour quantifier leurs influence sur la consommation énergétique, la distribution de chaleur et la sensibilité de la consommation énergétique de la pièce à la distribution de chaleur. Ces résultats montrent que la taille de la fenêtre, l'isolation de la

fenêtre et l'infiltration/exfiltration totale peuvent changer la distribution de chaleur associée au chauffage virtuel minimum. En augmentant chacun de ces trois paramètres, la distribution de chaleur a changé d'un chauffage uniquement au volume d'air à un chauffage qui progressivement chauffe davantage le plancher et par la suite le plafond. Les résultats ont aussi montré que la plupart des paramètres géométriques et d'isolation peuvent influencer la sensibilité de la consommation énergétique à la distribution de chaleur. Dans le pire des cas testés, la consommation énergétique maximum consomme 86% plus d'énergie que la consommation minimum. Le meilleur des cas montre que ce chiffre peut être réduit à 27%. L'isolation de la fenêtre est le paramètre qui a le plus d'influence sur la sensibilité à la distribution de chaleur.

Pour résumer, cette thèse présente une nouvelle façon d'aborder le problème de la distribution de chaleur optimale. Les chauffages virtuels permettent la définition de nouveaux indices de performance qui ont été utiles pour investiguer la performance des systèmes de chauffage et des pièces d'un point de vue de la distribution de chaleur. Par une comparaison expérimentale, il peut être conclu que la distribution de chaleur a une influence sur la consommation énergétique et devrait être considérée dans la conception d'un bâtiment. Le chauffage virtuel est sans doute un outil qui servira à mieux comprendre comment atteindre des distributions de chaleur optimales.

Mots-clés: vote moyen prédit, confort thermique, chauffage optimale, chauffage virtuel, efficacité énergétique, chauffage électrique

Integration, Evaluation and Modeling of Thermal Comfort in Energy Efficiency Measures: Comparing Electric Heating Systems

Jérémie LÉGER

ABSTRACT

Electric heating systems do not to perform all equally in terms of energy consumption. In fact, by changing the heat distribution, thermal comfort can be achieved with less energy consumed. In this thesis, the optimal heat distributions and the heat distributions of electric heating devices are investigated and compared. In the first part of this work, the design, construction, control and validation of a climatic chamber is presented. This experimental tool is essential to compare electric heaters at equal thermal comfort. In what follows, a novel method of investigating the optimal heat distribution numerically is presented. In this method, the concept of virtual heaters is introduced. Virtual heaters are a set of two heat distributions: one that maximizes the total heat loss of a room, while maintaining thermal comfort inside this room; whereas the other minimizes the total heat loss, while still maintaining the same thermal comfort. Using the virtual heaters energy consumption, three new performance indices are introduced. The first performance index measures the effectiveness of a heater to distribute heat; the second measure the significance of the heat distribution inside a room from an energy consumption standpoint; the third measure how the diference in energy from the virtual heater and a real heater. The minimum energy loss can also be used as a measure of the room's energy efficiency, while the maximum virtual heater gives an indication on heat distributions to avoid. Expanding the investigation on heat distribution, the bi-climatic chamber tool is then used to investigate the temperature distribution and energy consumption of three electric heating systems. The results from this experiment show that not all electric heating systems distribute heat in the same way, and from this fact, they do not all have the same energy consumption when providing similar thermal comfort. The convection heater experimentally tested here outperformed the radiant heater and baseboard heater. The experimental heat distribution results are also compared with those of the virtual heater. Both methods agree that avoiding to heating the windows is most efficient. This comparison also serves, in part, as a validation of the method used to find virtual heaters. Other validations for key calculations in the virtual heater models include: comparing tabulated results to calculated results for the thermal comfort model; and comparing simplified solutions calculated analytically by hand to the one calculated by the model for the heat transfer model. Finally, the virtual heaters are used to investigate how optimal heat distributions change with respect to the room geometry and insulation parameters. Investigated parameters were varied individually to quantify their effects on the energy consumption, the heat distribution, and the sensibility of the room heat loss to heat distribution. Interestingly, the window size, the window insulation level and the air infiltration/exfiltration rate can drastically change the minimum energy consumption heat distribution. It was observed that when increasing each of these three parameters, optimal heat distribution changed from heating the air volume to floor heating. The results also showed that most geometric and insulation parameters can influence the sensibility of heat loss to heat distribution. The percentage increase of energy consumption for the maximum virtual heater when compared to the minimum virtual heater

was observed to range from 27.4% to 86.0% for the tested cases. The window insulation was found to be the predominant factor influencing the sensibility of heat loss. In summary, this thesis presents a new concept termed virtual heater that is useful in the investigation of indoor heat distribution. Using the virtual heaters and their associated performance indices, the optimal heat distributions for different room geometry and insulation topologies, and the efficiency of some electric heating devices were assessed. Heat distribution can have a significant effect on the energy consumption of heaters and should be considered in building design. Virtual heaters are tools that can undoubtedly help to find more general understandings of optimal indoor heat distribution.

Keywords: predicted mean vote, thermal comfort, optimal heating, virtual heaters, electric heating, energy efficiency

TABLE OF CONTENTS

LIST OF TABLES

LIST OF FIGURES

LISTE OF SYMBOLS AND UNITS OF MEASUREMENTS

A	Surface area, [m^2]
$\mathbf{C}$	Conductance matrix, [W/K]
c_p	Heat capacity, [kJ/kg]
E	Energy, [J]
$\dot{E}$	Energy rate (heat rate),[W]
err	Error, [-]
f_{cl}	Clothing factor, [-]
F_{ij}	View factor of surface i with respect to surface j, [-]
h	Convection heat transfer coefficient, [W/m^2K]
I	Clothing level, [m^2K/W]
J	Radiosity, [W/m^2]
k	Conductivity, [W/Km]
m	Mass, [kg]
$\dot{m}$	Mass flow rate, [kg/s]
N	Number of sub-surfaces, [-]
$NDRE$	Normalized draft rate error, [-]
NP	Normalized power, [-]
P	Pressure, [Pa]
p	Percentage of cycle, [%]
PMV	Predicted mean vote, [PMV scale vote]
PPD	Predicted percentage of dissatisfaction, [%]
$\dot{Q}$	Heat distribution, [W]
$\mathbf{R}$	Radiation matrix, [W/K]
R_{eq}	Surface weighted equivalent thermal resistance, [K/W]

$RHDS$	Room heat distribution sensitivity, [-]
T	Temperature, [°C]
t	Time, [s]
$\dot{V}$	Volumetric flow rate, $[m^3/h]$
v	Velocity or air draft rate, [m/s]

Greek letters

α	, Damping factor, [-]
ε	, Surface emissivity, [-]
ε_{AH}	, Heater effectivness, [-]
σ	, Stefan-Boltzmann constant, $5.67 \times 10^8 [W/m^2K^4]$
Θ	, Normalized temperature, [-]

Subscripts

2D	Pertains to two dimensions
50Pa	At 50Pa of pressure
adj	Adjusted
AH	Actual heater
air	Air
av	Average
bal	Balance
cl	Clothing
cold	Cold room
comf	Comfort

cond	By conduction
conv	By convection
crawl	Crawl space
cycle	Pertains to a heater cycle
d	Desired
diff	Water vapour diffusion
dr	Dry respiration
du	Dubois
ELA	Equivalent leakage area
eq	Equivalent
ex	Air exchange (infiltration/exfiltration)
gain	Source in a volume
globe	Black globe
ih	Internal heat
in	Inside of enclosure
loss	Heat loss (sink in a volume)
lr	Latent respiration
m	Measured
met	Metabolic
mrad	Mean radiant
mVH	Minimum virtual heater
MVH	Maximum virtual heater
n	Neutral
op	Operative
out	Outside of enclosure
outm	Mean outdoor temperature

rad	Radiation
s	Wall surface
sk	Skin
Stan	Standard
sw	Sweat evaporation
TC	Thermal comfort constraints
test	Test room
tot	Total
var	Variation
vh	Virtual heater
w	Water vapour
warm	Warm room
WWR	Window to wall ratio

INTRODUCTION

Energy use in households has been on the rise for a number of years. In Canada, space heating alone represents 62% of the residential energy use (Canada, 2016). Nearly 25% of households are heated by electric systems (Snider, 2006). Electric heating thus represents an important part of the total Canadian energy use. As Canada tries to reach its greenhouse gas emission targets, efficiencies in the household heating sector could significantly contribute to these reductions, especially in regions of the country where electricity is produced with fossil fuels. Hence, in this thesis, the optimal energy consumption of electric heating systems to achieve thermal comfort is investigated.

For space heaters, design objectives can be interpreted in two ways: first, a minimum indoor temperature might be required; second, the heating system should provide thermal comfort to the occupant of the building. For example, an absent house owner will heat his house to a minimum temperature to prevent water pipes from freezing and bursting. On the other hand, when the house is occupied, the heating system should provide thermal comfort within the occupied indoor space. This thesis will focus on the system objective of thermal comfort. Thermal comfort being defined as the occupant's subjective response related to the satisfaction of a thermal environment. Apart from quality of life, thermal comfort has also been linked to work productivity (Mohamed & Srinavin, 2005) and sleep quality (Bischof *et al.*, 1993).

Thought there are many types of heating systems that may achieve thermal comfort, the particularity of electric heating systems is that they convert 100% of their electrical power to heat. Gains in efficiency for these systems are thus limited to how the produced heat is used within the indoor space to achieve thermal comfort. Particularly, this may pertain to the heat distribution of the system. Moreover, electric heaters are good for investigating heat distribution experimentally as they convert power to useful heat with the same efficiency. The objectives of this thesis are then further narrowed to the following two research questions:

- Do all electric heating systems consume the same amount of energy while providing an equal thermal comfort?
- What characterises an energy optimal indoor heat distribution constrained by thermal comfort?

To answer these questions, both a numerical and an experimental approach are utilized.

The experimental investigation aims at answering the first research question. Using a bi-climatic chamber, three electric heaters are compared on the basis of their energy consumption and their heat distribution.

The second research objective will be answered through a numerical investigation. From the formulation of the second research question, thermal comfort is interpreted as a constraint to satisfy, while energy consumption an objective to minimize. This formulation of the problem highlights how thermal comfort is interpreted in the context of indoor space heating for this thesis. Others have interpreted thermal comfort as being a secondary objective two optimize. In this way, optimal solutions compromise on thermal comfort to achieve energy efficiency. It is argued in this thesis that the constrained approach is more accurate than the secondary objective approach since occupants will eventually adjust the heating system to achieve thermal comfort. Furthermore, the constrained approach gives rise to a new method of investigating heat distribution called virtual heaters as defined in Chapter 4.

Virtual heaters are a set of two heat distributions that satisfy the indoor thermal comfort constraint: the minimum virtual heater minimize the total heat loss; while the maximum virtual heater maximizes the same. From the virtual heaters, new performance indices for characterizing the optimal heat distribution of heating systems and rooms are introduced. These performance indices along with the virtual heaters are the primary tools used in this work to characterize optimal heat distribution.

The first index measures the heat distribution performance of heating systems. Prior to the definition of this new performance index, the primary method for comparing the heat distribution performance was to compare heating systems with themselves. As it will be argued in this thesis, this approach can be limiting as there is no way to know if the best observed heat distribution can be improved. By using the minimum virtual heater in the performance index, this ambiguity is no longer present as the minimum consuming solution is known. The heat distribution effectiveness is also used in the context of this thesis to assess the heat distribution performance of the experimentally tested heaters.

The second performance index, room heat distribution sensibility (*RHDS*), measures the importance of heat distribution for energy efficiency in a single room. Though it can be know from experience that some rooms are prone to be sensible to heat distribution, this performance index measures the sensibility based on the virtual heaters. This becomes particularly important when comparing the optimal heat distributions of different rooms.

Since virtual heaters are room dependent, a parametric analysis of the room geometry and insulation parameters was used to investigate the optimal heat distribution characteristics of different rooms. Using the *RHDS*, the importance of heat distribution is assessed. The minimum virtual heater gives the desired characteristic of heat distribution, while the maximum virtual heater gives the heat distribution characteristics to avoid. Using this analysis, the second research question is answered.

This thesis is divided into 5 chapters. In the first chapter, a literature review discusses background information and recent works on thermal comfort, investigations of heat distribution and tools, and the effects of geometry and insulation on the total heat loss. This is followed by two chapters introducing the tools used in this work to investigate thermal comfort and heat distribution. In Chapter 2, a bi-climatic chamber is discussed for use with experimental investigations. In Chapter 4, the virtual heaters are introduced along with their solution methods. In

what follows, an experimental investigation of the energy consumption of three electric heaters at equal thermal comfort is presented and the first research question is answered. The second research question is more thoroughly answered in Chapter 5. In this chapter, a comparison of the heat distributions for different room geometries and insulations is provided. Conclusions and future perspectives are then given in the final chapter.

CHAPTER 1

LITERATURE REVIEW

An overview of the topics relative to optimal heat distribution is now presented. For optimal heating, thermal comfort is seen as a constraint to be achieved while energy consumption, a objective to minimize. It is therefore important to properly define thermal comfort and hence, a discussion of thermal comfort and its models is presented in Section 1.1.

Heat distribution has been studied using either numerical simulation or experiments. This thesis uses both. In Section 1.2, existing climate chambers are discussed as this is an important experimental tool. Thermostat control strategies are then discussed in Section 1.3.1. Heating methods are covered in Section 1.3.2.1. and experimental investigations on heat distribution using these systems are discussed in Section 1.3.2.2.

Investigating heat distribution using simulations and numerical models is reviewed in Section 1.3.2.3. The results of numerical models to investigate heat distribution are then discussed in Section 1.3.2.4.

To expand on the concept of optimal heating, the effects of room geometry and insulation are reviewed in Section 1.4.

The following sections highlight key contributions in each distinct topics for which this thesis will cover or improve upon. A summary of the relevant literature is presented in Section 1.5.

1.1 Thermal comfort

Thermal comfort is a central component in understanding how indoor heating and cooling systems perform. The Merriam Webster dictionary defines comfort as "a state or situation in which you are relaxed and do not have any physical unpleasant feeling caused by pain, heat, cold, etc." (Merriam-Webster, 2015). ASHRAE defines thermal comfort as "the condition of mind in which satisfaction is expressed with the thermal environment" (ASHRAE-55, 2013).

Based on these definitions, it is clear that thermal comfort is an interdisciplinary concept. The state of mind being related to psychology, the physical stimuli relating to physiology, and the science of controlling a thermal environment has historically been the work of HVAC engineers and practitioners.

To control a state of comfort, one must first be able to measure comfort. In the 1930's, Bedford (Bedford, 1936) was the first to proposed a thermal comfort scale, nowadays known as the Bedford scale. His experiment was simply to ask occupants what level of comfort they felt in a room, from much too cold on the lower end of the scale to much too hot on the upper end of the scale. This seems quite obvious, the best way to measure thermal comfort is simply to ask occupants what level of comfort they feel. Other scales have since been proposed, the differences being the words used to describe thermal comfort associated with a number on the scale. Each thermal comfort scale thus covers a limited range of responses. Table 1.1 shows a comparison of different thermal comfort scales.

Table 1.1 Thermal comfort scales

PMV (Fanger, 1970)		Bedford (Bedford, 1936)		SHASE (Rijal *et al.*, 2015)	
hot	3	much to warm	7	very hot	3
warm	2	too warm	6	hot	2
slightly warm	1	comfortably warm	5	slightly hot	1
neutral	0	neither cool nor warm, hence comfortable	4	neutral (neither cold nor hot)	0
slightly cool	−1	comfortably cool	3	slightly cold	-1
cool	−2	too cold	2	cold	-2
cold	−3	much to cold	1	very cold	-3

For building design purposes, it is also important to know what affects thermal comfort. A number of studies have been published on this topic and are carefully reviewed in (Djongyang *et al.*, 2010; Mohammad *et al.*, 2013). From these studies, two points of views can be identified: On one hand, the "engineer's" point of view sees the problem as a heat transfer problem between the occupant and his environment; while on the other hand, the "architect" point of view sees the problem as the human adaptation to his environment. In fact, both points of views

are correct and each has their own contributions to thermal comfort. Yau (Yau & Chew, 2014) provides a good review of both points of view.

1.1.1 Fanger's PMV

A number of heat balance models have been proposed in the literature (Fanger, 1970; Fiala & Havenith, 2015a; Fiala *et al.*, 2010; Stolwijk & Hardy, 1977; Nishi & Gagge, 1977; Wissler, 1961; Werner, 1990; Fiala *et al.*, 2007, 2012). In most cases, the human body is discretized in a number of concentric cylinders and a detailed heat transfer analysis is performed. In an effort to dynamically simulate thermal comfort, Fiala proposed numerous detailed adaptive heat transfer models of the human body (Fiala & Havenith, 2015b; Fiala *et al.*, 2010, 2012, 2007). A thermoregulation control model was developed by Stolwijk (Stolwijk & Hardy, 1977). Amongst these heat balance models, Fanger's thermal balance model (Fanger, 1970), similar to Wissler's model (Wissler, 1961), stands out as a practical model for use in evaluating thermal comfort. The standard effective temperature (SET) (Gagge & Gonzalez, 1972; Nishi & Gagge, 1977; Gagge *et al.*, 1986) has also been widely used. Fanger proposed a thermal comfort index based on observations that led him to formulate the following three requirements needed to achieve thermal comfort:

1. The body is in heat balance, i.e., the internal heat produced by the occupant is equal to the heat removed from the body by the surrounding environment.

2. The sweat rate and skin temperature affecting the heat balance are within certain limits.

3. No local discomfort exists, i.e. radiation asymmetry, cold draught, and air temperature gradient are kept to a minimum.

From the first statement, Fanger developed his heat balance model (Fanger, 1970):

$$\dot{E}_{\text{cond,cl}} = \dot{E}_{\text{gain,ih}} - \dot{E}_{\text{loss,diff,sk}} - \dot{E}_{\text{loss,sw,sk}} - \dot{E}_{\text{loss,lr,sk}} - \dot{E}_{\text{loss,dr,sk}} \tag{1.1}$$

$$\dot{E}_{\text{cond,cl}} = \dot{E}_{\text{loss,rad}} + \dot{E}_{\text{loss,conv}} \tag{1.2}$$

$$\dot{E}_{\text{bal}} = \dot{E}_{\text{gain,ih}} - \dot{E}_{\text{loss,diff,sk}} - \dot{E}_{\text{loss,sw,sk}} - \dot{E}_{\text{loss,lr,sk}} - \dot{E}_{\text{loss,dr,sk}} - \dot{E}_{\text{loss,rad}} - \dot{E}_{\text{loss,conv}} \tag{1.3}$$

where each term is in units of watts (W), $\dot{E}_{\text{gain,ih}}$ is the internal heat production, $\dot{E}_{\text{loss,diff,sk}}$ is the heat loss by water vapour diffusion through the skin, $\dot{E}_{\text{loss,sw,sk}}$ is the heat loss by skin surface sweat evaporation, $\dot{E}_{\text{loss,lr,sk}}$ is the latent respiration heat loss, $\dot{E}_{\text{loss,dr,sk}}$ is the dry respiration heat loss, $\dot{E}_{\text{loss,rad}}$ is the heat loss by radiation, $\dot{E}_{\text{loss,conv}}$ is the heat loss by convection, $\dot{E}_{\text{cond,cl}}$ is the conduction through the clothing.

Equations for the skin temperature T_{sk} and sweat heat loss $\dot{E}_{\text{loss,sw,sk}}$ were then obtained through an experimental study of thermal comfort performed in a climatic chamber on college age students wearing standardised clothing and performing standardised activities while being exposed to a steady state condition for a period of 3 hours. From the double heat balance equations, Eq. 1.1 and 1.2, and experimental data on thermal comfort, Fanger then derived his thermal comfort index (Fanger, 1970):

$$PMV = \left(0.303e^{\left(-0.036 \dfrac{\dot{E}_{\text{gain,ih}}}{A_{\text{du}}} \right)} + 0.028 \right) \dot{E}_{\text{bal}} \tag{1.4}$$

where A_{du}, the DuBois surface area, is the effective heat exchange surface area of the body. The PMV, which stands for predicted mean vote, is the comfort index related to the PMV scale shown in Table 1.1. $\dot{E}_{\text{bal}}$ is the heat balance, which should be zero when the body is in thermal equilibrium.

As a second method of considering thermal comfort, Fanger proposed a relation between the predicted percentage of dissatisfaction (*PPD*) and the *PMV* index:

$$PPD = 100 - 95e^{\left(-0.03353PMV^4 - 0.2179PMV^2\right)} \tag{1.5}$$

The *PPD* estimates the percentage of occupants that will be dissatisfied with the thermal environment. It is important to note that there will always be some level of dissatisfaction, therefore the best that can be achieved is to minimize the percentage of dissatisfaction. Using Fanger's *PPD* equation, Eq. (1.5), with 100 and 95 as embedded constants, the minimum *PPD* is 5% when $PMV = 0$.

The *PMV* and thus the *PPD* depends on six parameters: the air temperature T_{air}, mean radiant temperature T_{mrad}, humidity as represented by the water vapour pressure P_{w} and air velocity v are the four environmental parameters; and, the clothing level I_{cl}, and metabolic rate $\dot{E}_{\text{met}}$ are the two occupant parameters. Other factors such as radiation asymmetry could also be considered for thermally asymmetric environments (Halawa *et al.*, 2014), but will not be considered in the analysis of this thesis. A sensitivity analysis performed by Holz et al. (Holz *et al.*, 1997) showed that the most sensitive parameters of *PMV* are the clothing level, metabolic rate, air temperature and mean radiant temperature. The air velocity and humidity have less of an impact on *PMV* (Holz *et al.*, 1997); however, humid and windy environments make thermal comfort more sensitive to changes in temperature.

Fanger's thermal comfort is not without limitations, there have been numerous validations of the thermal comfort model. In some cases, the model predicted a level of comfort well within a certain range (Humphreys & Nicol, 2002; Parsons, 2002; Buratti & Paola, 2009). In other cases, the actual mean vote (*AMV*) was significantly different from the *PMV* (Fountain *et al.*, 1996; Doherty & Arens, 1988). Given that, the *PMV* thermal comfort index is inherently static, it does not perform well when occupants are used to variable thermal conditions. This is the case of naturally ventilated buildings, where the *PMV* fails to predict comfort (de Dear & Brager, 2001; de Dear, 2004). Naturally ventilated buildings provide less consis-

tent temperatures than HVAC controlled buildings in which *PMV* predicts comfort well. The comfort temperature range for naturally ventilated buildings given by adaptive models is generally broader than the range predicted by *PMV*. The broader range could be used to lower energy consumption as the comfort temperature can be set to a higher or lower setpoint (Holz *et al.*, 1997; Yang *et al.*, 2014; Kwong *et al.*, 2014). Despite its difficulties in predicting thermal comfort in naturally ventilated buildings, *PMV* is still the most widely used thermal comfort index (Van Hoof, 2008). In fact, standards such as ASHRAE 55 (ASHRAE-55, 2013) and ISO 7730 (ISO-7730, 2005) have adopted *PMV* as the primary method to predict thermal comfort; whereas an adaptive model has been adopted by ASHRAE only for naturally ventilated buildings under specific conditions (ASHRAE-55, 2013).

1.1.2 Adaptive approach

Adaptive models are useful in predicting thermal comfort in situations where Fanger's model is not compatible with the *AMV* (de Dear & Brager, 1998), as is the case for naturally ventilated buildings. They have generally tried to predict thermal comfort in changing conditions, whereas *PMV* is more of a static index. The premise of adaptive models is that occupants will adapt to their thermal environment. As such, they will find ways to achieve thermal comfort when the opportunity is provided (Humphreys *et al.*, 2015). The adaptive models also state that past thermal history will influence the thermal expectation and thus the thermal comfort (de Dear & Brager, 1998). The adaptation process can by subdivided into three major categories: physiological, psychological and behavioural adaptations (Nicol *et al.*, 2012). Physiological adaptation is how the body will adapt using its own mechanism of thermal regulation e.g. vasoconstriction and perspiration. Psychological adaptation pertains to the perception of thermal comfort based on past experiences. Behavioural adaptations are actions taken by a person to achieve thermal comfort. This may include personal, technological and even cultural adjustments. Some examples of these adjustments include changing one's clothing (personal), adjusting the thermostat (technological) or even taking a nap during warm periods of the day (cultural).

Adaptation to the outdoor temperature has received considerable attention (Chun *et al.*, 2008; Bouden & Ghrab, 2005; Luo *et al.*, 2016; Toe & Kubota, 2013; Humphreys, 1978; ASHRAE-55, 2013; BS-EN-15251, 2007). Relations between thermal history and indoor thermal comfort where investigated in Seoul Korea and Yokahama Japan by Chun (Chun *et al.*, 2008). Results showed that the thermal conditions experienced by the subjects during the 24 hour prior to the test in the climatic chamber did influence their thermal perception. In Tunisia, climatic chamber experiments were also conducted (Bouden & Ghrab, 2005). Correlations were given for the effective temperature and globe temperature to comfort votes and also between clothing levels and outdoor temperature. Concerning the mean outdoor temperature, a recent study conducted in China concluded that occupants that moved from northern China to southern China or vice versa, had lower comfort expectations, i.e. a wider range of acceptability, than occupants who had stayed in their respective regions (Luo *et al.*, 2016). Adaptation to mean outdoor temperature were also investigated for hot and humid climatic regions (Toe & Kubota, 2013). Using the ASHRAE RP-884 database, three correlations differing from those used in standard ASHRAE 55 were found. Correlations to outdoor temperatures are also used in some standards such as ASHRAE 55 (ASHRAE-55, 2013; BS-EN-15251, 2007).

Other studies focused on the adaptation of clothing (Parsons, 2010; Bouden & Ghrab, 2005; Linden *et al.*, 2008; de Dear & Brager, 1998; Mui & Chan, 2003; Wray, 1980; Parsons, 2014), air velocity (de Dear & Brager, 1998; Mui & Chan, 2003) and gender differences (Amai *et al.*, 2007). It is apparent from these studies and correlations, that adaptive comfort is difficult to measure and that it heavily relies on the collection and correlation of experimental data. Table 1.2 summarizes some adaptive relations found in literature.

In Table 1.2, T_{op} is the operative temperature, T_{out} is the outdoor temperature, T_{globe} is the globe temperature, T_{comf} is the comfort temperature, T_{n} is the neutral temperature, I is the clothing level, v is the air velocity and $\dot{E}_{\mathrm{met,av}}$ is the average metabolic rate. Field experimentations and curve fittings of the experimental data are the principal methods that have been used to find adaptive correlations such as those presented in Table 1.2. A review of experimental studies for the past 10 years on thermal comfort is given by Rupp et al. (Rupp *et al.*, 2015). The weakness

Table 1.2 Adaptive relations

Reference	Adaptive equation	Comment
(Humphreys, 1978)	$T_{\mathrm{n}} = 0.534T_{\mathrm{out}} + 11.9$	
(ASHRAE-55, 2013)	$T_{\mathrm{comf}} = 0.31T_{\mathrm{outm}} + 17.8$	Naturally ventilated buildings
(BS-EN-15251, 2007)	$T_{\mathrm{comf}} = 0.33T_{\mathrm{outm}} + 18.8$	
(de Dear & Brager, 1998)	$v = 0.03T_{\mathrm{op}} - 0.56$	Building with centralized HVAC
(de Dear & Brager, 1998)	$v = 0.0008e^{0.117T_{\mathrm{op}}}$	Naturally ventilated building
(Mui & Chan, 2003)	$v = 0.02T_{\mathrm{op}} - 0.35$	Office buildings
(Parsons, 2010)	$I = I_{\mathrm{stan}} \pm I_{\mathrm{adj}}I_{\mathrm{stan}}$	
(de Dear & Brager, 1998)	$I = -0.04T_{\mathrm{op}} + 1.73$	Building with centralized HVAC
(de Dear & Brager, 1998)	$I = -0.05T_{\mathrm{op}} + 2.08$	Naturally ventilated building
(Mui & Chan, 2003)	$I = -0.04T_{\mathrm{op}} + 1.76$	Office buildings
(Mui & Chan, 2003)	$I = -0.0075T_{\mathrm{out}} + 0.9898$	Office buildings
(Bouden & Ghrab, 2005)	$I = -0.0379T_{\mathrm{out}} + 1.3318$	Tunisian houses and offices
(Bouden & Ghrab, 2005)	$I = -0.0352T_{\mathrm{globe}} + 1.3875$	Tunisian houses and offices
(Mui & Chan, 2003)	$\dot{E}_{\mathrm{met,av}} = -0.0067T_{\mathrm{op}} + 1.35$	Office buildings

of these relations is that they do not give a full explanation of thermal comfort. Each relation was found for a specific set of conditions and upon varying these conditions the relations might change, e.g. by changing the location the comfort temperature found by a correlation could also change. This could explain why field studies tend to yield varying correlations. This lack of unity of the adaptive models was highlighted by Yang et al. (Yang *et al.*, 2014).

1.1.3 Hybrid models

In an effort to unify the *PMV* index and the adaptive models, some new adaptive models based on the *PMV* index were proposed (Linden *et al.*, 2008; Parsons, 2014; Yao *et al.*, 2009; Fanger & Toftum, 2002; Schweiker & Wagner, 2015). These are referred to herein as hybrid models. To modify his thermal model, Fanger proposed the *ePMV* (Fanger & Toftum, 2002). The *ePMV* model introduces an expectancy factor e which explains the differences between *PMV* and *AMV* in naturally ventilated buildings by taking occupant expectations into consideration. On the other hand, Yao et al. (Yao *et al.*, 2009) proposed the *aPMV* model. This model is based on a *PMV* feedback loop, i.e. a feedback loop is added to take into account the adaptive changes. These changes are included in one parameter λ that takes into account all

three adaptive categories. The $aPMV$ can be formulated as:

$$aPMV = \frac{PMV}{1 + \lambda PMV} \tag{1.6}$$

Similarly, Gao (Gao *et al.*, 2015) proposed the TSV_{se} and TSV_{sa} indices to measure thermal comfort using the expectancy factor and adaptive coefficient derived for $ePMV$ and $aPMV$, respectively. In an attempt to correct the data of PMV to AMV, Yang et al. propose PMV_a, related quadratically to the PMV based on empirical data (Yang *et al.*, 2015). More recently, the $ATHB$ model (Schweiker & Wagner, 2015) was proposed to define an adaptive equation for each of the six independent variables of Fanger's PMV. In the $ATHB$ model, these equations are then used as inputs to the PMV index to determine thermal comfort.

These hybrid models provide thermal sensation results that are closer to experimental data. This is to be expected given that they consider more information on the problem, i.e., the models may consider both a heat balance model and experimental correlations for adaptation processes.

Clearly, Fanger's model is still relevant. This thesis will use this model to measure thermal comfort as it gives a good estimate of comfort in steady state conditions, which is what will be considered in this work.

1.2 Climatic Chambers

To experimentally study thermal comfort and the energy efficiency of heating systems, climatic chambers are useful tools.

Climatic chambers are not new concepts. Many suppliers offer a range of climate or environmental chambers. To study a building environment, walk-in chambers are the most appropriate. The Cooper group (group, 2017), as do many other suppliers, builds their walk-in climate chambers with modular camlock panels. These panels allow for quick and easy on-site construction. The chamber comes with its own control system. Kvalitest Nordic (Nordic, 2017)

has successively built a climate chamber for testing the thermal resistance of windows and doors according to the standard ISO 12567 (12567, 2010).

In the context of experimental thermal comfort studies, a chamber with an area of 10.4m^2 was used to study the thermal comfort of young college students from Hong Kong (Chung & Tong, 1990). Similarly, Huimei et al. (Huimei *et al.*, 2010) used a chamber with a surface area of 10.6m^2 to study the thermal comfort in the hot and humid regions of China. In this same chamber, a study on the influence of sexe on thermal comfort was performed (Yongchao *et al.*, 2014). In a classroom context, a climatic chamber with a 44.9m^2 surface area was used to study thermal comfort in a classroom (Fong *et al.*, 2015).

The chambers (Chung & Tong, 1990; Huimei *et al.*, 2010; Yongchao *et al.*, 2014; Fong *et al.*, 2015) consist of a single room, whose wall temperature, humidity and air temperature are controlled. It also seems common practice in thermal comfort studies, to use a chamber with a surface area close to 10.5m^2.

To study the efficiency of heating and cooling systems, a bi-climatic chamber is needed. The particularity of these chambers is that they consist of two distinct rooms one within the other. The first is the test room where the heating system is to be tested. The second is the climate cold room where a climate can be created artificially by use of industrial refrigerators.

Olesen et al. (Olesen *et al.*, 1980) used a bi-climatic chamber with an 11.5m^2 test area to compare types of heating systems at temperatures as low as -5°C. In another study (Causone *et al.*, 2009), an environmental chamber with a test room floor area of 11.6m^2 was used to assess the heat transfer coefficient of a chilled ceiling.

In studying cooling systems, Rees et al. (Rees & Haves, 2013) used a climate chamber with a floor area of 16.72m^2. The chamber's wall temperature was controlled, i.e. thermally controlled fluid-filled pipes in the walls controlled the wall temperature.

Another interesting bi-climatic chamber is the one built at University of Salford (building & energy research group, 2011). Inside this controlled chamber a 1920's Victorian town house was

built. In the house, servomotors control the opening and closing of doors and appliances to simulate occupation. For the exterior portion of the house, inside the environmental chamber, winter, summer, rainy and sunny conditions can be simulated.

At Concordia university, Fazio et al. (Fazio *et al.*, 1997) built a bi-climatic chamber to test wall insulation. Inside the chamber, a test room with a surface area of up to 27.5m^2 can be constructed. The chamber has a wide range of potential applications given that many different constructions can be tested.

A bi-climatic chamber is also described in the C828-13 standard (CSA, 2013). This climatic chamber has the function of testing thermostat drift according to standard C828-13 (CSA, 2013). The test room floor area is 16.6m^2. This standard was the inspiration for the bi-climatic chamber described in Chapter 2 and later used in Chapter 3 of this thesis.

1.3 Energy efficiency, heat distribution and thermal comfort

Driven by the desire or need to reduce building and household energy consumption, there have been many studies on the subject of optimal heating and cooling. Heating and cooling systems may be viewed as a combination of three subsystems. The first is the heat or chill source, which may be a heat pump, electric heating element, central furnace, boiler or any other heat or chill source. The second is the diffusing element, which has the function of distributing, inside the occupied space, the heat generated by the heat source. Examples of diffusing elements include: the vents, the shape of convection heaters, the shape of baseboard heaters or even the shape of radiant heaters. Finally, the thermostat, which controls the first two sub-systems. This control may be accomplished via the measuring of air temperature, radiant temperature, humidity, draft, thermal comfort or a combination of the above. The heat or chill source, such as certain HVAC systems (Martín *et al.*, 2008), has little effect on thermal comfort apart from the temperature profile it generates. The effects of generated temperature can be considered in the heat diffusor element of the system when studying thermal comfort. The following sections focus on heat distribution and indoor control strategies to achieve thermal comfort at minimal

energy consumption. The discussion highlights how distributing heat and controlling thermal comfort can be used to lower energy consumption and maintain suitable living spaces from a thermal point of view.

1.3.1 Thermostats and control strategies

There have been many examples of comfort indices in the context of minimising the energy consumption of heating or cooling systems with various control strategies and thermostat settings.

The importance of a paradigm shift in the control strategies used to achieve energy efficiency and thermal comfort has been highlighted by Brager et al. (Brager *et al.*, 2015). In their work, shifts such as: personal control VS centralized control, still air to breezy air and even system disengagement to improved feedback loop where discussed. It was found that significant energy savings and an improvement in thermal comfort could be achieved by these small changes.

In another study, Corgnati et al. (Corgnati *et al.*, 2008) stated that to ensure good thermal comfort, having a monthly temperature set-point is necessary. They also highlight that it could be interesting to control the operative temperature instead of the air temperature as this would increase thermal comfort. Not surprisingly, they also showed that a thermostat achieving a PMV of -0.5 in the winter and 0.5 in the summer would lead to reduced energy consumption.

Varying HVAC control strategies have been developed (Castilla *et al.*, 2011, 2012, 2010; Yang *et al.*, 2003; Dounis & Caraiscos, 2009; Atthajariyakul & Leephakpreeda, 2004; Cigler *et al.*, 2012; Michailidis *et al.*, 2015). In their review, Dounis and Caraiscos (Dounis & Caraiscos, 2009) showed that On/Off controllers have yet to be used to control thermal comfort in buildings. They concluded that Fuzzy Logic, Neural Networks (Yang *et al.*, 2003), Neuro-Fuzzy Systems and other advanced control strategies are useful in achieving indoor requirements and reducing energy consumption. They also highlight some limitations to controlling PMV. No non-intrusive sensor is capable of measuring clothing insulation and the metabolic rate of a

person. *PMV* is therefore difficult to estimate in real time applications such as a control system. For future perspectives, they stated that more work is needed to find the balance between thermal comfort and energy usage. This shows a perspective on indoor thermal comfort where thermal comfort is not the primary objective but a joint objective along with minimum energy consumption.

Castilla et al. (Castilla *et al.*, 2010, 2011, 2012) showed that the energy savings of an HVAC system could be achieved with a model predictive controller. The objective function used for the controller interpreted the optimization problem as the minimizing of the square of energy and thermal comfort. A potential downside of such a method is that thermal comfort is not guaranteed. Also, adjusting the objective function will influence both thermal comfort and energy consumption. The results are thus dependent on the chosen optimization parameters. In another study on HVAC control systems (Atthajariyakul & Leephakpreeda, 2004), CO_2 levels, thermal comfort (*PMV*) and energy consumption was used in an objective function for a HVAC control system. They showed that CO_2 and *PMV* could be controlled within certain limits while minimizing the cooling load. Cigler et al.(Cigler *et al.*, 2012) showed that controlling *PMV* instead of the operative temperature could lead to energy savings of 10% to 15%. Although their controller reached the thermal comfort limits specified in standards, part of the energy savings was due to having a lower *PMV* than other control strategies. Considering the variations in mean radiant temperature (T_{mrad}), Nagarathinam et al. (Nagarathinam *et al.*, 2017) proposed a control system that is based on an optimal temperature setpoint vector. The optimal vector is used to take T_{mrad} into consideration and distribute hot air to provide thermal comfort accordingly. Energy savings of up to 21% could be achieved when compared to a baseline system.

Michailidis et al. (Michailidis *et al.*, 2015) developed a building optimization and control algorithm that learned to use the inertia of the building and predicted weather conditions in order to better control the indoor building climate. They tested the system in a high thermal mass building and a low thermal mass building. In both cases the system performed better than any other rule-based strategy.

In another study performed by Yang et al. (Yang & Su, 1997), it was concluded that energy savings upwards of 30% could be achieved by using Fanger's model to maintain thermal comfort, then replace the cooling load by an increase in ventilation. A smart controller was developed to adjust air drafts to achieve thermal comfort. Thermal comfort has also been used to find optimal humidity and temperature settings to minimize energy consumption in a room cooling context (Wan *et al.*, 2009). Another control system was also developed to provide local comfort using draft, cooling and heating (Katabira *et al.*, 2008).

In a recent review of literature in household heating (Nägele *et al.*, 2017), it was found that intelligent control, characterised by its automated setpoint variation, outperforms programmable thermostats. Median energy savings of up to 26% and better thermal comfort was observed for intelligent controllers when compared to programmable thermostats. They then concluded that significant amounts of energy could be saved by a simple change of thermostat to an intelligent thermostat. The drawback of fixed programmable thermostats is that occupants generally either do not program the thermostat or they use the manual mode disenabling the advantages of multiple setpoints in programable thermostats. This is primarily due to the fact that residents strive for thermal comfort and not energy efficiency. It is easier for them to set the thermostat at one fixed temperature. In the review, they also mentioned that most thermostats either operate with a PID controller or with an On/Off (Bang-Bang) controller.

Thermal comfort as measured by PMV can be difficult to measure from the perspective of indoor thermostats, therefore approaches to PMV control have mainly focused on simplified models (Castilla *et al.*, 2013; Donaisky *et al.*, 2007; Kuzuhara & Nishi, 2013). This includes models by neural network (Castilla *et al.*, 2013) other predictive models (Donaisky *et al.*, 2007; Kuzuhara & Nishi, 2013).

As it can be seen in the literature, many control strategies see the problem of thermal comfort and energy consumption as a multi-objective problem where the square of PMV and of energy are the two objectives to be minimized. In this study, the problem is interpreted as a single objective to be minimized, heat loss, with one constraint to be satisfied, thermal comfort. This

is coherent with the idea that heating and cooling systems have the primary function of providing thermal comfort and evidently energy consumption is a consequence of providing this thermal comfort. It is obvious from the literature that the control strategies employed for controlling heating and cooling systems can have a significant influence on both thermal comfort and energy consumption.

1.3.2 Diffusor heat distribution

Heat distribution is a major element of a heating system that may affect thermal comfort. By proper heat distribution it is possible to reduce energy consumption while maintaining thermal comfort. This subsection will first discuss the types of heat diffusors and some experimental investigations on how heat distribution affects thermal comfort and energy consumption. In what follows, numerical models useful to the study of heat distribution and thermal comfort are discussed on two fronts: the models themselves and the optimal thermal distributions found with these models.

1.3.2.1 Heat diffusors

Heat diffusors are an essential component to a heating system. They serve to distribute heat inside the occupied space and do so in different ways depending on the type, the size and the location of the diffusor. In general, diffusors are supplied by hot air, hot water, gas or electrical power through a resistance.

Electric heaters, as a single unit, can be of different types (Inc., 2017). Baseboard heaters are generally less expensive than convection heaters. The convection heaters are able, through natural convection or forced convection, to generate an air flow of higher velocity than baseboard heaters. This flow can then be used to propel hot air into the room. Other types of electric heating include radiant heating systems.

In gas heating, apart from centralized gas heaters, radiant panels and forced convection heaters are available (Products, 2017).

Hydronic systems, utilizing water, are classified by their inlet water temperatures (Ovchinnikov *et al.*, 2017). High temperature systems supply water temperatures of up to 95°C. They are classic radiators and baseboard radiators. Medium temperature systems supply temperatures close to 55°C. Low temperature systems with a supply flow at 45°C are ventilation radiators and ventilation baseboards. These systems are particular in that inlet supply air passes through the radiator before being diffused into the room. Very low temperature systems, water supply at 35°C or cooler, are radiant systems. This includes floor heating.

Radiant heating is a growing research trend, as shown by an increase in publications on the topic (Rhee & Kim, 2015). Radiant heaters diffuse heat by means of radiation (Rhee *et al.*, 2017). They can be classified in one of three categories (Rhee *et al.*, 2017). Systems embedded in surfaces have pipes or electric wires embedded into the surface of a wall, ceiling or floor. Thermally activated buildings have pipes or electric wires embedded into the building structure, e.g. pipes running through a concrete floor, wall or ceiling slab. Radiant panel systems are pipes or wires integraded into a panel. Radiant panels may also use air as a form of energy transport.

One advantage of radiant systems is that thermal comfort may be achieved with lower air temperatures for heating applications and higher air temperatures for cooling applications (Babiak *et al.*, 2007). Radiant floor and ceilings also tend to reduce vertical temperature gradients in the room (Olesen, 2007). Comparing radiant heating to all-air systems for thermal comfort, Karmann et al. (Karmann *et al.*, 2017) found that there is evidence that radiant systems provide equal or better thermal comfort when compared to all-air systems.

Different types of ventilation systems can be found in the literature: mixing ventilation, displacement ventilation, personalized ventilation, hybrid air distribution, stratum ventilation, protected occupied zone ventilation, local exhaust ventilation and piston ventilation are all types of ventilation (Cao *et al.*, 2014). Air inlet and outlet varies from one type of ventilation system to another. They are in some cases combined with other heating systems to provide thermal comfort. The location, opening area and flow rate of the vent will all be contributing factors

to thermal comfort and energy efficiency (Cao *et al.*, 2014). Though ventilation systems are used for heating and cooling, a second primary objective of reducing the amount of indoor air contaminants by air change is also of importance to ventilation systems (Tham, 2016).

1.3.2.2 Experimental investigations

Comparing heat distribution elements, many have found that the location, surface area and temperature of the heat distributor can be used to provide thermal comfort and minimize energy consumption.

Studying heating systems in a controlled environment such as a climatic chamber, Olesen et al, (Olesen *et al.*, 1980) experimentally compared two radiators at different temperatures, a convector, a heated ceiling, two floor heating configurations, two warm air inlet configurations and a skirting board. They found that floor heating was the most energy efficient at providing thermal comfort in all tested cases. They noted that the efficiency of a heating system cannot be evaluated apart from of the characteristics of the test room. Tests were conducted at an outdoor temperature of $-5°$C with an air change rate of 0.8 ACH and the outside facing wall insulated at $0.35\mathrm{W}/\mathrm{m}^2\mathrm{k}$ with one double glaze window. All tested systems were able to achieve thermal comfort. They concluded that convectors had increased heat losses due to an increase in air velocity near the window. Standards such as ASHRAE (ASHRAE-55, 2013) suggest placing heating systems below windows to compensate for cold drafts, but this indicator is incomplete and could lead to less efficient systems. In the example of the convector tested by Olesen et al. (Olesen *et al.*, 1980): to achieve energy efficiency, thermal comfort can be maintained by increasing insulation and lowering the setpoint temperature (Olesen *et al.*, 1980). Hannay et al. (Hannay *et al.*, 1978) also studied the effects of changing heating systems on thermal comfort and energy efficiency. They concluded similar results as Olesen et al. (Olesen *et al.*, 1980).

Air temperature gradients were measured for displacement ventilation coupled with floor heating and cooling (Causone *et al.*, 2010). Results show that as heat output from the floor increased, temperature gradients decreased. Significant temperature stratifications, up to 8°C,

were observed for floor cooling. Thermal discomfort, measured by a thermal manikin, could be observed in the case of floor cooling. Air temperature stratification was also studied by Schiavon et al.(Schiavon *et al.*, 2012) in the context of chilled ceiling coupled with displacement ventilation. Their findings show that temperature gradients may be affected by the proportion of heat removed by the chilled ceiling versus the ventilator, the temperature of the chilled ceiling and the air flow rate; however, temperature gradients were all within 1.5°C. Rees and Haves. (Rees & Haves, 2013) in their chamber experiment tested a cooled ceiling with displacement ventilation in the presence of indoor heat sources. The results showed that floor air temperature was greater than supply ventilation temperature. This was due to the presence of heat sources in the room radiating heat to the floor. They concluded that heat sources inside the room could significantly change the radiant exchange and thus the temperature distribution.

In a study comparing active chilled beams to radiant walls (Le Dréau *et al.*, 2015), it was found that radiant walls were more efficient. The active chilled beam at higher cooling demand reached lower air temperatures than the radiant wall. The temperature gradient in the room was greater for the radiant wall than for the chilled beam. Thermal comfort, measured by a thermal manikin, was achieved for both tested systems.

From experiments cited in the literature, air temperature distribution can cause difficulties in attaining thermal comfort. In heating and cooling systems, counteracting the natural flow of heat will provide a better temperature distribution. In the case of radiant floor heating or chilled ceiling cooling, heat tends to rise; thus, cold air accumulates below while hot air atop. It is then obvious that heating the cold air on the bottom or cooling the hot air at the top will tend to stabilize the temperature inside the room. Another technique to provide a more constant temperature distribution is to have sufficient air flow inside the room. The mixing of air, in this case, stabilizes temperature.

The effect of the heater position was studied by Ghaddar et al. (Ghaddar *et al.*, 2006), they showed that 14% savings could be achieved by changing the position of a stove. The position of the stove mainly influenced mean radiant temperature for thermal comfort. In an

experimental study comparing gas radiant heaters for industrial buildings to convective heaters (Petráš & Kalús, 2000), showed that a radiant heater fixed to the ceiling could provide better thermal comfort while consuming less energy. A minimum height was also suggested to prevent local thermal discomfort.

In areas with high ceilings, indoor air thermal gradients can become quite significant, while the occupied spaces remain a small portion of the total heated space (Huang *et al.*, 2007). It is thus useful to design a system that takes these effects into consideration. Local thermal comfort is a way of reducing energy consumption significantly by heating or cooling only the occupied space. In an effort to provide local thermal comfort, a heated/cooled office chair was tested (Hoffmann & Boudier, 2016). Thermal comfort was improved when focalizing on the chair. Another attempt to provide local thermal comfort includes personalised ventilation where air is blown on the occupant(Wang *et al.*, 2016; Krajčik *et al.*, 2016).

These experiments show that despite facing similar outdoor conditions, not all systems will be as efficient to achieve thermal comfort. The method of heat distribution in the room can greatly influence energy efficiency and thermal comfort.

Despite the widespread use of electric heating systems in residential spaces, no literature could be found comparing the different electric heating technologies from a heat distribution perspective. Rather, many studies focus on particular technologies with a few giving a broad comparison of the different systems available. Comparison of the most common electric heating systems will be the focus of Chapter 3.

1.3.2.3 Numerical models of room heat transfer

Numerical models in fluid flow and heat transfer have proven to be a useful tool to investigate heating and cooling systems. CFD along with other simplified models such as fast fluid dynamics, zonal models and one-node models have been used in the context of the building environment. In this sub-section, the type of models and parameters used within these models will be discussed.

Using computational fluid dynamics (CFD), a 3-D conjugate fluid flow and heat transfer model of a room was investigated and compared with published experimental data by Horikiri et al. (Horikiri *et al.*, 2014). In the model, a (RNG) k-ε model was used to simulate turbulence similar to what had been done in other studies (Horikiri *et al.*, 2015; Zuo & Chen, 2009). A CFD model was also used in a study of thermal comfort by Sevilgen and Kilic (Sevilgen & Kilic, 2011). In this model programmed with ANSYS Fluent, the SIMPLE algorithm (Patankar, 1980) was also used and turbulence was modelled with a (RNG) $k-\varepsilon$ model (Choudhury, 1993). Approximately 3 million elements were used in the model. Ahmed et al. (Ahmed *et al.*, 2016) performed a CFD computation on a room cooled by displacement ventilation with a thermal manikin. A total of 2.5 million cells were used in the computations. An (RNG) k-ε model was also employed for turbulence modeling.

In a review of models used to assess the performance of ventilation systems for buildings (Chen, 2009), it was found that 70% of papers published used CFD. Application of CFD techniques relating to building energy studies where reviewed by Oosthuizen and Lightstone (Oosthuizen & Lightstone, 2010). They found that the use of a $k-\varepsilon$ turbulence model was adequate for most design applications studying indoor spaces.

Studying radiant floor cooling with CFD, Fernádez-Gutiérrez et al. (Fernández-Gutiérrez *et al.*, 2015) constructed a model using ANSYS Fluent with 154,000 nodes in a finite volume discretization. Model results agreed with experimental PIV results. Using a CFD model, humidity could also be modeled by adding an extra conservation equation for water (Teodosiu, 2013).

In an attempt to reduce computation time, Zuo and Chen (Zuo & Chen, 2009) proposed to simulate indoor environments with fast fluid dynamics (FFD). They achieved speeds from 4 to 100 times faster than CFD.

Simplified models of indoor heat transfer have also been developed and carefully review by Megri and Haghighat (Megri & Haghighat, 2007). They are a less computationally expensive alternative to CFD. One-node models consider the room as having a single homogeneous temperature. They cannot describe the air temperature distribution inside a room. Multi-node

models are an extension of one-node models capable of simulating air temperature in different rooms or zones of a building. These two approaches are good for system sizing. Zonal model are an intermediate between the one-node model and CFD model. They are capable of describing the general air flow and temperature distribution inside a room. They are particularly useful for faster analysis of thermal comfort inside a room: faster than FFD, however they are also less accurate for detailed results.

Inard et al. (Inard *et al.*, 1996) developed a zonal model approach where the pressure field mainly determines flows as airflow momentum and is considered to be small. In a second model (Inard *et al.*, 1998) they used empirical correlation to model the heaters, empirical correlations to model convective heat transfer and the radiosity method, using analytical solutions, for the radiative heat transfer. Walls were discretized into 100 elements, refined near windows and heaters, while the ceiling and floor was a single element. The indoor volume was discretized with 12 and 13 zone elements, depending on the type of heating. The model was validated experimentally. A limitation of these models are the inherent empirical correlations that are needed for the models.

Musy et al. (Musy *et al.*, 2001) developed a zonal model that does not require prior knowledge of flow pattern. Their model requires only 24 cell elements. Ren and Stewart (Ren & Stewart, 2003) also proposed a zonal model and showed reasonably accurate results for flow and temperature profiles. Results could be achieved in a few minutes. Wurtz et al. (Wurtz *et al.*, 2006) showed how zonal models can be applied to full year analysis of heat transfer in a room.

A new robust zonal model was proposed by Megri and Wu (Megri & Yu, 2015). The model is capable of approximating the temperature distribution better than previous models. The model can be regarded as a simplification of the Navier-Stokes equation with the exception that conduction and viscous dissipation is ignored in the energy equation. A total of 60 elements were used for a 2D solution.

Although zonal models seem to be a better tool for fast analysis of temperature distribution, they have the drawback of being very sensitive to input parameters when compared to other

models (Wang *et al.*, 2016). For general applications, this limitation can lead to inadequate results.

In optimizing temperature distribution, the case of this thesis, a computationally efficient model is required since the optimization process itself can be time consuming and requires multiple solutions to the heat transfer problem. The topic of choosing an adequate model will be discussed further in Chapter 4.

1.3.2.4 Numerical results of room heat transfer

In investigating energy consumption and thermal comfort, computational fluid dynamics (CFD) has been a cost efficient way to study indoor environments. It has been used to optimize radiant heater position, surface area and temperature for energy efficiency (Tye-Gingras & Gosselin, 2012; Jahantigh *et al.*, 2015; Myhren & Holmberg, 2009; Ahmed *et al.*, 2017), to study the effect of furniture and humans in a room on thermal comfort (Horikiri *et al.*, 2015), to compute the effect of walls and window insulation (Horikiri *et al.*, 2014; Sevilgen & Kilic, 2011), to study the air temperature distribution (Myhren & Holmberg, 2006; Gan, 1995; Lu *et al.*, 1997; Ahmed *et al.*, 2016; Catalina *et al.*, 2009; Huang & Wang, 2009; Wang *et al.*, 2014) and to compare numerous heating and cooling systems (Myhren & Holmberg, 2008; Le Dréau & Heiselberg, 2014; Han *et al.*, 2014; Inard *et al.*, 1998).

Potential energy savings by considering thermal comfort in a building instead of a desired temperature was studied by Holtz et al. (Holz *et al.*, 1997) using DOE-2 (Hirch, 2015), a building simulation software. They concluded that using PMV, the energy consumption could be lowered by better temperature zone control. They finished their paper by stating that "Comfort is not just a side issue to saving energy, it is the issue", which highlights the importance of thermal comfort inside occupied buildings and its effect on energy efficiency.

With a model of a room with radiant ceiling and walls, Tye-Gingras and Gosselin (Tye-Gingras & Gosselin, 2012) studied the effects of changing the position of the radiant heating systems, the temperature of the radiant surface and the surface area of the system on thermal comfort and energy

consumption. They found that the radiant heating system's energy consumption could be lowered by changing the location, the temperature and the surface area of the system. In their analysis, they presented a multi-objective optimization as the combination of both minimizing thermal discomfort and energy consumption. This led to pareto fronts showing the trade-off between thermal comfort and energy efficiency. Jahantigh et al. (Jahantigh *et al.*, 2015) also concluded that heater surface area, temperature and location can all be used to reduce energy consumption while maintaining thermal comfort. Myhren and Holmberg (Myhren & Holmberg, 2008) compared floor heating, low temperature wall heating and medium-high temperature radiators in an office with exhaust ventilation via CFD. Their findings show that low temperature systems may improve indoor climate relative to high temperature systems by providing lower air velocities and temperature differences; however, they did not perform well in counteracting cold drafts. In a later study (Myhren & Holmberg, 2009), they showed that the position of an exhaust vent could also lead to increased energy efficiency.

The effect of the variation of the location of outlet diffusers in a displacement ventilation system for cooling was investigated by Ahmed et al. (Ahmed *et al.*, 2016). It showed that energy savings of up to 25% could be achieved by the proper location of the diffusor on the ceiling. Using CFD it was shown (Gan, 1995) that ventilation in an upwards displacement was more efficient in terms of energy use, but may cause local discomfort. It was also found that optimal ventilations for heating and cooling are different. Chen et al. (Chan *et al.*, 1995) used a CFD model to assess the most suitable position for a thermostat and corresponding temperature correlation to achieve thermal comfort, in order to better design and place thermostats. Another CFD simulation (Lu *et al.*, 1997) showed how a radiator could strongly affect the air flow and temperature distribution.

Numerically comparing radiant walls, a radiant ceiling, a radiant floor and an active chilled beam at different air exchange rates (Le Dréau & Heiselberg, 2014), it was found that the radiative technologies outperformed the active chilled beam. A simple explanation for this result is that radiative technologies achieve thermal comfort without lowering the air temperature as compared to convective systems. At a high air exchange rate, the convective system will have

an extra cooling load from the air change thus consuming more energy. It was also observed that the chilled ceiling provided a more uniform thermal comfort while the radiant floor had the least uniform thermal comfort. Using CFD and experimental data, Catalina et al. (Catalina *et al.*, 2009) showed that a good air temperature distribution, temperature gradients less than $1°C/m$, could be achieved using a chilled ceiling.

Using a zonal model to describe heat transfer inside a room (Inard *et al.*, 1998), two distributed heat sources, floor and ceiling heating, and two local heat sources, convector and radiator, were compared. It was shown that heated ceilings gave similar energy consumption as heated floor but with lower thermal comfort since temperatures varied with ceiling height. The energy consumption and thermal comfort of the convector and the radiator were similar, however, their energy consumption was found to be higher than those of the distributed heating systems. The increase in consumption for the local heat sources is because these heated the outside facing wall more than the distributed system and thus increased heat transfer to the outside.

Horikiri et al. (Horikiri *et al.*, 2014) concluded, after simulating and comparing different wall types and heaters, that window glazing and the heat source had significant impact on temperature distribution. For poorly insulated windows, the heating device heating the wall and window on which it is installed contributed to reducing the energy efficiency. Sevilgen and Kilic (Sevilgen & Kilic, 2011) studied, using CFD, a thermal manikin inside a room heated by two panel radiators. They found that windows contribute significantly to the heat loss and could also affect negatively thermal comfort because of their low temperatures. Myhren and Holmberg (Myhren & Holmberg, 2006) showed using CFD that cold drafts from cold windows and walls blocked by heat from radiators placed under the window leads to improved thermal comfort. They also stated that an increase in radiative heat reaching the human body could increase the energy efficiency of heating systems.

Investigating, via CFD, the effect of furniture and occupants inside a room on thermal comfort (Horikiri *et al.*, 2015), it was found that furniture could significantly change flow patterns inside the room, but had little effect on air temperature distribution. As for occupants, they tend

to generate thermal plume inside the room and also increase temperature. Thermal comfort, PMV, is thus increased with a higher number of occupants. This is to be expected as occupants releases heat to maintain thermal comfort.

In an effort to create local thermal comfort, the design of air conditioning systems for large spaces have been investigated (Huang & Wang, 2009; Wang *et al.*, 2014). A stratified air conditioning system was recommended for local air conditioning when less than 33% of the total height of the room is the occupied space. Evidently, with local cooling, less energy is consumed. Comparing a coupled radiant/air system to an all air system to cool a semi-enclosed space that opens up to an atrium, i.e. local cooling, Kim et al. (Kim *et al.*, 2001) used CFD to show that the coupled radiant/air system could dramatically save energy as compared to the all air system. In the case of high ceilings, it was also found using CFD that radiant panels would outperform convection systems in terms of energy consumption and thermal comfort (Han *et al.*, 2014). Another attempt to provide local thermal comfort includes a local exhaust system designed to be imbedded in an office workstation to provide local thermal comfort and air quality (Ahmed *et al.*, 2017). It was shown with a CFD model of the device, that thermal comfort could be achieved locally and that energy consumption was reduced by up to 30% when compared to normal office HVAC systems. A key aspect of thermal comfort for this system was hot air ventilation from the foot area to provide constant vertical temperature.

Optimizing the heat distribution in rooms is thus an important factor in achieving energy efficient heating systems. Depending on the room and its type of occupation, different heating or cooling systems may be optimal. Despite a large interest in indoor temperature distribution and energy consumption, there is no performance indicator in the literature that can be used to guide the designer in the evaluation of heat distribution in indoor environments. Most published papers focus on existing technologies for temperature distribution and energy consumption thus limiting the search for optimal heating and cooling of a space. This thesis will propose a way of quantifying the optimal heat distribution (see Chapter 4) without prior knowledge of how to design such a system.

1.4 Effects of room geometry and insulation on heating

Optimal heat distribution is room dependent. A system that performs well in one particular room might not do as well in another type of room. It is thus important when investigating heat distribution to consider the room parameters.

In this section, the effects of geometry and insulation parameters on the energy consumption of rooms are discussed.

1.4.1 Room geometry

The geometry of a room can have an influence on the power consumption. In commercial buildings, the effects of window-to-wall ratio and room width-to-depth ratio were investigated by Susorova et al. (Susorova *et al.*, 2013). In their analysis, varying the window-to-wall ratio effected solar heat gains and conduction losses; moreover, rooms with south oriented windows performed better than those facing other orientations. They also concluded that for cold climates, deep rooms performed better than shallow rooms and that window-to-wall ratios could be increased for deeper rooms. As Susorova et al. (Susorova *et al.*, 2013) pointed out, the geometry of a room with respect to its heat consumption is often neglected. This is made evident by the lack of publications on this topic (Ruparathna *et al.*, 2016; Chwieduk, 2017), especially for colder climates.

Papers in literature have focused on the influence of the geometry and the insulation parameters of a building or room on the cost and energy consumption. Particular attention has been given to optimal insulation to achieve a cost optimal construction.

Most of the papers that discuss the effect of geometry on the room's heat balance focus on solar heat gain management by varying the window-to-wall ratio (Tzempelikos *et al.*, 2007; Goia, 2016; Ochoa *et al.*, 2012). Goia (Goia, 2016) concluded that for buildings in most European climates and for non-south-facing facades, the optimal window-to-wall ratio is between 30 to 45% while optimal south-facing facades had more variability. The optimal window-to-

wall ratio was also investigated in (Ochoa *et al.*, 2012). In their analysis, they considered the power consumption, but also natural lighting quality. They found that an optimal window size is between 50 to 70% of the wall's surface, considering both light quality and energy consumption. Results show that the lowest energy consumptions were found when the window-to-wall ratio is in the range of 20 to 40%. This is consistent with the findings of Goia (Goia, 2016).

The shapes of buildings in general have been investigated (Randelovic *et al.*, 2014; Ruparathna *et al.*, 2016; Chwieduk, 2017; Raji *et al.*, 2017), but publications on the optimal dimensions of individual rooms are scarce (Susorova *et al.*, 2013; Kalmár & Kalmár, 2012). Kalmár and Kalmár (Kalmár & Kalmár, 2012) investigated how the room geometry could affect the mean radiant temperature and thus thermal comfort. In their simulations, thermal comfort and mean radiant temperature were calculated at the geometric center of the room. Floor heating and radiators were tested as heating systems. They found that ceiling height had more influence on thermal comfort for rooms with a smaller floor area. They also found that floor heating would increase the radiant temperature less than a radiator, because of the high radiator temperature and low floor temperature.

In a study on the retrofitting of existing industrial buildings for residential use (Valančius *et al.*, 2015), it was found that floor heating was unable to counteract cold air currents generated by tall windows. This is in fact a source of discomfort. It was especially true when higher ceilings and window heights were involved.

From an architectural point of view, the floor plan and utility rooms can also be contributing factors to energy efficiency (Randelovic *et al.*, 2014). The floor plan, room geometry and heat distribution should therefore be combined in a synergetic way to provide rooms with good thermal comfort, while reducing energy consumption.

The reviewed literature mostly focused on how the window-to-wall ratio can be used with the sun irradiation to lower the heating needs of rooms. Some other parameters such as room depth

and height have also been covered, but their effect on optimal heat distribution has not been thoroughly discussed.

1.4.2 Room insulation

The literature also focused on the influence of the insulation parameters of a building or room on the costs and energy consumption. Particular attention was paid to optimal insulation to achieve a cost optimal construction.

Zhao et al. (Zhao *et al.*, 2015) varied the infiltration rate, the thickness of insulation, the window U-value, the orientation of the building, the shading coefficient and the window-to-wall ratio. They found that the most sensitive parameters able to affect heating consumption in cold climates were the air tightness and wall insulation thickness. Window U-value was also found to have a significant effect, but less than air tightness and wall insulation.

Pikas et al. (Pikas *et al.*, 2014) compared different window-to-wall ratios and window glazing types and found that triple pane windows with a 23% window-to-wall ratio was cost optimal.

Özkan and Onan (Özkan & Onan, 2011) showed that the cost-optimal insulation thickness was most effective in buildings with low window-to-wall ratio. In a recent review of thermal insulation and its applications in the building environment (Aditya *et al.*, 2017), cost optimal insulation thicknesses were reported to be between 1.5cm to 26cm depending on the cost of energy and the considered climate. In a study by Ozel (Ozel, 2014), it was shown that insulating on the outside of the walls would reduce the indoor temperature swings when compared to insulating the inside of the wall; however, the location of insulation with respect to the inside or outside of the wall did not influence the yearly consumption. Considering the insulation distribution, it was also found that wall insulation thickness should be increased for minimal energy consumption when coupled to radiant heating systems (Cvetković & Bojić, 2014).

It is clear from the literature that a balance between cost of insulation and cost of heating is an important point. Clearly, increasing insulation decreases the heating cost by a reduction

of the total heat loss to the outside environment and increases the construction cost, but an undiscussed topic of interest is how the optimal heat distribution might change with these different levels of insulation.

1.5 Conclusions

In summary, optimal heat distribution is a multifaceted problem that requires a good understanding of both the indoor heat transfer and thermal comfort.

Two major approaches to thermal comfort have been reviewed in the available literature. On the one hand, there is the thermal model approach as made famous by Fanger's PMV, and on the other hand, the adaptive approach, which considers the measures that a person will take, may it be consciously or unconsciously, to achieve thermal comfort. Each of the approaches misses part of the problem, even Fanger acknowledged this when he modified his PMV to accommodate adaptive processes in a new model he called $ePMV$. Hybrid models like $ePMV$, $aPMV$ and $ATHB$ unify the thermal heat balance to the adaptive processes; there is great potential in their ability to more accurately predict thermal comfort. Further work still remains on properly modeling adaptive measures.

Fanger's PMV is found to be valid for climate-controlled buildings. Such is the case for the rooms studied in this thesis. The PMV is thus adopted as the measure of thermal comfort in this work.

Applying thermal comfort, there are many examples both in cooling and heating applications where energy efficiency could be enhanced using heat distribution. Experiments performed in climatic chambers mostly concluded that floor heating is the most efficient way to heat a room. A convector installed below windows was found to be inefficient since they heat the window, hence increasing heat transfer to the outside environment. These experiments were mostly performed in the 1980s. Heating devices have since evolved; therefore, it would be interesting to test the conclusion that convectors are the least efficient heaters. Improvements in the outlet flow design of convectors could potentially reduce the heating of the window that is above the

heater; thus, the new convector could be more efficient than other systems installed below the window. This will be tested in this thesis.

To do so, a climatic chamber with a thermal comfort control system must be utilized. In the past, this has been done by adjusting a temperature thermostat until thermal comfort was achieved. Reviewing existing climatic chambers, it has also been identified that most chambers have fixed test room geometries and insulations. Those that do not have fixed parameters, require a new construction every time a new configuration is tested. A chamber that does not require new wall construction to change its geometry would thus be an interesting new experimental research tool. Especially when considering that the geometry and insulation of a room can affect the energy consumption results.

In fact, the effect of the room geometry and insulation on heat distribution has been tested for specific cases involving selected heating devices, geometries and insulations. These have shown that the room height, window-to-wall ratio, room depth, window insulation, wall insulation, and air exchange rate could all contribute significantly to energy savings. The example cases in the literature have also shown the importance of position, temperature, and surface area of the heater in achieving energy efficient systems for providing thermally comfortable spaces. Reviewed studies on optimal heat distribution revealed that their results are technology specific, i.e. they depend on the chosen heater for the experiment or simulation. A method that is independent of a selected heater could then generalize optimal heat distribution conclusions. This is the primary innovation of the virtual heaters introduced in this thesis.

With this new method, an investigation of optimal heat distribution in different types of rooms could then benefit from being independent of the type of heating device.

A general understanding of optimal heat distribution could lead to better architectural designs and more efficient heating devices.

CHAPTER 2

THE CLIMATIC CHAMBER

In this chapter, the design, construction, and computer programming of a bi-climatic chamber is discussed. The bi-climatic chamber is a useful tool for comparing the energy consumption of different heating systems. The main innovation of this particular climate chamber is that walls are modular; therefore, it is easy to perform experiments with different test room sizes, insulation levels, and window or door configurations. The bi-climatic chamber presented here is used in Chapter 3 for the experimental investigation of the energy consumption of electric heating systems.

The bi-climatic chamber is called Klimat and was intended to provide a residential electric heaters company with the capabilities of testing different heating systems and comply with CSA C828-13 standard (CSA, 2013) to test thermostat reliability.

In a first section of this chapter, a general description of the Klimat is given. The section that follows discusses the control system for the chamber that was programmed. The measurement equipments and their locations inside the chamber is then presented in Section 2.3. In Section 2.4, the innovations of the Klimat are highlighted and discussed. The critical innovation is the modular walls. A complimentary climatic/air flow visualisation chamber is also presented in the section that follows. This chamber is primarily used to visualise the airflow generated by the heating systems; whereas, the Klimat is useful for measuring their energy consumption. Finally, conclusions are drawn on the bi-climatic chamber project.

2.1 Description of the basic chamber

The Klimat chamber used to study the heaters is a C828-13 standardized chamber (CSA, 2013). The chamber, see Figures 2.1 and 2.2, is made of four primary rooms. The cold room is capable of achieving $-37.5°C$ to $35°C$ to simulate the extreme Canadian outdoor climates. The warm room allows a range of temperature from $15°C$ to $25°C$. The test room is the room adjacent to

the warm and cold rooms. It is in this room that heaters are tested. The crawl space is the area under the warm room and the test room. This crawl space can have temperatures profile similar to those of the warm room. The test room, in the Klimat CSA configuration, is thus positioned to simulate a corner room with three exposed outdoor surfaces, i.e. the ceiling and two walls.

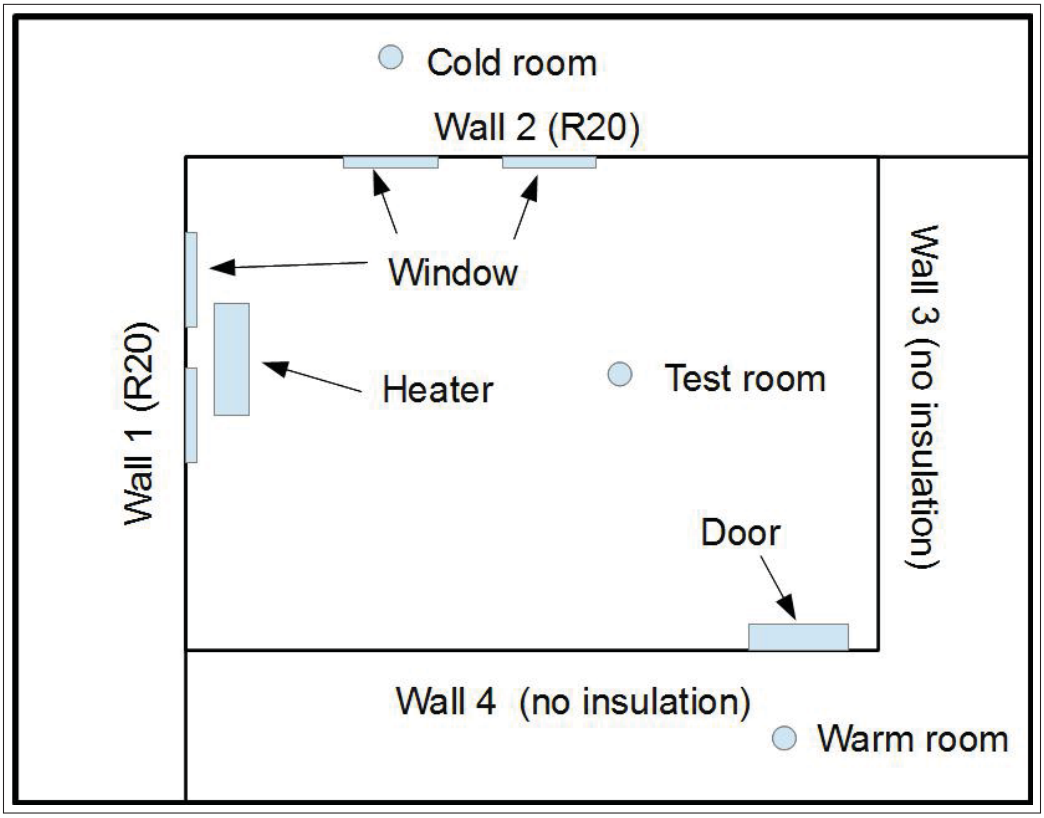

Figure 2.1 Bi-climatic chamber plan view. Source: C828-13 (CSA, 2013)

The outer shell of the chamber is insulated at R40 along with the test room ceiling; while the test room floor is insulated at R30. The exterior facing walls of the test room are insulated at R20; while the other walls are insulated at R10. Four windows are present on both cold walls, see Figures 2.3 and 2.4 for dimensions and positions. A wooden door gives access to the test room via the warm room, its dimensions and position are given in Figure 2.5.

The walls are constructed from metal studs, while the floor and ceiling are constructed with wooden studs. Aligned with wall 2, two I-beams made from steel reinforce the ceiling and the

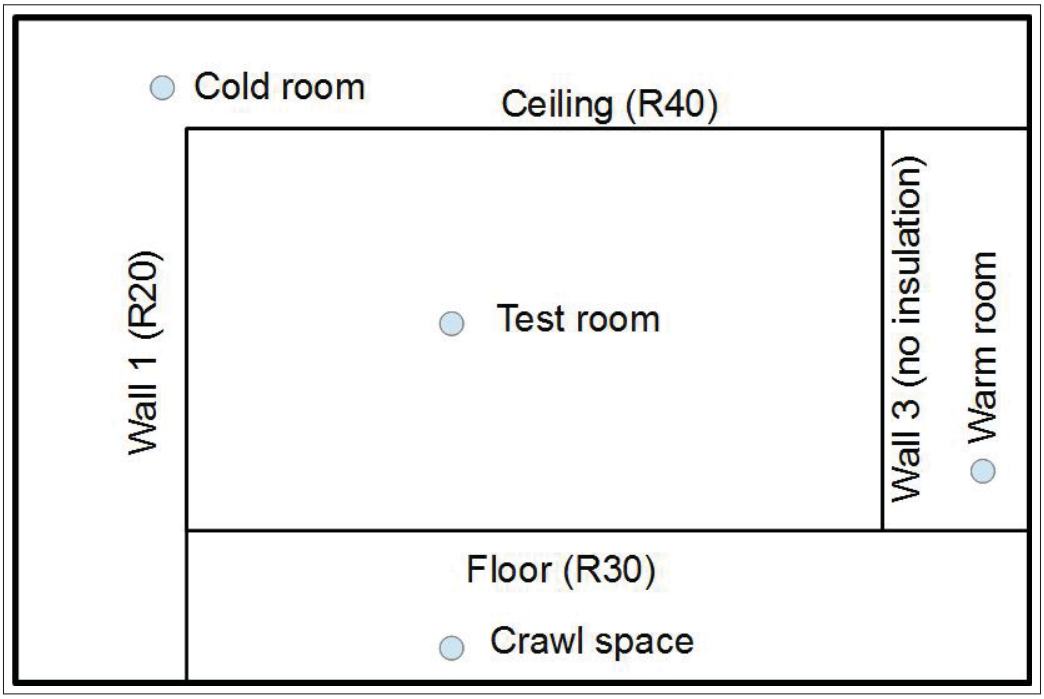

Figure 2.2 Bi-climatic chamber elevation view. Source: C828-13 (CSA, 2013)

floor. On each of the four corner of the ceiling and floor rest metal screw columns that support the structure. These columns are hidden from view as they are surrounded by wooden frames.

The chamber's refrigeration and heating systems are controlled via a LabView program. Figure 2.6 shows the different components of the heating and cooling systems to control temperature inside the Klimat. Four evaporator units, two per cold room corridor, can provide the deep cold temperature in the cold room. The warmer temperature are assured by four industrial heaters placed on each corner of the cold room. In the warm room and crawl space, two heaters and one air conditioning unit assure a temperature control within these spaces. Given that the cold room has a ceiling height of 4.88m(16ft), fans at the ceiling level homogenises the air temperature in the cold room by a proper air circulation.

No humidity control system is available; however, the warm room and test room humidity can be indirectly lowered at very low levels of humidity in the cold room and by infiltration/exfiltration between the cold room, warm room, exterior environment and test room. The cold

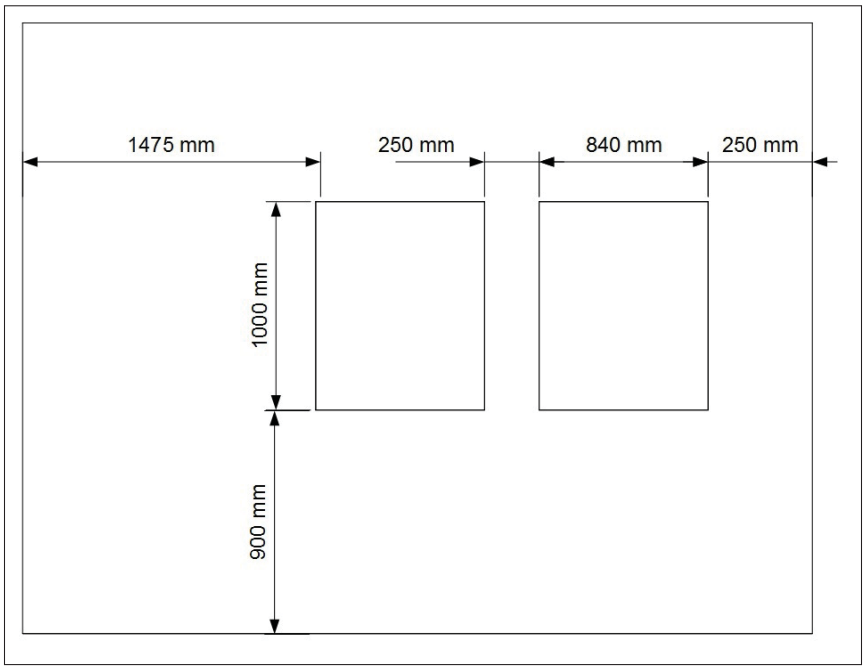

Figure 2.3 Bi-climatic chamber windows on wall 1

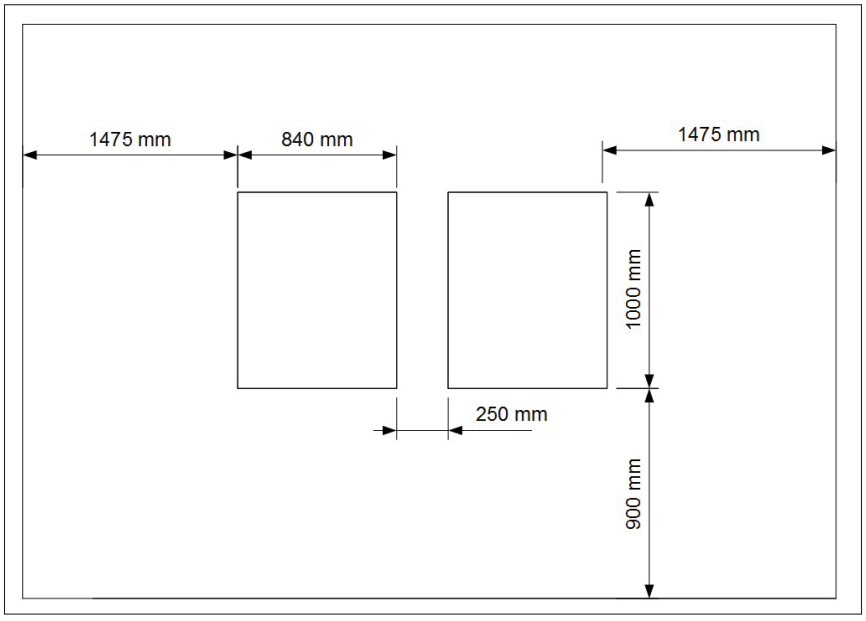

Figure 2.4 Bi-climatic chamber windows on wall 2

room, by having a cold temperature will naturally be much dryer than the test room and warm room. It should also be noted that the evaporators of the refrigeration system is even colder

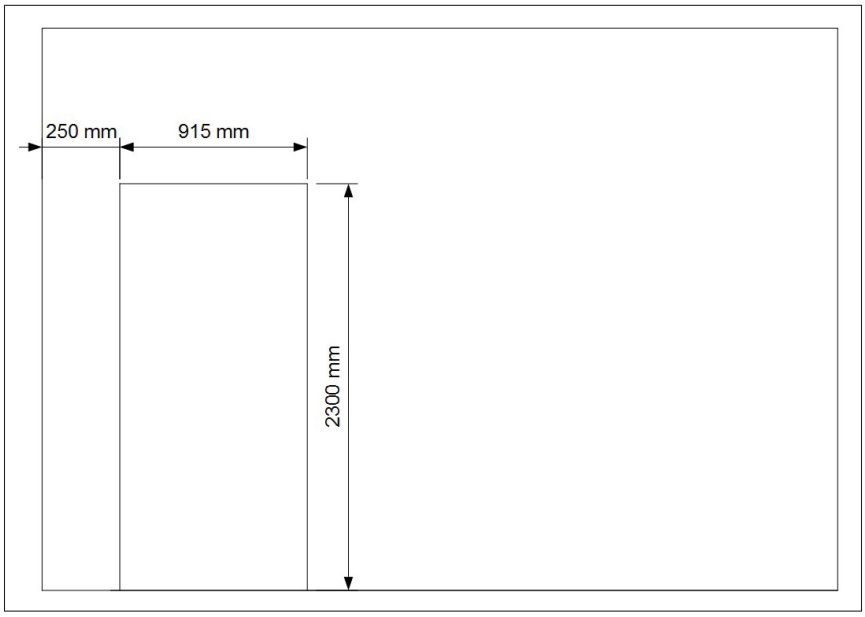

Figure 2.5 Bi-climatic chamber door on wall 4

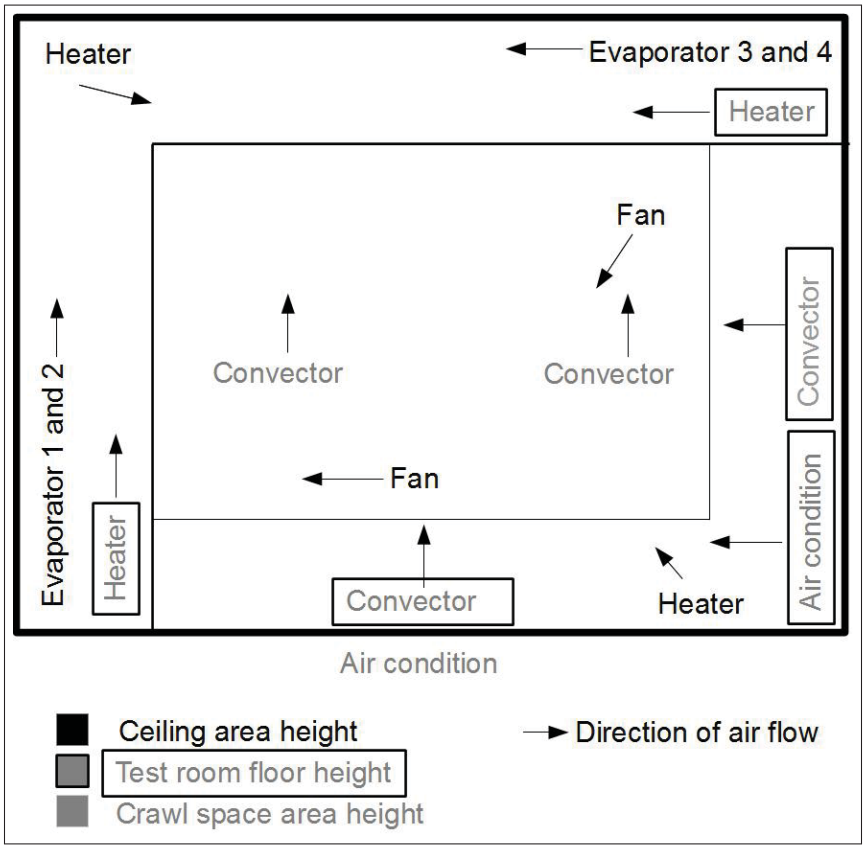

Figure 2.6 Heating and cooling components of the Klimat

than the cold room temperature, thus drying the air further. The cold room can then be used to dry the air inside the warm sections; however, no tools are presently available in the chamber to humidify the air. To prevent humidity differences between tests, the relative humidity is intentionally kept at a steady low value below 30%.

2.2 The chamber's controller

In the cold room, a *PID* controller is used to control the refrigeration by opening and closing a valve to the evaporators. For the heating part of the cold room and the heating and cooling part of the warm room and crawl spaces, an intelligent ON/OFF controller is used. The ON/OFF controller is similar to Bang Bang controller (van Breemen & de Vries, 2001) as it turn the system completely ON or OFF according to some rule. It calculates the heat that must be added to achieve the desired temperature and converts these results to a percentage of cycle time. This percentage of cycle time is the percentage of the cycle that the heater is in its ON states. One cycle typically last 2min. This fast cycle time is fine for testing in a laboratory, but would not be recommended in a consumer product as the cycle time would wear the thermostat relay. The fast cycle time is used here to provide a more constant temperature through time. Similar to the intelligent ON/OFF controller, the test room can be controlled via a thermal comfort controller. This controller calculates the heat that must be added for the next cycle, not to achieve the desired temperature, but to achieve the desired comfort. The derivation of this controller is shown thereafter.

It is known that *PMV* is a function of four environmental parameters. Two of which the heating system can significantly effect, mean radiant temperature and air temperature. For convection heaters, the case of interest, it may be supposed that the heater will heat the air and not the walls, or at least a more significant portion to the air. With that in mind, the variation of energy required to increase the air temperature by one degree is written as:

$$\frac{dE_{\text{air}}}{dT_{\text{air}}} = mc_{\text{p}} \tag{2.1}$$

where m is the mass of air inside the room and c_{p} is the heat capacity of air. The variation of PMV with respect to the air temperature is

$$\frac{dPMV}{dT_{\mathrm{air}}} = \left(0.303e^{-0.036\frac{\dot{E}_{\mathrm{gain,ih}}}{A_{\mathrm{du}}}} + 0.028 \right) \left(0.0014\dot{E}_{\mathrm{gain,ih}} - \frac{d\dot{E}_{\mathrm{loss,rad}}}{dT_{\mathrm{air}}} - \frac{d\dot{E}_{\mathrm{loss,conv}}}{dT_{\mathrm{air}}} \right) \quad (2.2)$$

where

$$\frac{d\dot{E}_{\mathrm{loss,conv}}}{dT_{\mathrm{air}}} = \begin{cases} \dfrac{-1.25 f_{\mathrm{cl}} h_{\mathrm{cl}}}{1 + 0.19375 f_{\mathrm{cl}} h_{\mathrm{cl}} I_{\mathrm{cl}} (1+\chi)} & \text{if} \quad 2.38 \left(\mathrm{T_{cl}} - \mathrm{T_{air}} \right)^{0.25} \geq 12.1\sqrt{\mathrm{v}} \\ \dfrac{-f_{\mathrm{cl}} h_c}{1 + 0.155 f_{\mathrm{cl}} h_{\mathrm{cl}} I_{\mathrm{cl}} (1+\chi)} & \text{if} \quad 2.38 \left(\mathrm{T_{cl}} - \mathrm{T_{air}} \right)^{0.25} < 12.1\sqrt{\mathrm{v}} \end{cases} \quad (2.3)$$

and

$$\frac{d\dot{E}_{\mathrm{loss,rad}}}{dT_{\mathrm{air}}} = \chi \frac{d\dot{E}_{\mathrm{loss,conv}}}{dT_{\mathrm{air}}} \quad (2.4)$$

with

$$\chi = \frac{-2.4552 \times 10^{-8} I_{\mathrm{cl}} f_{\mathrm{cl}} \left(T_{\mathrm{cl}} + 273.15 \right)^3}{1 + 2.4552 \times 10^{-8} I_{\mathrm{cl}} f_{\mathrm{cl}} \left(T_{\mathrm{cl}} + 273.15 \right)^3} \quad (2.5)$$

where all the relevant parameters are defined in the list of symbols and follows Fanger's nomenclature (Fanger, 1970). The PMV error is written as

$$err_{\mathrm{PMV}} = PMV_d - PMV_m \quad (2.6)$$

where PMV_d is the desired PMV and PMV_m is the measured PMV. The heat that must be added or removed to achieve PMV_d can thus be computed using the chain rule and then multiplying this result by the PMV error err_{PMV}.

$$\Delta E_{\mathrm{air,var}} = \frac{dE_{\mathrm{air}}}{dT_{\mathrm{air}}} \left(\frac{dPMV}{dT_{\mathrm{air}}} \right)^{-1} err_{\mathrm{PMV}} \quad (2.7)$$

Heaters and air conditioning systems both are either ON or OFF. To avoid fast cycling (ON/OFF), a constant cycling time is chosen, i.e. they can only be in the ON state once per cycle. The number of ON/OFF cycle is thus regulated. The added percentage of cycle time that the heater

must remain in the ON state compared to the previous cycle can be calculated in the following way to achieve thermal comfort:

$$dt = \frac{\alpha \Delta E_{\text{air,var,av}}}{\dot{E}_{AH}} \tag{2.8}$$

where α is a damping factor to be adjusted for each controller, $\dot{E}_{AH}$ is the power of the heater when it is in its ON state and $\Delta E_{\text{air,var,av}}$ is the average heat that must be added calculated from the previous cycle.

$$\Delta E_{\text{air,var,av}} = \frac{\int_0^{t_{\text{cycle}}} E_{\text{air,var}} dt}{t_{\text{cycle}}} \tag{2.9}$$

The percentage of cycle time that the heater remains in its ON state is calculated using the previous percentage of cycle as

$$p_{\text{i}} = dt + p_{\text{i}-1} \tag{2.10}$$

where i denote the i^{th} cycle. In an expanded form this leads to

$$p_{\text{i}} = \frac{\alpha}{P} \frac{\int_0^{t_{\text{cycle}}} \frac{dE_{\text{out}}}{dT_{\text{air}}} \left(\frac{dPMV}{dT_{\text{air}}} \right)^{-1} err_{PMV} dt}{t_{\text{cycle}}} + p_{i-1} \tag{2.11}$$

If it is assume that both $\frac{dE_{\text{air}}}{dT_{\text{air}}}$ and $\frac{dPMV}{dT_{\text{air}}}$ remain constant trough one cycle, the percentage of cycle time can be written in a new form

$$p_{\text{i}} = \beta \int_0^{t_{\text{cycle}}} err_{PMV} dt + p_{\text{i}-1} \tag{2.12}$$

This form of the percentage of cycle time is similar to Newton's method of solving the roots of a nonlinear equation where the function is the integral of the PMV error $f(p)$, β represents the gradient of the function at one specified point and $p_{\text{i}-1}$ is the previous percentage of cycle time. Each heater cycle is interpreted as one iteration of Newton's method.

To derive eq.(2.12), the major assumption that gradients remained constant over one cycle was made. This is, in fact, not far from reality if humidity, clothing factor, metabolic rate and draft

remains constant. In this case $\frac{dPMV}{dT_{\text{air}}}$ is barely effected by T_{mrad} and T_{air}. As for $\frac{dE_{\text{air}}}{dT_{\text{air}}}$, it depends on c_{p} and m, for which, changes are negligible as we approach thermal comfort and a steady state condition. This is why, for the controller of the climate chamber, gradients where chosen for a set of conditions that achieve thermal comfort. As thermal comfort is approached it can then expected that the gradient information becomes more accurate; consequently, the controller will performs better. For the controller given by eq.(2.12), the gradient β is calculated via the constant $alpha$, and the gradients $\frac{dE_{\text{air}}}{dT_{\text{air}}}$ and $\frac{dPMV}{dT_{\text{air}}}$ at thermal comfort conditions.

This *PMV* controller can also be modified to control other parameters such as temperature. Changing the *PMV* function for temperature, one of the gradient functions will become unity while the other remains the same. The controller can then be used as such with $err = T_{\text{d}} - T_{\text{m}}$.

As it will be shown in Chapter 3, this controller is adequate for achieving a set point *PMV* values when the *PMV* is directly measured in the test room.

2.3 Measurement equipments

The measurement equipments that measure the performance of the heaters and the temperature profiles inside the Klimat are now discussed. Globally, the data acquisition system for the Klimat involves two redundant power measurements, 63 thermocouple temperature measurements and one thermal comfort measurement.

For the power measurements, one device measures power directly and two other equipments measures voltage and current from which power can be deducted. Two of these redundant instruments are available to take measurements inside the test chamber on two independent heating systems. This allows for more flexibility in experiments.

The logged temperature measurements include 64 K type thermocouple temperature measurements on the walls, windows, and hanging from the ceiling inside the chamber. In the cold room, 8 thermocouples hang from the ceiling at different locations to measure the cold room temperature. In this way, the temperature stratification inside the cold room is monitored. The

average of these 8 temperatures is taken as the measure of the cold room temperature for the control system.

The warm room temperature is taken at the geometric center of its two hallways by two thermocouples. These thermocouples are offset from the heating devices installed inside the warm room to not be influenced by their ON or OFF states.

The crawl space has one thermocouple hanging from its ceiling placed at the geometric center of this space.

Four thermocouples also monitor the temperature of the evaporators. They are mostly used for controlling the defrost cycles of the evaporators and monitoring their proper functioning. They serve in the experiment to check if the evaporator were properly functioning.

In the test room lays the remaining installed temperature measurements. Figure 2.7 shows the locations of the temperature measurements taken on wall 1, wall with the installed heater.

On the wall, 13 thermocouples measurements are carried-out. Three thermocouples located directly over the heating system provide a vertical temperature profile above the heater. Three thermocouples on the left hand side window provide a temperature profile of that window. Two thermocouples on each side of the heater provide a horizontal temperature profile and three thermocouples at three corners of the wall provide a general wider distribution of the wall temperature.

For the other room surfaces, Figure 2.8 depicts the locations of the thermocouples installed on walls, while Figure 2.9 show the location of the temperature measurements taken on the ceiling and floor.

For the walls other than wall 1, there is two thermocouples measurements (Figure 2.8). With two thermocouples, a mapping of the wall temperature can be performed across the wall section. The floor and ceiling also both involve two thermocouples measurements to get a one dimensional temperature distribution of both surfaces (Figure 2.9). On each surface, one ther-

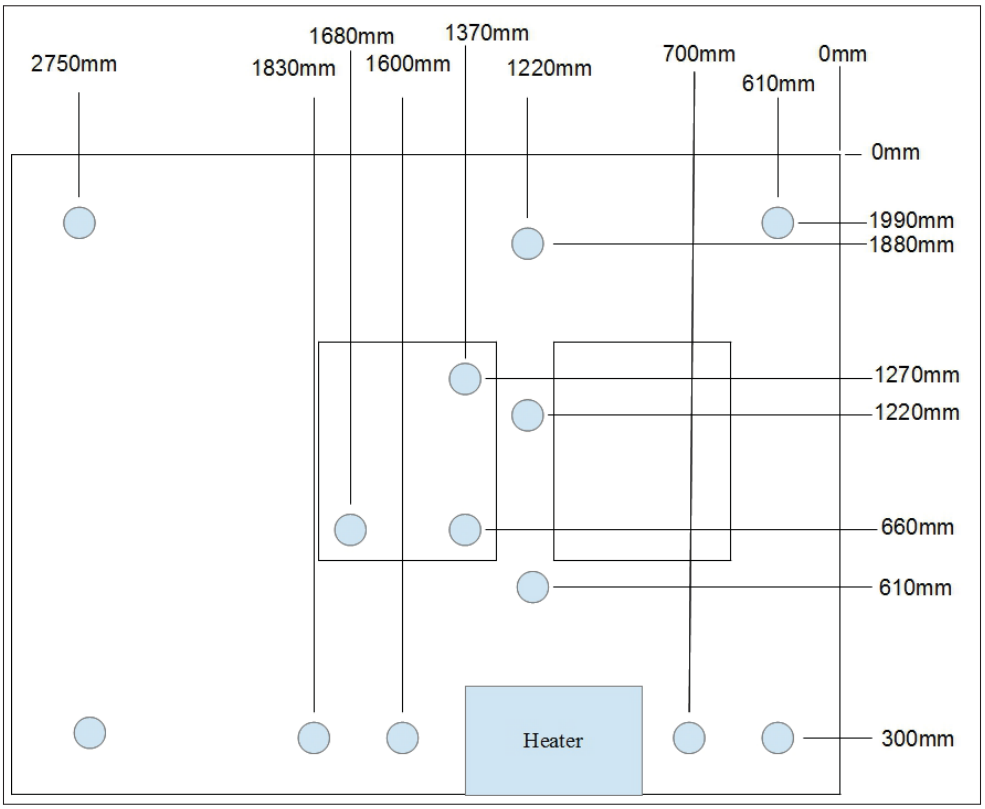

Figure 2.7 Thermocouples on wall with the heating system

mocouple is located in the corner expected to be the hottest and the other in the one expected to be the coldest.

In total, 23 surface temperatures are measured inside the test room.

To complement these 23 surface temperature measurements, four columns of air and radiant temperature measurements, each containing three pair of thermocouple, hang from the ceiling. Each pair of measurement consists of: 1) air temperature measurement with a thermocouple and 2) black globe temperature measurement. Each pair provides the required values to estimate thermal comfort at different vertical locations. The pairs are positioned at a height of 0.61m, 1.22m and 1.83m from the floor level.

Finally, one black globe temperature measurement is collected in the geometric center of the room. In total, 25 air temperature and radiant temperature measurement are logged. The

Figure 2.8 Thermocouples on walls with no heating system

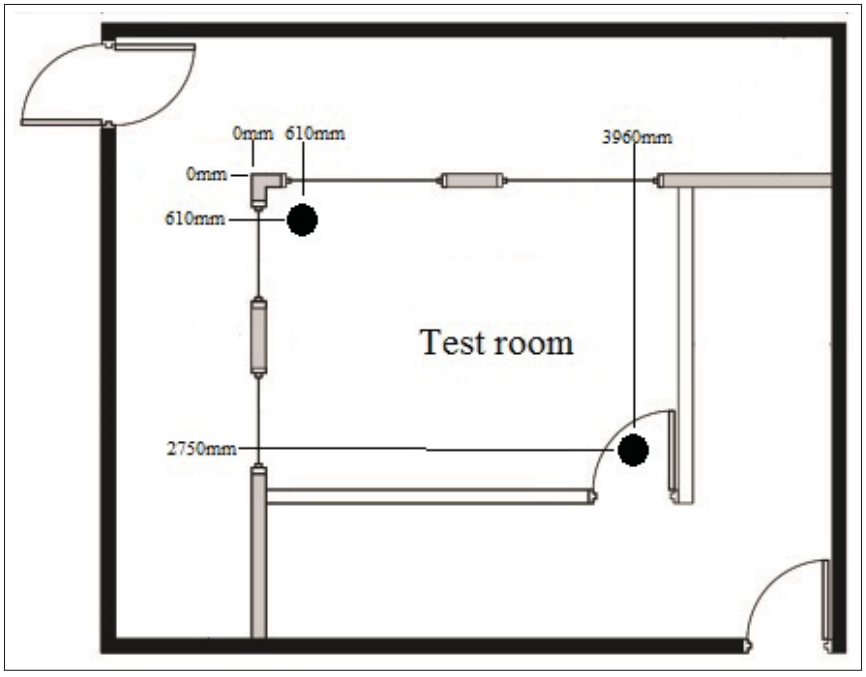

Figure 2.9 Thermocouples on ceiling and floor

columns of thermocouple are shown in Figure 2.10 with the black globe schematically depicted in the center.

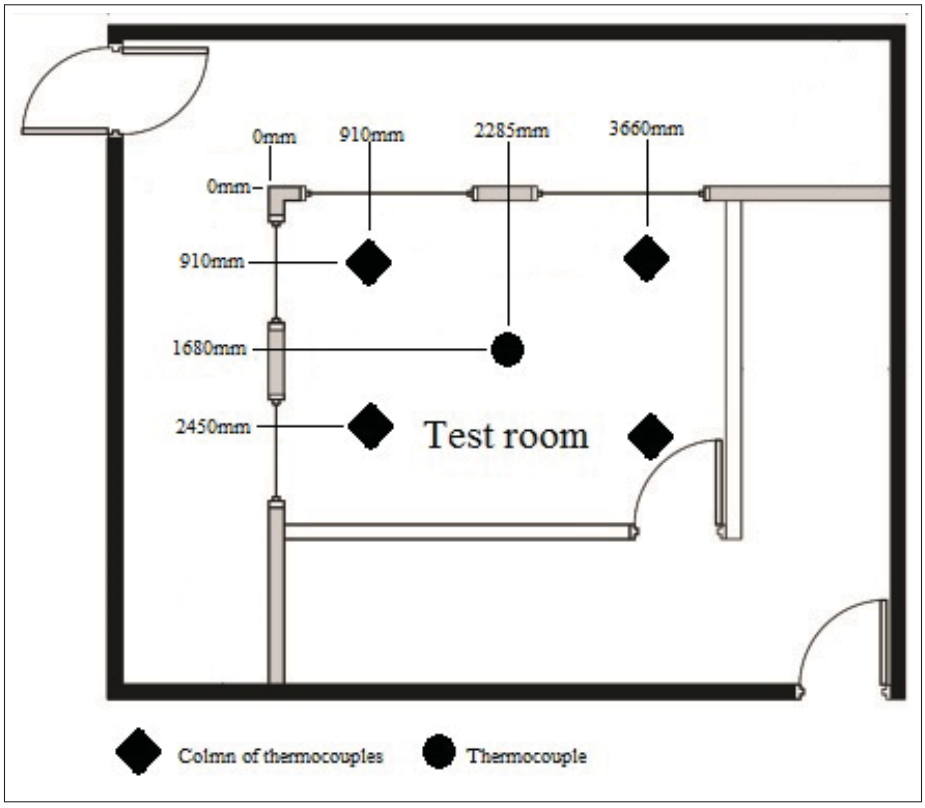

Figure 2.10 Thermocouples hanging from the ceiling

To measure thermal comfort, two methods are used to calculate the *PMV*. The first is to measure the four environmental parameters (humidity, air velocity, radiant temperature and air temperature), to assume the personal parameters (clothing insulation and metabolic rate) and then to calculate *PMV*. The second method measures the air temperature and radiant temperature, assumes the other four parameters then calculate *PMV*. The assumption that humidity, clothing level, metabolic rate and draft remains constant through the room is made for this second method. It is used where no humidity and air velocity measurements were taken, but radiant and air temperatures were taken. This is the case of the four thermocouple columns depicted in Figure 2.10. In this way, a mapping of thermal comfort can be done throughout the room without the need for expensive extra air velocity and humidity measurement probes.

As for the geometric center of the test room, the *PMV* is measured using the Dantec system for measuring thermal comfort displayed in Figure 2.11. The Dantec system uses the first

method described of measuring thermal comfort which involves four probes, one that measure the magnitude of air velocity, one that measure the operative temperature, one that measure air temperature and one that measure humidity. Radiant temperature can be deducted from the operative temperature and air temperature. Clothing and activity levels are set in the LabView program and *PMV* is then calculated.

Figure 2.11 Comfort sense probes. Source: Dantec.com

The calibration of the Dantec system was performed by Dantec who then provided the calibration certificates. The accuracy of the system is of 0.5°C for temperature measurements, 1.5% for humidity measurements and 0.02 m/s for air draft measurements.

As for the other temperature measurements, calibration of the thermocouples was done following the procedure outlined in Appendix I. Thermocouples are accurate to 0.5°C as per the limitation of the hardware.

To measure power, a voltmeter, ammeter and power meter are used. The power meter has an accuracy of 1%. The voltmeter and ammeter, providing a redundant measure of power, have accuracies of 0.1% and 1% respectively. All were purchased calibrated.

The Klimat is thus instrumented with temperature, power and thermal comfort measurements that enable for measuring the performance of heating systems. It is also noteworthy that all measurement equipments are either purchased calibrated or calibrated on site. In this way, the Klimat produces accurate and reproducible results.

2.4 Bi-climatic chamber improvements

One of the key features of the CSA standardized climatic chamber is the possibility to control three environments around the test room, i.e., the cold room, crawl space, and warm room. Another interesting feature of this equipment is that both the refrigeration and heating systems are powerful enough to impose temperature variations akin to what can be found in a Canadian climate. As seen from the literature (see Section 1.2), these properties are common for bi-climatic chambers.

The innovation in the Klimat is its ability to simulate other wall configurations than those of the lay-out displayed in Figures 2.1 and 2.2. The innovative wall construction allows for quickly (less than one hour) interchanging the type of walls or windows used for the test room. Hence, although the actual configuration used in this thesis is precisely that shown in the aforementioned figures, the walls can be moved within the chamber and extra walls can be added to: (1) change the aspect ratio of the test room; (2) add and remove windows of different shape, size and locations; (3) add doors; (4) transform the crawl space into a outdoor space; (5) add a short wall on the top of the test room (see Figure 2.2) so that the upper part of the cold room becomes a warm room; (6) expose 1, 2, 3, or even 4 test room walls to the cold conditions; (7) change the thermal resistance of the walls. All of this by a simple switching of existing walls that is possible with no damage to the floor and ceiling.

The removable walls are designed so that each section of wall may be added or removed independently. These new modular walls provided enhanced abilities when comparing to other climate chambers. No other experimental bi-climatic chamber is able to change walls without rebuilding a new section of wall for each experiment unless they are built from modular wall for

refrigeration. What is innovative about the interior walls in the Klimat is that it also simulates a standard construction, e.g. type of insulation and studs inside the wall, while being modular. The refrigeration panels do not have studs and do not use common residential insulation materials. They are then not as good of a representation of a wall for residential spaces.

In essence, each section of wall is constructed with two leg screws at the bottom that allows the wall to be compressed between the ceiling and the floor. With this mechanism, the wall is fixed to the floor and ceiling, not to other wall sections. Since they are held by compression, no screw or bolt damage the ceiling or floor section. The wall are $1.22\text{m}\,(4\text{ft}) \times 2.44\text{m}\,(8\text{ft})$ and are made of metal studs spaced every 16 inches with fiberglass insulation between studs. Figure 2.12 shows a sketch of a cold room facing wall section.

To prevent air infiltration, rubber seals are used on the top and bottom of the walls along with air sealing tape. For the sides of the wall sections, sealing tape is used between two adjoining sections. On the inside of the wall, a plastic vapour barrier is installed on the wall and helps reduce air infiltration. To install the drywall, a magnetic system is used. On the metal studs, magnets are attached in order to secure the drywall section to the wall. The drywall sheets are fitted with metal strips on their borders that serve not only to protect the drywall, but also to attach the sheets to the magnets. A similar system is used on the outside portion of the exterior walls where a plastic fridge liner and a foam insulation sheet are installed to achieve R20 insulation. The magnetic attachment system was preferred in order to have reusable drywall sheets. Drilling trough the sheets would render them useless once the wall section is changed.

To measure the infiltration/exfiltration between the test room and adjacent rooms, a blower door test was performed. A description of the test and results is shown in Appendix II. An air change rate between the cold room and test room of 14.9ACH at 50Pa was observed. This would be considered high as blower door test at 50Pa for per 1945 housing in Canada showed air change rates of less than 14ACH (Parekh *et al.*, 2007)

The control and acquisition of the Klimat is also an improved part of the laboratory. Custom programmed with LabView, it give the operator access to the source code which allows for

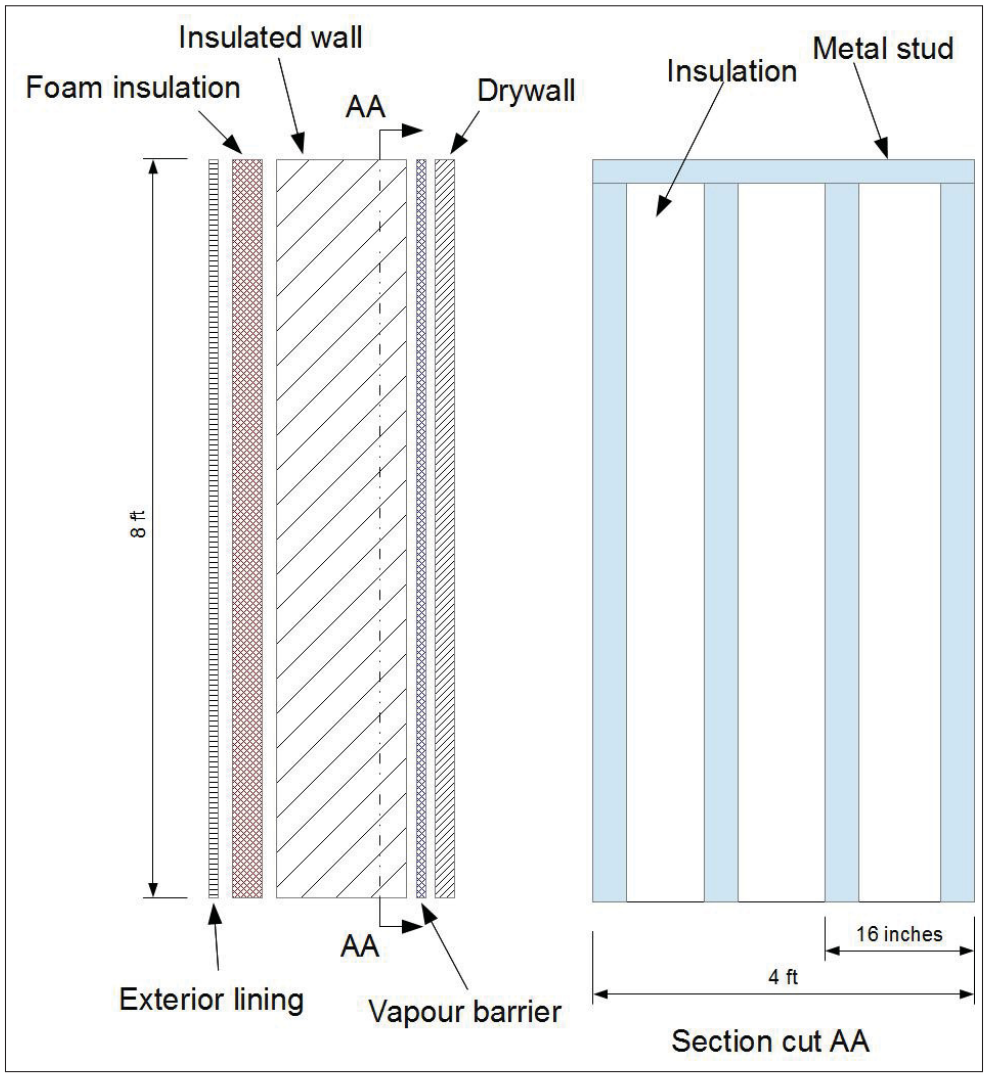

Figure 2.12 Sketch of the modular cold room facing wall section

testing different control strategies on one single platform. It is also important to mention that *PID* and Bang Bang controllers have yet to have been used as a method of controlling thermal comfort (Nägele *et al.*, 2017). The thermal comfort controller used and developed here is original when comparing to literature.

In summary, the Klimat (Léger *et al.*, 2017), also see Figures 2.13 and 2.14, can be modified to simulate a corner apartment exposed to a cold ceiling and warm basement, a corner apartment sandwiched between a similar one, an apartment with only one wall exposed to the external

environment, etc.. The tool is also capable of controlling the test room temperature and thermal comfort. These special features distinguish the Klimat from other bi-climatic chambers and can open a plethora of possible projects outside the proposed experiments of this thesis.

Figure 2.13 Picture of the finished bi-climatic chamber (Klimat) and visualization chamber (Vortex)

2.5 A second climatic chamber

While designing and constructing the Klimat, the partner company also pointed out the need to update another test facility that is designed to carry-out flow visualization experiments. The room called Vortex (Figure 2.15) involves light particles that stay afloat for long durations coupled with a laser that illuminates these particles on a specific plane. The lite up particles allow for visualisation of the air flow inside the room on one plane. A few thermocouple measurements have also been installed to monitor the wall temperature above the heating unit and the air temperature in middle of the room. On the other side of the wall that the heating system is installed, a room is cooled with an air conditioning unit to temperatures as low as $10°C$.

Figure 2.14 Picture of the test room in the bi-climatic chamber

The Vortex is not yet equipped with a particle interferometry visualisation system (PIV). There is no quantitative measurement of air flow available from the experiment. However, qualitative conclusions may be drawn from the Vortex. This tool is used to support some conclusions on experiments presented in Chapter 3.

2.6 Conclusions

In this second chapter, attention was focussed on the design, construction, controls, and validation of the equipment that will be used to reach the experimental goals mentioned in Chapter . This equipment is called the Klimat chamber. Specific interest was given to create a research instrument that could later be used to tackle different challenges in the domain of building thermal engineering. The flexibility in geometry, climatic conditions, controls and types of equipments to be tested makes this facility unique and led to a conference publication (Léger *et al.*, 2017) that is summarized in Appendix 1.

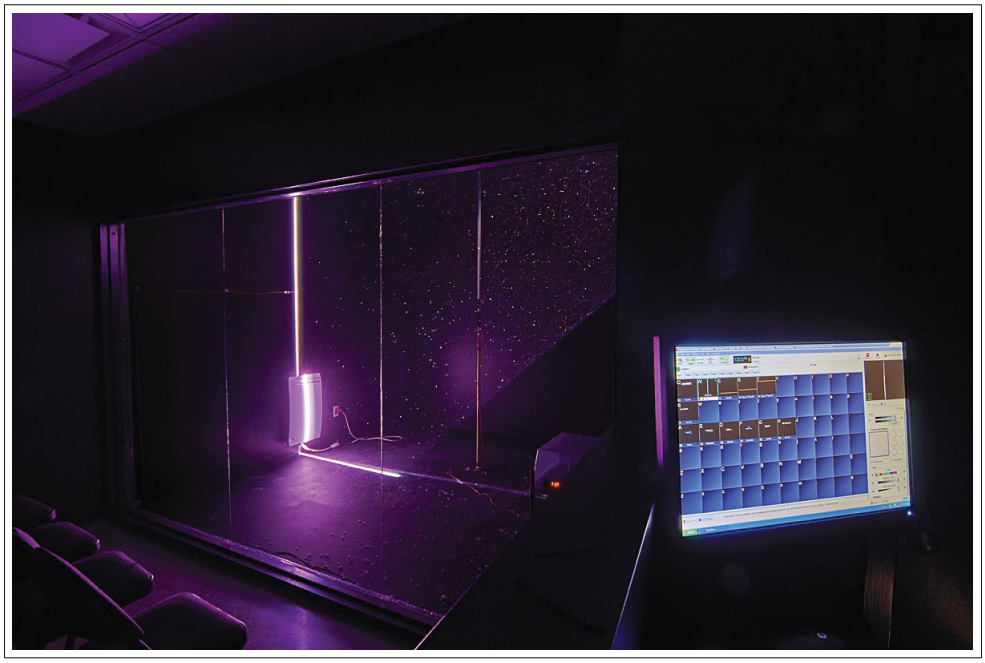

Figure 2.15 Picture of the finished fluid mechanics chamber : The VORTEX

A visualisation chamber of air flow was also discussed as it is used to support some conclusions of this thesis. This chamber is not yet equipped with the appropriate PIV or other system to actually measure fluid flow, but it can be used to provide qualitative descriptions of the thermally induced fluid flow about heating systems.

CHAPTER 3

EXPERIMENTAL INVESTIGATION

In this chapter, the bi-climatic chamber Klimat discussed in chapter 2 is used to produce experimental results on the energy consumption of three different electric heating systems at equal thermal comfort: a convection heater, a radiant heater and a baseboard heater. The experimental investigation is intended to answer the following: Do electric heaters consume the same amount of energy when providing the same thermal comfort? In answering this question, the differences of the three tested electric heaters are highlighted.

In a past research, Olesen et al. (Olesen *et al.*, 1980) showed that convection heating tends to increase heat loss if the heater is located at the base of the wall, directly under the window. Locating the device below windows increased the convection heat transfer due to high air velocity on the window surface. Sevilgen and Kilic (Sevilgen & Kilic, 2011) also showed that heating the windows consumes more energy; however, they mentioned that heating below the windows would counteract uncomfortable cold drafts. Myhren and Holmberg (Myhren & Holmberg, 2006) stated that radiant heating and cooling could potentially save energy as compared to convection technologies. A specific case of these comparisons will be tested in this experiment.

Nowadays, developments in convection heaters have made them able to push air further down the room. This becomes important to reduce heat loss as there will be less air movement directly above the heater and thus near the window. In fact, initial qualitative experimental results obtained with the Vortex visualization and climate chamber indicate that convection-based devices heat the surface on which they are installed less than baseboard heaters.

The advantage of comparing electric heating systems in this work is that differences in energy consumption will be based purely on heat distribution alone as each heater convert 100% of their loads to heat. It is then significant to demonstrate quantitatively that convection heaters indeed evolved to distribute heat in a more efficient way to increase their energetic performance.

By doing so, convection heater would now perform better than what was observed by Olesen et al. (Olesen *et al.*, 1980). This is the hypothesis of this experimental campaign.

In the first part of this chapter, the experiment is described. This is followed by an error analysis of the experiment and tools. Results are then presented and show that convection heaters have indeed improved in their heat distribution performance. The differences between heaters are then discussed in what follows. The results are put into relation with the virtual heaters. Conclusions are then drawn on heat distribution characteristics of the different tested heaters.

3.1 Description of experiment

Equipped with the Klimat, the following experiment was performed.

First, the chamber's cold room was set at $-35°$C for 24h so as to dry the air inside and reach a stable humidity point in the bi-climatic chamber. Note that no humidity control is available so it was decided to keep the air inside the cold room, and by infiltration the test room, as dry as possible in order to maintain a level of control over this parameter via the cooling system. It can also be noted that to prevent icing of the evaporator unit of the main refrigeration system inside the chamber, defrost cycles of the evaporators were performed first at a temperature lower than the minimum experimental temperature and also before each measurement sequence. This prevents the need to defrost during the experiments, which might affect the cold room temperature as refrigeration power is lost for a few minutes. In the warm room and crawl space, heaters were set at 22°C for the duration of the experiment. In the test room, a proportional thermal comfort controller controls the heater so as to achieve, on average, $PMV = 0$ at the geometric center of the room. Not achieving $PMV = 0$ would lead to an increase or decrease in energy consumption. The controller was tested statistically in the section that follows. The PMV is not directly measured, the relative humidity, air velocity, operative temperature and air temperature are measured. By specifying a metabolic rate and clothing levels, values of 1met and 1clo respectively, the PMV can then be calculated.

Once the initial stabilisation is achieved, a temperature of $-30°C$ is set in the cold room for 36h. The first 24h serve to stabilize at the new temperature and the remaining 12h serve as the measurement period. Measurements are thus taken in quasi-steady state conditions. Quasi-steady is employed here as the ON/OFF heaters cannot maintain a steady state temperature, but over multiple ON/OFF cycles, the temperature cycle is constant.

The process at $-30°C$ was then repeated at $10°C$ intervals for temperatures of $-20°C$, $-10°C$, $0°C$ and $10°C$. All measurements were stored at 5s intervals taking the mean measured value over a 5s period. These values were then averaged on a 12h period for comparison.

3.2 Error analysis

Comparing heating equipment's, it is important to quantify the experimental error to truly understand the significance of the differences found between systems. The error can be characterised in two ways: the accuracy characterise how close a measurement is from the real value, while precision quantify the reproducibility of that measure. For this experiment, it is most important that measurements be precise as the difference between heater energy consumptions is wanted to draw conclusions rather that the consumption themselves which pertain to the accuracy. Nonetheless, the accuracy and precision of measurements is presented in this section. Different types of measurements are taken and could be sources of error. These include the air and radiant temperature, power, tension, electric current, humidity, and air velocity. Another source of error is the thermal comfort control system. A higher PMV would consume more energy, it is thus important that thermal comfort be consistent throughout experiments. Similarly, the cold room, warm room and crawl space temperature differences could also contribute to the error on energy consumption. The accuracy of the installed sensors as reported in the supplier's documentation is shown in Table 3.1.

In the table, it can be seen that the temperature error is in the order of $0.5°C$ since type K thermocouple are used. This accuracy could be increased by proper calibration. The power is estimated to be accurate at 1% which is sufficient for the experiment.

Table 3.1 Accuracy of measurements

Type of measurement	Uncertainty
Temperature	$\pm 0.5°C$
Humidity	$\pm 1.5\%$
Air velocity	$\pm 0.02 m/s$
Voltage	0.1%
Current	1%
Power	1%

It is important that the measured difference between heaters be also properly assessed. A thermal comfort controller is used in the experiment and it can be difficult to assess the uncertainty caused by the controller without some statistical analysis. An increase in thermal comfort would lead to an increase in power consumption as the indoor temperature would increase. A statistical approach to measure the total error caused from sensor precision and from the control systems is chosen as the preferred method to assess the precision of the experiment.

The test for the convection heater was reproduced a number of times to get several samples of the same experiment. Then, constructing a 95% confidence interval (Ryan, 2007), the experimental precision was estimated. Statistical results of the repeated experiment are shown in Figures 3.1 and 3.2 where the number of samples for each temperature is shown in Table 3.2.

Table 3.2 Number of samples for each tested temperature

Temperature [°C]	Number of samples [-]
-20	4
-10	7
0	7
10	5

On Figure 3.1, the normalized temperature errors are shown for the different temperature measurements. Temperature is normalized using

$$\theta_{\mathrm{i}} = \frac{T_{\mathrm{i}} - T_{\mathrm{cold}}}{T_{\mathrm{av,air,conv}} - T_{\mathrm{cold}}} \tag{3.1}$$

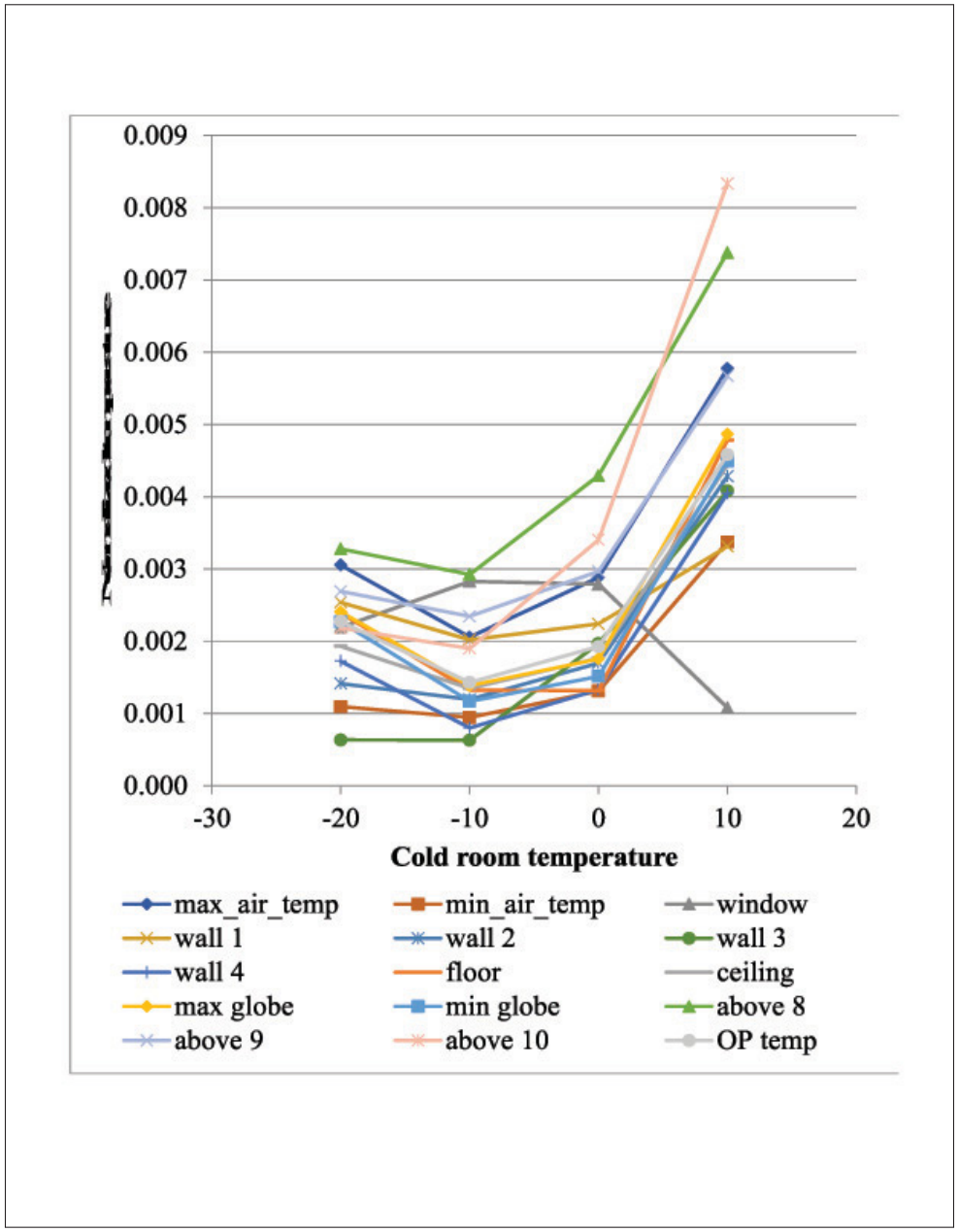

Figure 3.1 Normalized temperature errors (95% confidence)

where T_i is the temperature to be normalized, T_{cold} is the cold room temperature and $T_{av,air,conv}$ is the average air temperature of the convector. The average air temperature ($T_{av,air}$) is computed from the arithmetic average of all air temperature measurement averages taken in the test room, see Figure 2.10. The temperature errors are clearly less than 1%.

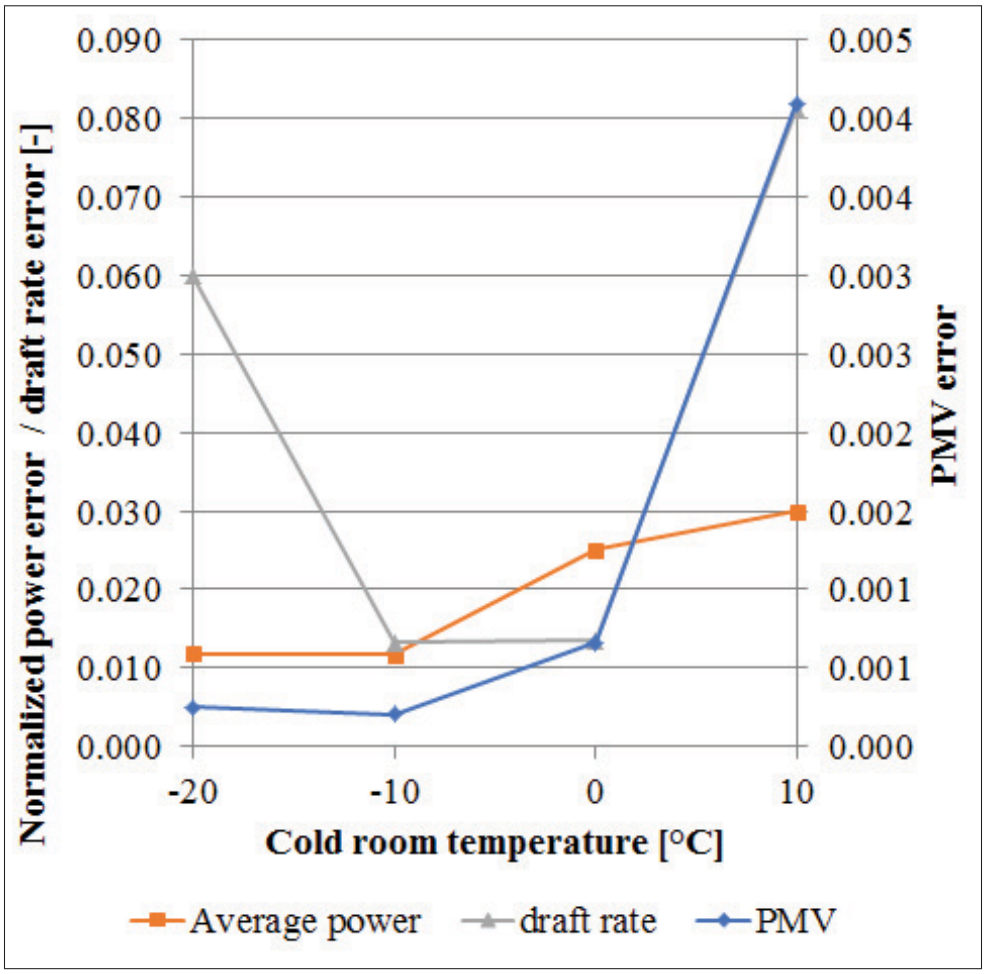

Figure 3.2 Normalized error of draft rate and power (left axes) along with *PMV* error (95% confidence) (right axes)

On Figure 3.2, the normalized draft rate error is shown to be less than 9% and the normalized power error varies from 1.2% to 3%. On the secondary axis, the PMV varies less than 0.005 which is likely within the undetectable range of comfort since it is a 100 times smaller than the thermal comfort range defined by ASHRAE (ASHRAE-55, 2013). Power is normalized using the following equation:

$$NP_i = \frac{P_i}{P_{conv,av}} \tag{3.2}$$

where $P_{\text{conv,av}}$ is the average power consumption of the convector and P_{i} is the power consumption to be normalized. Similarly, the normalized draft rate error is:

$$NDRE_{\text{i}} = \frac{DRE_{\text{i}}}{DR_{\text{conv,av}}} \tag{3.3}$$

where DRE_{i} is the draft rate error and $DR_{\text{conv,av}}$ is the average draft rate of the convector.

From figures 3.1 and 3.2, it is clear that the experiment is repeatable. The samples were taken over a span of two months, showing that the experiments are not affected by external conditions. The high draft rate error is due to the low air velocities measured. The air inside the test room is relatively still which makes it hard to measure. This is more obvious when looking at Figure 3.2.

Note that the number of samples varies between cold room temperature levels. This is due to the way the trajectory was programmed. It increased the temperature level from $-20°$C to $10°$C then decreased the temperature level from $10°$C to $-20°$C. The extremities were not repeated between an increase and a decrease in temperature thus reducing the amount of samples for the temperature extremities.

The statistical errors presented here account for variations in load due to the thermostat controlling the process. Relative errors tend to be higher as the cold room temperature warms. This is likely due to the fact that at colder temperatures, heat transfer increases along with temperature differences while random errors tend to remain stable. The increased difference between random errors and measured values then make for more precise relative measurements at lower cold room temperatures.

3.3 Results

The results of the experiment are now shown in normalized form to highlight the differences between heaters. Interestingly, although all heaters where rated at 1000W, they did not, under the same voltage, produce the same power. This is caused by small differences in the resistance

of each heater. Since at $-30°C$ the heaters were on their ON state 100% of the time, they did not all achieved the same thermal comfort because of these differences in resistance value. The point at $-30°C$ was omitted from the results. Error bars are deliberately not shown on the Figures follow to improve their readability.

The normalized power consumptions of the three heaters are presented in Figure 3.3 with a secondary axis of the graph showing the convector power. The term norm is used in Figures 3.3 and in the figures that follow to denote the denominator of the normalization used. The norm helped retrace the normalized power and normalized temperatures to their respective units in $[W]$ and in $[°C]$. In these figures, the terms conv, rad and base are short for values that relate to the convector, radiant heater and baseboard heater respectively. Blue is employed for conv, red for rad, purple for base and green for norm. This nomenclature is applied for all the figures presenting results.

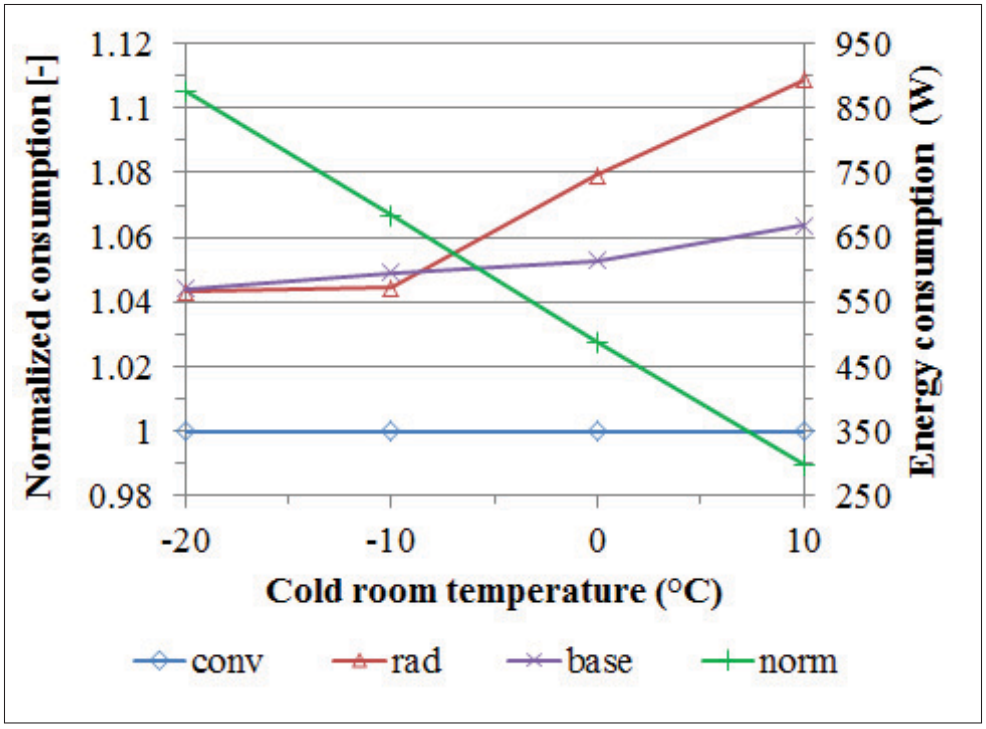

Figure 3.3 Comparison of power consumptions

From Figures 3.3, it is shown that the convector consumes less energy than the baseboard and the radiant heaters. The baseboard heater performance relative to the radiant heater increased with higher outdoor temperatures. The radiant and baseboard heaters consumed just over 4% more than the convector at low cold room temperatures which is significant considering a potential variation of 1.2% on the average power consumption. At higher cold room temperatures, the radiant heater consumed almost 11% more than the convector, though the error on this measurement was closer to 3%. The baseboard heater at higher cold room temperatures consumed 6% more than the convector. This is barely significant as it is within the range of the experimental error.

The minimum, maximum and average normalized air temperatures are presented in Figure 3.4 with a secondary axis showing the average temperature difference between the test room air temperature and cold room temperature for the convector. This secondary axis is repeated for all temperature graphs and is only useful for the norm curve. The circle symbol is used to denote an average temperature, the triangle for a maximum temperature and the diamond for the minimum temperatures. This nomenclature is repeated for the figures showcasing maximum, minimum and average temperatures.

Figure 3.4 shows that the radiant heater induced less air temperature stratification followed by the baseboard and the convector. There is a spread between the maximum and minimum air temperature of close to 9% for the convector. This is significant, since the temperature error could be up to 2%. The average temperatures were all similar for the three heating devices. The minimum air temperature for all cases was found in the lower plane of the corner of walls 1 and 2. The maximum was found in the upper plane of the corner of walls 3 and 4.

The minimum, maximum and average radiant temperatures calculated from the black globe temperature and an average draft rate (Kuehn *et al.*, 1970) taken from Figure 3.12 is presented in Figure 3.5.

As expected, the radiant heater has a higher mean radiant temperature than the convector or the baseboard heaters. A mean radiant temperature stratification can also be observed.

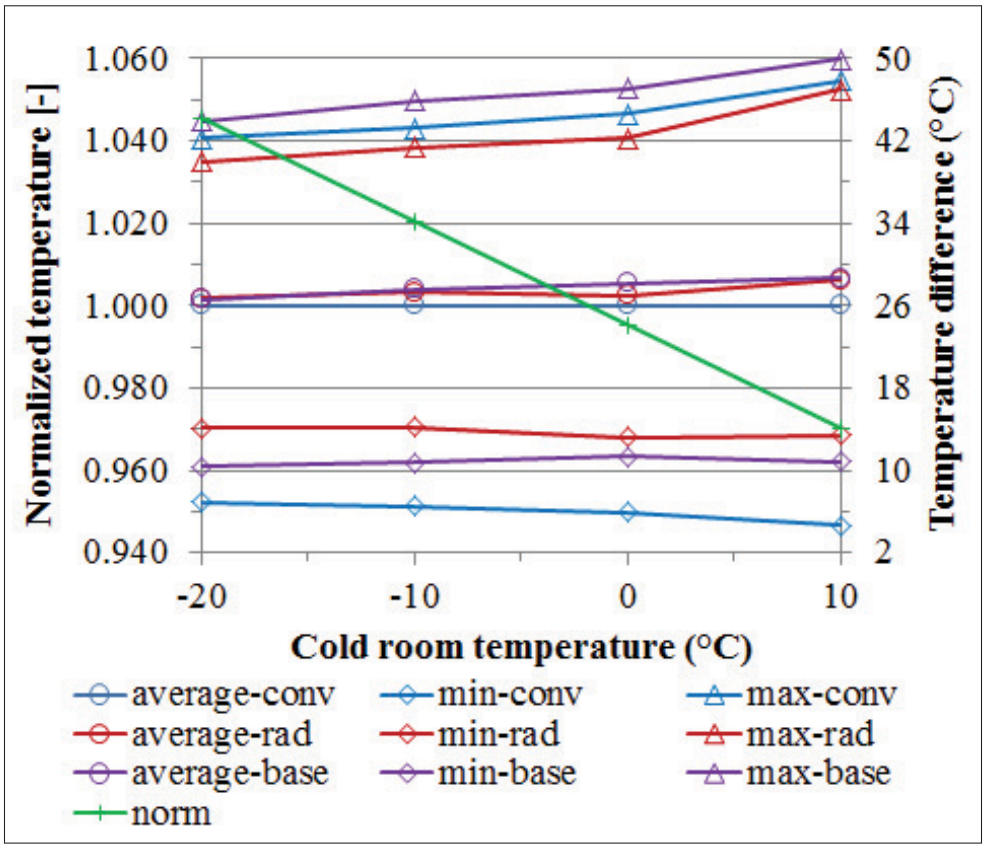

Figure 3.4 Normalized air temperatures overall

The air temperature and radiant temperature on the mid plane, the plane on which thermal comfort is measured, are presented in Figures 3.6 and 3.7, respectively.

From these two figures, the trade-off between radiant heat and convective heat to maintain thermal comfort can be observed. The radiant heater had higher radiant temperatures followed by the baseboard and then the convector. Inversely, the convector had higher air temperatures followed by the baseboard and then the radiant heater. This is to be expected as thermal comfort was controlled on the mid plane.

The temperatures on wall 1, wall 2, the ceiling and the window above the heater are shown for each cold air temperatures in Figure 3.8.

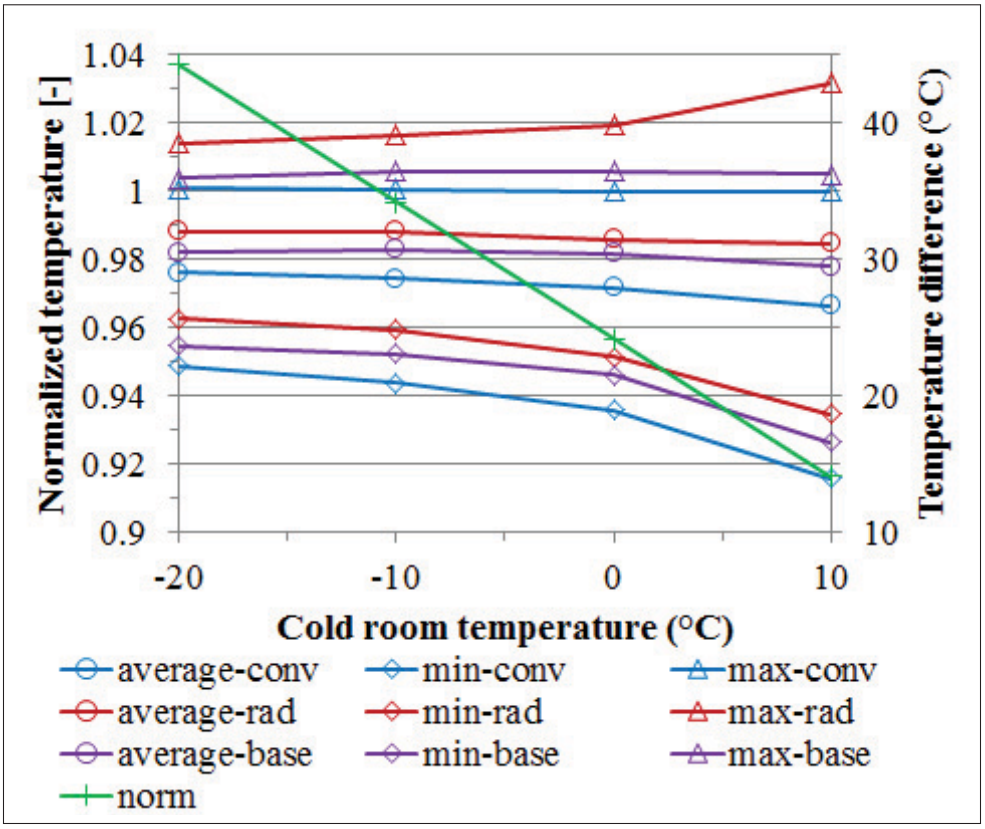

Figure 3.5 Normalized mean radiant temperatures overall

Clearly the windows are the coldest surfaces while the ceiling, most insulated part exposed to the cold room, is the warmest. It is also interesting to note that the radiant heater and baseboard heater heated the windows more than the convector.

For wall 3, wall 4 and the floor, i.e. surfaces exposed to a warmer temperature, the normalized measured temperatures are shown in Figure 3.9.

Figure 3.9 shows that the radiant heater significantly heated the floor more than the other heaters. As for the other surfaces, the radiant heater also provided consistently warmer surface temperatures. This was followed by the baseboard heater heating the surfaces more than the convector. This is consistent with the results of the mean radiant temperatures presented in Figures 3.5 and 3.7.

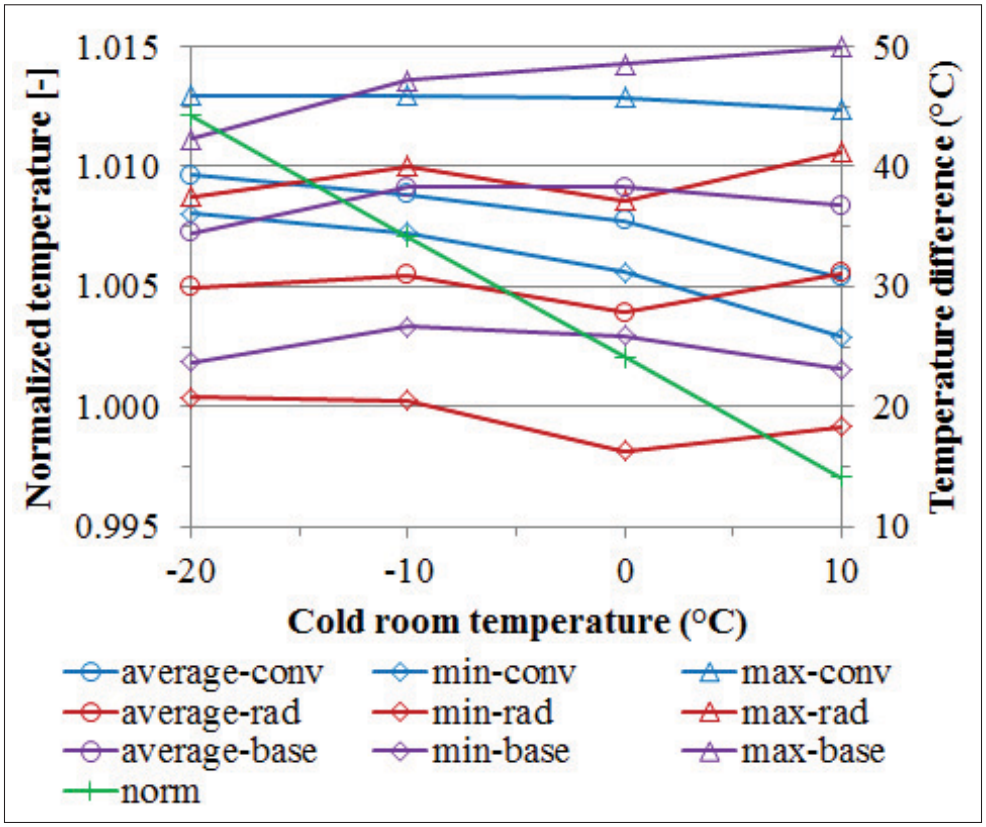

Figure 3.6 Normalized air temperatures on mid plane

To complete the presentation of surface temperatures, the temperature of the wall above the heaters (TC_{ab} in Figure 2.7) is presented for three heights in Figure 3.10. These heights are: 0.41m (low), 1.02m (med) and 1.60m (high). These are spaced out equally along the height of the room.

The baseboard heater heated the wall above it more than the radiant heater then followed by convector. It is also noted that the baseboard and radiant heaters progressively heated the wall less as height increased. This indicates that the hot thermal plume from both heaters was cooled by the above wall and windows. The convector did not have the same behaviour, as the highest temperature was found at the highest point.

The environmental parameters affecting thermal comfort were also measured. The variation of the relative humidity is presented in Figure 3.11.

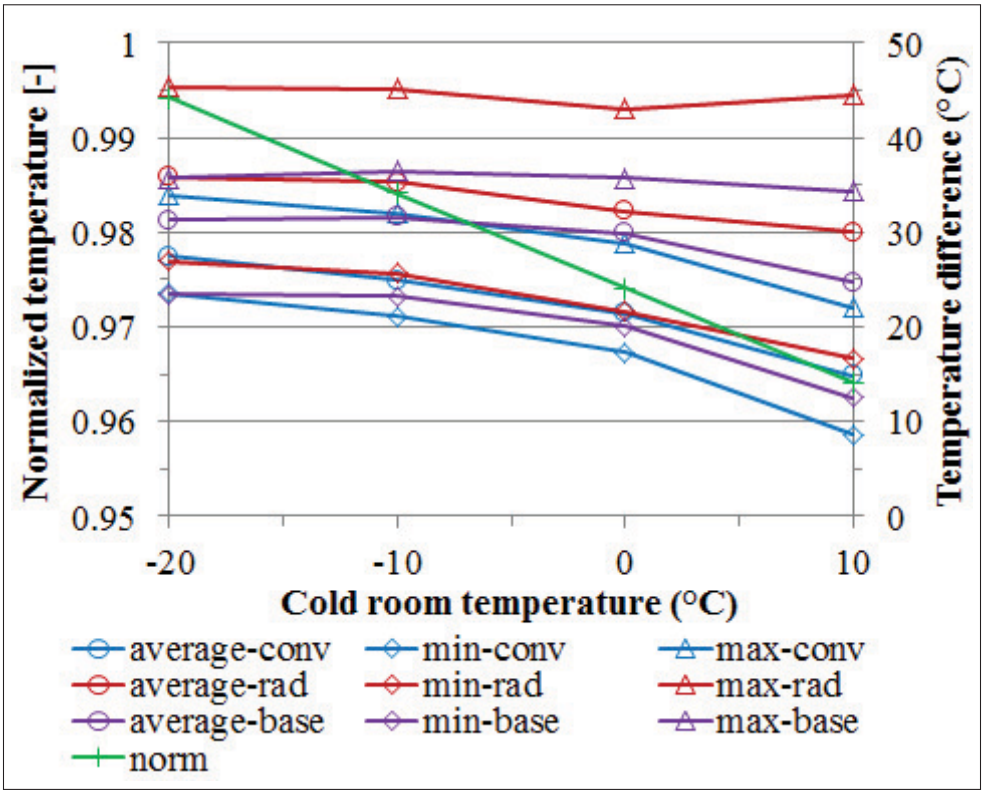

Figure 3.7 Mean radiant temperatures on mid plane

The humidity remained relatively constant despite having no control over this parameter. Humidity when testing the convector was slightly higher than when testing the baseboard heater and radiant heater. Statistical testing with the convector showed that humidity varied from 6% to 12% at lower cold room temperatures while it varied from 11% to 15% at warmer cold room temperatures. The change in relative humidity does not change the final heat consumption results.

The average air velocity is presented in Figure 3.12.

In Figure 3.12, the convector is seen to have higher air velocities than the other two heaters, though still relatively low. The average air velocity was also higher for lower outdoor temperatures and gradually increased. This can be explained by the convector providing increased air flow when it is in operation. With decreasing cold room temperature, the rate of heating is also reduced; thus, the reduction in average natural convection flow for the convector is observed.

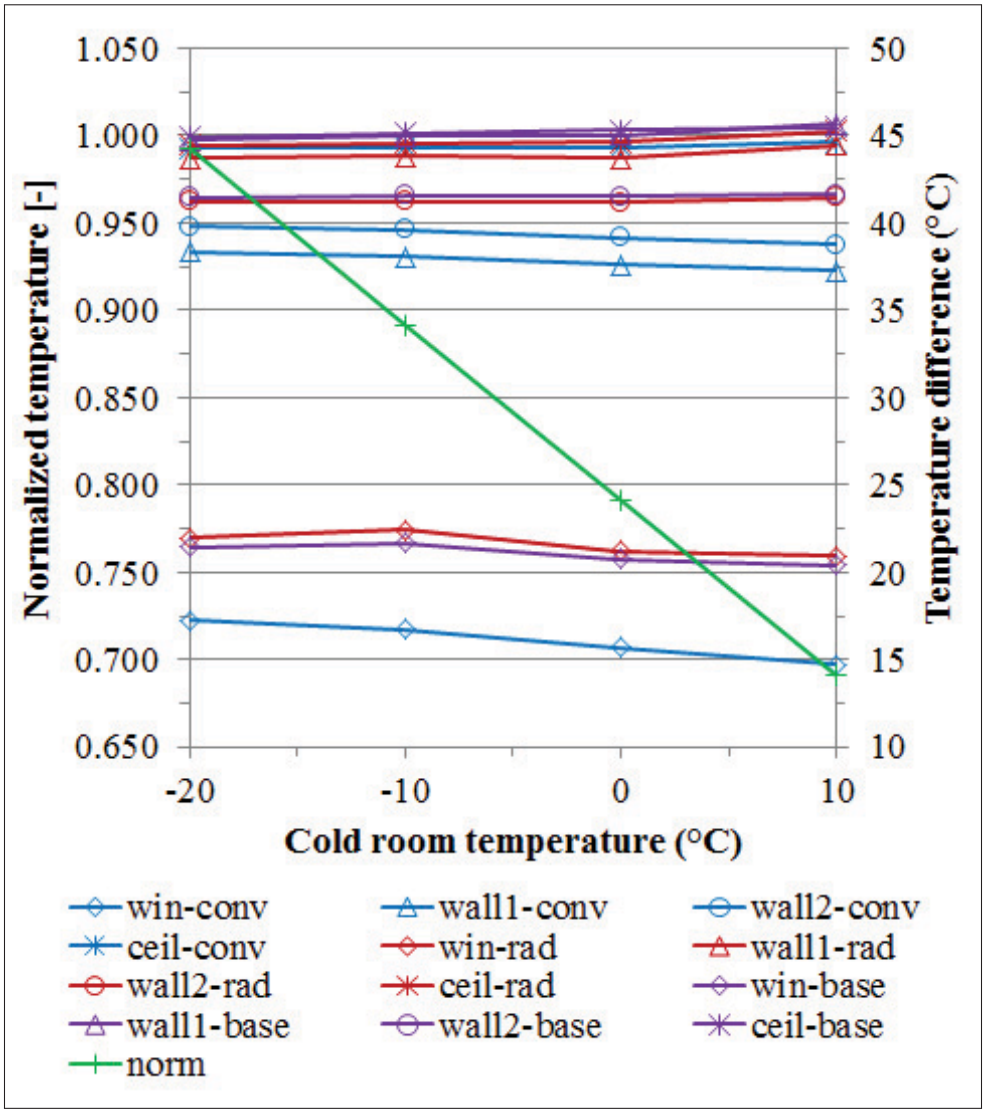

Figure 3.8 Cold room exposed surfaces normalized temperatures

The *PMV*, measured at the geometric center of the room, is presented in Figure 3.13.

The measured *PMV* at the center of the room remained relatively constant when changing heating systems. This is not surprising as the thermostat controlled the set point $PMV = 0$. Thermal comfort was then well controlled and consistent for each heating system.

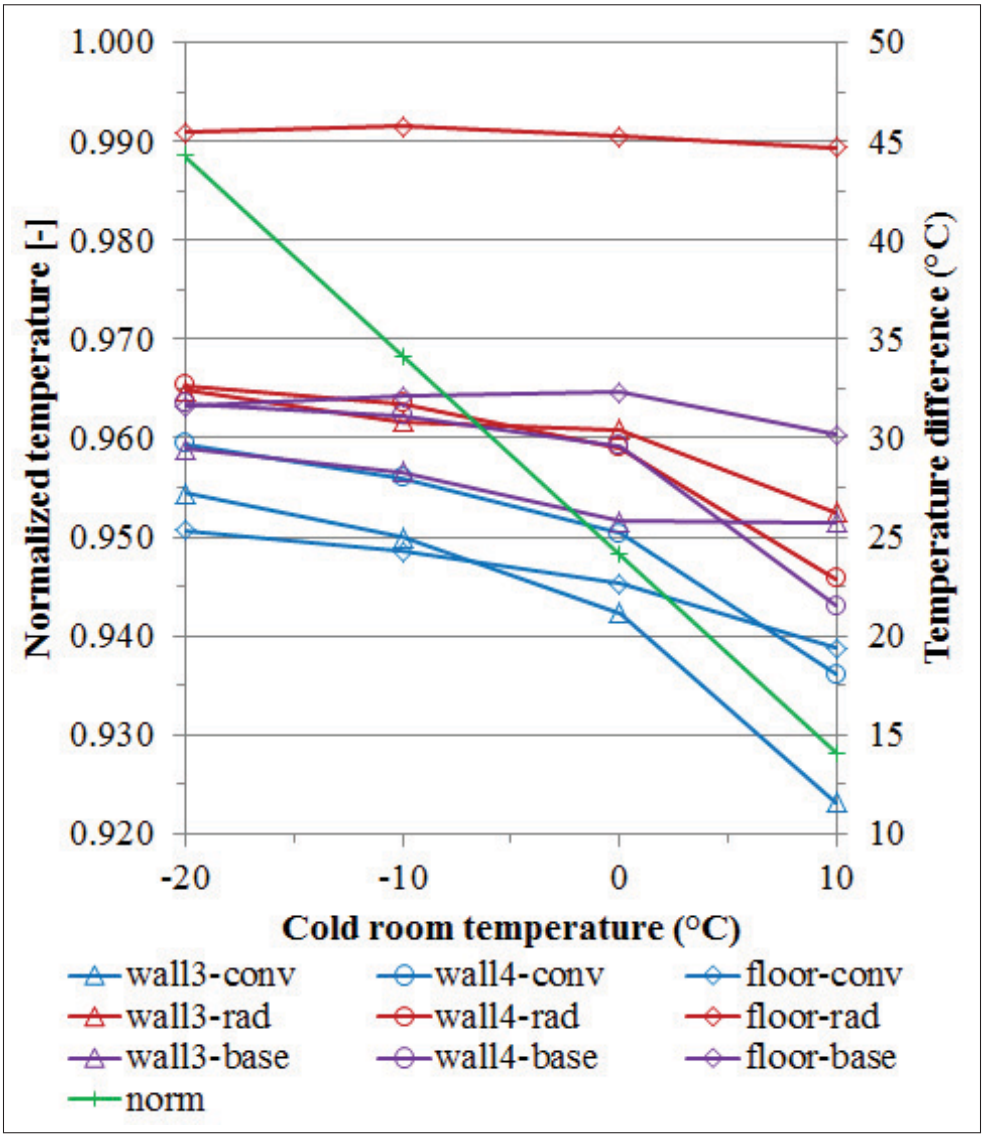

Figure 3.9 Warm rooms exposed surfaces normalized temperatures

3.4 Comparing electric heaters

The question of whether electric heating systems all consume the same amount of energy to achieve thermal comfort is now answered. From the results, it is clear that they do not have all the same energy performance because they distribute heat differently. All tested heating systems achieved an average thermal comfort of $PMV = 0$ at the geometric center of the room. The convector achieved this by consuming less energy than the radiant and baseboard heaters.

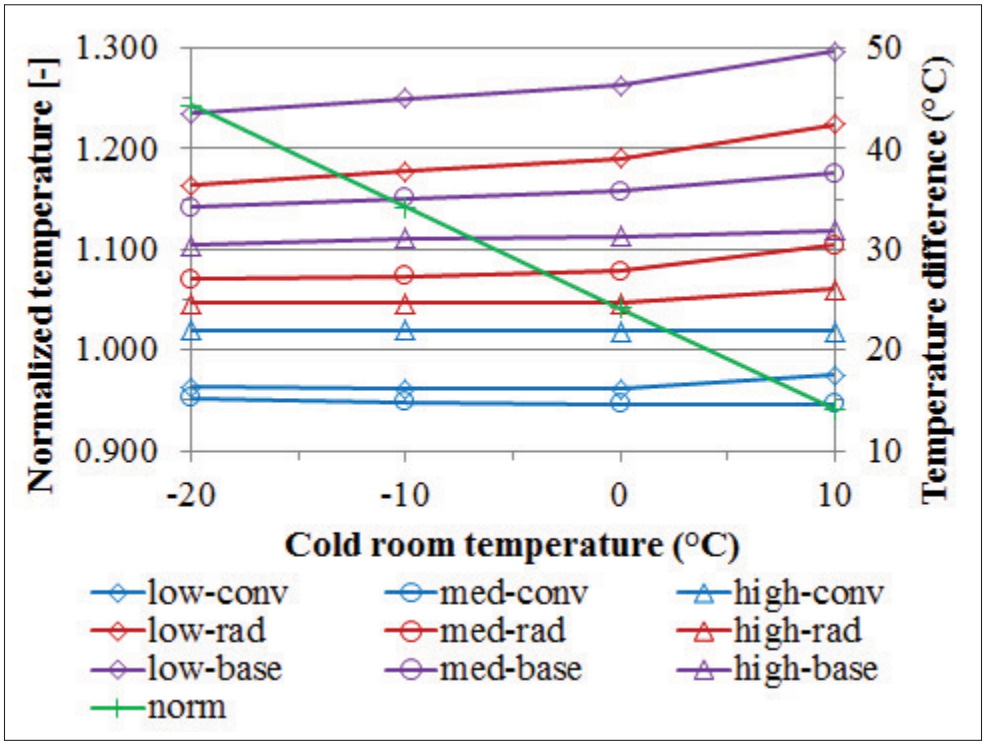

Figure 3.10 Wall temperatures above heater

The temperature stratification was however more important for the convector and less for the radiant heater. The radiant heater consumed the most; it also heated most surfaces more than the other equipment.

From the results presented in Figure 3.8, it is clear that the convector heats the window much less. This is likely an important source of gain in effectiveness that the convector has over the baseboard and the radiant heaters since the heat loss through the windows is most sensitive to a temperature change. The wall and window temperatures above the heater was heated less by the convector. The convector, by its air outlet design, is able to push the hot air into the room before the hot thermal plume reattaches to the adjacent wall. This phenomenon was observed in a visualization chamber prior to these experiments, as shown in Figure 3.14.

On Figure 3.14, a sheet is placed parallel to the outlet air flow; then, using a thermal camera, a picture of the thermal plume is taken. Clearly, the thermal plume seen on Figure 3.14 does

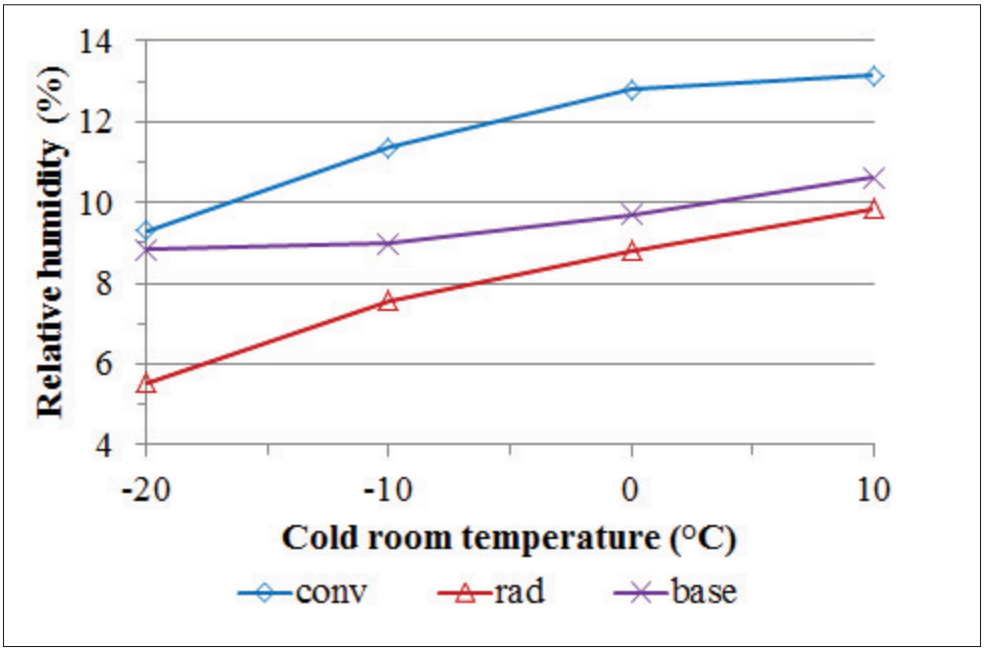

Figure 3.11 Average relative humidity at the geometric center of the test room

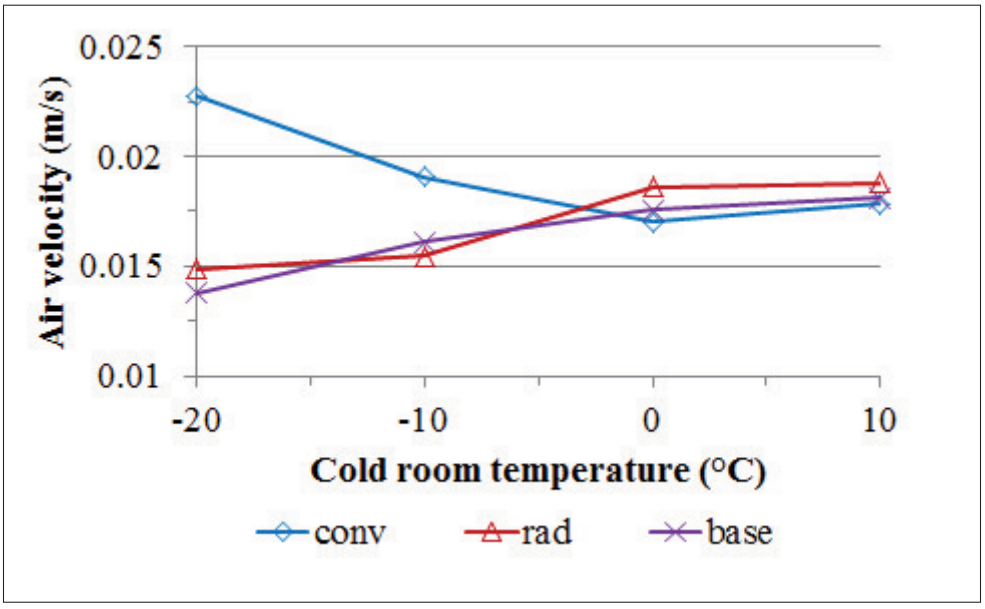

Figure 3.12 Average air velocity at the geometric center of the test room

not immediately attach to the wall on which the convector is installed. This late reattachment would reduce the heat transmitted to the wall and window above the heater for the same reason.

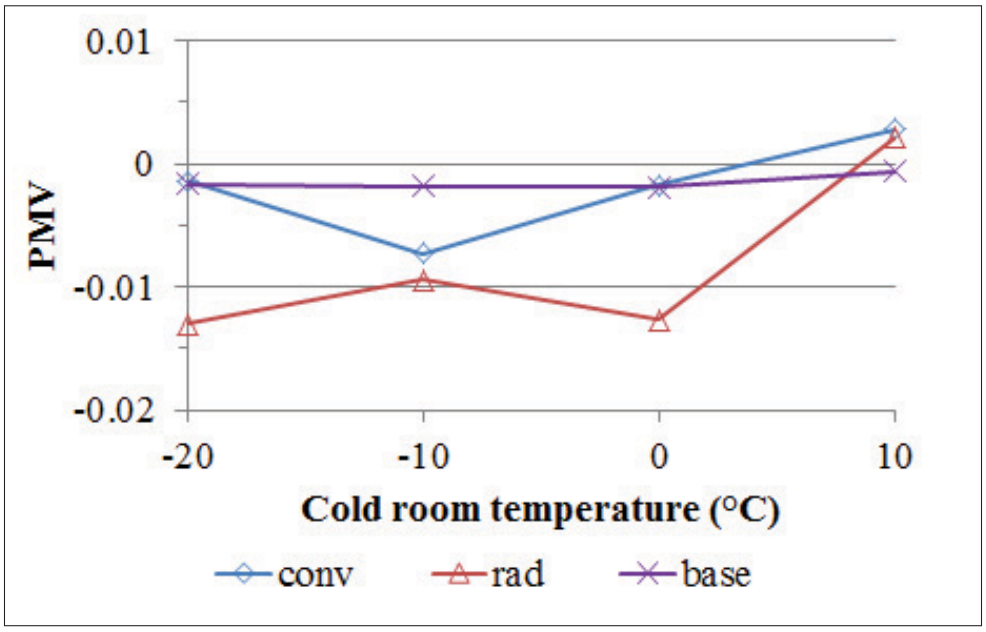

Figure 3.13 Average thermal comfort at the geometric center of the test room

The convector involves an inner vertical cavity where air is heated. Cold air penetrates at the bottom, is heated, and gains momentum inside the equipment by natural buoyancy effect. It is then ejected at the top where louvers redirect the air flow toward the inside of the room. This momentum characterises the convector. When done well, as is the case observed here, the air thermal plume inside the room and after the outlet, will not attach immediately to the wall.

The radiant heater and baseboard heater do not push the thermal plume into the room. In fact, the tested radiant heater, although called radiant, was investigated in a previous experiment by its manufacturer. The results showed that only up to 30% of the produced heat is emitted by radiative effects; this depending on the total heating load of the heater. There is then 70% or more convection heat transfer, which is quite significant. The design of the radiant heater is such that the air flow generated by natural convection inside the heater exits straight up at the outlet instead of pushing the plume inside the room. The heat transfer to the above window and wall is thus increased relative to the convector and the performance reduced. As for the

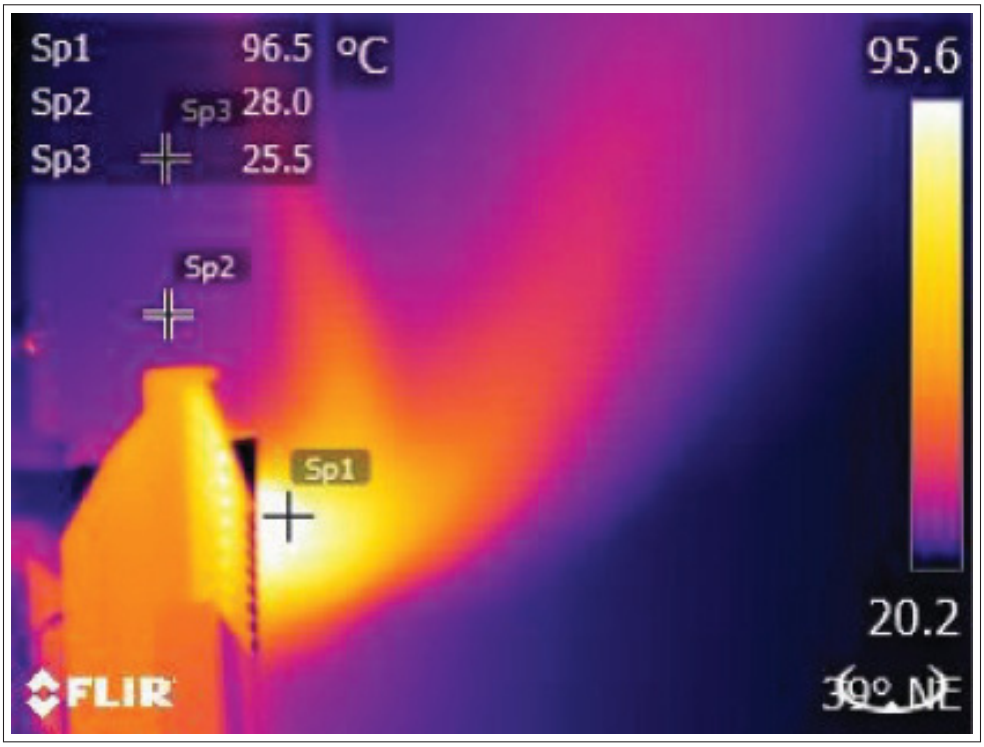

Figure 3.14 Thermal plume of the tested convector

baseboard heater, a similar phenomenon is observed where the thermal plume attaches early to the wall.

Inefficient heating of windows located above heaters has also been reported by Olesen et al. (Olesen *et al.*, 1980). However, in their study, the convector tested produced thermal plumes that were not pushed into the room. The design of convectors with louvers to direct air horizontally has thus improved their effectiveness.

Other significant heat losses are due to infiltration/exfiltration. As the average air temperature remained constant when comparing heating systems, there was likely no increase or decrease in energy consumption due to infiltrations.

It is also interesting to note that the radiant heater did in fact increase the overall radiant heat on the plane where the thermal comfort is measured. This allowed for a reduction in air temperature and is an expected result as the other two heaters are not designed to heat the room by

radiation. The required air temperature on that plane was also found to be lower to maintain thermal comfort.

The results from the experiment agree with those of the calculated virtual heaters. It is inefficient to heat the windows. Moreover, the *RHDS* for the test room has evaluated at 35%. Considering that the *RHDS* give the maximum relative energy consumption difference between two heaters, a difference of 4% to 11% in heating consumption is quite significant for this particular test room. It represents a change in heat distribution effectiveness (see eq. (4.1)) of 11% and 31% respectively.

3.5 Conclusions

In summary, three electric heaters were compared for energy effectiveness at equal thermal comfort in a bi-climatic chamber. A special thermostat that worked with the thermal comfort measure was implemented to control the heating element of each equipment. Results were compared at cold room temperatures of $-20°$C, $-10°$C, $0°$C and $10°$C, successively.

The results showed that not all electric heaters have equal energy effectiveness to maintain thermal comfort and this is most likely due to their indoor heat distribution mechanisms. The convector consumed less energy since it heated its adjacent windows and wall less than the radiant heater and baseboard heater. This is contrary to prior results observed by Olesen et al. (Olesen *et al.*, 1980) and is likely due to the improved flow outlet design involved in the convector tested herein.

Although some differences could be observed between heaters; overall, these differences were minimal. The study nevertheless showcases the fact that heat distribution may influence the effectiveness of a heating device as it strives to maintain thermal comfort. Electric heaters are not all equal: the design of the heat diffusor can affect its overall performance. The results were also concurrent with those of the virtual heaters found in Chapter 4, heating the window is not energy efficient.

CHAPTER 4

VIRTUAL HEATERS

In light of the interest to find an optimal heat distribution for indoor spaces, a new concept termed virtual heater is introduced in this chapter. This numerical tool finds the solution to an optimization problem that distributes heat to either minimizes or maximizes the heat loss of a room while being constrained by thermal comfort. The solution found is called a virtual heater. A virtual heater is then an imaginary heater that distributes heat in an optimal way, with steady state conditions, and that is constrained by thermal comfort.

In this chapter, the concept and usefulness of virtual heaters will be investigated in a first section. In a second section, a solution to the virtual heater problem will be proposed. This is a four part process as the heat loss objective function, heat distribution, thermal comfort constraint and the optimization algorithm all form important milestones for the solution. A third section will then use the proposed solution scheme to solve a case study that approximate the heat distribution in the test room of the Klimat chamber. Finally, the chapter is summarised in a final section.

First, some definitions related to virtual heaters are introduced; then, applications of virtual heaters and associated performance indices are highlighted. In steady state conditions, a virtual heater is an indoor heat distribution that is energy optimal and that is constrained by thermal comfort.The following definitions related to virtual heaters are useful in the discussion that follows.

Definition 4.1 (minimum virtual heater, mVH)**.** *A heat generation device that distributes heat in a room in such a way as to* **minimize** *total steady-state heat loss to the outside environment and maintain a prescribed level of thermal comfort in an occupied volume inside the room.*

Definition 4.2 (maximum virtual heater, MVH)**.** *A heat generation device that distributes heat in a room in such a way as to* **maximize** *total steady-state heat loss to the outside environment and maintain a prescribed level of thermal comfort in an occupied volume inside the room.*

Definition 4.3 (actual heater, AH)**.** *A real heat generation device that distributes heat in a room to maintain a prescribed level of thermal comfort in an occupied volume inside the room. This includes all existing heat distributors. It is self-evident that:* $\dot{E}_{\mathrm{mVH}} \leq \dot{E}_{\mathrm{AH}} \leq \dot{E}_{\mathrm{MVH}}$

Thus, the virtual heaters are a set of two theoretical heaters: one that minimizes and one that maximizes heat loss, respectively. Virtual heaters are best described in mathematical form as the infinitesimal heat injected into the room at each point as a function of space, i.e. $\dot{Q}_{\mathrm{VH}}(x,y,z)$ where $\dot{Q}_{\mathrm{VH}}$ is the power density distribution, fully describing the virtual heater as a function of spatial coordinates x, y and z. It is also noted that all actual heaters' total heat loss should fall within the range of the mVH and MVH total heat losses as per definition 4.3.

4.1 Usefulness of the virtual heaters

An analogy of virtual heaters with a well-known problem is the Carnot cycle in thermodynamics (Çengel & Boles, 2008). Just like the Carnot cycle defines theoretical limits on the efficiency of a thermal machine, the virtual heaters bound the actual heaters to what is theoretically achievable with heat distributions in terms of heat loss at equal thermal comfort. No other method of evaluation of heat distribution is able to give an effectiveness of the heat distribution as it is unknown if a better heat distribution exists.

Since the heating needs of indoor spaces are all different, it should be expected that virtual heaters are functions of the room geometry, thermal parameters, outdoor temperatures and chosen thermal comfort volume. There is thus one set of virtual heaters for each room, thermal comfort space and each set of outdoor temperature.

From the literature, it is also clear that the heat distribution has an influence on energy consumption. Many experimental and numerical investigations of heating concluded that heater type and location of heater can contribute to a reduction of energy consumption at equal thermal comfort (Olesen *et al.*, 1980; Myhren & Holmberg, 2008, 2009; Tye-Gingras & Gosselin, 2012; Ghaddar *et al.*, 2006). Although these showed that distribution of heat is important, none have yet computed an optimal heat distribution, the objective of this chapter. This op-

timal distribution of heat may not always be achievable by a real heat distribution system. Comparing experimentally different heaters would enable the investigator to find the optimal existing heating system, but would not guarantee the optimal heat distribution. Simulation of heating systems, as done in literature (Tye-Gingras & Gosselin, 2012; Ghaddar *et al.*, 2006), gives more flexibility to the solution, but still constrains the search space for an optimal heat distribution to known types of heating. By defining more general heating systems such as virtual heaters, this constraint is removed and optimal heat distributions may be found.

Virtual heaters are also useful on multiple fronts:

1. The minimum and maximum heat losses $\dot{E}_{\mathrm{mVH}}$ and $\dot{E}_{\mathrm{MVH}}$, respectively given by the mVH and MVH, can be used to normalize heating system energy consumption, generalizing the results for comparison;
2. $\dot{E}_{\mathrm{mVH}}$ and $\dot{E}_{\mathrm{MVH}}$ can be used to assess the thermal performance of a room: the lower both are, the better the performance;
3. $\dot{E}_{\mathrm{mVH}}$ and $\dot{E}_{\mathrm{MVH}}$ can be used to assess the total heat loss sensitivity to heat distribution based on the interval between mVH and MVH losses;
4. $\dot{E}_{\mathrm{mVH}}$ and $\dot{E}_{\mathrm{MVH}}$ can be used to determine the performance of an actual heating $\dot{E}_{AH}$ device and how close the actual heater is to the minimum heat loss relative to the interval or range between the consumption of the mVH and MVH;
5. $\dot{E}_{\mathrm{mVH}}$ and $\dot{E}_{\mathrm{AH}}$ can be used to determine the maximum potential power savings for a given room if the ideal minimum virtual heater replaced the actual heater.

From the above, performance indices of heat distribution effectiveness and sensitivity and potential savings are readily defined as follows:

Heat distribution effectiveness

$$\varepsilon_{\mathrm{AH}} = \frac{\dot{E}_{\mathrm{MVH}} - \dot{E}_{\mathrm{AH}}}{\dot{E}_{\mathrm{MVH}} - \dot{E}_{\mathrm{mVH}}} \quad 0 \leq \varepsilon \leq 1 \tag{4.1}$$

With $\varepsilon_{\text{AH}} \Rightarrow 0$ when the actual heater tends to perform as badly as the MVH and $\varepsilon_{\text{AH}} \Rightarrow 1$ when the actual heater performs almost as ideally as the mVH. The heat distribution effectiveness essentially measures how close the actual heater is from the minimum virtual heater. It can then be interpreted as a measure of the heat distribution performance of heat distributors.

Room heat distribution sensitivity

$$RHDS = \frac{\dot{E}_{\text{MVH}} - \dot{E}_{\text{mVH}}}{\dot{E}_{\text{MVH}}} \quad 0 \leq RHDS \leq 1 \tag{4.2}$$

With $RHDS \Rightarrow 0$ when the room is almost insensitive to the type of heating device that could be installed to ensure thermal comfort ($\dot{E}_{mVH} \Rightarrow \dot{E}_{MVH}$) and $RHDS \Rightarrow 1$ when the room is very sensitive to the type of heating because the difference between the mVH and MVH is high. The room heat distribution sensitivity can then be interpreted as a measure of the heat distribution performance of a room.

Maximum power savings

$$MPS = \frac{\dot{E}_{AH} - \dot{E}_{mVH}}{\dot{E}_{AH}} \quad 0 \leq MPS \leq RHDS \tag{4.3}$$

With $MPS \Rightarrow 0$ when the AH tends to be close to the mVH. This index is very useful to assess the potential savings from replacing a heating system in a room.

The concept of virtual heaters is an attempt like no other to define optimal heating. It does not have a bias toward one technology in particular. It also gives rise to three new performance indexes for the built environment, i.e. the distribution efficiency (ε_{AH}), the room heat distribution sensitivity (*RHDS*), and the maximum power savings (*MPS*). To give an examples of how these performance indexes might be used together in a design decision: a designer could first assess the *RHDS* of a room to conclude if the heat distribution sensitivity is significant enough to consider heat distribution for the heater selection. For more sensitive rooms, if a heater already exist in the room, he then could use the *MPS* to assess the maximum power saving that

could entail from changing this heating system. Then, his selection of a new heating device for better heat distribution would be done by comparing $\varepsilon_{\mathrm{AH}}$ for different heaters. The concept of virtual heaters should allow a better understanding of optimal heating systems, but also provide a better understanding of optimal thermal performance of indoor spaces.

4.2 A model for solving virtual heaters

The optimization problem for the minimum virtual heater is written as

$$\begin{aligned} \min_{\dot{Q}} \quad & \dot{E}_{\mathrm{loss}}(\dot{Q}) \\ \text{subject to} \quad & \mathrm{TC}(\dot{Q}) \\ & \dot{\mathbf{Q}} > 0 \end{aligned} \tag{4.4}$$

where $\dot{E}_{\mathrm{loss}}$ is the total heat loss, the design variable $\dot{\mathbf{Q}}$ is the heater's heat distribution and TC is the thermal comfort constraint function. The maximization problem is the same except one wishes to maximize $\dot{E}_{\mathrm{loss}}$ instead of minimizing this value.

Since steady-state conditions are assumed for virtual heaters, the total power given by the heat distribution $||\dot{\mathbf{Q}}||$, which is the amount of heat generated by the heating system, equals the total heat loss $\dot{E}_{\mathrm{loss}}$.

A heat transfer model and a thermal comfort model must be used to calculate the virtual heaters. However, as thermal comfort models and heat transfer models are more easily calculated from the temperature field ($\mathbf{T}$) the problem is expressed as:

$$\begin{aligned} \min_{\mathbf{T}} \quad & \dot{E}_{\mathrm{loss}}(\mathbf{T}) \\ \text{subject to} \quad & \mathrm{TC}(\mathbf{T}) \\ & \dot{\mathbf{Q}}(\mathbf{T}) > 0 \end{aligned} \tag{4.5}$$

This formulation is used in this chapter for the solution of the virtual heaters. It is important to realize that the formulation of eq. (4.5) is general, and any valid heat transfer model and thermal comfort model may be used to solve the optimization.

Virtual heaters also depend on the room geometry, thermal parameters and the selected definition of thermal comfort, all three of which must first be well defined before attempting to solve the minimum or maximum virtual heaters problem. A few important assumptions are formulated to solve the virtual heater problem:

1. First, the room is in steady state conditions. If dynamic effects were to be considered, it would significantly and unnecessarily complicate the interpretation of the virtual heater solutions and related performance indices. Many studies of heat distribution (Olesen *et al.*, 1980; Myhren & Holmberg, 2006; Sevilgen & Kilic, 2011; Inard *et al.*, 1998; Ghaddar *et al.*, 2006; Tye-Gingras & Gosselin, 2012) have focused their attention on steady state conditions for this exact reason. The analysis of dynamic conditions is interesting for optimal heating, but is not the focus of virtual heaters. However, an analysis of virtual heaters in different conditions, e.g. different infiltration rates and outdoor temperatures, could later be used to determine how optimal heating might change with these parameters;

2. A second assumption made for the virtual heater problem is that thermal comfort should be considered as a constraint and not a second objective in a multi-objective optimization scheme. The problem with including the thermal comfort as a second objective lies in that colder indoor environments naturally consume less energy; thus, it is trivial to say that the mVH would converge towards a comfort level that is colder. Given that the purpose of a heating system is to provide thermal comfort within a space, it then makes sense to evaluate systems, and hence calculate the mVH and MVH, at a predetermined level of equal thermal comfort.

To solve the virtual heaters using the temperature as the design variable, three thermal models and one optimization are formulated and programmed. In this section, all four essential

elements are described. First, the total heat loss of the room given a temperature distribution will be discussed. In a second sub-section, the heat distribution calculated from the temperature distribution is presented. A third sub-section shows the thermal comfort model. In sub-section 4.2.4, the optimization scheme to solve the virtual heater is shown. In this sub-section, some key elements such as the objective function and constraint gradients are presented. The choice of a simplified heat transfer model is also justified. A validation of the model is given in sub-section 4.4.

4.2.1 Total heat loss

Two primary means by which heat is lost are considered: the first is conduction through the walls and windows, $\dot{E}_{\text{cond}}$, while the second is infiltration/exfiltration through cracks and windows, $\dot{E}_{\text{ex}}$.

Radiation heat exchanges between the indoor and outdoor spaces is excluded from this model. Although solar gains contribute significantly to the heat balance of a room, the bi-climatic chamber modeled in this study is located indoors, hence no solar heat gains are present. Moreover, the assumption of no solar heat gain does not change the final results of this study. A comparison of a real heater to theoretical heaters can still be achieved.

The heat balance, eq. (4.6) as applied to the control volume formed by the complete enclosure, Figure 4.1, is then:

$$\dot{E}_{\text{gen}} = \dot{E}_{\text{loss}} = \dot{E}_{\text{cond}} + \dot{E}_{\text{ex}} \tag{4.6}$$

where $\dot{E}_{\text{gen}}$ represents the energy generated by the heating system (and other means of any similar equipment, lighting etc) and $\dot{E}_{\text{loss}}$ corresponds to the above-described heat losses through the boundaries of the calculation domain delimited by the enclosure.

The conductive heat rate, $\dot{E}_{\text{cond}}$, is the sum of the convective heat rate, $\dot{E}_{\text{conv,out}}$, and net radiative heat rate, $\dot{E}_{\text{rad,out}}$, between the outer surface and the surroundings minus the absorbed

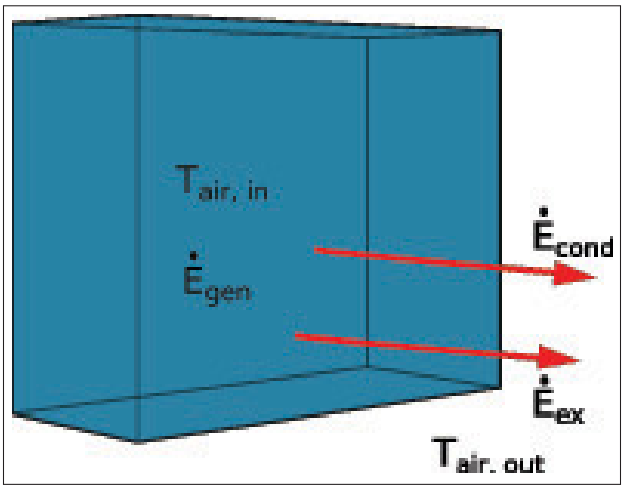

Figure 4.1 Schematic representation of the energy balance on the complete enclosure considered in this study

fraction of the solar irradiation, $\alpha A_{\text{tot}} G$. Hence, to avoid calculating these heat rates, the conductive rate is retained in the calculation.

In the implementation of the energy balance over the surfaces of this volume, the six walls of the enclosure are discretized into N equal square surfaces, $L \times L$, without loss of generality in the description. Moreover the conditions outside each surface are assumed to be uniform, which creates 6 different conditions outside. The discretized heat balance on the enclosure, eq. (4.6), then becomes

$$\dot{E}_{\text{gen}} = \sum_{i=1}^{N} \dot{E}_{\text{cond,i}} + \sum_{j=1}^{6} \dot{E}_{\text{ex,j}} \tag{4.7}$$

In this discretization each of the N conductive heat rates across each discretized subsurface can be represented by standard relations:

$$\begin{aligned}\dot{E}_{\text{cond,i}} &= \frac{T_{\text{air,in}} - T_{\text{air,out,j}}}{\dfrac{1}{L^2 h_{\text{in}}} + \dfrac{t}{L^2 k_{\text{eff,i}}} + \dfrac{1}{L^2 h_{\text{out,j}}}} \\ &= \frac{T_{\text{s,in,i}} - T_{\text{air,out,j}}}{\dfrac{t}{L^2 k_{\text{eff,i}}} + \dfrac{1}{L^2 h_{\text{out,j}}}} \\ &= \frac{T_{\text{s,in,i}} - T_{\text{s,out,i}}}{\dfrac{t}{L^2 k_{\text{eff,i}}}}\end{aligned} \tag{4.8}$$

Where t is the total thickness of the wall; $k_{\text{eff,i}}$ is the effective conductivity in x (normal to the wall in Figure 4.1 of the ith element that accounts for all materials; h_{in} and h_{out} are the convection heat transfer coefficients; and $L \times L$ represent the surface area of an element.

Each of the six exfiltration heat rates are given by:

$$\dot{E}_{\text{ex,j}} = \dot{m}_{\text{j}} c_{\text{p}} (T_{\text{air,in}} - T_{\text{air,out,j}}) \tag{4.9}$$

In which $\dot{m}_{\text{j}}$ is the mass flow rate of exfiltration air exiting the enclosure through the wall j; c_{p} is the specific heat as air is considered as a perfect gas; and the temperature difference is what occurs between indoor air and air outside the six surfaces (of course some of these temperatures could be similar depending on the problem to be solved).

In each of these equations, the index i refers to one of the N subsurfaces and index j refers to one of the 6 surfaces that determines the whole enclosure or the 6 possibly different air temperatures outdoors.

There is no index associated with the indoor air temperature because at the implementation level, the air volume is not discretized and is considered to be represented by one constant temperature throughout the volume. Reasons for not discretizing the air volume are provided in subsection 4.3.

Strictly speaking, the thermophysical properties of air (density, specific heat, conductivity, diffusivity, etc.) and building materials vary with temperature. These variations are neglected here with no significant impact on eqs.(1-3) as these equations are expressed in terms of relative differences and serve as guidelines in the selection of a proper heating system for a given room.

Eq. (4.7) is linear in temperature and therefore can be cast in vector form as:

$$\dot{E}_{\text{loss}} = \mathbf{e}_{\text{loss}}^{T}\mathbf{T} + e_{\text{loss,const}} \tag{4.10}$$

where $\mathbf{e}_{\text{loss}}$ is a vector containing the conduction, exfiltration and radiation constants that multiply the temperature vector and $e_{\text{loss,const}}$ is a constant computed from the temperature boundary condition and conduction/infiltration constants.

Here, the temperature vector used in the remainder of the description is

$$\mathbf{T} = \left[\begin{array}{cccc} T_{s,1} & \ldots & T_{s,N} & T_{air} \end{array} \right]^{\text{T}} \tag{4.11}$$

In the thermal model, as the indoor air temperature is an unknown, there is a total of $N+1$ values in the temperature vector. To solve eq. (4.10), one needs to express the conduction term, eq. (4.8), in terms of the unknown indoor temperature, $T_{\text{s,in,i}}$, and know the outdoor temperature $T_{\text{air,out,j}}$. Hence, the second expression on the right hand side of eq. (4.8) is used at the implementation level.

4.2.2 Heat distribution

The heat balance, eq. (4.6) as applied to the control volume formed by a single surface element of area $L \times L$, Figure 4.2, is then:

$$\dot{Q}_{s,i} + \dot{E}_{\text{conv,i}} + \dot{E}_{\text{cond,2D,tot,i}} + \dot{E}_{\text{rad,i}} - \dot{E}_{\text{cond,i}} - \dot{E}_{\text{cond,i}} \tag{4.12}$$

To respect energy conservation, each term has to be expressed according to the direction shown in Figure 4.2. In eq. (4.12), one notices that the exfiltration rate is not included as this energy penetrates the control-volume from the inner surface and then crosses the outer surface.

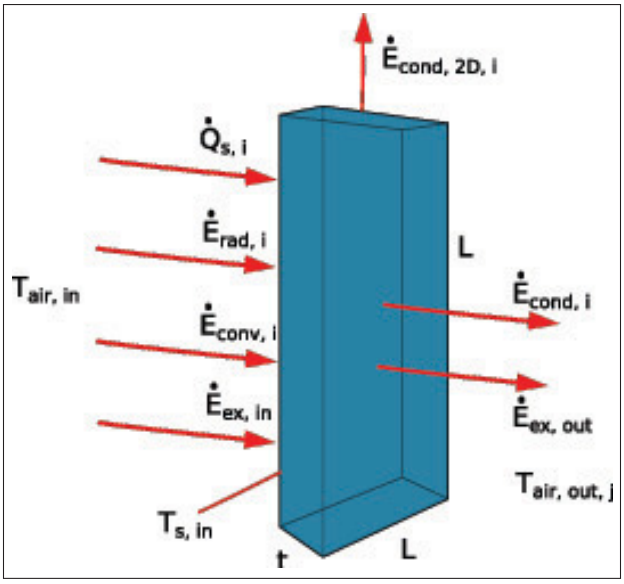

Figure 4.2 Energy balance on a control-volume defined by a surface element of surface area $L \times L$ and thickness t.

The term $\dot{Q}_{\mathrm{i}}$ is the actual heat of the virtual heater on sub-surface i and this discretized heat rate is the unknown value to be resolved. The convection loss between the air volume and surface element i is computed using the following standard equation:

$$\dot{E}_{\mathrm{conv,i}} = h_{\mathrm{i}} A_{\mathrm{i}} (T_{\mathrm{air,in}} - T_{\mathrm{s,in,i}}) \tag{4.13}$$

where A_{i} is the surface area of the element and h_{i} is the convection coefficient for each element. A constant h_{i} was chosen so that the heat distribution model could be expressed as a vector/matrix multiplication, thus speeding up computation for the optimization.

With respect to the square elements shown in Figure 4.3, the two-dimensional conduction heat transfer across two adjacent wall surface elements can be described as

$$\dot{E}_{\text{cond,2D}} = (L \times t)k\frac{\Delta T}{L} = tk\Delta T \tag{4.14}$$

In eq. (4.14), k is the effective thermal conductivity in directions normal to the main gradient (in x) in Figure 4.3; A is the surface area through which heat transfer occurs in directions normal to that of the main gradient $(L \times t)$, ΔT is the finite temperature difference between one node and its neighbor, and L is the distance between two nodes. The expression is valid in either the y or the z direction in Figure 4.3 and more generally for any surface of the enclosure.

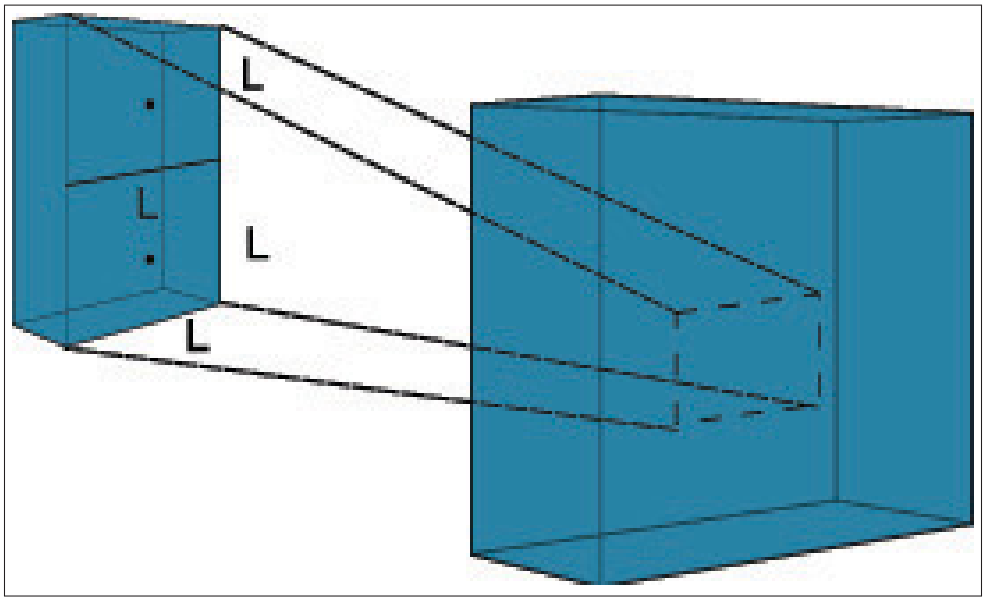

Figure 4.3 Two elemental sub-surfaces on the right wall and related geometrical parameters

This particular nomenclature is in accordance with that proposed by Patankar (Patankar, 1980). As the walls are composite, it is supposed that heat conduction along the wall surface primarily happens through the drywall section as it is more conductive than the subsequent insulation layers. Thus, the effective thickness $t^* \leq t$ considered here for heat transfer calculations is only

that of the drywall. On the other hand, conduction across windows and doors occurs mainly through the entire thickness of the glass and door material.

Now, the effective thermal conductivity, k, used to compute heat transfer between adjacent cells has to be the conductivity at the interface between to adjacent cells: it is the harmonic mean of the conductivity of these cells as prescribed by Patankar (Patankar, 1980). This ensures an adequate and consistent representation of the heat flux at the interface.

One has to understand that heat conduction represented by eq. (4.14) is at least an order of magnitude below the other conductive flux (along the x-axis in Fig. 4.3). Therefore, one could think of neglecting such a term. However, this term smooths the variations of temperature on surfaces in the y-z plane of Figure 4.3 when it comes to presenting results and therefore it is kept herein to enhance the representation of the isothermal curves presented in the results section.

One final comment on eq. (4.14) pertains to the fact that it could be improved to handle 3D effects at the interface between a wall and a window for instance. But to provide such a level of accuracy in a term that is close to negligible with respect to what is desired in this study.

The total loss (or gain) by conduction in a given element can then be expressed by the sum of all conduction terms established with adjacent elements. This sum involves 4 neighbors for a subsurface located in the middle of a wall, 3 neighbors when the element is the first or last in a row or in a column, and 2 neighbors when the element is located next to a corner, linking three walls together.

Combining all linear conduction and convection terms together, the conduction/convection problem can be expressed as

$$\dot{\mathbf{E}}_{\text{cond/conv}} = \mathbf{C}\mathbf{T}_{\mathbf{s}} \tag{4.15}$$

where $\mathbf{T_s}$ is the surface temperature vector, $\dot{\mathbf{E}}_{\text{cond/conv}}$ is the conduction and convection loss vector and $\mathbf{C}$ is a matrix containing the conduction and convection parameters. The i^{th} element of $\dot{\mathbf{E}}_{\text{cond/conv}}$ is the sum of all conduction and convection heat losses for the i^{th} surface.

Radiation gains are calculated with the net radiation method (Incropera & DeWitt, 2011). Since the mesh involves equally aligned squares, view factors F_{ij} were found analytically using the expressions from Howell's catalogue of view factors (Howell, 2016).

The net radiation gain of one surface is then expressed as

$$\dot{E}_{\mathrm{rad,i}} = \frac{A_{\mathrm{i}}\varepsilon_{\mathrm{i}}}{1-\varepsilon_{\mathrm{i}}}(J_{\mathrm{i}} - E_{\mathrm{b,i}}) = \sum_{m=1}^{N} A_{\mathrm{i}} F_{\mathrm{k,m}}(J_{\mathrm{m}} - J_{\mathrm{i}}) \tag{4.16}$$

where ε_{i} is the surface emissivity of surface i and J_{i} is the radiosity of the same. In eq 4.16, $\dot{E}_{\mathrm{b,i}}$ is the black body emissive power. Radiosities vector $\mathbf{J}$, containing all surface radiosities, can then be found by solving

$$\mathbf{A}_{\mathrm{rad}}\mathbf{J} = \mathbf{T}_s^4 \tag{4.17}$$

where $\mathbf{A}_{\mathrm{rad}}$ is a matrix computed from eq.(4.16) and $\mathbf{T}_s^4$ is the vector of surface temperatures elevated to the power of four. Substituting the radiosities in eq.(4.16), the following expression is found for the net radiative gain.

$$\dot{\mathbf{E}}_{\mathrm{rad}} = \mathbf{diag}\left(\frac{A_{\mathrm{i}}\varepsilon_{\mathrm{i}}}{1-\varepsilon_{\mathrm{i}}}\right)(\mathbf{A}_{\mathrm{rad}}^{-1} - \mathbf{diag}(\sigma))\mathbf{T}_s^4 \tag{4.18}$$

where $\mathbf{diag}(i)$ is a diagonal matrix with its i^{th} diagonal element evaluated as i and $\dot{\mathbf{E}}_{\mathrm{rad}}$ is the radiative heat gain vector. This can be expressed in a compact form as

$$\dot{\mathbf{E}}_{\mathrm{rad}} = \mathbf{R}\mathbf{T}_s^4 \tag{4.19}$$

where matrix $\mathbf{R}$ is expressed as

$$\mathbf{R} = \mathbf{diag}\left(\frac{A_{\mathrm{i}}\varepsilon_{\mathrm{i}}}{1-\varepsilon_{\mathrm{i}}}\right)(\mathbf{A}_{\mathrm{rad}}^{-1} - \mathbf{diag}(\sigma)) \tag{4.20}$$

The complete heat transfer model required to compute the heat balance of each surface element and the air volume, required to compute the heat distribution that is used to estimate the virtual

heater, is finally expressed as

$$\dot{\mathbf{Q}} = \mathbf{AT} + \mathbf{BT}^4 \tag{4.21}$$

where

$$\mathbf{A} = \begin{bmatrix} \mathbf{C} & -\mathbf{vect}(h_i A_i) \\ -\mathbf{vect}(h_i A_i) & \sum_j \dot{E}_{\mathrm{ex,j}} + \sum_i h_i A_i \end{bmatrix} \tag{4.22}$$

$$\mathbf{B} = \begin{bmatrix} \mathbf{R} & \mathbf{0} \\ \mathbf{0}^T & 0 \end{bmatrix} \tag{4.23}$$

where $\mathbf{vect}(i)$ is a vector with its i^{th} element being i. This is the final matrix form of the model used for estimating the virtual heaters in this work. Since **A** and **B** depend only on the geometry and thermal properties, both matrices can be computed before the optimization process. The model can be seen as a linearization of the real heat transfer problem around one temperature point. The model can be updated to get a better approximation of the heat transfer around the current temperature point.

4.2.3 Thermal comfort

PMV is originally defined over one point in space; however, one may suggest that it would be more useful to have a thermal comfort constraint that is defined over the occupied volume of the room. One could then first define thermal comfort for this volume by discretizing the volume in equal subvolumes and then computing *PMV* on the geometric center of each of these subvolumes. The thermal comfort constraint could then be that $PMV = 0$ on each sub-volume; however, it would be too constraining for a heating system: No real heating system is able to provide a constant *PMV* throughout a volume in such a way. In fact, even for virtual heaters this would significantly limit the allowed surface and air temperatures.

A more reasonable approach is to limit *PMV* on each subvolume to a predefined range of values. It is proposed here to use $-0.5 < PMV < 0.5$. This comfort range, used in Standard ASHRAE 55 (ASHRAE-55, 2013), allows for a maximum of 10% of occupants to be dissatis-

fied with the thermal environment. Since achieving $PMV = -0.5$ consumes less energy than achieving $PMV = 0.5$ in heating mode, the average PMV over the entire volume is also considered as a thermal comfort constraint. This ensures that heaters are compared to a similar heating load, while allowing for some variations in PMV and energy consumption.

In this research, thermal comfort is computed on a volume that is offset by 1m from the walls, 0.1m from the floor and a height of 1.7m. This is in accordance with the measurement location given in ASHRAE 55 (ASHRAE-55, 2013). The volume is discretized in equal subvolumes, i.e. a grid of $9 \times 9 \times 9$ volumes for which PMV is calculated on the geometric center of each. Thermal comfort is achieved when all subvolumes lie in the comfort range $-0.5 < PMV < 0.5$ and the average thermal comfort over the volume is $\overline{PMV} = 0$. To computationally reduce the number of inequality constraints, the condition $-0.5 < PMV < 0.5$ is rewritten as $PMV^2 < 0.5^2$ at the implementation level.

4.2.4 Solving the optimization problem

The thermal comfort and heat transfer models are now defined and ready to be used to solve the optimal heat distribution problem. In this sub-section, a solution method to the virtual heaters is discussed.

Posing the question of efficient heating as an optimization problem of the temperature field, the objective function is the test room total heat losses, constraints are thermal comfort inside the room, and the temperature field is the design variable. To ensure that the solution found is a heating device, a positive heat gain constraint is also imposed $\dot{\mathbf{Q}} > 0$.

The objective and constraint functions defined in sub-sections 4.2.1, 4.2.2 and 4.2.3 are differentiable. In a first step of this sub-section, the gradients of the three functions presented in sections 4.2.1, 4.2.2 and 4.2.3 are derived. In what follows, an algorithm is shown for solving the optimal heat distribution problem using the introduced heat transfer and thermal comfort models.

4.2.4.1 Gradient of the heat loss and heat distribution

When using a gradient-based approach to solve the optimization problem of the virtual heaters, it is useful to determine the gradient of the objective function and the gradient of the constraints in their analytical forms (Nocedal & Wright, 1999). By doing so, computational time can be significantly reduced as numerical gradients must not be computed. The gradient of the objective function, the total heat loss from eq.(4.10), is:

$$\frac{d\dot{E}_{\text{loss}}}{d\mathbf{T}} = \mathbf{e}_{loss} \tag{4.24}$$

Since the heat distribution is used as a constraint, it is also useful to know its gradient. The gradient of the heat distribution given by eq.(4.21) regarding temperature is

$$\frac{d\dot{\mathbf{Q}}}{d\mathbf{T}} = \mathbf{A} + \mathbf{B}\mathbf{diag}(4T_{\text{i}}^3) \tag{4.25}$$

Note that the vector/matrix form of the heat transfer problem enables quick computation of the gradient function. In this case, the total heat loss is a linear function, therefore its gradient is a constant vector. However, the gradient of heat distribution $\dot{\mathbf{Q}}$ is not a constant function; nevertheless, part of it can be computed before the optimization process.

4.2.4.2 Gradient of thermal comfort

In the optimization algorithm that follows, it is also useful to have the gradient of the thermal comfort constraints in an analytical form. Differentiation of the constraints with respect to temperature yields:

$$\frac{\partial PMV_i^2}{\partial \mathbf{T}} = 2PMV_i \frac{\partial PMV_i}{\partial \mathbf{T}} \tag{4.26}$$

$$\frac{\partial \overline{\mathbf{PMV}}}{\partial \mathbf{T}} = \overline{\frac{\partial \mathbf{PMV}}{\partial \mathbf{T}}} \tag{4.27}$$

where **PMV** is the vector containing the thermal comfort values, index i indicates the i^{th} value of the vector and $\overline{\mathbf{PMV}}$ is the mean value of thermal comfort. To find the gradient of the constraint, $\partial\mathbf{PMV}/\partial\mathbf{T}$ must first be found. Using the chain rule, the gradient of PMV for one thermal comfort point is

$$\frac{dPMV}{d\mathbf{T}} = \frac{dPMV}{d\begin{bmatrix} T_{\text{mrad}} \\ T_{\text{air}} \end{bmatrix}} \frac{d\begin{bmatrix} T_{\text{mrad}} \\ T_{\text{air}} \end{bmatrix}}{d\mathbf{T}} \tag{4.28}$$

The partial derivatives $\partial PMV/\partial T_{\text{mrad}}$ and $\partial PMV/\partial T_{\text{air}}$ must be found. Upon differentiation of PMV (see (Fanger, 1970)) with respect to T_{air}, the following is found

$$\begin{aligned}\frac{\partial PMV}{\partial T_{\text{air}}} = M\Bigg(&-0.0014\frac{\dot{E}_{\text{gain,ih}}}{A_{\text{du}}} - 15.84\times10^{-8} f_{\text{cl}} T_{\text{cl}}^3 \frac{\partial T_{\text{cl}}}{\partial T_{\text{air}}} \\ &- f_{\text{cl}} h_{\text{c}} \left(\frac{\partial T_{\text{cl}}}{\partial T_{\text{air}}} - 1\right) - f_{\text{cl}} \frac{\partial h_{\text{c}}}{\partial T_{\text{air}}} (T_{\text{cl}} - T_{\text{air}})\Bigg)\end{aligned}$$

where

$$M = \left(0.303e^{\left(-0.036\frac{\dot{E}_{\text{gain,ih}}}{A_{\text{du}}}\right)} + 0.028\right) \tag{4.29}$$

and the derivative of the convection factor being

$$\frac{\partial h_{\text{c}}}{\partial T_{\text{air}}} = \begin{cases} \text{if} \quad 2.38(T_{\text{cl}} - T_{\text{air}})^{0.25} > 12.1\sqrt{v} \\ 0.5013(T_{\text{cl}} - T_{\text{air}})^{-0.75}\left(\dfrac{\partial T_{\text{cl}}}{\partial T_{\text{air}}} - 1\right) \\ \\ \text{otherwise} \\ 0 \end{cases} \tag{4.30}$$

The derivative of the clothing temperature is found as

$$\frac{\partial T_{\mathrm{cl}}}{\partial T_{\mathrm{air}}} = \begin{cases} \text{if} \quad 2.38(T_{\mathrm{cl}} - T_{\mathrm{air}})^{0.25} > 12.1\sqrt{v} \\ \dfrac{0.19375 I_{\mathrm{cl}} f_{\mathrm{cl}} h_{\mathrm{c}}}{1 + 0.155 I_{cl} f_{cl} [15.84 \times 10^{-8} T_{\mathrm{cl}}^3 + 1.25 h_{\mathrm{c}}]} \\ \\ \text{otherwise} \\ \dfrac{0.155 I_{\mathrm{cl}} f_{\mathrm{cl}} h_{\mathrm{c}}}{1 + 0.155 I_{cl} f_{cl} [15.84 \times 10^{-8} T_{\mathrm{cl}}^3 + h_{\mathrm{c}}]} \end{cases} \tag{4.31}$$

Differentiating by T_{mrad}

$$\frac{\partial PMV}{\partial T_{\mathrm{mrad}}} = M \left(-15.84 \times 10^{-8} f_{\mathrm{cl}} \left[T_{\mathrm{cl}}^3 \frac{\partial T_{\mathrm{cl}}}{\partial T_{\mathrm{mrad}}} - T_{mrad}^3 \right] - f_{\mathrm{cl}} h_{\mathrm{c}} \frac{\partial T_{\mathrm{cl}}}{\partial T_{\mathrm{mrad}}} \right) \tag{4.32}$$

where

$$\frac{\partial h_{\mathrm{c}}}{\partial T_{\mathrm{air}}} = \begin{cases} \text{if} \quad 2.38(T_{\mathrm{cl}} - T_{\mathrm{air}})^{0.25} > 12.1\sqrt{v} \\ 0.5013(T_{\mathrm{cl}} - T_{\mathrm{air}})^{-0.75} \dfrac{\partial T_{\mathrm{cl}}}{\partial T_{\mathrm{mrad}}} \\ \\ \text{otherwise} \\ 0 \end{cases} \tag{4.33}$$

and

$$\frac{\partial T_{\mathrm{cl}}}{\partial T_{\mathrm{mrad}}} = \begin{cases} \text{if} \quad 2.38(T_{\mathrm{cl}} - T_{\mathrm{air}})^{0.25} > 12.1\sqrt{v} \\ \dfrac{2.4552 \times 10^{-8} I_{\mathrm{cl}} f_{\mathrm{cl}} T_{\mathrm{mrad}}^3}{1 + 0.155 I_{cl} f_{cl} [15.84 \times 10^{-8} T_{\mathrm{cl}}^3 + 1.25 h_{\mathrm{c}}]} \\ \\ \text{otherwise} \\ \dfrac{0.155 I_{\mathrm{cl}} f_{\mathrm{cl}} h_{\mathrm{c}}}{1 + 0.155 I_{cl} f_{cl} [15.84 \times 10^{-8} T_{\mathrm{cl}}^3 + h_{\mathrm{c}}]} \end{cases} \tag{4.34}$$

The air temperature is part of the design variable, and eq. (4.29) gives the final component of $\partial PMV / \partial \mathbf{T}$. The gradients $dT_{\mathrm{mrad}}/d\mathbf{T}$ for each comfort point must now be found. The mean

radiant temperature gradient using the chain rule is

$$\frac{dT_{\text{mrad}}}{d\mathbf{T}_s} = \frac{dT_{\text{mrad}}}{dT^4_{\text{mrad}}} \frac{dT^4_{\text{mrad}}}{d\mathbf{T}^4_s} \frac{d\mathbf{T}^4_s}{d\mathbf{T}_s} \tag{4.35}$$

From eq.(4.35), the following gradient is known

$$\frac{d\mathbf{T}^4_{\text{rad}}}{d\mathbf{T}^4_{\text{s}}} = \mathbf{F} \tag{4.36}$$

where $\mathbf{T}^4_{\text{rad}}$ is the mean radiant temperature vector knowing that its element i is the radiant temperature of the i^{th} thermal comfort point elevated to the power of four. $dT_{\text{rad}}/dT^4_{\text{rad}}$ and $d\mathbf{T}^4_{\text{s}}/d\mathbf{T}_{\text{s}}$ can be found knowing that

$$\frac{d\mathbf{T}^4}{d\mathbf{T}} = \mathbf{diag}(4T_i^3) \tag{4.37}$$

The gradient of the constraint is then found using eqs.(4.26) and (4.27).

4.2.4.3 Choice of an optimization algorithm

With the objective function, the constraint functions and their gradients well defined, the solution to the virtual heater optimization problem is now discussed. To find the appropriate optimization algorithm, it is important to properly classify the problem at hand (Nguyen *et al.*, 2014). The constraint functions are continuous and differentiable and so is the objective function. In fact, the objective function is linear with respect to the design variable. The search space has a high number of dimensions. Equality and inequality constraints are present and are nonlinear.

Although the objective function is linear, the nonlinear constraints require that the optimization problem be solved by nonlinear programming techniques.

Evolutionary optimization algorithms such as genetic algorithms have widely been used in optimizing the built environment (Machairas *et al.*, 2014; Nguyen *et al.*, 2014). These algorithm, generally utilized to find a global solution to an optimization problem, suffer from a large number of function evaluations. In some cases, when either the objective or constraints are expensive to compute, a surrogate model based on neural network have been used to reduce these function computation time (Nguyen *et al.*, 2014).

In most studied cases of heat transfer utilizing genetic algorithms, a popular class of evolutionary algorithms, less than 100 variables are considered. Most often, no more than 10 variables are used (Gosselin *et al.*, 2009; Nguyen *et al.*, 2014). This is a far cry in the complexity of the search space considered in the solution of virtual heaters where the number of variables considered is in the order of 1000 or more. This class of optimization problems are called *l*arge scale due to the high dimension of the search space. Global optimization algorithms for solving large scale optimization problem of that sort are in their early developments and few have been tested at above 1000 variables (LaTorre *et al.*, 2015). In a comparison of these top performing algorithms, MOS algorithms has the best overall performance (Cabrera, 2016; LaTorre *et al.*, 2015).

Large scale optimization also arises in machine learning such as neural networks (Bottou *et al.*, 2016). Common methods used to solve this problem are gradient based approaches (Bottou *et al.*, 2016). Gradient based methods generally fall into the realm of local optimization. They are then likely to find a local optimum over a global optimum, but are much faster to find a solution than global optimization approaches (Nocedal & Wright, 1999). The advantage of gradient based methods is that variable steps are guided by the gradient, a descent direction, at each iteration. A gradient based approach is preferred here to solve the virtual heater optimization problem due to the high number of design variables.

When unconstrained, these reduce to a line search method where the next iterate of the algorithm is computed as:

$$\mathbf{T}_{k+1} = \mathbf{T}_k + \alpha_k \mathbf{s}_k \tag{4.38}$$

where T_k is the design variable at iteration k, α_k is some constant at the current iteration and $\mathbf{s}_k$ is a descent direction. There are different ways that a descent direction could be computed. For unconstrained problems when $\mathbf{s}_k = -\nabla f$, this is called the steepest descent method where f is the objective function (Nocedal & Wright, 1999). Other methods include $\mathbf{s}_k = -\mathbf{H}^{-1}\nabla f$ where $\mathbf{H}$ takes the form of the hessian matrix of f. These methods are called Newton methods. In the case where an approximate hessian is used, these are called quasi-Newton. The advantage of using quasi-Newton methods is that the objective function is approximated quadratically while only using gradient information.

To handle equality constraints, one popular method is to use Lagrange multipliers (Bertsekas, 2014). In this approach, the Lagrangian function,

$$L(\mathbf{x}, \lambda) = f(\mathrm{x}) + \lambda^T \mathbf{h}(\mathbf{x}) \tag{4.39}$$

is optimized instead of the objective function $f(\mathrm{x})$. At a stationary point of the Lagrangian function, it can be readily verified by differentiation that the constraints $\mathbf{h}(\mathbf{x}) = \mathbf{0}$ and first order optimality conditions $\nabla f(\mathbf{x}) = -\nabla \mathbf{h}(\mathbf{x})\lambda$ are stratified. A second approach to equality constrained optimization is to search for a solution in the null space of the constraints. This is what is proposed in the orthogonal decomposition algorithm (ODA) (Angeles *et al.*, 1990). In ODA, the search step $\mathbf{s}$ described in eq. (4.38) is separated into two orthogonal components:

$$\mathbf{s} = \delta\mathbf{v} + \mathbf{L}\delta\mathbf{u} \tag{4.40}$$

where $\delta\mathbf{v}$ is a step towards satisfying the constraint, $\delta\mathbf{v} = \mathbf{0}$ if the constraint is satisfied, and $\mathbf{L}\delta\mathbf{u}$ is a step in the null space of the constraint, hence orthogonal to $\delta\mathbf{v}$ when $\delta\mathbf{v} \neq \mathbf{0}$. The step $\mathbf{L}\delta\mathbf{u}$ is aimed at reducing the objective function, i.e. is a descent direction. Using a linear approximation of the constraints $\mathbf{h}(\mathbf{x})$, the null space can then be locally approximated by a set of vectors $\mathbf{L}$ orthogonal to $\nabla\mathbf{h}(\mathbf{x})$, i.e. $\nabla\mathbf{h}(\mathbf{x})\mathbf{L} = \mathbf{0}$. The ODA algorithm is especially useful when the null space $\mathbf{L}$ can be easily found. It is not the case for the virtual heaters. For this reason, a Lagrange multiplier approach is preferred to solve the virtual heaters. By such, the Lagrangian

function to be solved is a nonlinear function, unlike the original linear function involved in the objective function. A quasi-Newton approach to solving the optimization is then preferred. Particularly, the hessian matrix is updated using the Broyden–Fletcher–Goldfarb–Shanno (BFGS) algorithm (Nocedal & Wright, 1999).

A more difficult type of constraint to satisfy is the inequality constraint. The major difficulty of handling inequality constraints is that linear algebra can no longer be used to define the derivative of the normality conditions; linear algebra being a useful tool in the analysis of vector spaces that are involved in optimization algorithms. This is a direct result of the inequality defining a subspace that is not a vector space. Too satisfy inequality constraints, two major methods can be used. The first is the penalty function approach where a penalty/barrier functions is introduced into the objective function, in the case of minimization it increases the value of the objective function when an inequality constraint is violated. The search for a solution can then be performed within a vector space. This approach can also be used to solve equality constraints (Nocedal & Wright, 1999). Another approach introduces slack variables into the inequality constraints to transform these constraints to equality constraints (Nocedal & Wright, 1999). The new equality constraints are then handled in one of the previously discussed ways.

Using MatLab, a selection of optimization algorithms are at disposal using the *fmincon* function for constrained nonlinear optimization. The sequential quadratic programming (SQP) optimization scheme was selected (MATLAB, 2017). The particular SQP implementation chosen makes use of slack variable to transform inequality constraints to equality constraints; handles the equality constraints using Lagrange multipliers; and updates the hessian matrix using a quasi-Newton methods, in this case a BFGS update. The algorithm was chosen for its robustness and speed of convergence.

As it was discussed in sub-section 4.2.2, the convection factor between the wall and air volume is constant in the model. To have a more accurate convection factor, the constant convection factor is updated through a new model calculated from the current optimal temperature estimate that is given by *fmincon*. This is done at each 8 iterations of the SQP method and must be

updated at least 12 times before convergence can be declared on the algorithm. Convergence is found when the temperature distribution no longer varies and the convection factor has also converged.

Peeters et. al. (Peeters *et al.*, 2011) give a review of convective heat transfer coefficient expressions. Convection coefficient were calculated from the different cases outlined in this paper (Peeters *et al.*, 2011). These include expression for the coefficient of the window, walls, floor and ceiling. As the temperature solution evolves at each iteration, the convection factor can take the new temperature distribution into consideration so to have a more accurate representation of the convection.

To summarize, the virtual heaters are found by first optimizing the temperature distribution using SQP with the models discussed in sections 4.2.1, 4.2.2 and 4.2.3. Second, the convection factor and associated model is updated at regular iterations of the algorithm. Third, once convergence is observed, the virtual heater can then be calculated with the model discussed in section 4.2.2. The optimal heat distribution is then found.

4.3 Choice of a simplified model

An explanation as to the choice of the simplified model is now provided. The main advantage of the current simplified model is that matrices **A**, **B** and parts of $d\dot{\mathbf{Q}}/d\mathbf{T}$ can be pre-calculated before the iterative procedure, thus significantly speeding up the optimization process. Had a CFD model been used, the required time for finding the virtual heaters would likely have been too long for practical purposes. The current model makes it possible to find the optimal solutions in one hour in the best case scenario, and in some cases, over 10 hours depending on the room geometry and discretization selected. Some major assumptions are responsible for this form of the model. The first is to set constant indoor and outdoor convection heat transfer coefficients h_i. Typically, convection heat transfer coefficients for natural convection, the case at hand, vary with temperature in the form of $h = C(T_s - T_{air})^n$. Accounting for such variations would then lead to a convection heat transfer equation that cannot be expressed in a vector/-

matrix multiplication form, which in turn would slowdown each iteration of the optimization as the matrices would have to be recalculated for each update. Similarly, if the air volume was discretized in subvolumes to solve the heat transfer problem, numerous flow equations would readily be introduced. This would require a volumetric discretized grid leading to several more algebraic equations and thus a larger design vector for the optimization. This would necessarily penalize the optimization time significantly due to the heat transfer problem's complexity.

The proposed simplified model was thus chosen not to describe heat transfer as accurately as possible, but rather to approximate it so that heat losses could be reasonably estimated and heat distribution also considered.

4.4 Model validation

The heat transfer model presented here was validated in two ways:

1. The conduction, convection and radiation parts of the heat transfer model were first compared with simple hand calculations to verify that no formulation and implementation errors were present. The convergence rate of the algorithm was monitored. The total heat transfer model and heat distribution model were then tested to be consistent. As expected, the sum of the distributed heat components $\dot{\mathbf{Q}}_i$ was equal to the total heat loss $\dot{\mathrm{E}}_{\mathrm{loss}}$;

2. Second, the model was compared to selected experimental results obtained from experiments carried out in a climatic chamber (Léger *et al.*, 2018). In this climatic chamber, three electric heaters were tested at equal thermal comfort in the center of the test room (Léger *et al.*, 2018). The climatic chamber used is the case study described in Chapter 2. Wall, floor, ceiling, window and air temperatures were recorded during the experiments and were used as an estimate to the inputs of the model described here. These average values are displayed in Table 4.1. Several operation cold room temperatures were used. Here, the values displayed in Table 4.1 are for a cold room temperature set at -20°C.

Table 4.1 Boundary conditions for temperature distributions used to validate the model

Building element	Assigned surface temperatures from measurements, [°C]		
	Type of heater		
	Convection	Radiant	Baseboard
Wall 1	21.3	23.7	21.2
Wall 2	22.1	22.6	22.7
Wall 3	22.2	22.7	22.4
Wall 4	22.5	22.7	22.6
Ceiling	23.9	24.0	24.3
Floor	22.1	23.9	22.6
Windows above heater	12.0	14.1	14.0
Other windows	10.0	10.5	10.0
Air	24.3	24.3	24.3

The total heat transfer, equivalent to the total heat loss was measured during the experiment. Table 4.2 compares the modeled total heat loss results with the experimental results.

Table 4.2 Comparison of modeled vs measured total average power consumption

Type of data	Average power consumption of the heater, [W]		
	Type of heater		
	Convection	Radiant	Baseboard
Modeled [W]	818	845	830
Measured [W]	891	929	930
Difference [W](%)	73 (8%)	84 (9%)	100 (11%)

From Table 4.2, it can be concluded that the model is able to predict the total heat loss with a discrepancy of up to 11% when the external temperature is $-20°C$. The model underestimates the total heat loss and does so consistently. Consistent discrepancies could be explained from the assumptions embedded in the model for air infiltration/exfiltration, radiation exchanges between indoor and outdoor, or even errors in the approximations of the wall insulations.

As for the *PMV*, it was compared with *PMV* tables at different environmental and personal parameters. The model agreed with the thermal comfort tables and thus accurately computes *PMV*.

The computed gradients calculations were also validated by comparing analytical solutions with numerical solutions. The comparison showed that the analytical calculation of the gradient is correct.

4.5 Case study: the Klimat test room

This section presents a case study that demonstrates the calculation of the virtual heaters for a typical room (Klimat test room). First, a solution with no constraints on temperature is calculated. Then upon realizing that this solution is not practical, a second solution to the virtual heaters is calculated with a constraint on the maximum allowable temperature.

The investigated room is based on a test room in a bi-climatic chamber (Léger *et al.*, 2017). The floor plan is approximately 3.75m $\times$ 5m with a ceiling height of 2.5m. Two double glazed windows are installed on two walls exposed to a cold environment. A door gives access to the test room from the warm side of the chamber. Figure 4.4 schematically illustrates the test room.

For the purpose of the model, the four windows are 0.75m $\times$ 1m and are installed at a height of 1m above the floor level. For each set, a distance of 0.25m separates each window. The door is 1m $\times$ 2m and is located 0.25m from the corner.

The effective thermal resistance and conductivity across the surfaces are given in Table 4.3. The effective wall thermal resistance including the outdoor convective resistance was measured experimentally (Léger *et al.*, 2017).

The infiltration rate of the test room is considered to be neglegible for all surfaces except for walls 1 and 2 where it is evaluated at 12.6m^3/h (Léger *et al.*, 2017). Infiltration was mostly considered for both windows which are located on walls 1 and 2. These constants represent the flow boundary conditions. The thermal resistance displayed in Table 4.3 include the outdoor convective resistance and has experimentally measured using a heat flux meter and a temperature measurement of the inside wall.

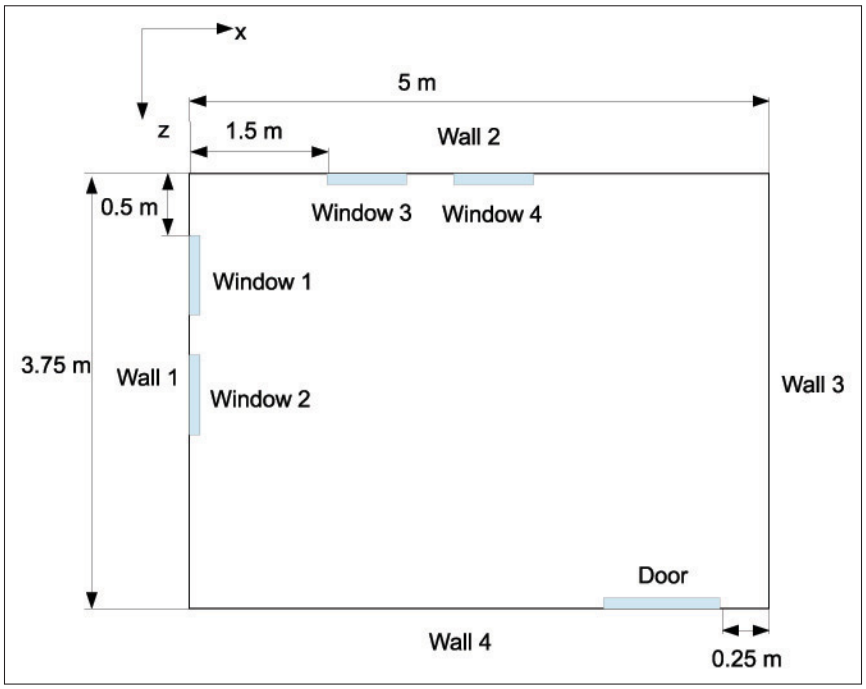

Figure 4.4 Test room top view

Table 4.3 Wall conductivity, thermal resistance and thickness

Surface	Thermal resistance [W/m°C]	Conductivity of first layer [m²°C/W]	Thickness of first layer [cm]
Wall 1, 2	2.94	0.17	0.95
Wall 3, 4	1.06	0.17	0.95
Floor	5.28	0.17	1.91
Ceiling	7.16	0.17	2.86
Door	0.80	0.08	4.00
Windows	0.41	0.80	0.48

The entire optimization process is divided in a sequence of four successive optimizations to make it possible to update the indoor convection coefficient h_i. The first three sequences involve 50 iterations before an update of h_i. The fourth optimization is then carried out until convergence. Convergence here has achieved when the variable, objective function and constraints stopped varying there respective value less then $10^{-}6$. The convection coefficient are calculated according to the vertical and horizontal plates correlations given in ASHRAE (ASHRAE, 2009).

In this study, Wall 1, Wall 2 and the ceiling are exposed to a cold environment maintained at $-20°C$. Wall 3 and 4 are considered to be indoor walls and the crawl space is also considered to be heated. The warm air temperature (exterior side of wall 3 and 4) is maintained at 22°C. These exterior temperatures are the temperature boundary conditions of the model.

For the radiation model, the total emissivity of surfaces must be specified. The walls and the floor have an emissivity of 0.90, the ceiling emissivity is 0.91 while the emissivity of the windows and door is 0.93 (Léger *et al.*, 2018).

A mesh size of 0.25m for the discretized square surface areas is used as further refinement was found to practically produce results that were insensitive to grid refinement. In fact, a mesh size of 0.5m would have been enough but 0.25m is retained since it is the actual smallest dimension found in the room model (see Figure 4.4).

The thermal comfort parameters for a person dressed in typical winter clothing sitting watching TV in a dry environment with relatively still air, is used (Fanger, 1970): metabolic rate , 1MET; clothing value, 1clo; draft rate or flow velocity, 0.02 m/s and relative humidity, 10%. Note that these parameters where selected to match typical conditions observed in the experimental setup where no warm air humidifier is available.

Given the significant amount of design variables (1301 temperatures), local optimization is favoured. The objective function is a linear function of temperature; however, the constraints have a higher degree of nonlinearity. Sequential quadratic programming (SQP) (Nocedal & Wright, 1999) is chosen for the optimization algorithm as it is a gradient-based approach that handles general C2 continuous nonlinear functions. The problem is programmed with Matlab and the optimization is solved using *fmincon* in the optimization toolbox.

4.5.1 Results without temperature limits

The virtual heaters were found in 158 iterations for the minimum and 179 iterations for the maximum. This is equivalent to a computation time of over 1h.

The minimum virtual heater has an energy consumption of 853W while the maximum virtual heater consumes $1,153$W. The room's heat distribution sensitivity using eq.4.2 is $RHDS = 0.35$. In other words, the maximum virtual heater consumes 35% more energy than the minimum virtual heater. An actual heater was measured and it consumes 915W to maintain thermal comfort at the geometric center of the room. The heater's heat distribution effectiveness using eq. (4.1) would then be 79%.

Some of the heat is distributed on the floor, see Figure 4.5. From this figure, it can be seen that the temperatures are unrealistic for real applications. The temperatures for the minimum virtual heater are too hot. Even if virtual heaters are conceptual heaters that may or may not exist, they should still satisfy basic regulatory requirements for indoor spaces since they simulate an indoor heater. It is recommended, in a second problem formulation, to limit the maximum allowable temperature to a safe level with lower maximum temperatures.

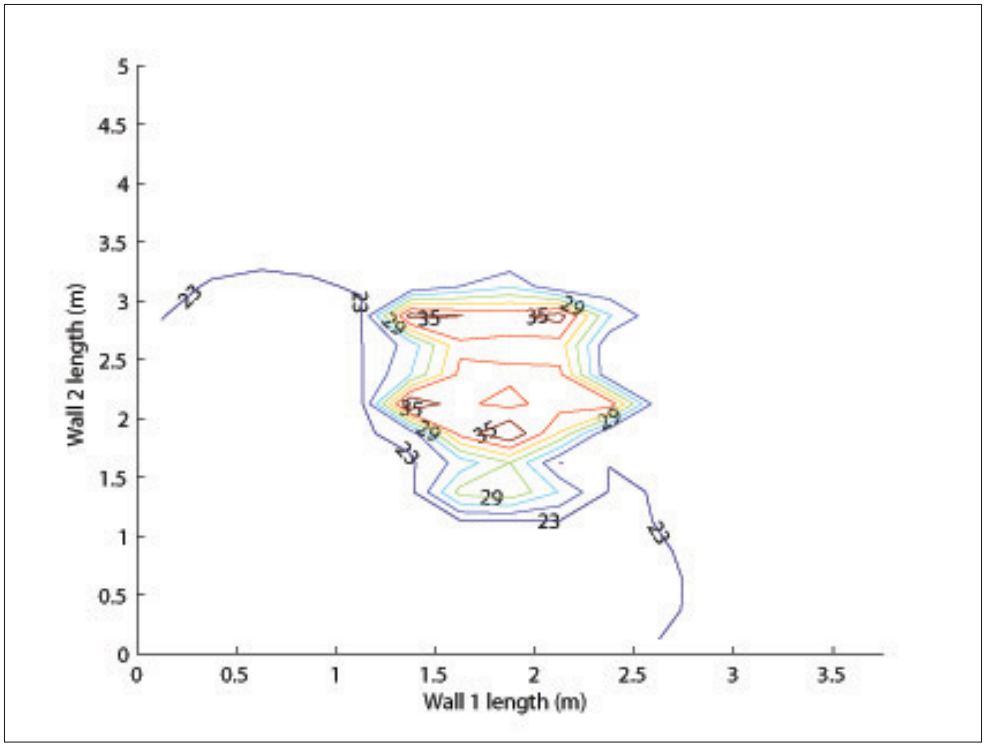

Figure 4.5 Floor temperatures for mVH (no temperature limit)

4.5.2 Results with limited temperatures

A first set of virtual heaters was obtained through an iterative process for which the temperature was limited to a maximum of 40°C for the wall and ceiling surfaces and a maximum of 27°C for the floor. These temperature limits are employed to prevent divergence of the solution. For example, the floor temperature at the center could have diverged to a infinitely high value only limited by the thermal comfort constraint near this surface. The virtual heaters were determined after 158 iterations for the mVH and 179 iterations for the MVH. This is equivalent to a computation time of over 1h on a standard PC involving an Intel Core i7-3740QM CPU at 2.70Ghz. The computation were set up in parallel computation to utilize all four cores at once.

Table 4.4 Simulation results

Variable	**Value**
T max floor, $[^{\circ}C]$	27
T max air, $[^{\circ}C]$	24
Surface/air heat rate mVH, [W]	56/798
Surface/air heat rate MVH, [W]	1153/0
$\dot{E}_{\mathrm{AH}}$	929
$\dot{E}_{\mathrm{mVH}}$	854
$\dot{E}_{\mathrm{MVH}}$	1153
$\varepsilon, [\%]$	0.9
$RHDS, [\%]$	25.9
$MPS, [\%]$	8.1
$CPUtime, i7-3740QM, 4Core, 2.70Ghz, [h], [\%]$	1.12

Table 4.4 indicates that the actual power dissipated in steady-state by the heater in the bi-climatic chamber is 929W (Léger *et al.*, 2018) while the power consumption of the mVH and MVH were found to be 854W and 1153W, respectively.

Hence, the associated heater effectiveness, ε, room heat distribution sensitivity, *RHDS*, and maximum power savings, *MPS*, were found to be 74.9%, 35.9% and 8.1%, respectively.

It is interesting to note how differently the mVH and MVH distribute heat: The mVH preferably heats the center of the floor (56W) as well as the air volume (798W) above. While the

MVH distributes 1153W on the surfaces (windows) and none in the air volume to obtain the same comfort. Hence, as the surfaces with low thermal resistance, i.e. windows, have the greatest influence on total heat loss, this is why the MVH distributes the heat on windows.

Conversely, a highly insulated surface of the room is selected to be heated when the minimum virtual heater solution is wanted. In this case, the floor has the highest thermal resistance along with the air volume which was also heated. This result is concurrent with other experimental results (Olesen *et al.*, 1980; Myhren & Holmberg, 2006; Sevilgen & Kilic, 2011).

Figure 4.6 shows the unit heating profile for the mVH in W/m^2 for the floor. Figure 4.6 shows that heating the center of the floor is preferred when the minimum virtual heater is wanted; in this case, the heat flux on the floor is approximately $27W/m^2$ for that particular room. There is no symmetry in the iso-flux contours because of the presence of windows on wall 1 and 2. But most of the heat is directed towards the center of the floor. This can be explained by the fact that the center of the surfaces have, on average, higher view factors to all thermal comfort points. With this information at hand, it is logical that the minimum virtual heater solution heats points that have more influence on thermal comfort by taking advantage of the radiant heat increases of these surfaces.

For the MVH, all of the heat is distributed to the windows. Figure 4.7 shows the heating profile on the windows of wall 1. After convergence of the optimization process, the MVH (Figure 4.7) heats the edges of the windows, and heats the window since it is the least insulated surface in the room. The view factor of the centered window (results on the left) on the thermal comfort volume is higher than the view factor for the window that is not centered (results on the right). A higher view factor for the thermal comfort volume leads to a surface having a greater influence on thermal comfort.

When comparing Figure 4.6 and 4.7, one acknowledges that it is logical that the minimum virtual heater solution heats points that have more influence on thermal comfort by taking advantage of the radiant heat increases of these surfaces. Conversely, the maximum virtual

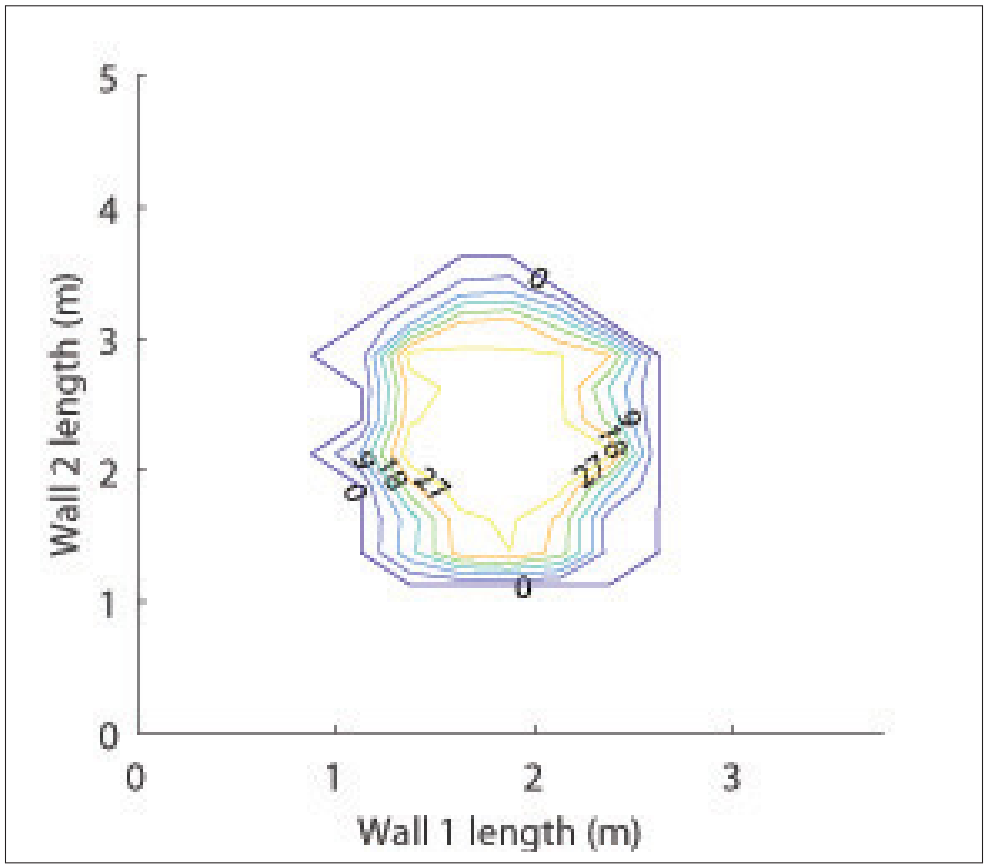

Figure 4.6 Top view of the temperature distribution on the floor with the mVH, [°]

heater tries to mitigate the mean radiant temperature of the comfort points by heating surfaces that have less of an influence on the volume, i.e. those with low average view factors.

The view factor effect supports the hypothesis that heating close to the objective, i.e. local thermal comfort, is more energy efficient than to heat far from the same space (Han *et al.*, 2014; Wang *et al.*, 2016; Krajčik *et al.*, 2016; Ahmed *et al.*, 2017). It is expected that the view factor effect is more significant in large spaces such as heating an atrium. In these spaces, the occupied thermal comfort volume is small relative to the indoor space, which is not the case in the specific room discussed here. There is also more of an opportunity to heat far from the comfort volume in these spaces, hence potentially increasing the required heat input to achieve similar thermal comfort when considering the MVH heat distribution.

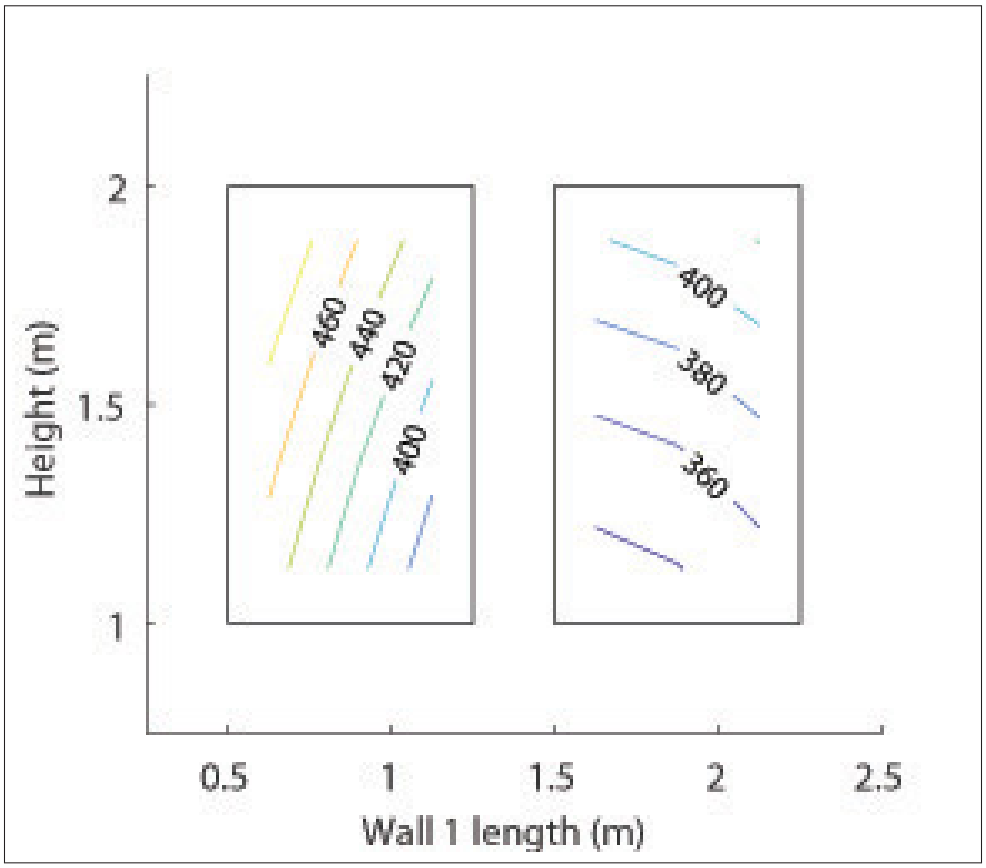

Figure 4.7 Temperature distribution on the windows of wall 1 for the MVH seen from the outside, [°]

The mVH and MVH results thus show that it is more energy efficient to heat surfaces that will have a high influence on the thermal comfort and more efficient to heat well-insulated surfaces for a similar comfort. Here, it is clearly indicated that it is better to heat the floor rather than the windows. Although, this could be said to be trivial, ASHRAE still recommends locating heaters below windows.

The average, minimum and maximum temperatures for each surface, for the mVH and MVH are given in Table 4.5. In the table, the first temperature presented (on the left) is for the mVH while the second is for the MVH (on the right).

The windows, walls and ceiling temperatures were maintained as low as possible for the mVH by providing no heating to these surfaces. On the other hand, MVH clearly produces higher

Table 4.5 mVH and MVH average, minimum and maximum temperatures predictions for the climate chamber [°C]

	average (mVH/MVH)	maximum (mVH/MVH)	minimum (mVH/MVH)
Wall 1	21.4/22.4	21.7/23.3	21.0/21.4
Wall 2	21.4/22.7	21.8/24.7	20.6/21.4
Wall 3	23.2/24.2	23.5/24.5	23.0/23.3
Wall 4	23.0/24.4	23.5/25.3	21.7/21.5
Floor	23.6/24.7	27.0/25.8	22.6/23.2
Ceiling	22.6/24.2	23.3/26.2	21.8/22.5
Wall 1 windows	12.5/51.0	12.7/58.2	12.4/45.3
Wall 2 windows	12.7/48.0	12.9/53.3	12.5/43.7
Indoor air	26.5/23.8	-	-

surface temperatures. Thus, the overall radiant temperature will also be higher. However, it did not heat the air volume. Higher window temperatures, for this particular room, leads to more losses for the same comfort level. In fact, the mVH shows that, for this particular room, heating air instead of surfaces is energy efficient. One should be aware of the very low window surface temperatures calculated for the mVH (below 13°C). This could lead to moisture condensation if the air inside is humid, when boiling water in the kitchen in winter, for instance.

Figures 4.8a and 4.8b show the temperature distributions on Wall 1 for the mVH and MVH, respectively: the mVH and MVH (isotherms) behavior. The windows on Wall 1, delimited by solid black rectangles, have higher temperatures towards the outside of the windows for the MVH. This can be explained by radiation exchange. For the MVH, heating toward the outside of the window is governed by the fact that these points will have less of an influence on the overall mean radiant temperature, thus allowing a same wall element located towards the outside to be at a higher temperature with the same influence on the thermal comfort volume. However, the main difference between the mVH and MVH, is still that one is found to heat the poorly insulated windows while the other is found to heat the floor and air volume.

In Figures 4.9a and 4.9b, the floor temperature distributions for the mVH and MVH are shown respectively. The mVH is found to heat the floor in the center of the surface. To increase radiant heat transfer, a higher local temperature is desired. Note that a thermal comfort model taking

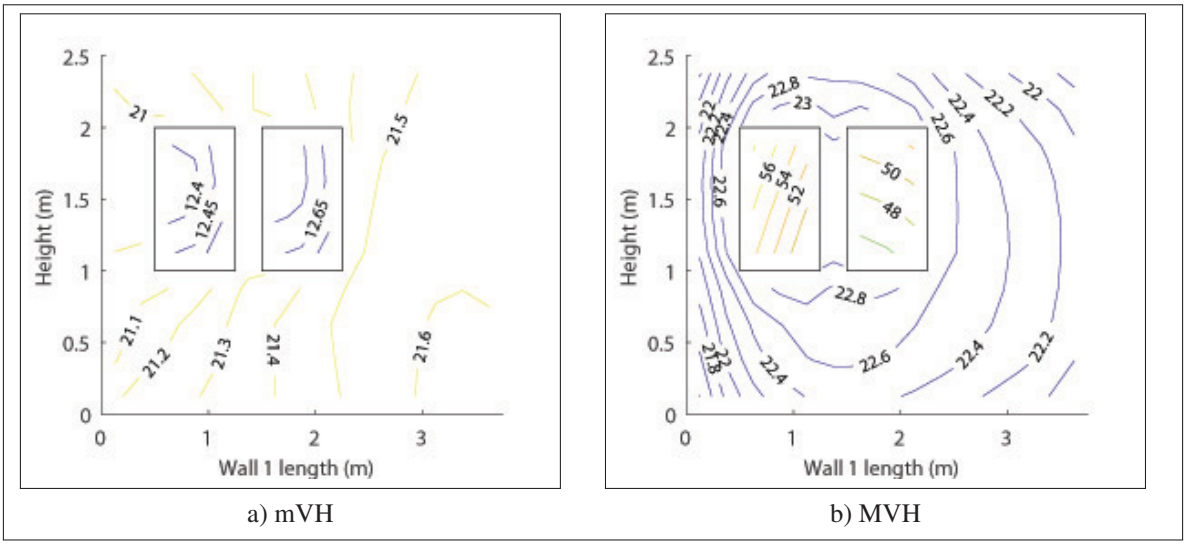

a) mVH b) MVH

Figure 4.8 Temperatures distributions on wall 1 [°C]:(a) mVH; (b) MVH

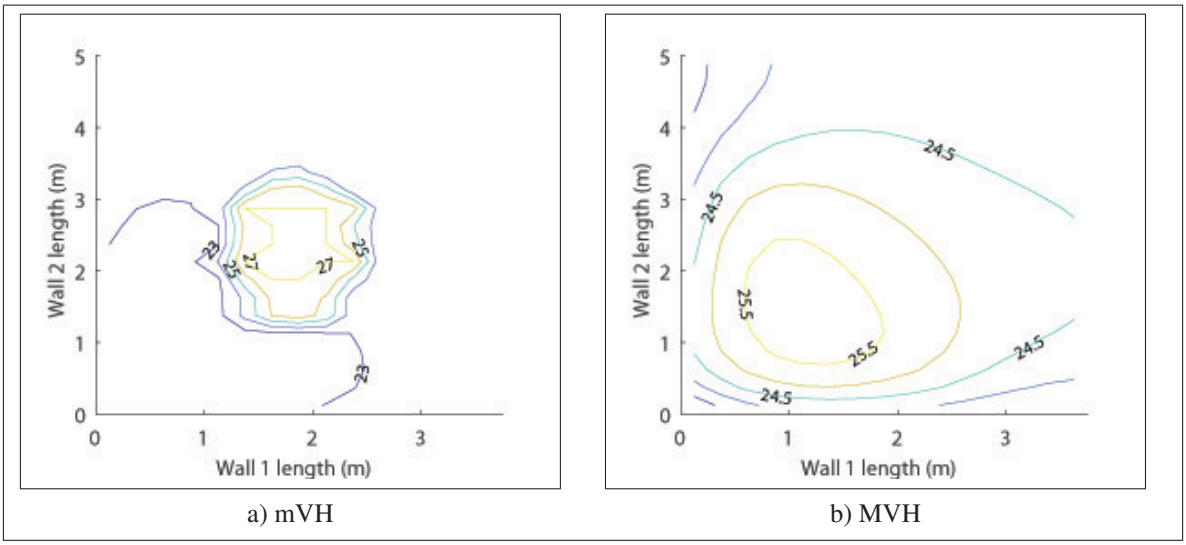

a) mVH b) MVH

Figure 4.9 Temperature distributions on the floor [°C]: (a) mVH; (b) MVH

into account the radiation asymmetry would reduce the occurrence of this type of optimum. A single hot point would generate significant radiation asymmetry.

The mVH and MVH thermal comfort distributions on three section cuts of the comfort volume are shown in Figure 4.10.

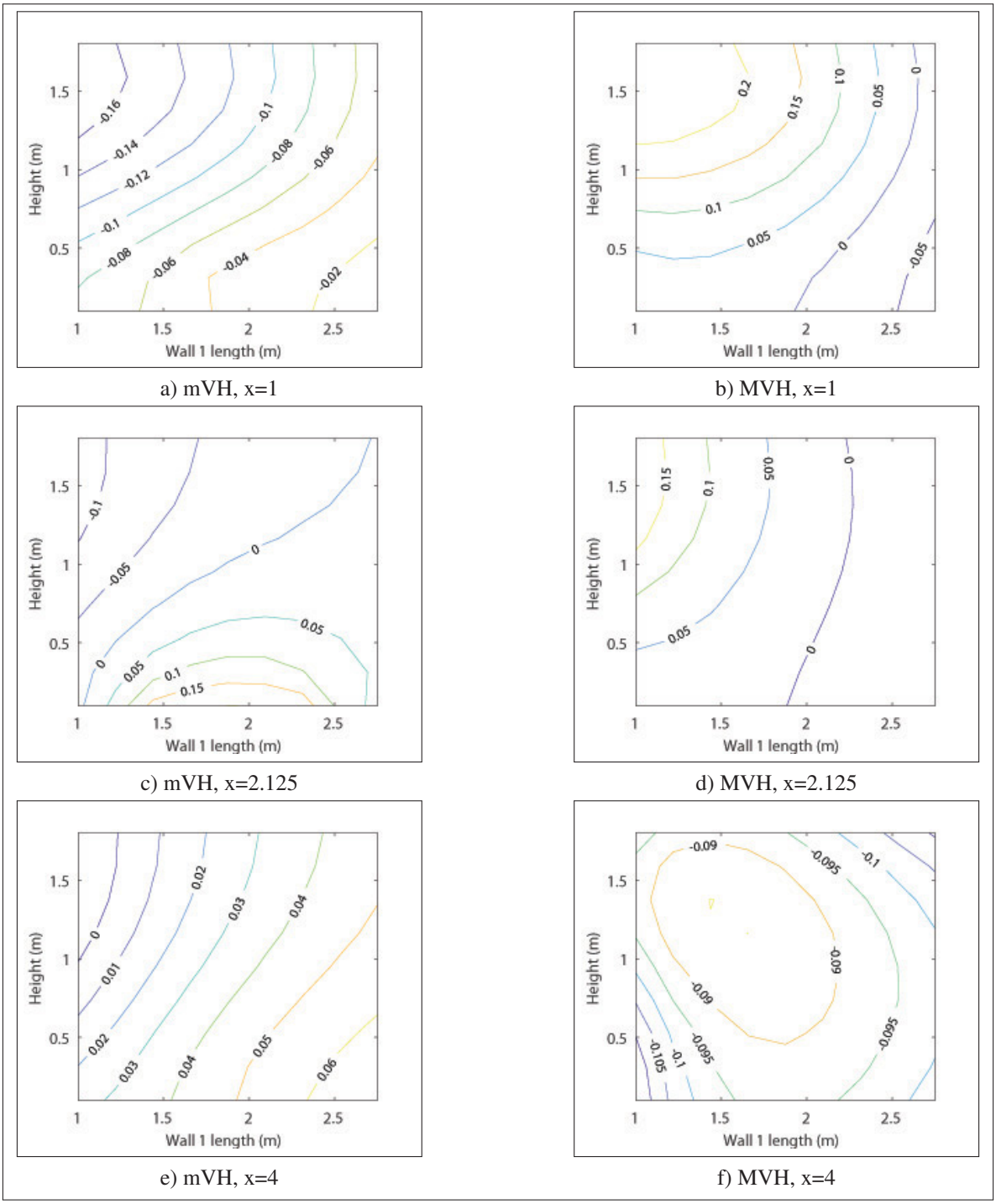

Figure 4.10 Thermal comfort distributions of three vertical occupied sections of the comfort volume, [PMV]: (a) mVH and x=1; (b) MVH and x=1;(c) mVH and x=2.125; (d) MVH and x=2.125;(e) mVH and x=4; (f) MVH and x=4;

The first result when one looks at a glance at Figure 4.10 is that both heaters provide comfort for all locations selected along the x-axis. For most locations $0 \leq |PMV| \leq 0.2$, comfort is even more uniform as x increases with $0 \leq |PMV| \leq 0.1$ of $x = 4$m. Then, as expected, the PMV is higher near the hot surfaces. It is clear from these figures that the corner mostly exposed to the cold room (the top corner in Figure 4.10b) was heated more for the MVH while the center and warm side of the room, which are well-insulated sections, were heated more for the mVH.

4.5.3 Discussion

The former case study, clearly exemplifies how virtual heaters can be used to assess the heat distribution performance with respect to a given comfort level.

4.5.3.1 Effectiveness, sensibility and power savings

First, the effectiveness, eq. 4.1 of the actual heater (Léger *et al.*, 2018) is found to be 74.9%, which means that this heater is closer to the mVH than to the MVH for this room. Second, the room has an $RHDS$ of 0.249, eq. 4.2, which is equivalent to saying either that the mVH consumes 24,9% less than the MVH and that not all heating systems will be able to maintain the same comfort level at the same operating cost. The $RHDS$ attains the maximum possible power savings, MPS, that is, if the actual heater was replaced by the MVH, the maximum savings would be 24,9%. Here, $MPS = 8.1\%$ is a fraction of that full range, meaning that care must be taken before replacing the actual system for low MPS based on a "simple" pay back period.

One should note that the maximum potential power savings can be expressed in terms of the effectiveness and room heat distribution sensitivity such that: $MPS = RHDS((1-\varepsilon))/(1-\varepsilon RHDS)$ and this clearly shows the upper limit of the MPS.

Had a different room been tested, a very different conclusion could have been made upon comparing the importance of heat distribution between the two rooms. Clearly, the room with an $RHDS = 0.1$ is less sensitive to heat distribution than the actual one with an $RHDS = 0.249$.

When $RHDS = 0.1$, the designer could choose to neglect the heat distribution in his design analysis for a heating system. On the other hand, a room with a large *RHDS* would require more attention to select the proper system.

This example for which the performance indices based on virtual heaters are used to help designers make informed decisions on heat distribution is of importance as significant energy savings can entail from the process.

A second and less obvious dominant governing effect is the thermal comfort point view factors found in the constraints. The minimum solution favoured heating the centers of the surfaces. This can be explained by the fact that the center of the surfaces have, on average, higher view factors to all thermal comfort points. With this information at hand, it is logical that the minimum virtual heater solution heats points that have more influence on thermal comfort by taking advantage of the radiant heat increases of these surfaces. Conversely, the maximum virtual heater tries to mitigate the mean radiant temperature of the comfort points by heating surfaces that have less of an influence on the volume, i.e. those with low average view factors.

The view factor effect supports the hypothesis that heating close to the objective, i.e. local thermal comfort, is more energy efficient than to heat far from the same space (Han *et al.*, 2014; Wang *et al.*, 2016; Krajčik *et al.*, 2016; Ahmed *et al.*, 2017). It is expected that the view factor effect is more significant in large spaces such as heating an atrium. In these spaces, the occupied thermal comfort volume is small relative to the indoor space. There is also more of an opportunity to heat far from the comfort volume in these spaces, hence potentially increasing the required heat input to achieve similar thermal comfort when considering the MVH heat distribution in section 4.5.2.

4.5.3.2 Heat transfer model limitations

The heat transfer model used has some limitations. The air temperature stratification was not considered in the model. Including air temperature stratification would have favored floor heating and heating the air volume close to the floor. Heating at the floor level reduces thermal

stratification and hence increases thermal comfort, thus approaching the case model herein for the mVH since it heated the floor. For the MVH, some thermal stratification would have occurred as the MVH heats the window. Since thermal stratification has a negative contribution to thermal comfort, it is expected that the MVH energy consumption would have been higher.

Moreover, it can be said that the virtual heater computed with the model used here was incapable of proposing where to heat the air inside the room. This is not a limitation of the virtual heater, but rather a limitation of the model used to find them.

4.5.3.3 PMV model range limitation

As for the thermal comfort distribution, no thermal comfort point reached its limits: $PMV = -0.5$ or $PMV = 0.5$. This result shows that the average thermal comfort for the volume is very constraining. It is also interesting to note that the MVH had higher thermal comfort in the corner of the wall exposed to cold outdoor temperature, whereas the mVH had higher PMV towards the center of the room and closer to the warm room walls. This could be linked to the window locations for the MVH. Had the windows been located differently, the thermal comfort distribution for MVH might have changed significantly. For the mVH, this is simply explained by the view factor effect and the floor heating.

Some aspects of thermal comfort that were not modeled by considering only PMV include radiant asymmetry and the effect of conduction through floor contact. The effect of radiation directionality on comfort was also neglected, i.e. is the hot surface on top, below or beside the occupant. To limit discomfort through hot floors, a floor temperature limit was imposed. As for radiation asymmetry, this was limited by construction of the thermal comfort volume. Having thermal comfort points close to each surface limits radiation asymmetry, but does not eliminate it.

4.5.3.4 Adequate compromise

Although more accurate heat transfer models and thermal comfort models exist and would have provided more accurate heat transfer and thermal comfort results, the chosen model was sufficient to show how the virtual heaters could be used to assess the coupled heat distribution/thermal comfort problem. The computation time to find both mVH and MVH is approximately 1h. Increasing the computation time required by the heat transfer model or the thermal comfort model would likely lead to a significant increase of the total optimization time. Currently, both models run under 0.25s. This is in part due to the fact that the heat transfer problem can be computed with matrix/vector multiplications where the matrix is not updated at each iteration; hence it is assumed that the convection heat transfer coefficient is constant and no air distribution model is incorporated. The ideal thermal model would be a CFD simulation, however, it will be hard to find an optimization algorithm able to efficiently find the optimal solution using CFD in a reasonable amount of time.

4.5.3.5 Upcoming work

More work should be done that will increase the complexity of the model while keeping a close eye on computation time. The optimization time is significantly affected by the number of nodes in the model, which is also the number of variables in the optimization, thus making efficient modeling and optimization techniques essential. Decoupling the discretization of the heat input from the discretization used for the flow and heat transfer calculations is one possible solution to this problem, and it is left for future research.

4.6 Conclusions

Addressing the optimal heat distribution of indoor spaces for both energy efficiency and thermal comfort is a challenging problem as it involves a combination of optimizing and modeling fluid flow, heat transfer and thermal comfort.

In this context, this chapter asked how an existing system is actually performing in ensuring thermal comfort with respect to an ideal system that would minimize energy consumption for the same comfort level in the same room? And how good is the performance of the actual system with respect to the worst theoretical system that would maximize energy consumption at constant thermal comfort?

To answer these questions, the chapter proposes a new concept termed virtual heater (VH) to assess the optimal heat distribution at a given or prescribed thermal comfort level for a specific room. Using both the minimum VH and maximum VH energy consumptions, three performance indices were introduced to evaluate the heat distribution of rooms and their heating devices:

1. The heat distribution effectiveness, ε, of a real heat diffuser/distributor which assesses how close a heater is to the mVH, $0 \leq \varepsilon \leq 1$;
2. The energy consumption sensitivity of a room to heat distribution, $RHDS$, which quantifies the difference between the best and the worst heater performances, $0 \leq RHDS \leq 1$;
3. The maximum potential power saving, MPS, that could be achieved if the ideal minimum virtual heater replaced the actual heater, $0 \leq MPS \leq RHDS$.

The interest of these performance indexes is that they provide a unique comparison basis for several heating technologies.

The case study example estimating the virtual heaters' performance demonstrated the usefulness of the VH concept. Results showed that the climatic chamber has an $RHDS = 35\%$ while a convection heater used inside the climatic chamber has a heat distribution effectiveness of 75%. This indicates maximum potential power savings of 9.5% at equal thermal comfort.

Results also generally showed that it is more efficient to heat well-insulated surfaces and surfaces that have a high average view factor on the thermal comfort volume. These two factors

were found to provide the most optimal solution. The virtual heaters thus produced results that are coherent with what was found in the literature.

Nevertheless, several ongoing studies will help to generalize the results:

1. More complex rooms will be investigated, as floor heating might not always be the best heating option. Investigating how the geometry of a room and its thermal parameters might affect the optimal heat distributions, the minimum consumption and the energy consumption sensitivity is of interest for future research;

2. A more complete fluid flow and heat transfer model of the room could be considered to account for air temperature stratification. However, the more complex model should not make the computational time become overly lengthy for practical use;

3. Improvements could be made on the thermal comfort model itself to propose a more accurate approximation of the virtual heaters.

As a final remark, one can conclude that applying the concept of virtual heaters could lead to the construction of more efficient buildings while providing them with optimal heating. The performance indices and virtual heaters introduced in this work provide an opportunity to evaluate the heating aspects of buildings in a new way.

CHAPTER 5

THE EFFECT OF GEOMETRY AND INSULATION ON OPTIMAL HEATING

The effect of the room geometry and thermal parameters on optimal heat distribution is investigated in this chapter. This is an interesting topic of investigation for both engineers and architect as it discusses the relation between the room parameters and its optimal heating distribution system.

The chapter is divided as follow: In Section 5.1, the tested parametric cases are presented. Two categories of parameters variations are considered: variations of the base case with respect to its geometry; and, variation of the base case with respect to its thermal parameters. Section 5.2 then summarizes the interesting results of the different test cases. Each parameter variation is compared on the basis of the heat distribution, the energy consumption, and the *RHDS*. In section 5.3, it is discussed how some room parameters have a strong influence on the *RHDS* and heat distribution.

5.1 Parametric analysis

The virtual heaters are examined for several geometries and thermal parameters topologies. Each parameter is varied individually from a base case. This base case is presented in Figures 5.1 and 5.2.

The window, centered on wall 1, has dimensions 2.5m $\times$ 1.25m and its base is 0.5m high from the floor. The double glazed window has an effective resistance of R2. Wall 1 has dimensions 5m $\times$ 2.5m and is insulated at R20. This wall along with the ceiling is exposed to a cold climate of -20°C. The ceiling as an insulation of R40. Walls 2, 3 and 4 are exposed to an indoor climate with a temperature of 22°C. They are insulated at R10. The floor is also exposed to a warm temperature of 22°C. It has dimensions 5m $\times$ 5m and is insulated at R30. The thermal comfort volume is outlined by the dashed lines on Figures 5.1 and 5.2, and give the room layout, thermal parameters, and the nomenclatures for each surface.

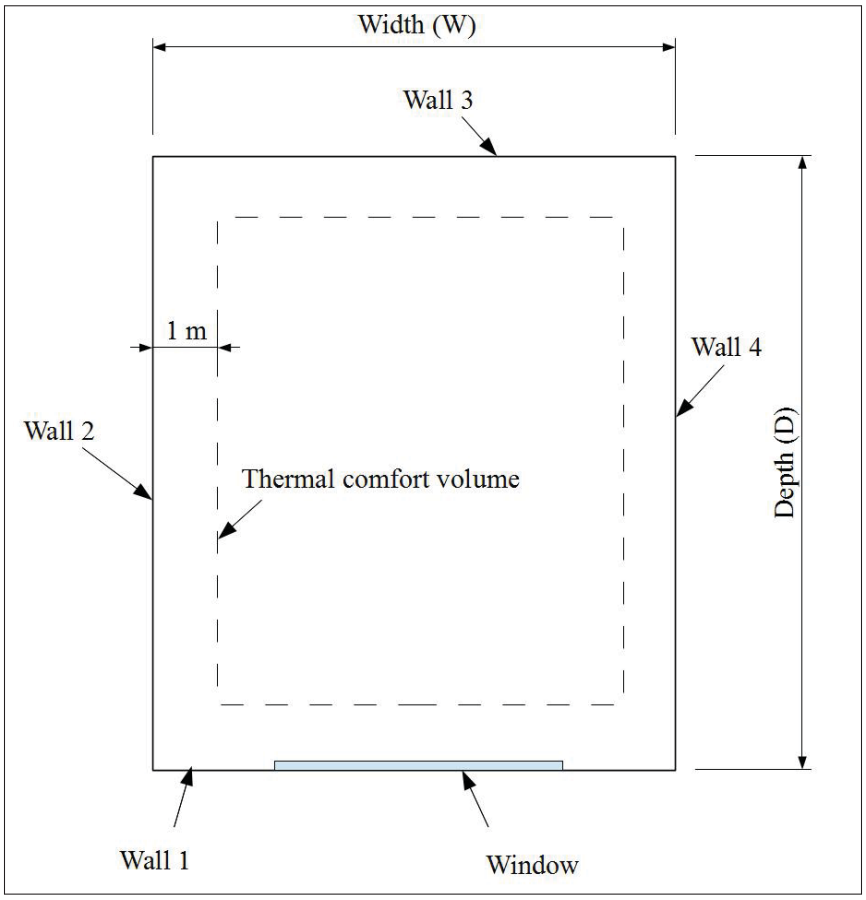

Figure 5.1 Plan view of the tested room

For thermal comfort, it was assumed that occupants are dressed with 1Clo of insulation and have a metabolic rate of 1MET (Fanger, 1970). It is also assumed that the indoor relative humidity is 10% and the average air velocity felt by the occupant is 0.02m/s.

For the optimization, the initial temperature field guess is that all temperature nodes are set to 0°C. To limit the floor temperature and wall temperatures to reasonable values, a maximum floor temperature of 27°C and a maximum temperature of 80°C for the walls and ceiling are imposed in the optimization. This is in relation with the findings of Chapter 4 where it was found that floor temperatures could exceed reasonable limits if they are not considered as a constraint.

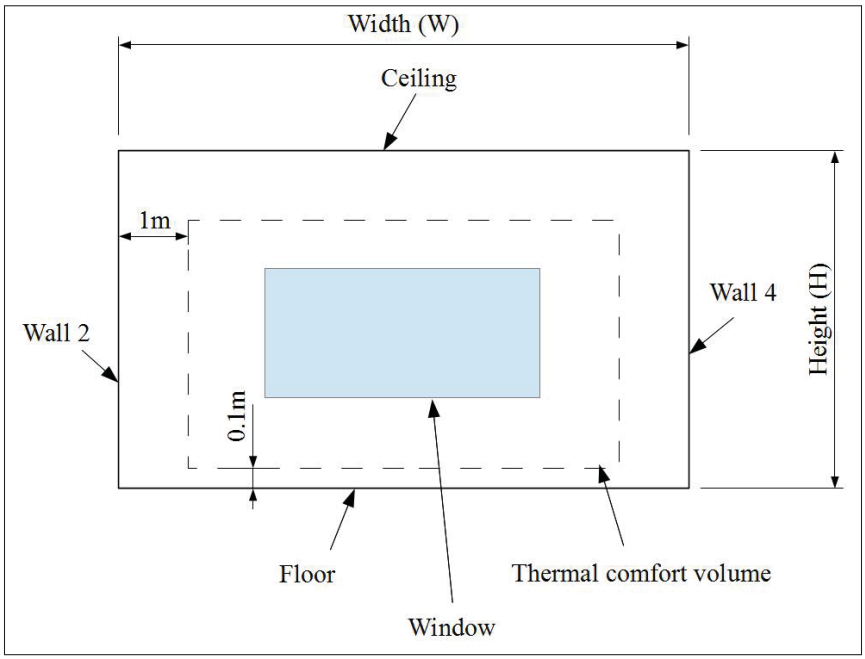

Figure 5.2 Elevation view of the tested room

In section 5.1.1 and 5.1.2 that follows, the different parametric cases tested are presented. Each case varies one parameter from the base case presented above, i.e. case 1. The procedure outlined in Chapter 4 is used to find the virtual heaters

5.1.1 Effect of geometry

The tested cases for different geometries are shown in Table 5.1.

Case 1 is considered as a base case. The other cases are parametric variations of the base case by one parameter, either the height (H), the depth (D) or the window-to-wall ration (WWR): cases 2 to 5 account for the variation of the depth; cases 6 to 9 investigate the variation of the height; and cases 10 to 14 study the variation of the WWR.

5.1.2 Effect thermal parameters

The test cases for variations in thermal parameters is presented in Table 5.2

Table 5.1 Test cases for the effect of geometry

	H [m]	W [m]	D [m]	WWR [%]
Case 1 (base case)	2.5	5.0	5.0	25
Case 2	2.5	5.0	7.5	25
Case 3	2.5	5.0	10	25
Case 4	2.5	5.0	12.5	25
Case 5	2.5	5.0	15	25
Case 6	3.0	5.0	5.0	25
Case 7	3.5	5.0	5.0	25
Case 8	4.0	5.0	5.0	25
Case 9	6.0	5.0	5.0	25
Case 10	2.5	5.0	5.0	16
Case 11	2.5	5.0	5.0	36
Case 12	2.5	5.0	5.0	49
Case 13	2.5	5.0	5.0	64
Case 14	2.5	5.0	5.0	81

The variable thermal parameters considered are insulation of wall 1, of walls 2, 3 and 4, of the floor and of the ceiling. Other variable parameters include the air exchange rate, the number of panes in the window and the outdoor temperature. The intended purpose of each cases, where a comparison is made with respect to the base case, is: cases 15 to 17 studies effect of wall 1 insulation; cases 18 and 19 studies the effect of wall 2, 3 and 4 insulation, where case 19 is an adiabatic indoor wall; cases 20 to 22 studies the effect of the floor insulation; cases 23 to 25 studies the effect of the ceiling insulation; cases 26 and 27 studies the effect of the number of pane for the window; cases 28 and 29 studies the effect of the air exchange rate; cases 30 and 31 study the effect of a change in outdoor temperature. These parameter cases cover some old and new constructions.

With the 31 parametric variations of Tables 5.1 and 5.2, the virtual heater solutions should provide an adequate understanding of the effect of thermal parameters and geometry on optimal heat distribution.

Table 5.2 Test cases for the effect of thermal parameters

Case	Wall 1 $[\frac{^\circ F ft^2 h}{BTU}]$	Wall 2-4 $[\frac{^\circ F ft^2 h}{BTU}]$	Floor $[\frac{^\circ F ft^2 h}{BTU}]$	Ceiling $[\frac{^\circ F ft^2 h}{BTU}]$	Window $[\frac{^\circ F ft^2 h}{BTU}]$	Air change [ACH]	T_{out} $[^\circ C]$
1 (base case)	20	10	30	30	2	0.1	-20
15	10	10	30	30	2	0.1	-20
16	30	10	30	30	2	0.1	-20
17	40	10	30	30	2	0.1	-20
18	30	5	30	30	2	0.1	-20
19	30	200	30	30	2	0.1	-20
20	30	10	20	30	2	0.1	-20
21	30	10	40	30	2	0.1	-20
22	30	10	50	30	2	0.1	-20
23	30	10	30	20	2	0.1	-20
24	30	10	30	40	2	0.1	-20
25	30	10	30	50	2	0.1	-20
26	30	10	30	30	0.9	0.1	-20
27	30	10	30	30	3.2	0.1	-20
28	30	10	30	30	2	0.3	-20
29	30	10	30	30	2	0.7	-20
30	30	10	30	30	2	0.1	-10
31	30	10	30	30	2	0.1	0

5.2 Results

The optimisation results for the three parametric variations are presented in the following sub-sections. Since all solutions are variations of the base case, the mVH and MVH for the base case are first investigated in more detail.

The mVH consumed 27.44W/m^2 (per floor area) while the MVH consumed 38.96W/m^2 which gives an $RHDS = 0.42$. For the base case, the MVH thus consumed 42% more power than the mVH. An $RHDS = 0$ would state that the heat distribution has no effect on the room's energy consumption, while a value of 1 would state that there is a massive difference, i.e. as large as the MVH itself.

For the mVH, the heat is found to be entirely distributed to the air volume. This is likely a consequence of the low air exchange rate simulated for the room. The MVH, on the other

hand, distributes all the heat to the window. The window is the least insulated part of the room, heating this part is thus less efficient.

The air temperature for the mVH is 26.2°C and 24.7°C for the MVH. The temperature of the cold wall is shown in Figures 5.3a and 5.3b for the mVH and the MVH, respectively.

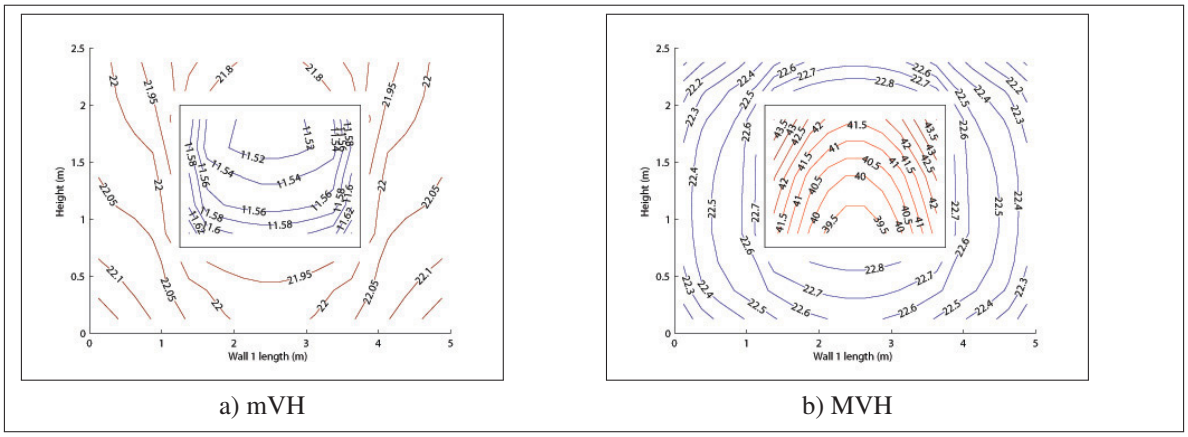

a) mVH b) MVH

Figure 5.3 Wall 1 temperatures for the base case

In Figures 5.3a and 5.3b, the window on wall 1 is depicted by a black rectangle at the center of the wall.

For the mVH, the window is at its equilibrium temperature. In this case, the heat is directed towards the air volume.

For the MVH, the heat distribution produces window temperatures that are not only warmer than all other surfaces, but also warmer at the extremities of the window. These results are consistent with those found in (Léger *et al.*, 2019) and presented in Chapter 4.

The thermal comfort distribution for the base case is shown in Figure 5.4 for the MVH and mVH for three vertical planes parallel to the window.

The first slice or vertical plane is located at 1m from wall 1 (and window), the second is at the center of the volume (2.5m) while the third is at a distance of 4m from wall 1 (it is at 1 m from the end wall). The thermal comfort is clearly lower near the window, Figure 5.4b, for the mVH

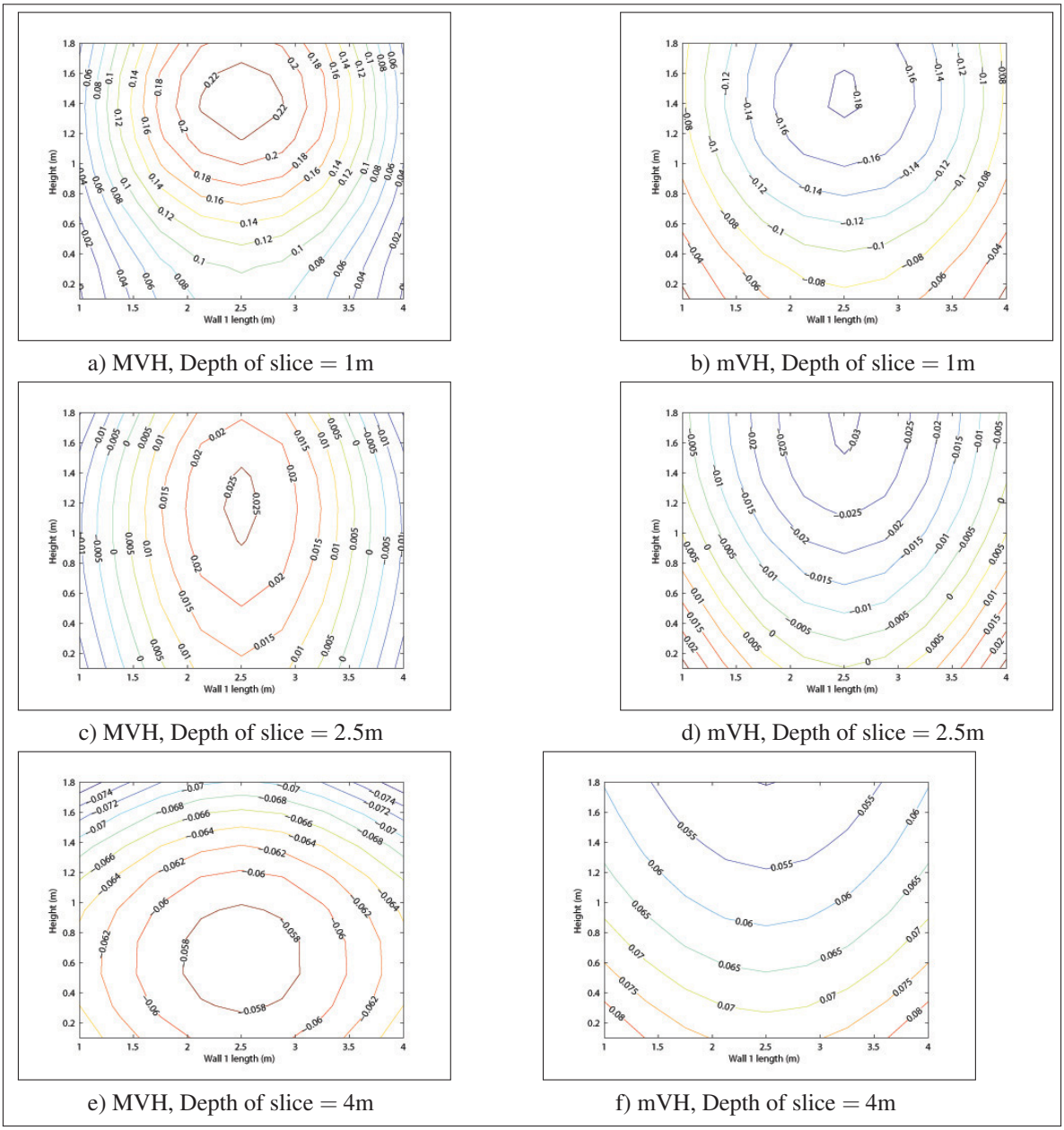

a) MVH, Depth of slice = 1m

b) mVH, Depth of slice = 1m

c) MVH, Depth of slice = 2.5m

d) mVH, Depth of slice = 2.5m

e) MVH, Depth of slice = 4m

f) mVH, Depth of slice = 4m

Figure 5.4 Thermal comfort (*PMV*) at different depth values for the base case mVH and MVH

and higher near the window for the MVH, Figure 5.4a. However, it remains within a tolerable range. The maximum *PMV* for the mVH and MVH are respectively 0.22 and 0.08; while the minimum values are respectively -0.076 and -0.18, well within the comfort range.

5.2.1 Effect of geometry

The results for the test cases that vary geometric parameters are now presented. These include changes in window-to-wall ratio (WWR), depth of the room (D), and height of the room (H).

5.2.1.1 Window to wall ratio

The effect of the window-to-wall ratio (WWR) on the optimal heat distribution is presented in this subsection. Figure 5.5, shows the *RHDS* index (left vertical axis) and the power consumptions per floor area (right vertical axis) for the mVH and MVH as a function of the WWR.

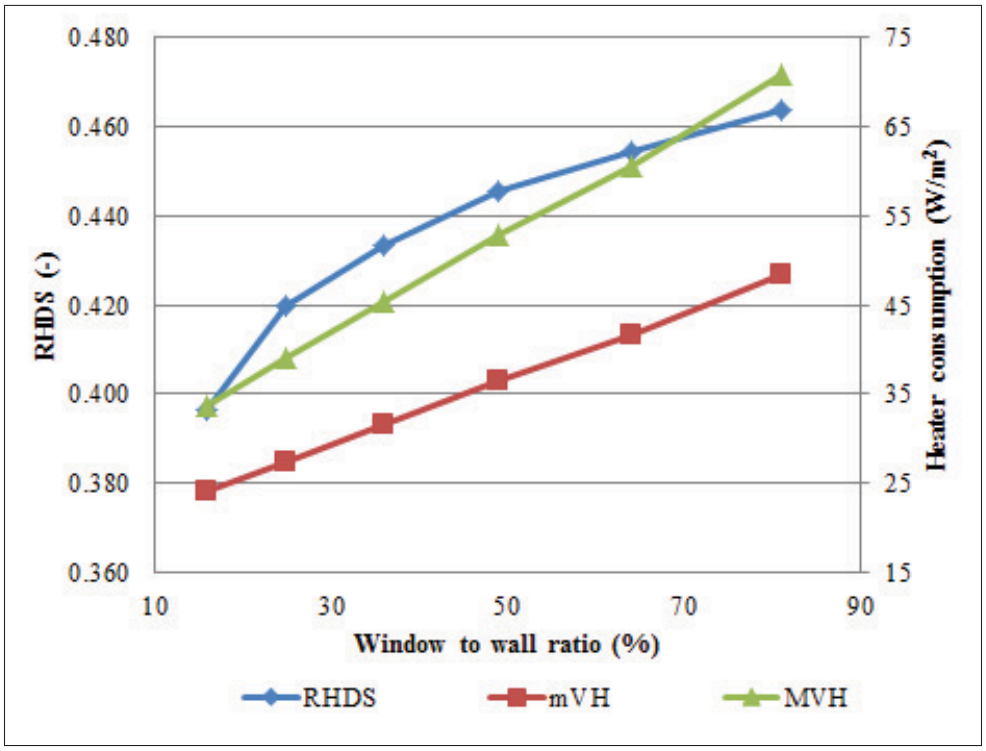

Figure 5.5 Room heat distribution sensibility (RHDS) as a function of window to wall ratio

At low WWR, the *RHDS*, as observed in Figure 5.5, is more sensitive to a change in WWR. In total, from a WWR of 16% to 81%, the *RHDS* increased by 0.033. This corresponds to the

MVH increasing its consumption relative to the mVH by 3.3% while the WWR increased by a factor of 5. The higher value of *RHDS* can be explained by the fact that a larger window is more likely to provide inefficient heating since it represents a bigger portion of the total heat loss. Moreover, it presents more opportunities to heat far from the thermal comfort volume (indicated by low view factors) at the window corners.

Table 5.3 shows the percentage of power that is distributed on the floor and on the air volume for these higher WWR. The MVH only heated the window while, at a WWR lower than 49%, the mVH heated the air volume only. Above WWR of 49%, the mVH heated both the floor and the air volume where the proportion of floor area-to-air volume heating increased with the WWR. Although floor heating is present, most of the heat is still distributed to the air volume.

Table 5.3 mVH heat distribution per heated room elements as function of WWR

WWR [%]	air volume [%]	floor [%]
49	100	0
64	98.5	1.5
81	94.6	5.4

The room air temperature for the mVH and MVH is presented in Figure 5.6.

It is observed that the room air temperature for the mVH increases as the WWR increases. This is to be expected since the window is a cold surface in the solution of the mVH and would contribute to lowering the mean radiant temperature for points inside the thermal comfort volume. The air temperature must then be increased accordingly to maintain thermal comfort. Note also that the temperatures are above normal ASHRAE 55 recommended values (ASHRAE-55, 2013). This can be explained by the metabolic rate and clothing factors chosen in the simulation. However, the absolute values of temperature are of little interest for this study as conclusions are drawn from variations in temperature. The effect of adding floor heating at higher WWR is also seen in Figure 5.6 as the air temperature slope for the mVH is lower at higher WWR.

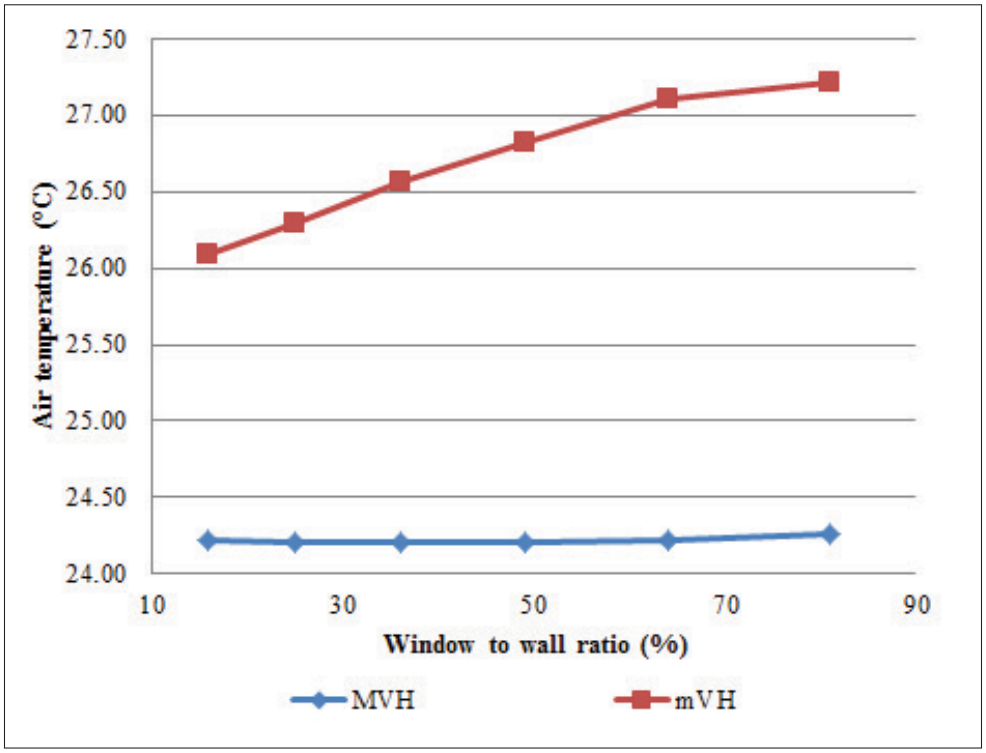

Figure 5.6 MVH and mVH air temperatures as a function of window to wall ratio

The air temperature for the MVH remains stable with respect to the WWR. This is also to be expected as the MVH heats the window and not the air volume. The air temperature is thus maintained by natural convection between the window and the air volume.

The effect of the variation of WWR on the window temperature (wall 1) is reported in Figure 5.7. The temperature of the windows for the mVH ($T \approx 11.5°C$) remained relatively constant with respect to the WWR. The temperatures of wall 1 and the window for three different window-to-wall ratios and for the MVH are shown in Figure 5.7.

In this figure, it is clear that the window temperature for the MVH decreases with an increase in WWR. It can also be noted that the corners of the window, especially those in the upper part, are heated more than the center and lower part of the window.

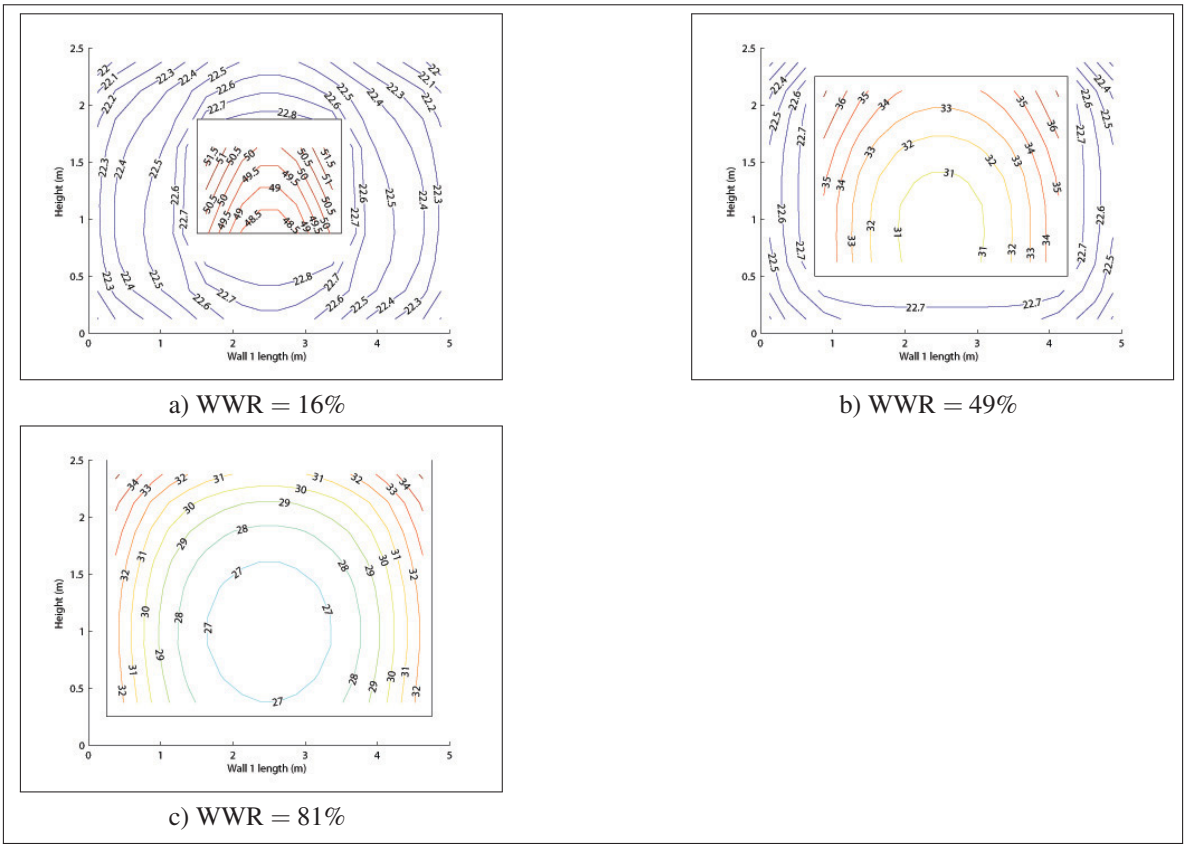

Figure 5.7 Wall 1 temperatures for different window to wall ratio and for the MVH

The decrease in window temperature leads to less thermal comfort variations near the window as can be seen in Figure 5.8.

The thermal comfort volume slices presented in Figure 5.8 are taken at 1m from the wall. It can be observed in Figure 5.8 that an increase in WWR for the MVH leads to a decrease in the peak PMV value as the window temperature is not as extreme.

Figure 5.9 presents selected results at floor temperature distribution for different values of WWR for the mVH. At high WWR, the mVH also heats the center of the floor. The floor temperature is presented in Figure 5.9 for two WWR.

In Figure 5.9, it can be seen that increasing the WWR leads to a larger portion of the floor being heated. The floor temperature was limited in the optimisation to a maximum temperature of

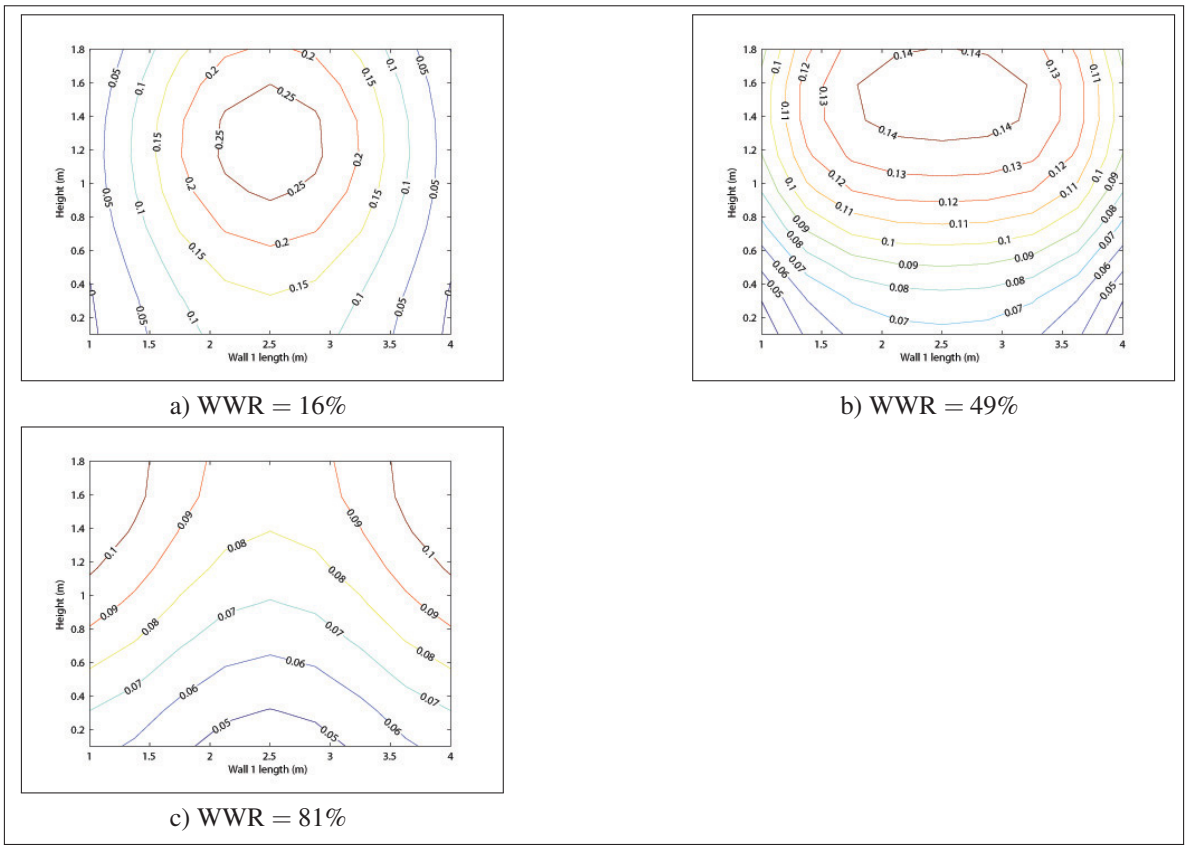

a) WWR = 16%

b) WWR = 49%

c) WWR = 81%

Figure 5.8 Thermal comfort at 1m offset from wall 1 for different window to wall ratio and for the MVH

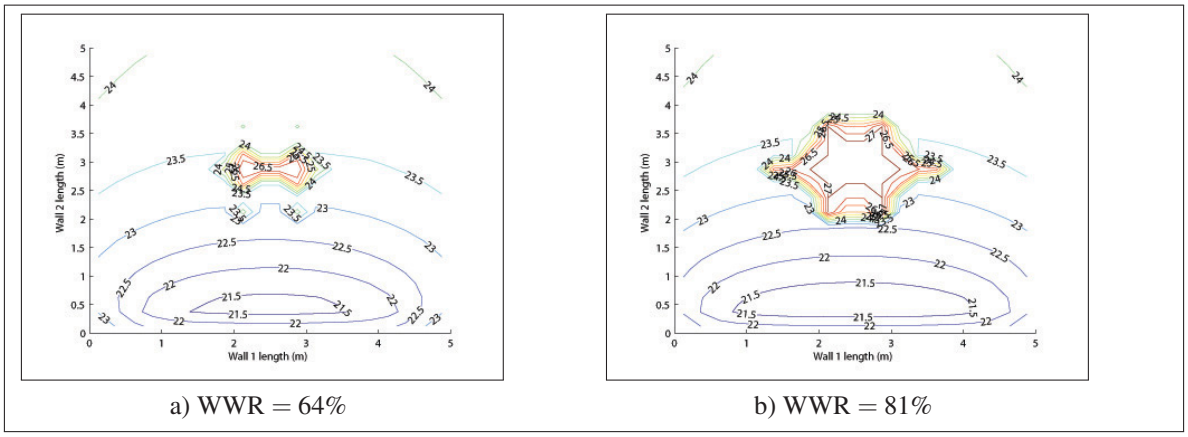

a) WWR = 64%

b) WWR = 81%

Figure 5.9 Floor temperatures for different window to wall ratio and for the mVH

27°C, thus the only way to increase the floor heating once a maximum temperature is achieved is with a larger surface area.

Figure 5.10 shows the thermal comfort for a WWR of 81% and for the center thermal comfort volume slice parallel to wall 1 (Depth= 2.5m).

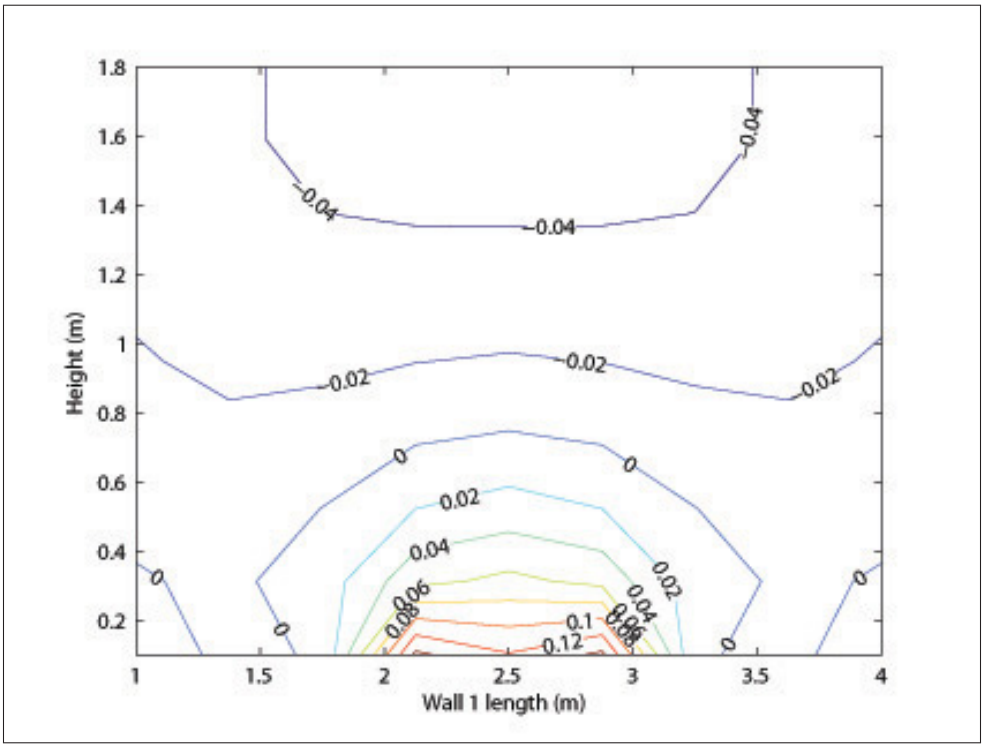

Figure 5.10 Thermal comfort at the center of the room for a WWR=81%

The thermal comfort is shown to locally increase near the floor. This increase in *PMV* is within the range of thermal comfort $-0.5 < PMV < 0.5$.

5.2.1.2 Room depth

The effect of the room depth is presented in Figure 5.11. In this Figure, the *RHDS* of the room along with the MVH and mVH energy consumption per floor area are reported as a function of room depth.

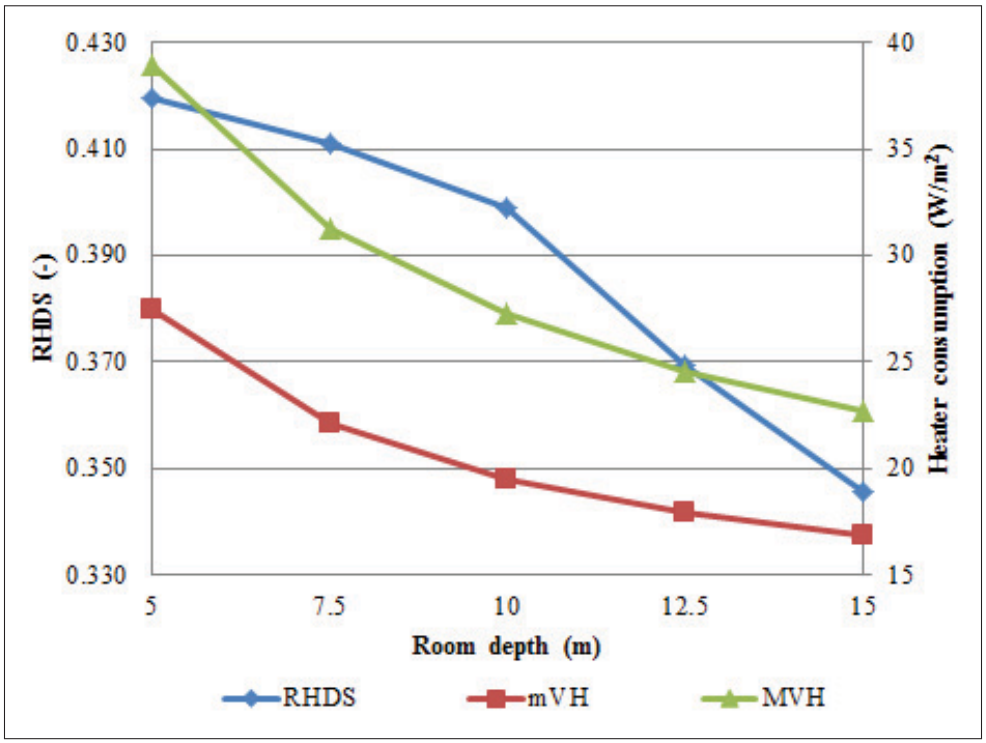

Figure 5.11 Room heat distribution sensibility (RHDS) and heat consumption as a function of room depth

From the results, it can be seen that a deep room is more energy efficient than a shallow room for both the mVH and MVH.

A negative variation of the *RHDS* of 3.9% can be observed in Figure 5.11, when the room depth is increased to 15m, three times the base case depth. This is a significant variation when compared to the WWR.

The air temperatures for mVH and MVH and for different room depths are shown in Figure 5.12.

It can be seen from this figure that the air temperature for the MVH slightly increases, but it still remains relatively stable while the air temperature for the mVH decreases with an increase in room depth.

Figure 5.13 shows the window temperature for the MVH and for different room depths.

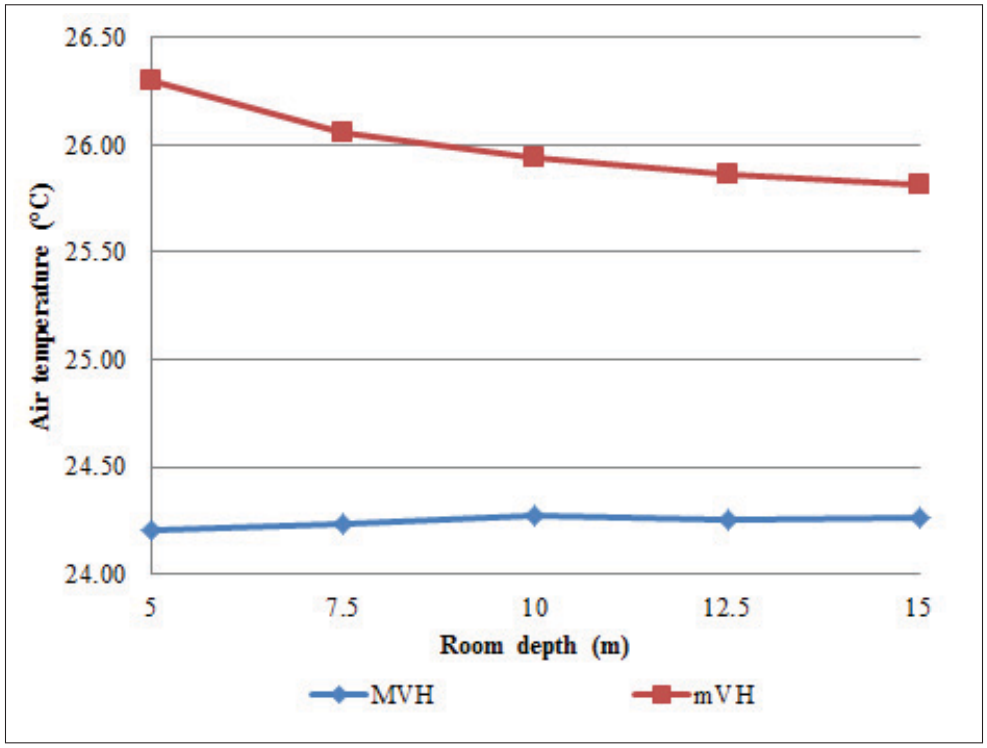

Figure 5.12 MVH and mVH air temperature as a function of room depth

In Figure 5.13, the maximum window temperatures increase with the room depth when comparing depths of 7.5m and 10m. The average window temperature increases from 46.5°C to 51.1°C between these two depths. As a consequence, the thermal comfort stratification is increased near the window.

Figure 5.14 shows the thermal comfort distribution at a distance of 1m from wall 1 for increasing room depths.On Figure 5.14, the PMV is shown not to surpass the comfort limits of $|PMV_i| < 0.5$; however, at a depth of 10m, the thermal comfort peak value of $PMV = 0.5$ is achieved.

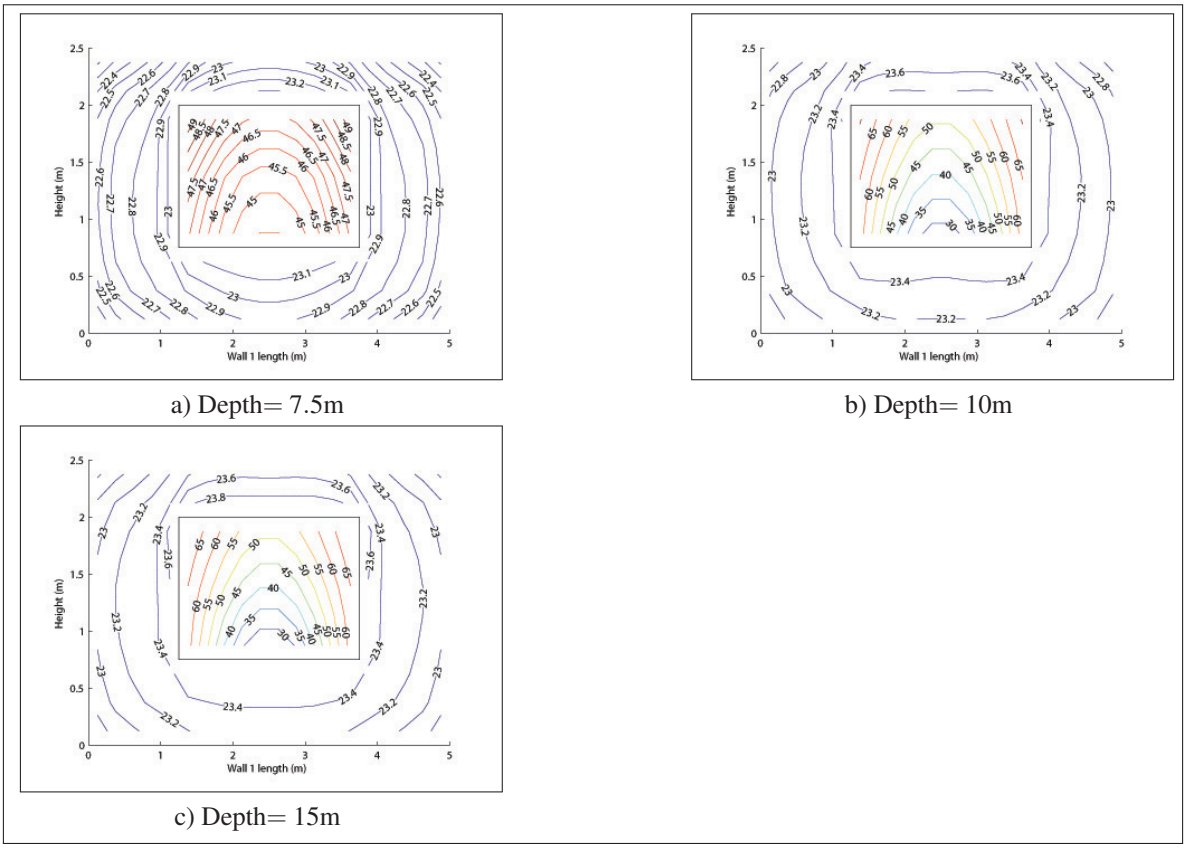

a) Depth= 7.5m

b) Depth= 10m

c) Depth= 15m

Figure 5.13 Wall 1 temperatures for three room depths, 7.5, 10, and 15 m, and for the MVH

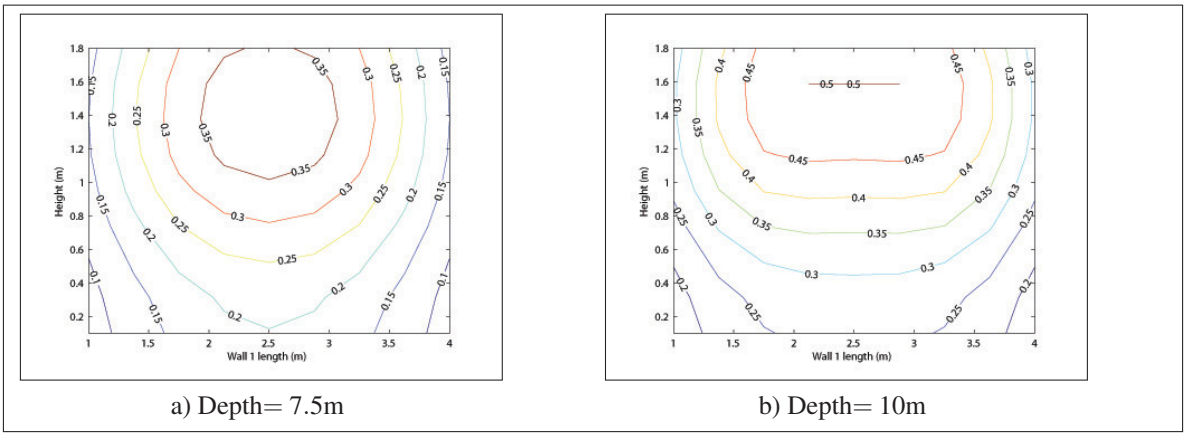

a) Depth= 7.5m

b) Depth= 10m

Figure 5.14 Thermal comfort (*PMV*) at 1m offset from wall 1 and for different depths of 7.5 and 10 m

5.2.1.3 Room height

In investigating the effect of room height, it is important to note that the thermal comfort volume has a constant height; hence, when the height of the room increases, the ceiling gets further away from the thermal comfort volume.

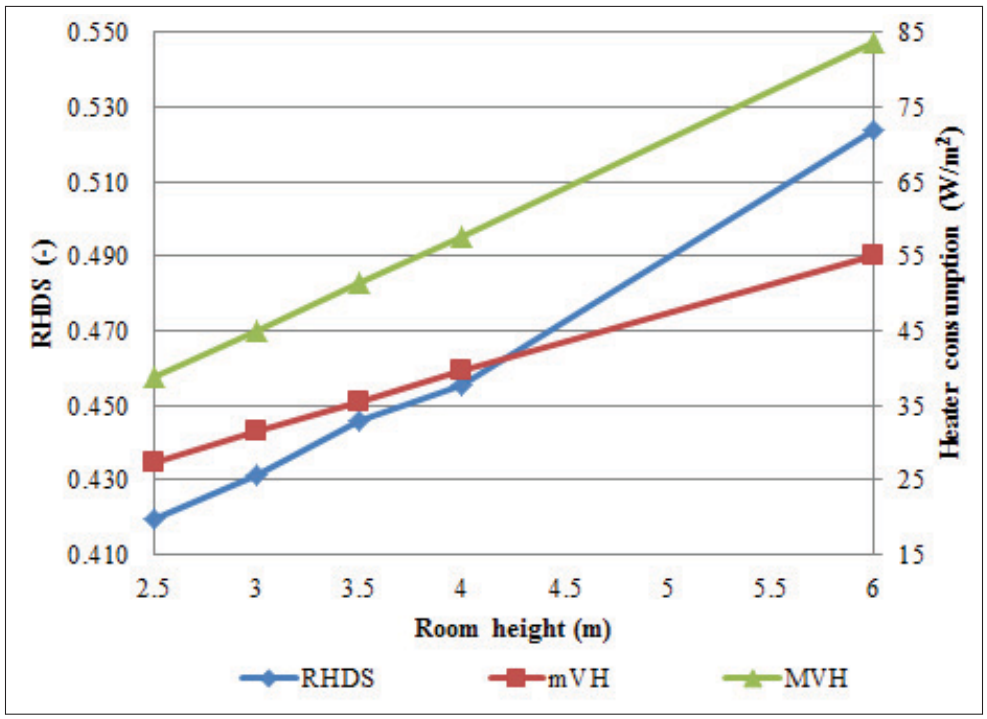

Figure 5.15 Room heat distribution sensibility (RHDS) and heater consumption as a function of the room height

Figure 5.15 shows the *RHDS* and the energy consumption per floor area of the mVH and MVH as a function of the room height. From Figure 5.15, it is reported that taller rooms consume more energy per floor area for both the mVH and the MVH.

An increase in room height of 240% led to an increase in *RHDS* of 4.8%. At 6m ceilings, the tallest tested room, the maximum $RHDS = 0.344$ was calculated.

For the MVH, similarly to the base case, the window was the only heated room element for all tested heights. In investigating the mVH, the air volume is heated except when a room height of 6m is considered. In this case, floor heating also contributes to providing thermal comfort.

For a room height of 4 m, the power is entirely distributed to the air volume. For a room height of 6 m, 11.9% of the power is distributed to the floor whereas the remainder is transmitted to the air volume. Although the floor is heated for a room height of 6m, the air volume is still the predominant element of the room that is heated.

Figure 5.16 shows the air temperature of the mVH and MVH as a function of room height.

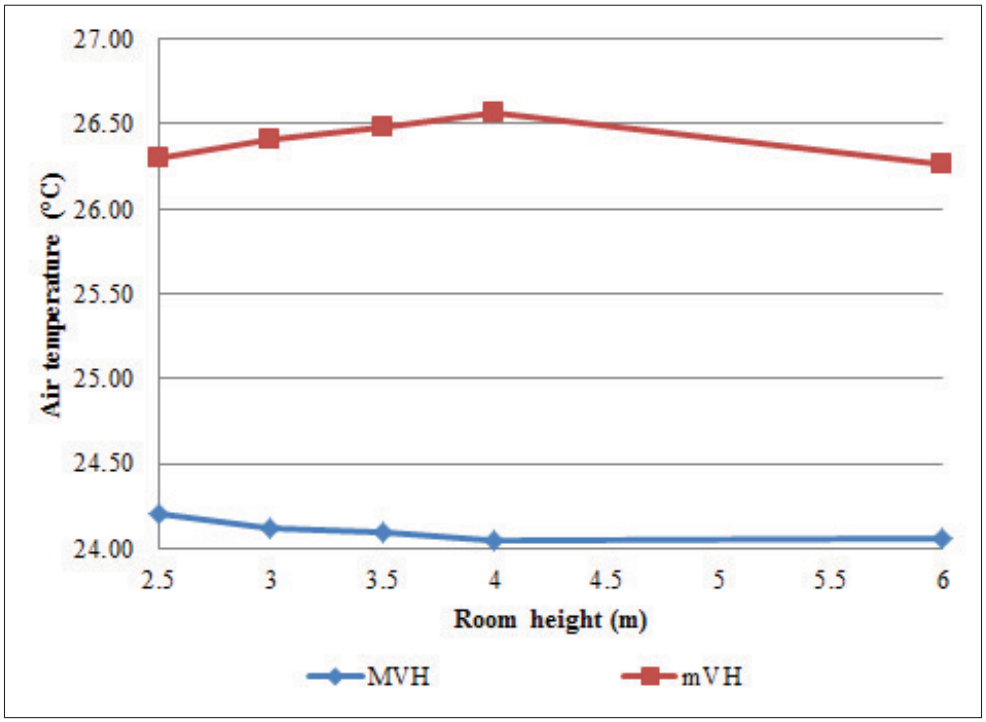

Figure 5.16 Room air temperatures for the mVH and MVH

Figure 5.16 shows the air temperature of the mVH and MVH as a function of room height. Results show that the room temperature for the mVH increases with the room height except for the last tested height where it decreases. The decrease in air temperature is related to the

increase in floor heating. For tall rooms, it becomes more effective to heat the floor instead of the air volume.

The temperature distribution on wall 1 for the MVH and for different heights is presented in Figure **??**.

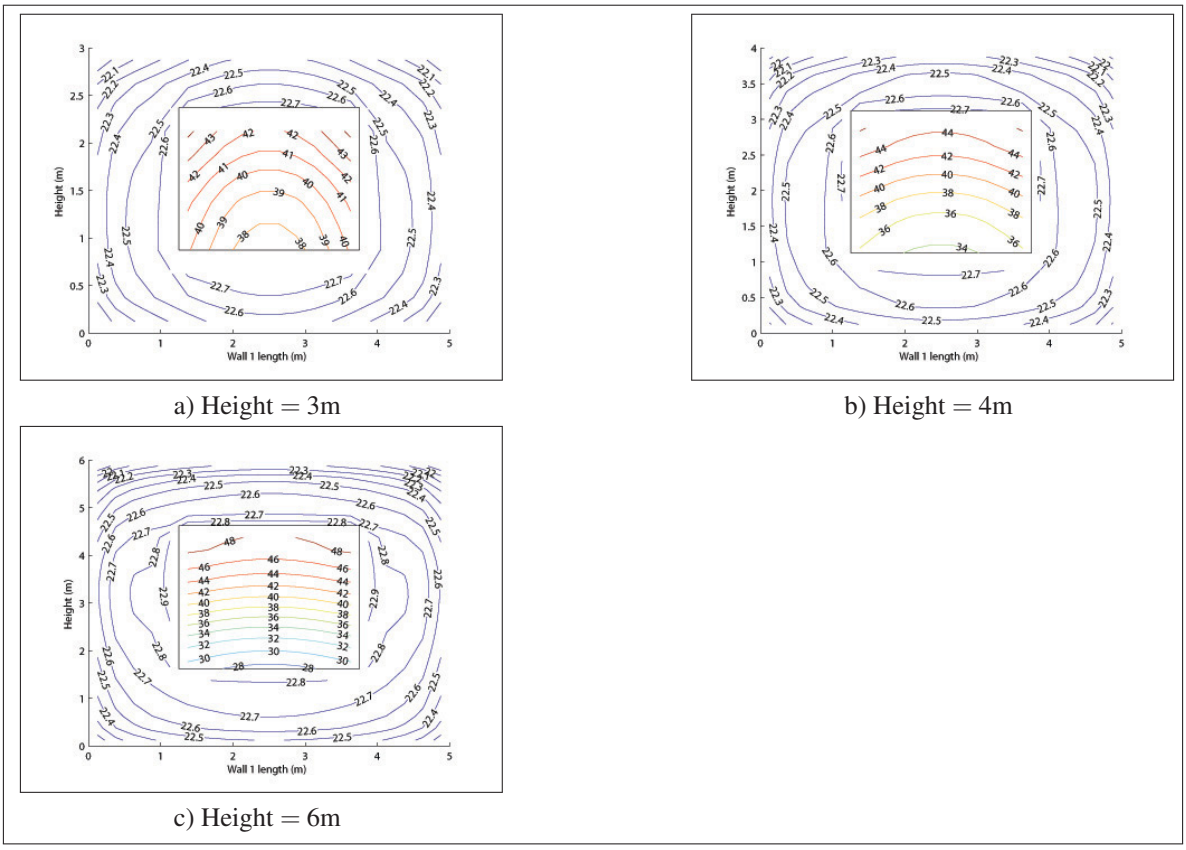

a) Height = 3m

b) Height = 4m

c) Height = 6m

Figure 5.17 Wall 1 temperatures for the MVH and for different heights

In Figure **??**, the effect of heating far from the thermal comfort volume is apparent from a view factor perspective. As the height of the room increases, the top of the window is heated.

The upper central part of the thermal comfort volume is the highest *PMV* as seen in Figure **??**. The peak *PMV* location is higher as the height of the room is increased.

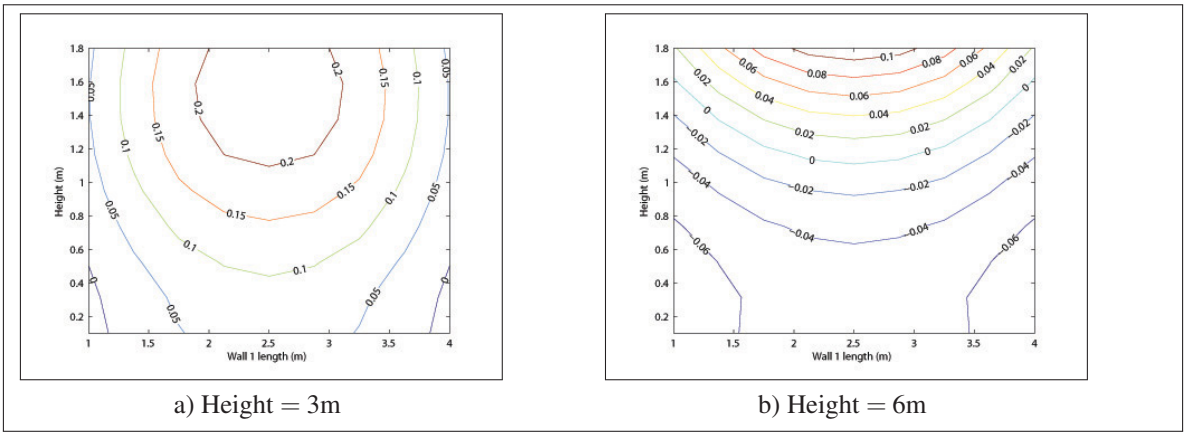

a) Height = 3m b) Height = 6m

Figure 5.18 Thermal comfort (*PMV*) at 1m offset from wall 1 for MVH and for different room heights of 3 and 6 m

The floor was also heated for the mVH when considering the case of a room having a 6m tall ceiling. This floor temperature profile is presented in Figure 5.19, which shows that the center of the floor is heated up to a maximum specified temperature of 27°C.

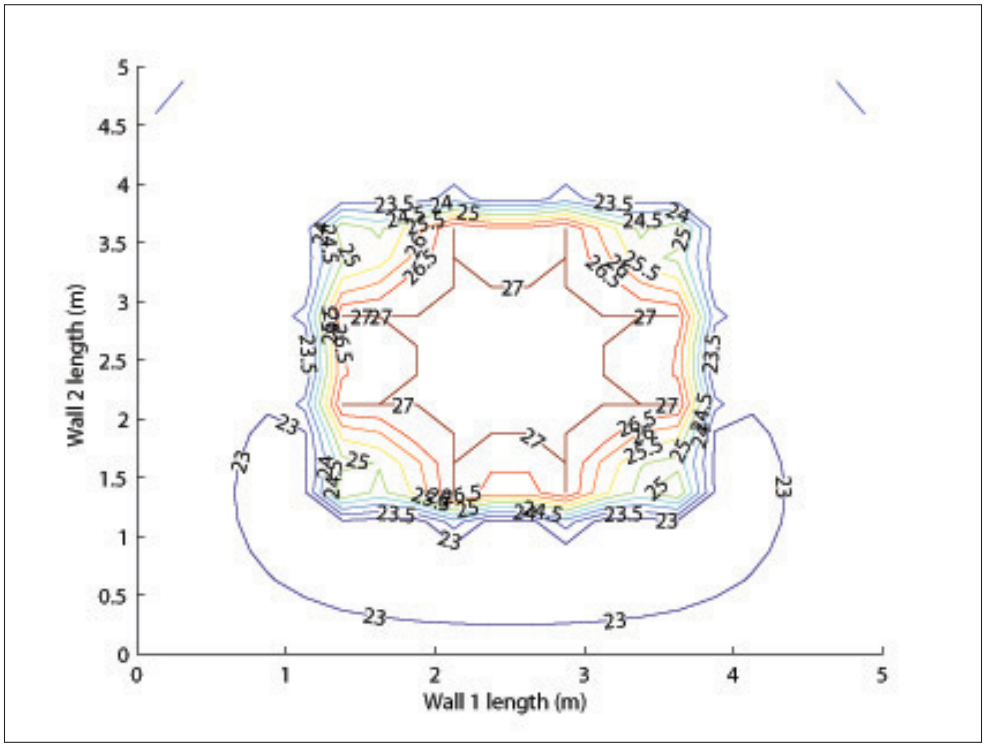

Figure 5.19 Floor temperature for the mVH with a room height of 6m

Floor heating modifies the thermal comfort distribution. Figure 5.20 shows a thermal comfort slice at the center of the volume that is parallel to wall 1.

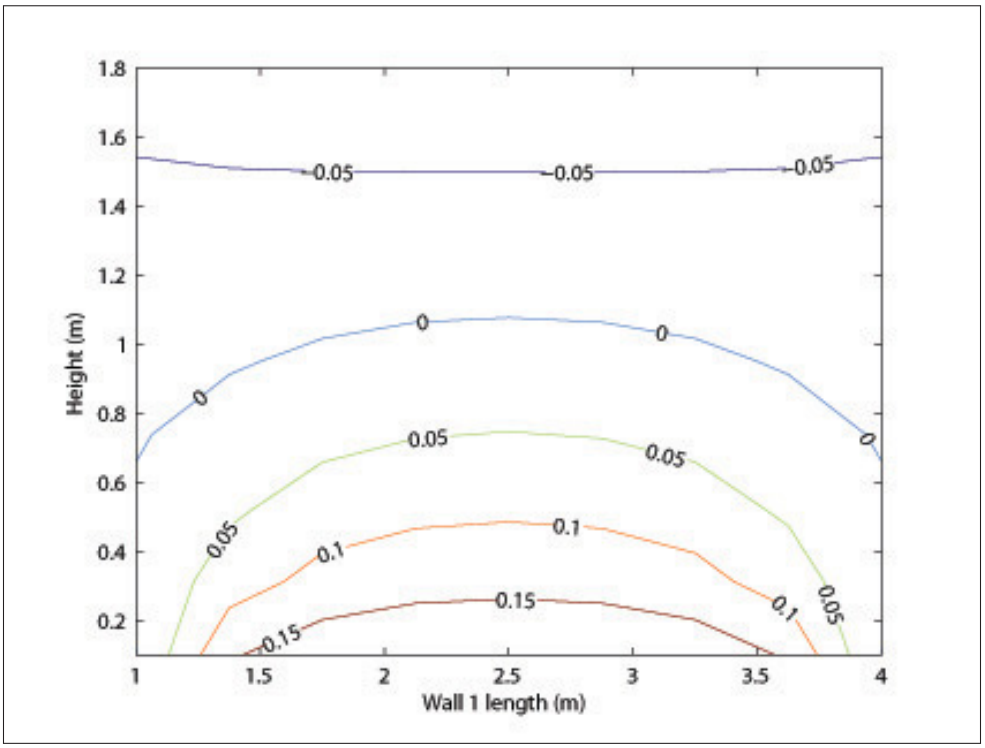

Figure 5.20 Thermal comfort volume slice at the center of the room (parallel to wall 1) and for the mVH

From the figure, the effect of floor heating is apparent. Close to the floor, the *PMV* increases locally, but not to a level where it is thermally uncomfortable.

The room height clearly has an influence on the *RHDS* and can have some influence, particularly for very high ceilings, on the mVH heat distribution.

5.2.2 Effect of changing R-value

Results for variations in thermal parameters are now presented in this section. These include changes in wall 1 insulation, wall 2, 3 and 4 insulation, floor insulation, ceiling insulation, window pane number, air exchange rates, and outdoor temperature.

5.2.2.1 Wall 1 insulation

In Figure 5.21 the virtual heater consumptions per floor area and the *RHDS* is shown as a function of wall 1 insulation.

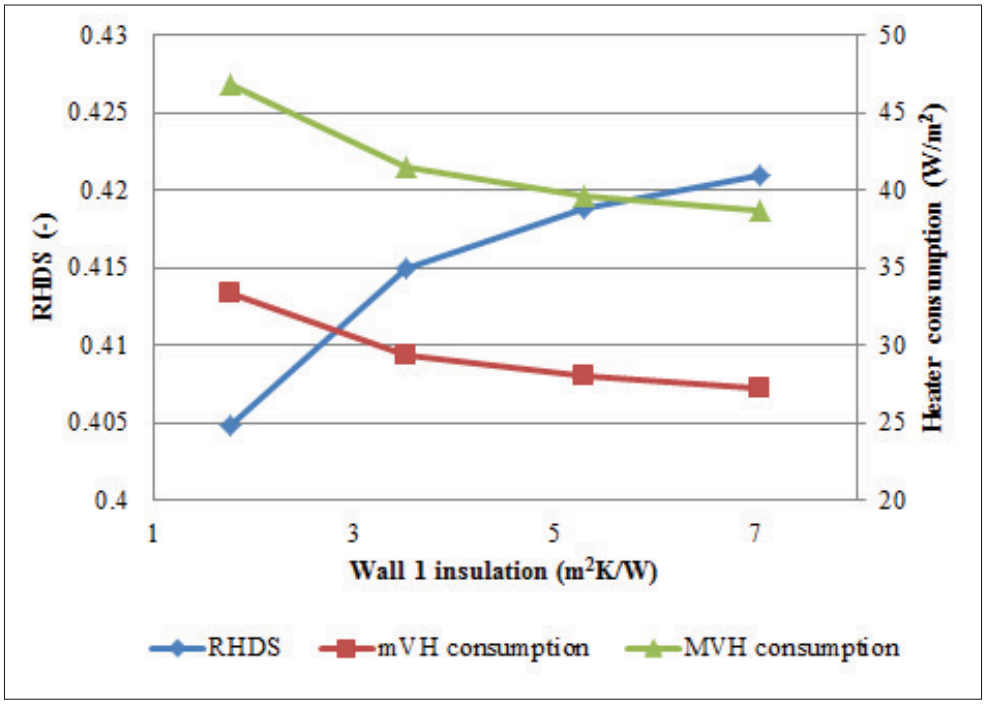

Figure 5.21 RHDS and energy consumption of virtual heaters as a function of wall 1 insulation

On the primary (left) axis, the *RHDS* increases from 0.405 to 0.421 which is a 4% increase in *RHDS* with a 300% increase in wall 1 insulation. On the other hand, the gradient of *RHDS* decreases as wall 1 insulation increases. The *RHDS* is thus more sensitive to lower values of wall 1 insulation. The 4% increase in *RHDS* is small considering the 300% increase in insulation level. Wall 1 could therefore be considered to have a marginal effect on the *RHDS* for this particular room.

On the secondary (right) axis, the virtual heater power consumptions are shown. As expected, an inverse relation is observed between heat consumption and wall 1 insulation. Clearly, adding insulation decreases the energy consumption of the room while thermal comfort is maintained.

The heat distribution for all tested wall 1 insulations follow a similar pattern to the base case. The air temperature for the mVH and MVH is presented in Figure 5.22.

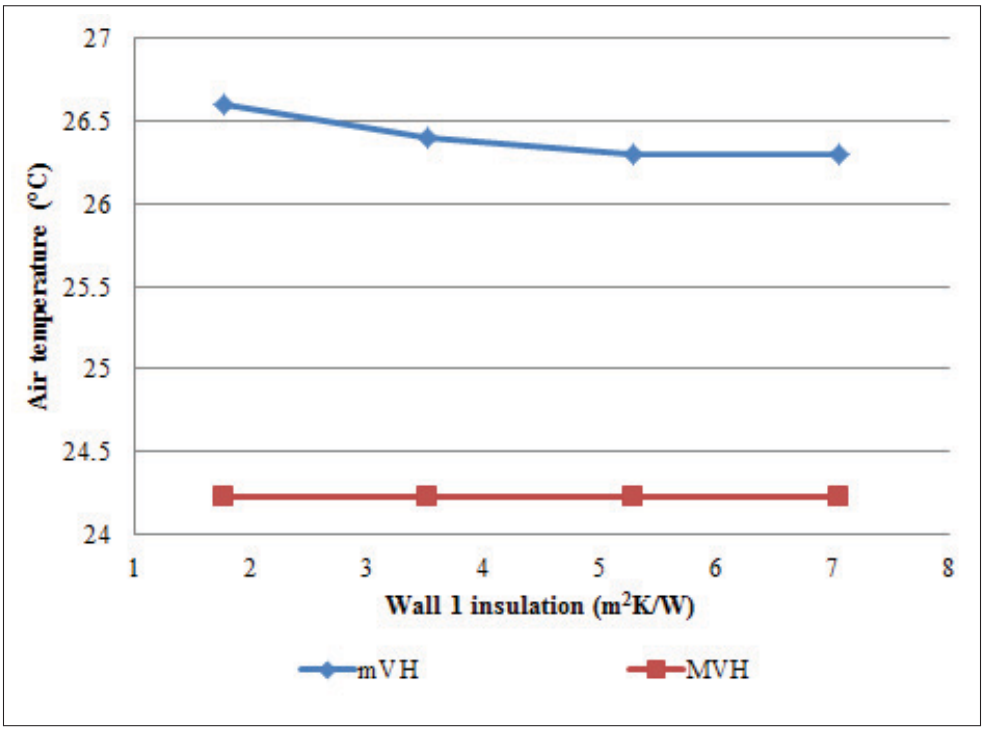

Figure 5.22 Room air temperatures for the mVH and MVH as a function of wall 1 insulation

The MVH temperature remains constant at 24.2°C as the heat is distributed entirely on the window. The mVH temperature slightly decreases as the level of insulation increases. This is expected as the increase in wall insulation yield's a warmer wall 1, hence increasing the mean radiant temperature. The air temperature can then be decreased as to maintain thermal comfort. A small decrease of 0.3°C was observed for the mVH.

The wall 1 temperature profile for the MVH is shown for different insulation levels (R_{wall1}) in Figure 5.23.

The window temperature decreases as the wall 1 insulation increases. This result is coherent with the consumption results shown in Figure 5.21. The higher insulation increases the mean

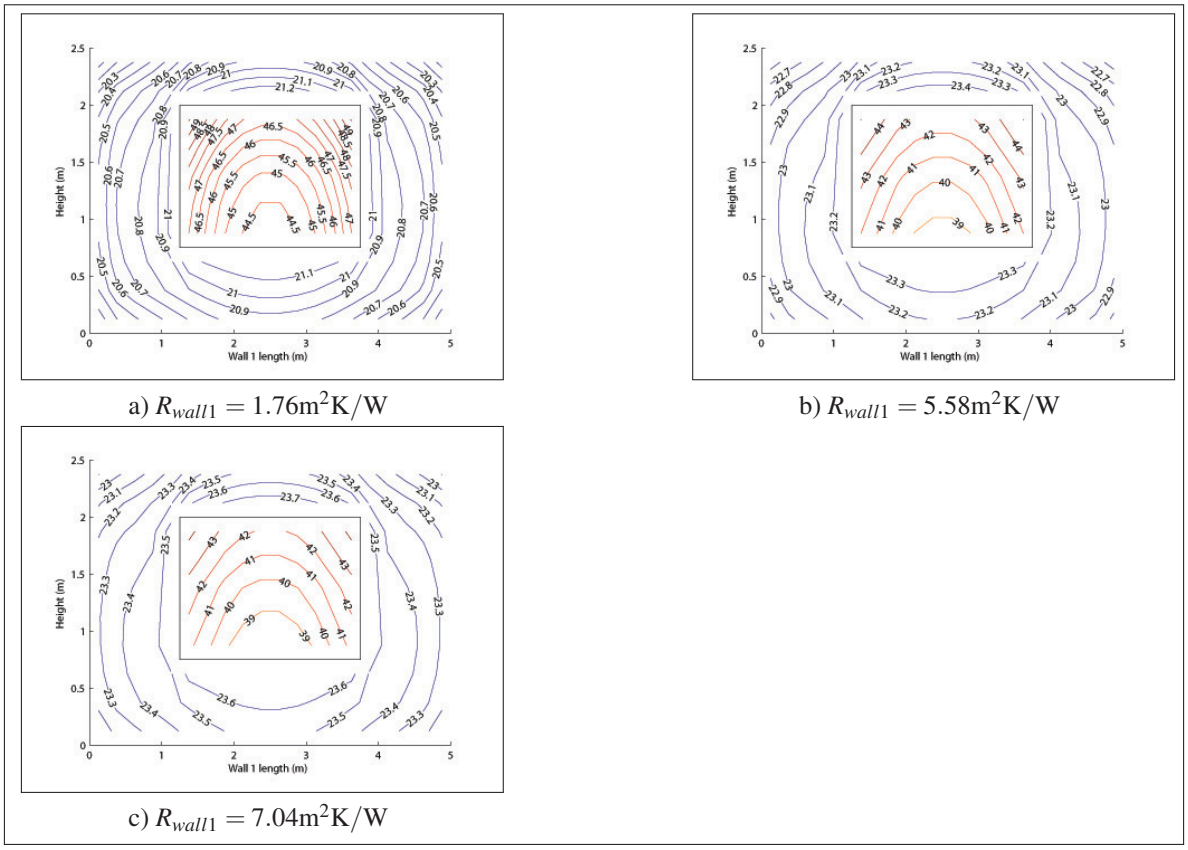

a) $R_{wall1} = 1.76 \mathrm{m^2K/W}$

b) $R_{wall1} = 5.58 \mathrm{m^2K/W}$

c) $R_{wall1} = 7.04 \mathrm{m^2K/W}$

Figure 5.23 Wall 1 temperatures for the MVH and for different wall 1 insulations

radiant temperature. The window temperature must not be as high to maintain a comfortable mean radiant temperature on the thermal comfort volume.

Based on these results, wall 1 insulation has a small effect on the optimal heat distribution and the *RHDS*.

5.2.2.2 Wall 2, 3 and 4 insulation

The results for wall 2, 3 and 4 insulation are now discussed. Figure 5.24 shows the *RHDS* (primary axis) and the mVH and MVH consumption per floor area (secondary axis) as a function of the indoor wall insulation.

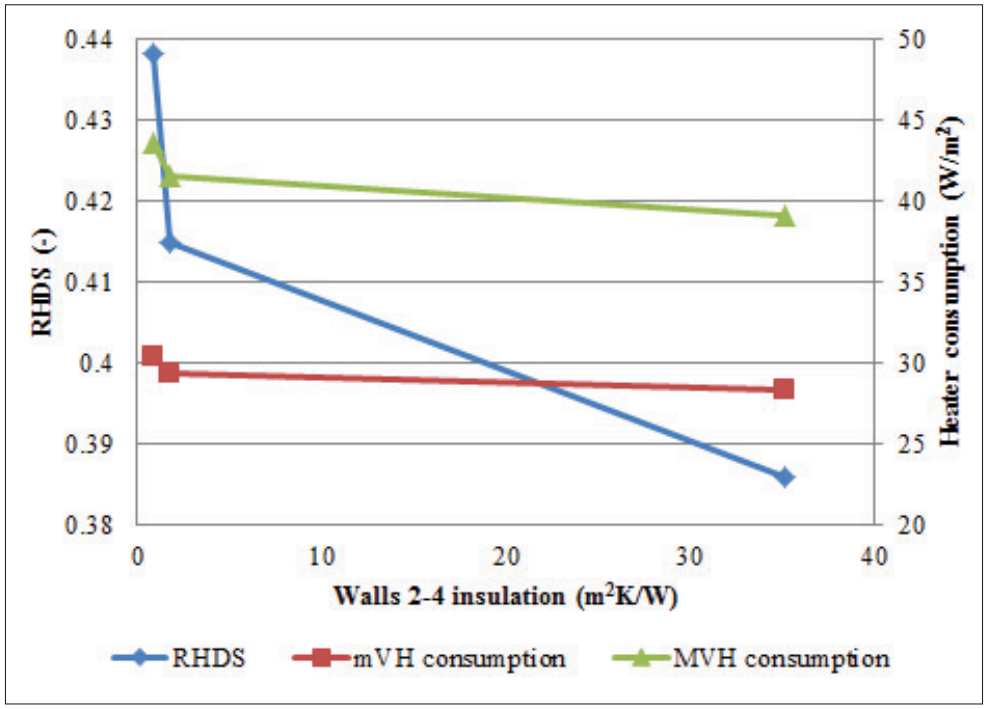

Figure 5.24 RHDS and energy consumption of virtual heaters as a function of walls 2 to 4 insulations

It can be seen from Figure 5.24 that the heat consumption decreases for both the mVH and MVH when the indoor wall insulation is increased. The *RHDS* also asymptotically decreases with a total variation of 12% when the insulation increases by 3900%. The final insulation point($R = 35.22\text{m}^2\text{K/W}$) is considered as a adiabatic wall in order to simulate adjacent occupied and heated rooms.

The air temperature for the mVH and MVH is shown on Figure 5.25.

There is no variation of air temperature for the MVH since the equilibrium air temperature is barely affected by a change in indoor insulation. The equilibrium point remains unchanged because the majority of the air volume heat loss is through the air exchange and the convection with the outdoor facing walls. As for the mVH, a slight decrease of 0.2°C in air temperature is observed. The decrease is likely because of the warmer wall, due to higher insulation, provides

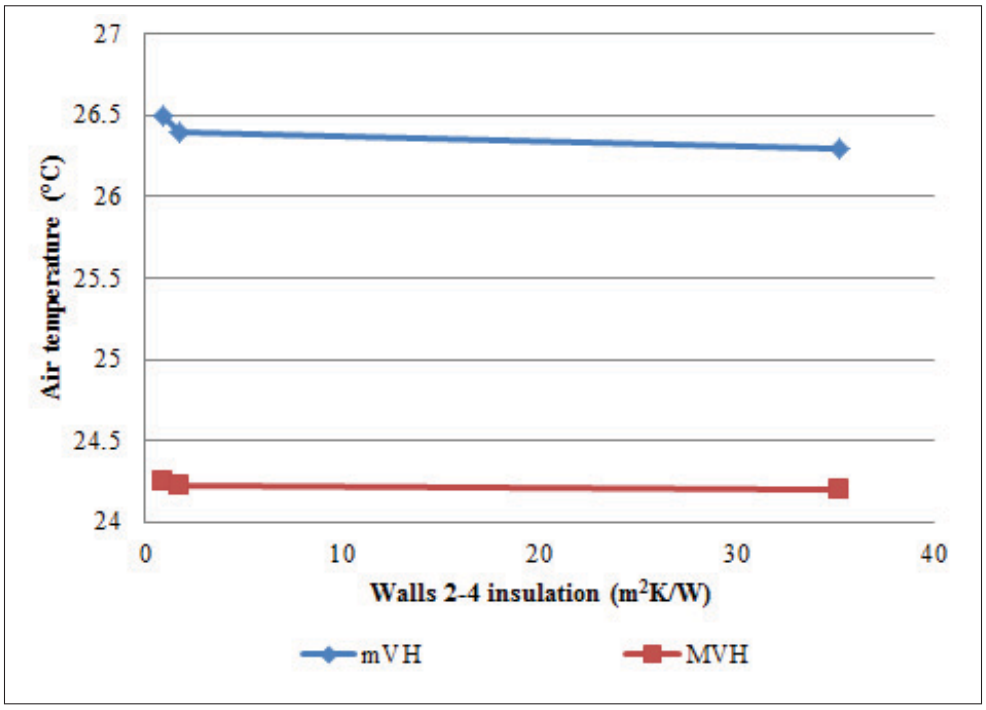

Figure 5.25 Room air temperatures for the mVH and MVH as a function of walls 2 to 4 insulations

a higher radiant temperature. The air temperature must then not be set to high to maintain thermal comfort.

A reduction in window temperature is also observed for the MVH as depicted in Figure 5.26. Its effect on the total energy consumption is greater than the effect of lowering air temperature, hence the reduction in *RHDS*.

In Figure 5.26, wall 1 temperature profile is presented. The temperature of the window is slightly lower when the insulation is increased. This is because wall 2-4 are warmer and thus there is less need to provide heat to the window.

The insulation of walls 2-4 only have a small effect on the *RHDS* when considering the tested insulation parameters. Also, the heat distribution also does not undergo dramatic changes with an increase in indoor wall insulation.

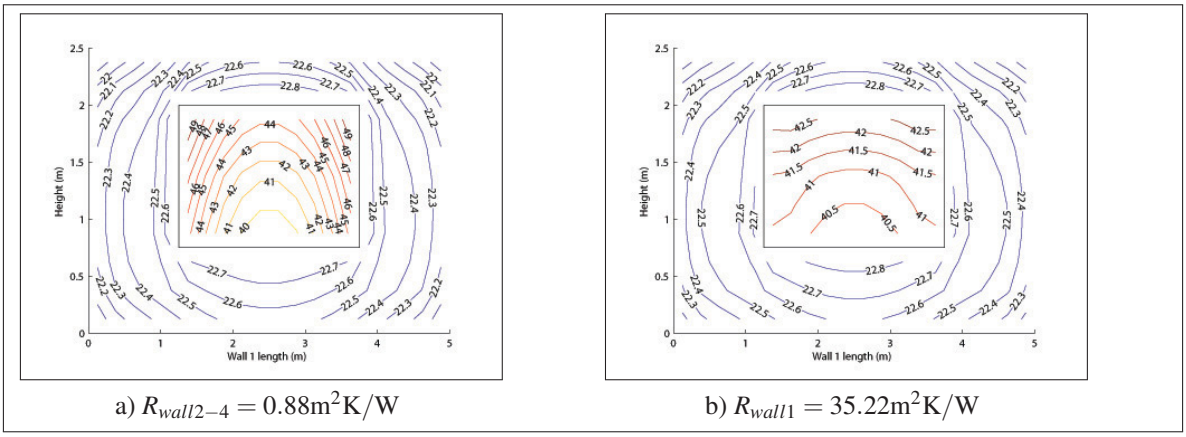

a) $R_{wall2-4} = 0.88\text{m}^2\text{K/W}$ b) $R_{wall1} = 35.22\text{m}^2\text{K/W}$

Figure 5.26 Wall 1 temperatures for the MVH and for different insulation of wall 2 to 4 insulations

5.2.2.3 Floor insulation

The variation in floor insulation is presented here. The *RHDS* along with the mVH and MVH consumptions are shown in Figure 5.27.

The energy consumption per floor area remains close to constant with respect to the floor insulation for both the mVH and MVH. Slight variations of the energy consumption are apparent through the *RHDS*. The value of *RHDS* varies from 0.419 to 0.412 (loss of 1.5%) with a 150% increase in floor insulation. Clearly, the floor insulation has little effect on the *RHDS* for this room.

The heat distribution when varying floor insulation is very similar to the base case. The air temperature as a function of floor insulation is presented in Figure 5.28.

In Figure 5.28, it is apparent that the optimal air temperature is not affected by floor insulation. Wall 1 temperatures for the MVH and for different floor insulations is presented in Figure 5.29.

From Figure 5.29, one can observe that there is no variation in the optimal heat distribution on wall 1, and particularly on the window.

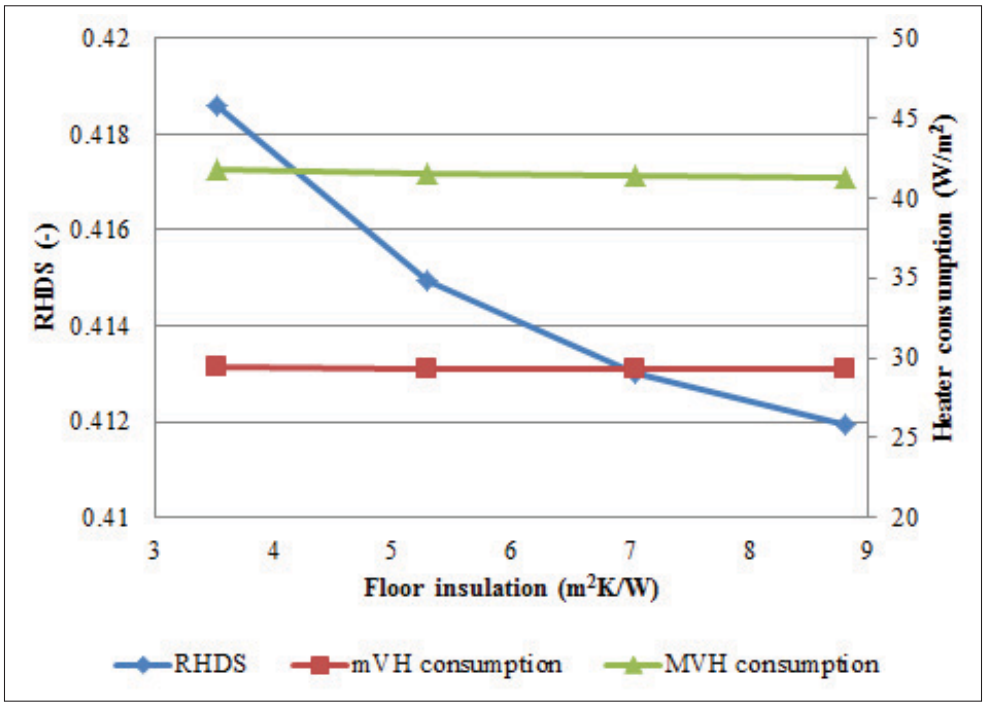

Figure 5.27 RHDS and energy consumption of virtual heaters as a function of floor insulation

The floor insulation has no effect on the optimal heat distribution and it barely affects the *RHDS*. The heat transfer through the floor surface does not sufficiently change as a function of its insulation; therefore, the heat distribution remains constant.

5.2.2.4 Ceiling insulation

The effect of the ceiling insulation is now investigated. While the ceiling has similar insulation levels as the floor, it is different because it is further away from the thermal comfort volume than the floor and it is exposed to a cold outdoor surface. The *RHDS* and energy consumptions per unit area are presented in Figure 5.30.

From Figure 5.30, it can be observed that the energy consumption decreases as ceiling insulation increases. This is not surprising given that the overall insulation of the room is increased. Figure 5.30 is also shows that the *RHDS* increases with ceiling insulation from 0.407 to 0.423

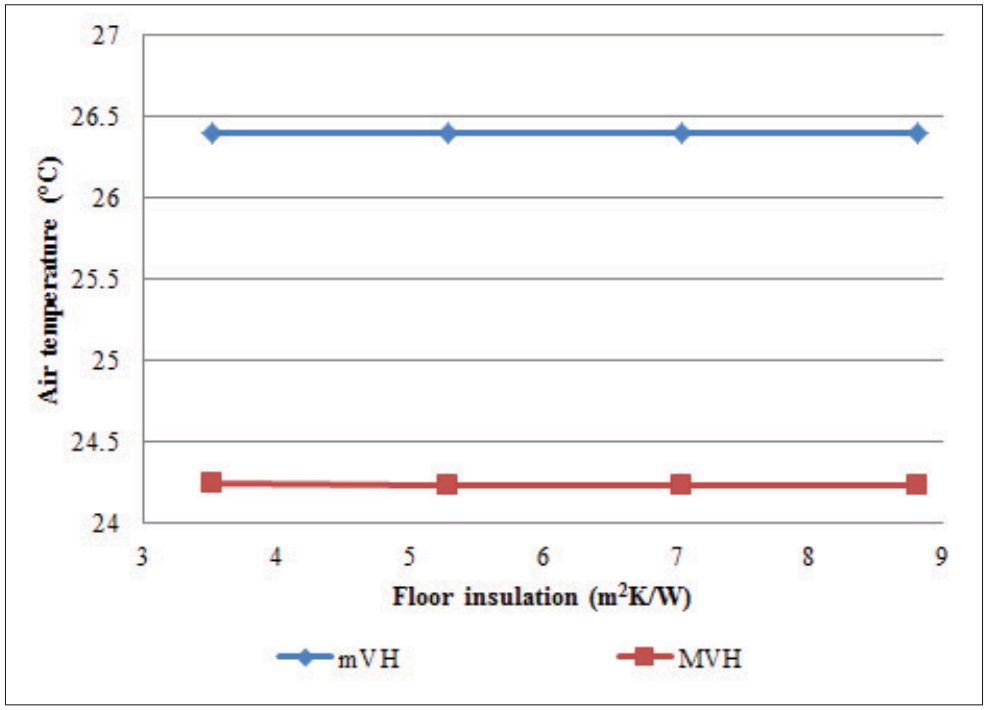

Figure 5.28 Room air temperatures for the mVH and MVH as a function of floor insulation

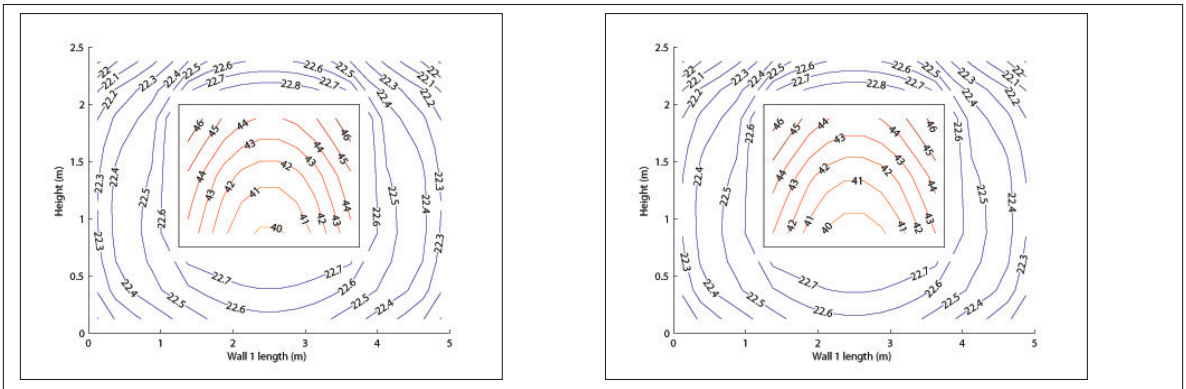

a) $R_{floor} = 3.52\text{m}^2\text{K/W}$ b) $R_{floor} = 8.81\text{m}^2\text{K/W}$

Figure 5.29 Wall 1 temperatures for the MVH and for different floor insulations (R_{floor})

(4% increase). The increased insulation leads to a higher ceiling temperature. In turn, this leads to the mVH having a lower air temperature, and the MVH, a lower window temperature.

The air temperature for both the mVH and MVH is presented in Figure 5.31.

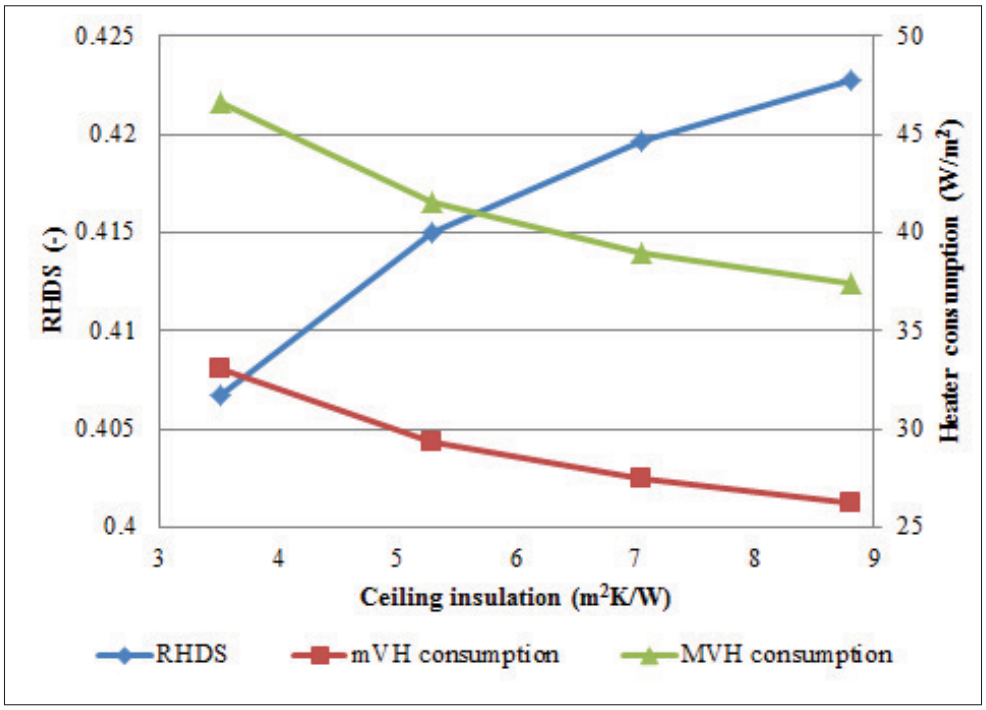

Figure 5.30 RHDS and energy consumption of virtual heaters as a function of ceiling insulation

In Figure 5.31, one notes that the air temperature for the MVH is constant while the air temperature for the mVH decreases as the ceiling insulation increases.

The wall 1 temperature for the MVH is shown in Figure 5.32.

The window temperature for the MVH decreases with an increase in ceiling insulation. This is not surprising as less power is needed to sustain thermal comfort when insulation is increased.

From the results, lowering the air temperature allows for other walls to have lower temperatures. Lowering the air temperature for the mVH is thus more significant, from a comfort and energy consumption point of view, rather than lowering the window temperature for the MVH, but it is still more efficient to heat the air volume and less efficient to heat the window. The *RHDS* is then increased given that the mVH energy consumption decreases faster than the MVH energy consumption. A similar behaviour is observed for the wall 1 insulation.

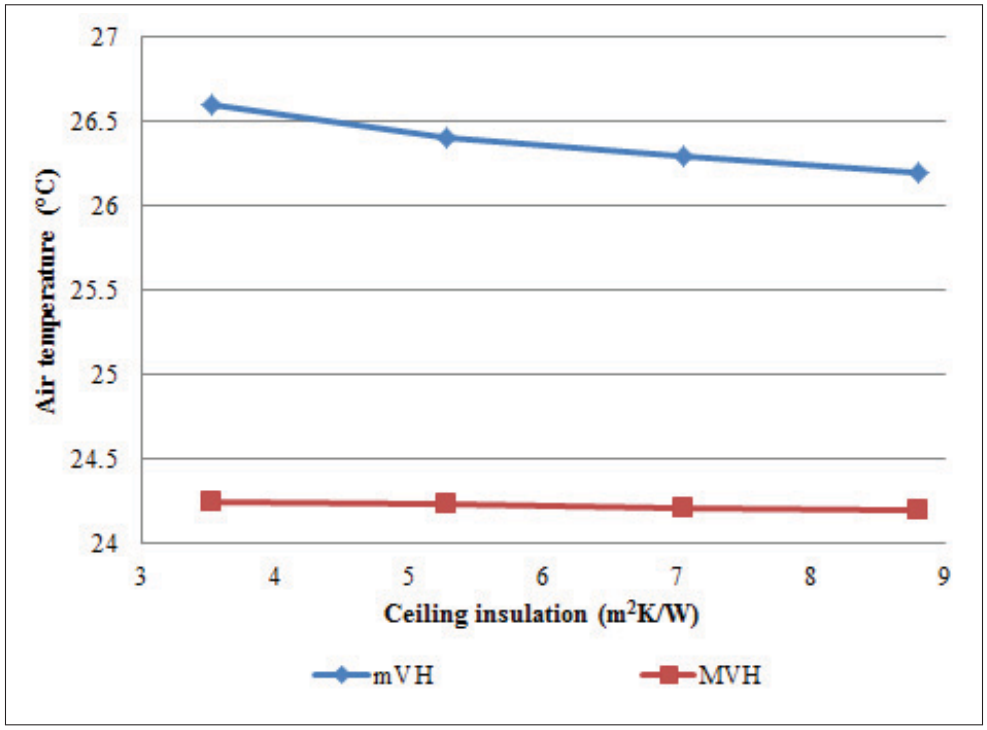

Figure 5.31 Room air temperatures for the mVH and MVH as a function of ceiling insulation

5.2.2.5 Number of window panes

The effect of the number of window panes, as simulated by a change in window thermal resistance, is now presented. In Figure 5.33, the *RHDS* along with the energy consumption per floor area for the mVH and MVH is shown.

As expected, both the mVH and MVH energy consumptions decrease with an increase in window R-value. However, the MVH is more affected with a 52% decrease compared to 29% decrease for the mVH when comparing single pane to triple pane windows. This is to be expected as the MVH heats the window; thus, an increase in window thermal resistance would have more of an effect.

There is a significant difference in *RHDS* between single ($0.158 m^2K/W$), double ($0.352 m^2K/W$) and triple ($0.564 m^2K/W$) pane windows. The value of *RHDS* decreases by 68% with a 250%

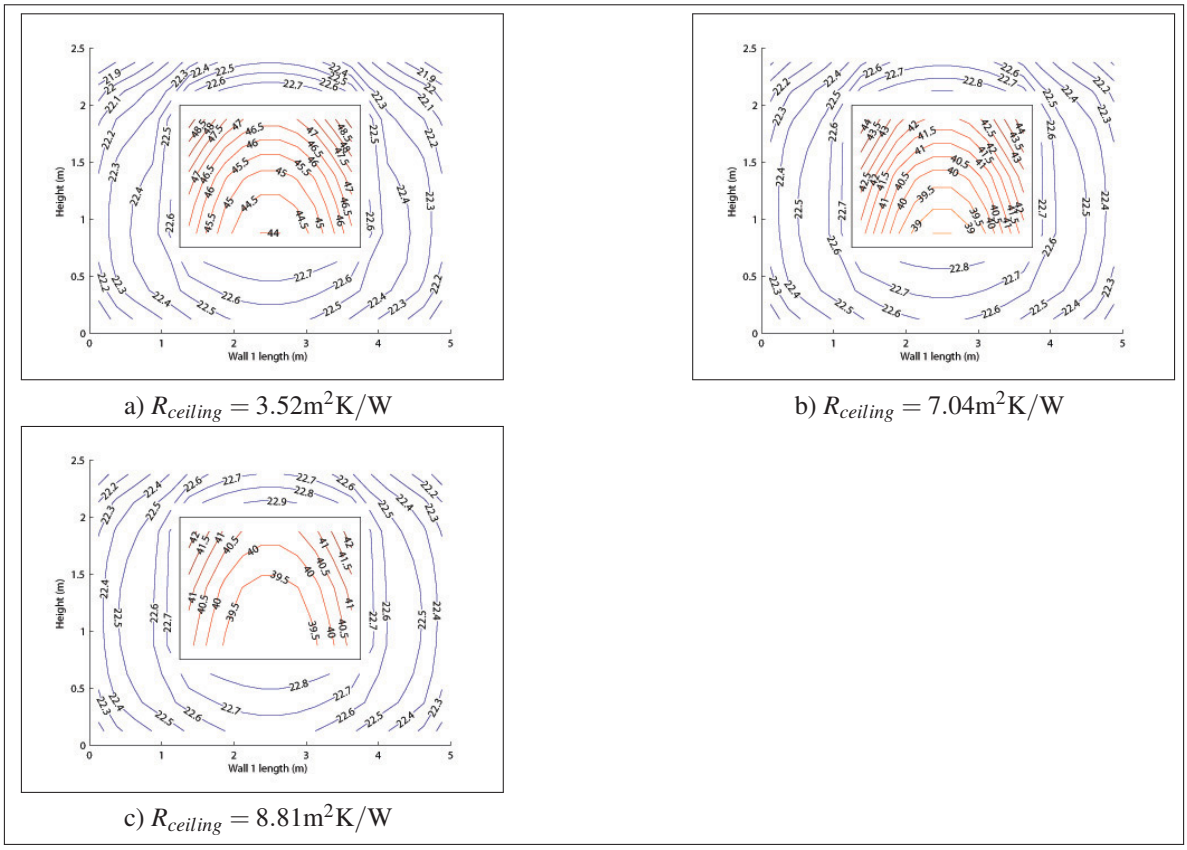

a) $R_{ceiling} = 3.52\text{m}^2\text{K/W}$

b) $R_{ceiling} = 7.04\text{m}^2\text{K/W}$

c) $R_{ceiling} = 8.81\text{m}^2\text{K/W}$

Figure 5.32 Wall 1 temperatures for the MVH and for different ceiling insulations

increase in window resistance. The $RHDS = 0.274$ for triple pane windows is the lowest observed value for all tested cases.

The decrease in *RHDS* can be attributed to a decrease in the effect of inefficient window heating that governs the MVH. By increasing the window resistance there are less opportunities for inefficient heat loss through the window; hence, the MVH energy consumption approaches that of the mVH.

Despite the drastic change in *RHDS* (0.87 to 0.28), the profile of the heat distribution remains similar to the base case. Figure 5.34 shows the air temperature inside the room as a function of the window resistance.

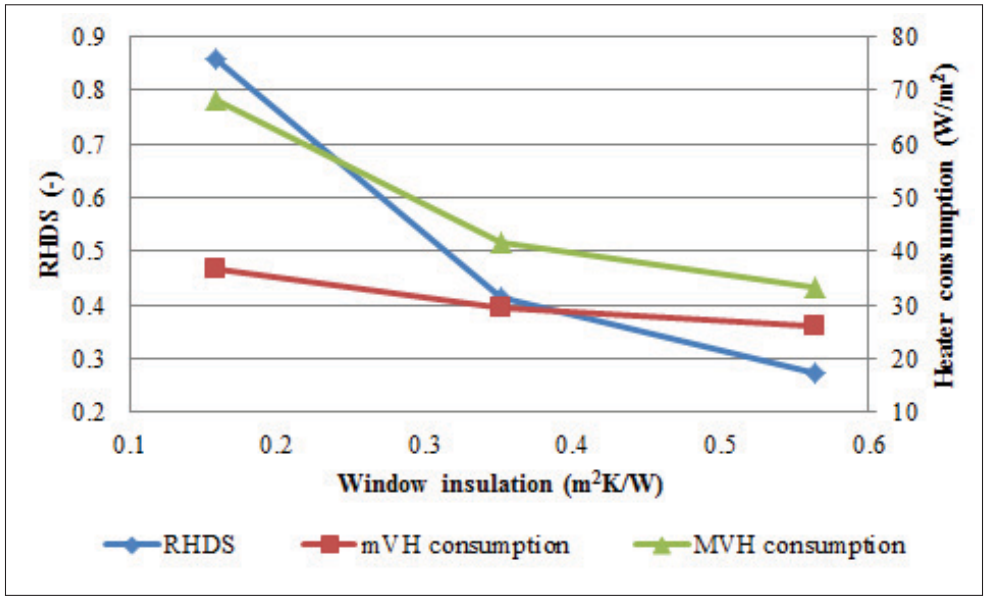

Figure 5.33 RHDS and energy consumption of virtual heaters as a function of window thermal resistance

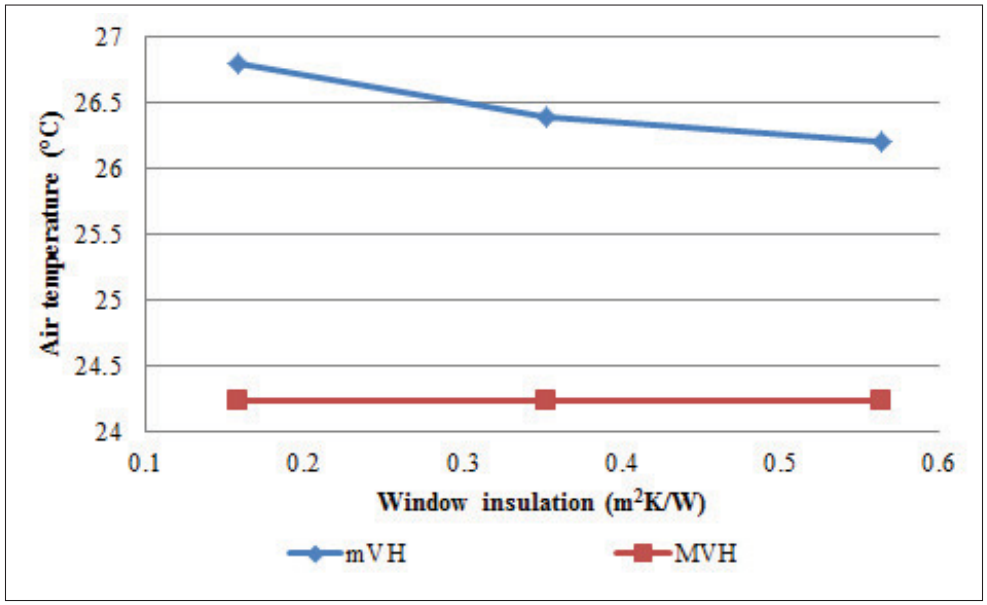

Figure 5.34 Room air temperatures for the mVH and MVH as a function of window thermal resistance

On Figure 5.34, it can be seen that the air temperature for the MVH does not change with an increase in window resistance. On the other hand, the air temperature for the mVH decreases

with an increase in window resistance. This is to be expected as a well-insulated window is warmer thus increasing the mean radiant temperature. To maintain thermal comfort, a lower air temperature setpoint is required.

The wall 1 temperatures for the MVH are shown in Figure 5.35.

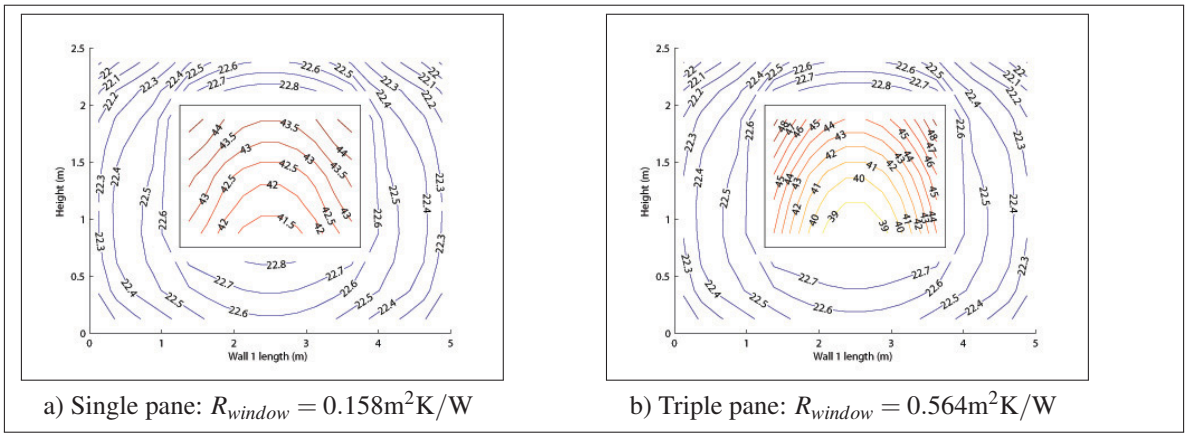

a) Single pane: $R_{window} = 0.158\text{m}^2\text{K/W}$ b) Triple pane: $R_{window} = 0.564\text{m}^2\text{K/W}$

Figure 5.35 Wall 1 temperatures for the MVH and for different window thermal resistance

Figure 5.35 shows that the increase in window thermal resistance leads to a MVH solution that has higher window temperature stratification. It is important to note here that two major effects govern the MVH. The first is that the MVH tends to heat the least insulated surface while the other is that the MVH tends to heat the surface where it will have the least effect on the mean radiant temperature. The increase in temperature stratification when window thermal resistance is increased is believed to be caused by a combination of these two predominant effects. As the window thermal resistance increases so does the potential of losing heat through its surface; however, the view factors in the room remain unchanged. It then becomes progressively more inefficient to heat surfaces that have low global view factors and more efficient to heat the entire window as window thermal resistance is increased. Since the other thermal parameters remain unchanged, a similar average temperature must still be achieved to maintain thermal comfort. The average temperature of the window thus remains relatively constant.

From a thermal comfort perspective, the increase in peak window temperature for the MVH leads to higher local discomfort. On the contrary, the increased window temperature for the mVH leads to lower local discomfort.

Therefore, it can be generally stated that increasing the window thermal resistance leads to better performance. Firstly, both the mVH and the MVH are lower; secondly, the *RHDS* is also lower thus reducing the risk of having an inefficient heat distribution.

5.2.2.6 Air exchange rate

Like the window, the air exchange can also be responsible for a significant amount of heat loss. The heat distribution results for the variation in the air exchange rate are now presented. Figure 5.36 shows the mVH and MVH energy consumptions per floor area and the *RHDS* for varying air exchange rates.

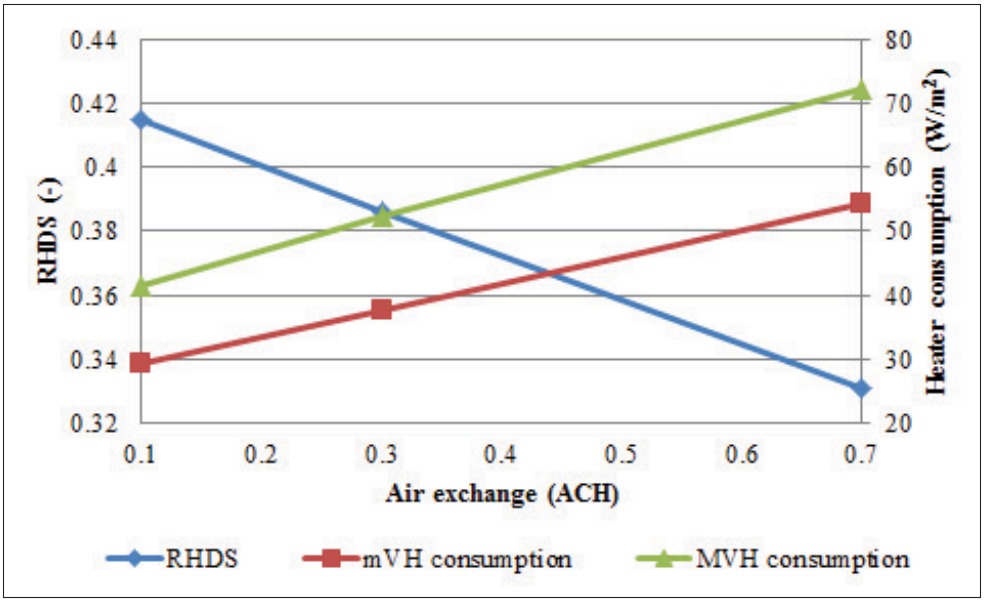

Figure 5.36 RHDS and energy consumption of virtual heaters as a function of the air exchange rate

Both the mVH and MVH energy consumption increase with the air exchange rate; however, the *RHDS* decreases with air exchange rate. The decrease in *RHDS* is due to the fact that the mVH heats primarily the air volume and thus will be more sensitive to an increase in the air exchange rate. Since the air exchange has a greater effect on the mVH, its increase will increase the mVH energy consumption faster than that of the MVH, thus the reduction in *RHDS*.

The heat distribution as a function of air exchange undergoes a drastic change for the mVH but not for the MVH. Figure 5.37 shows the air temperature for the mVH and MVH as a function of the air exchange rate.

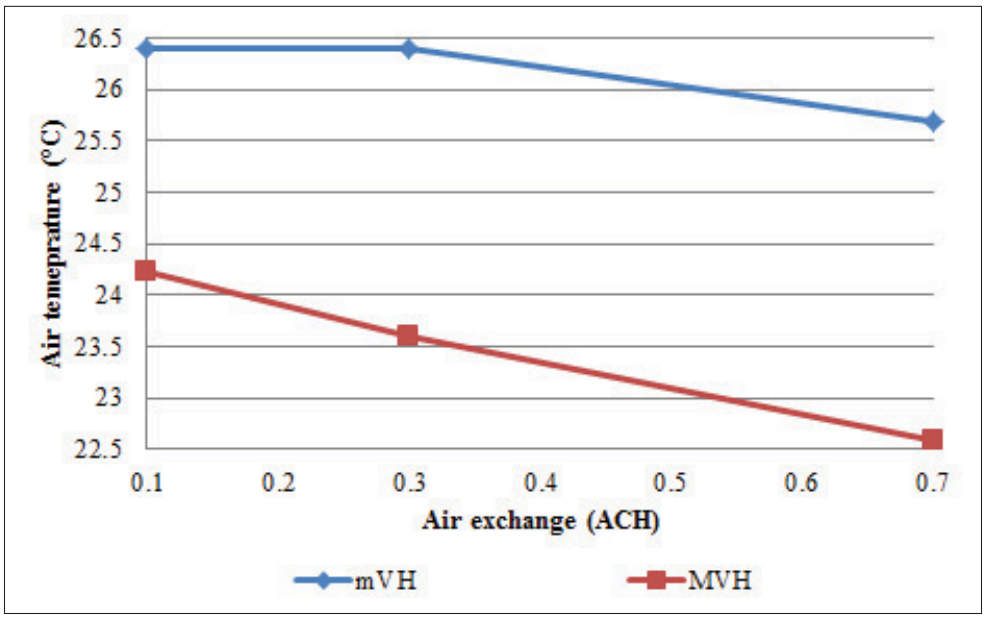

Figure 5.37 Room air temperatures for the mVH and MVH as a function of the air exchange rate

The air temperature for the MVH decreases with an increase in air exchange rate. This is to be expected since the MVH only heats the window and not the air volume. The equilibrium temperature for the air volume is decreased as the air exchange heat loss increases. As for the mVH, heating the air volume is progressively less efficient as the air exchange rate increases. Surface heating then appears in the mVH solution (see Figures 5.39 and 5.40). The split between surface heating and air volume heating is presented in Table 5.4.

Table 5.4 mVH heat distribution per heated room element as a function of air exchange rate

Air change (ACH)	air volume [%]	floor [%]	ceiling [%]
0.1	100	0	0
0.3	98.5	1.5	0
0.7	85.0	14.5	0.5

In the table above, the ceiling, floor and air volume percentage of total distributed power are shown. Clearly, a significant portion of heat is still given to the air volume. However, the floor and ceiling heating do take on more importance as the air exchange rate increases.

The wall 1 temperatures for the MVH are shown in Figure 5.38.

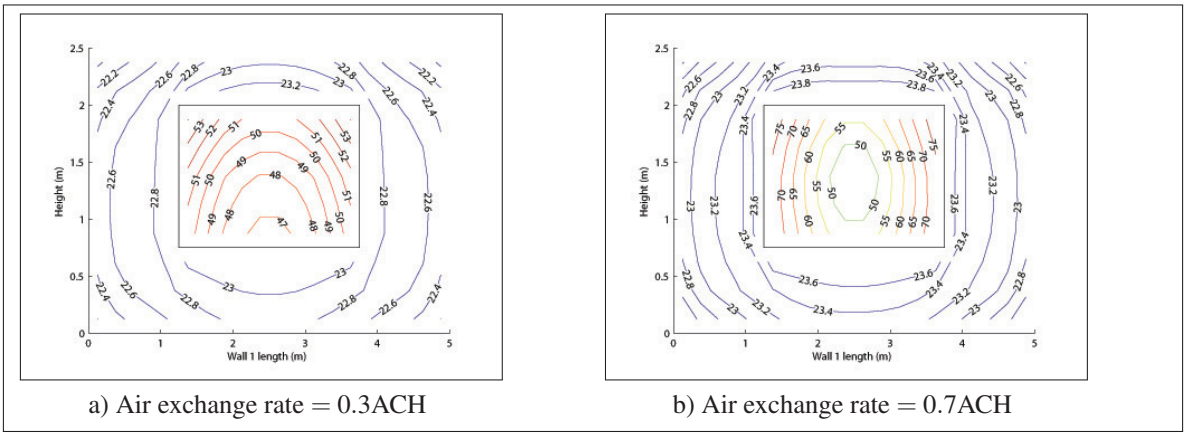

a) Air exchange rate = 0.3ACH b) Air exchange rate = 0.7ACH

Figure 5.38 Wall 1 temperatures for the MVH and for different air exchange rates

As the air temperature drops for the MVH, the window temperature is increased to maintain thermal comfort. This is shown in Figure 5.38 where the minimum window temperature increases by 3°C and the maximum temperature by 22°C when the air exchange rate increases from 0.3ACH to 0.7ACH.

As stated earlier, the mVH solution evolves from an air volume heating solution to a mixed surface-heating and air-volume heating when the air exchange rate is increased. The affected

surfaces are the floor and the ceiling. They are also the most insulated surfaces of the room. The floor temperature solution is presented in Figure 5.39 for two air exchange rates.

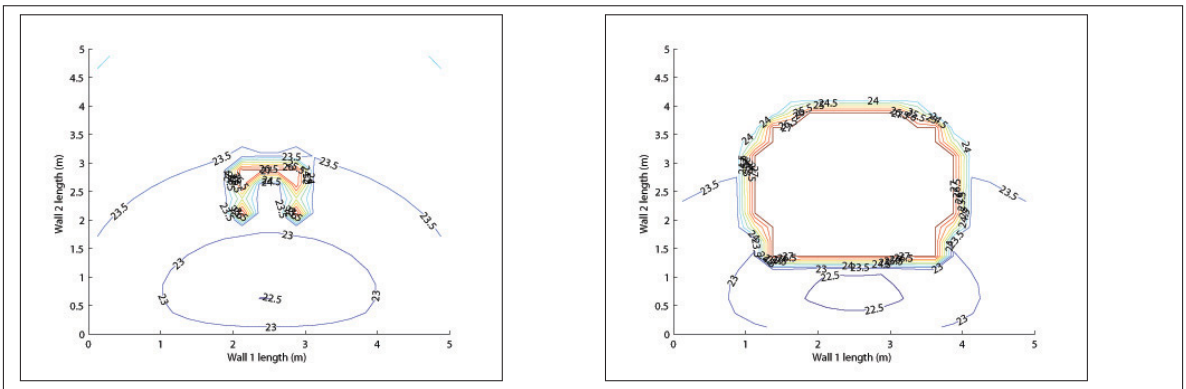

a) Air exchange rate = 0.3ACH

b) Air exchange rate = 0.7ACH

Figure 5.39 Floor temperatures for the mVH and for different air exchange rates

Figure 5.39 shows that some floor heating is present for an air exchange of 0.3ACH; however, at a high air exchange rate of 0.7ACH, almost the entire floor is heated to a maximum temperature of 27°C and the ceiling is also heated. Figure 5.40 shows the ceiling temperature for the mVH solution at an air exchange rate of 0.7ACH.

Figure 5.40 clearly indicates that the center of the ceiling is heated. The center is preferred here as it has the highest average view factor on the thermal comfort volume. It is the same reason that floor heating was preferred over ceiling heating. The floor has a higher view factor globally on the thermal comfort volume than the ceiling because it is closer to it. There are other arguments for floor heating instead of ceiling heating such as air temperature stratification, but the model used here does not take these effects into consideration.

As floor heating becomes more predominant, the thermal comfort inside the room undergoes some changes. Figure 5.41 shows two section cuts offset from wall 1 of the thermal comfort volume.

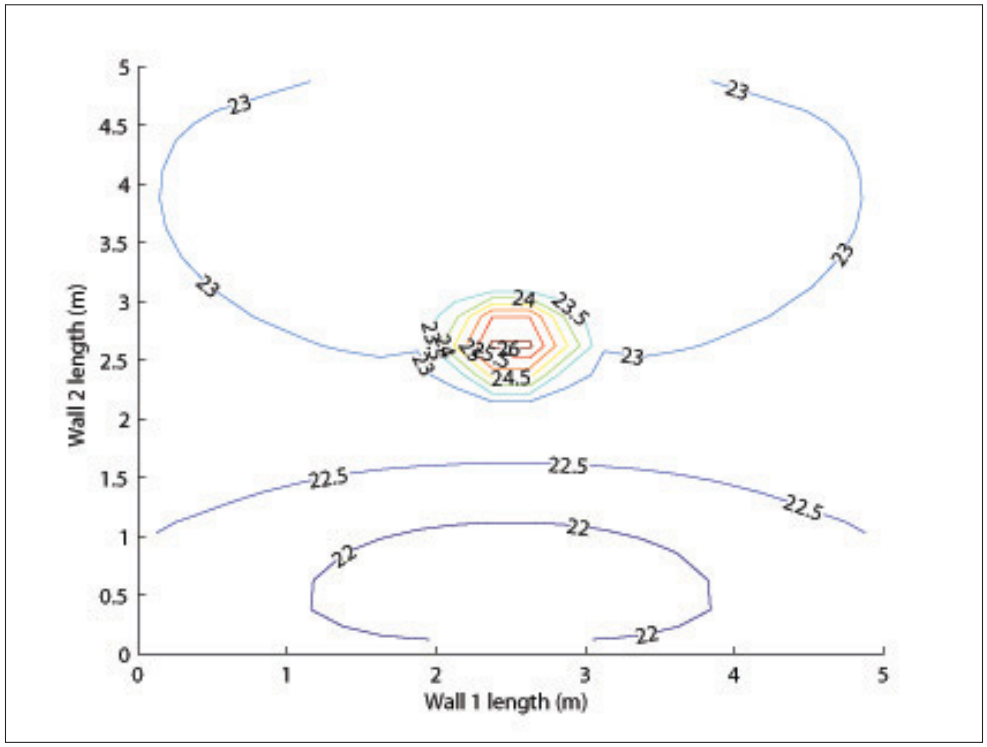

Figure 5.40 Ceiling temperatures for the mVH at an air exchange rate of 0.7ACH

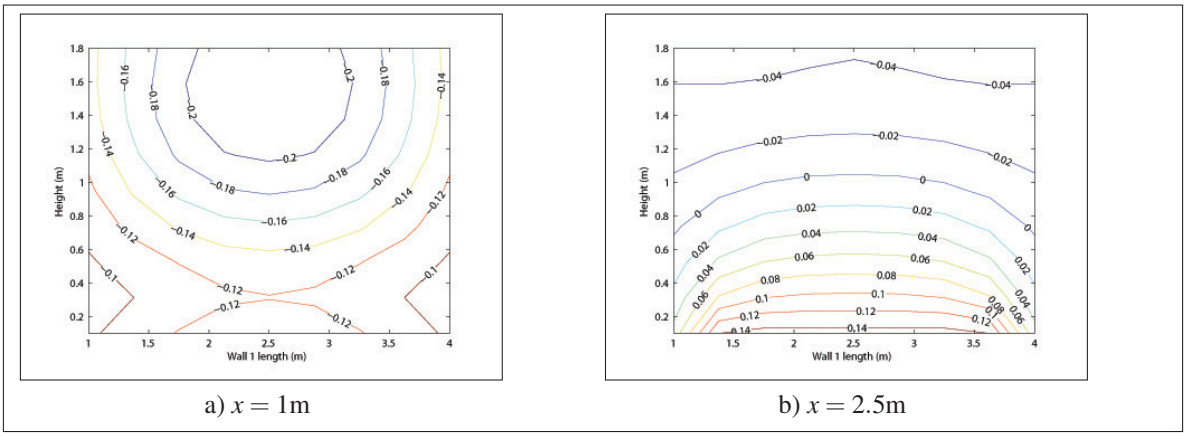

a) $x = 1$m b) $x = 2.5$m

Figure 5.41 Thermal comfort for the mVH at 0.7ACH and for different section cuts parallel to wall 1 where x is the distance from wall 1

It is obvious that the floor heating increases the *PMV* near the floor. The cold window still produces a local drop in *PMV* near the window. There is however no significant local discomfort so that $-0.5 < PMV < 0.5$ is not respected.

From these results, the floor and ceiling heating are interesting for rooms that have high air exchange rate. The *RHDS* is sensitive to air exchange rate and so is the mVH. Increasing the air tightness of a room leads to greater energy efficiency. In such a case, the heat distribution also becomes more important. Building designers should be aware of this.

5.2.2.7 Outdoor temperature

One final parameter that was studied is the effect of the outdoor temperature on optimal heat distribution. In Figure 5.42 the *RHDS* is shown along with the heat consumptions per floor area for the mVH and MVH as a function of outdoor temperature.

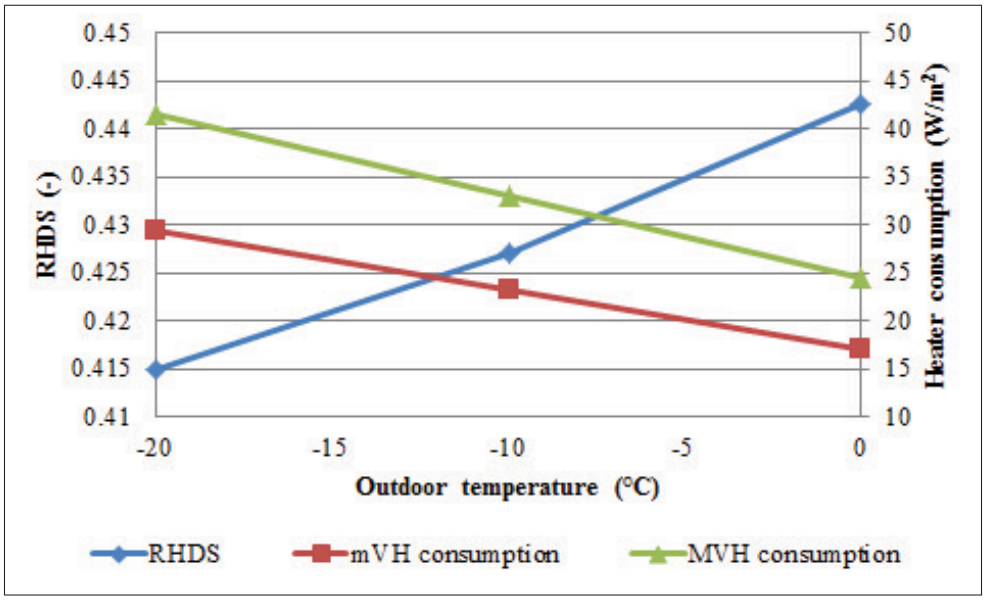

Figure 5.42 RHDS and energy consumption of virtual heaters as a function of the outdoor temperature

The energy consumption per floor area decreases as the outdoor temperature decrease: since there is less of a temperature difference between the room and the outdoor environment. The *RHDS* is shown to increase with a variation of outdoor temperature from 0.415 to 0.443, a 7% difference while the outdoor/indoor temperature difference decreased by 44%. The increase in *RHDS* can be explained by first considering that the mVH heats the air volume while the MVH

heats the window. With higher outdoor temperatures, the window and the exterior walls are at a higher equilibrium temperature. For the mVH, this has the consequence of increasing the mean radiant temperature, especially from the hotter window. The ambient air temperature setpoint must then not be too high to maintain thermal comfort (see Figure 5.43) and achieve significant energy savings. For the MVH, the decrease in outdoor temperature does not have as much of an effect since the heated window provides the radiant heat. There is thus less energy saved for the MVH when the outdoor temperature increases; hence, the increase in *RHDS* when the outdoor temperature is increased.

The air temperature for both the mVH and MVH is presented in Figure 5.43

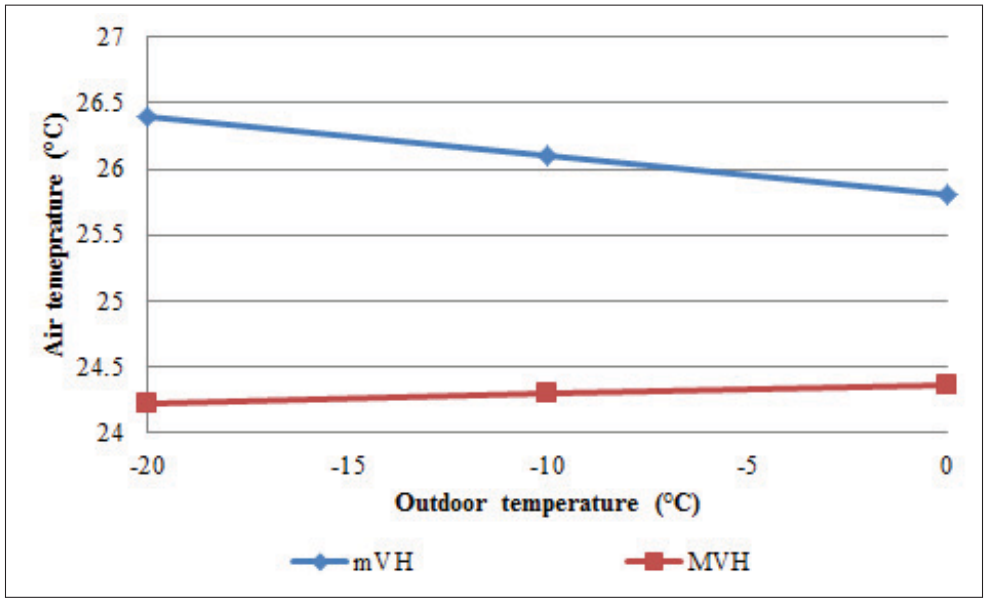

Figure 5.43 Room air temperatures for the mVH and MVH as a function of the outdoor temperature

It is clear from this figure that the air temperature for the mVH drops as the air temperature for the MVH increases. For the mVH, this is explained by an increase in wall and window temperature. The comfortable air temperature is thus lower. As for the MVH, the temperature increases as a result of the decreases in air exchange heat loss.

The MVH wall 1 temperatures at different outdoor temperatures are presented in Figure 5.44.

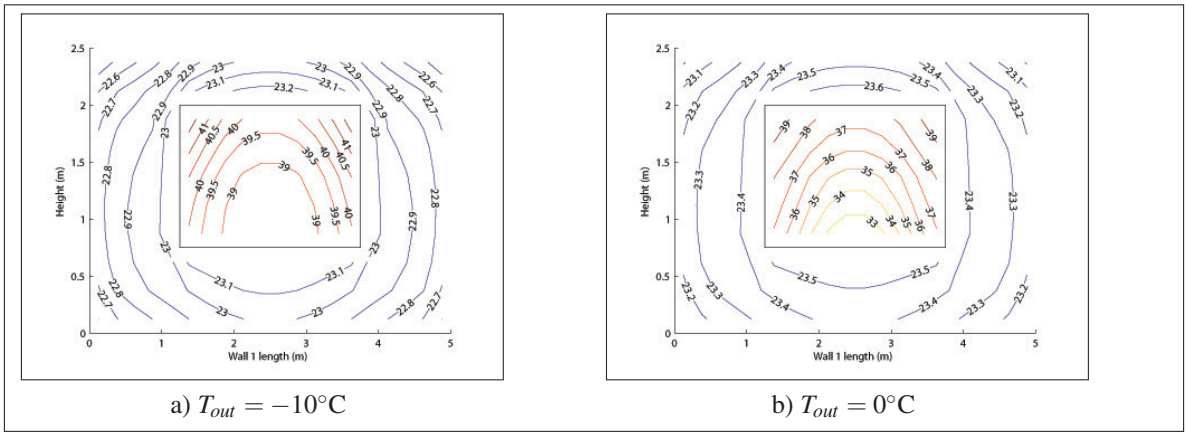

a) $T_{out} = -10°C$ b) $T_{out} = 0°C$

Figure 5.44 Wall 1 temperatures for the MVH and for different outdoor air temperatures

Figure 5.44 highlights that the window temperature decreases as the outdoor temperature increases. Since all the other surfaces and the air volume are naturally warmer, it is not surprising that the window in the MVH solution must be progressively colder as to maintain thermal comfort. Lowering the window temperature does contribute to reducing the MVH's consumption.

There is a definite link between the outdoor temperature and the *RHDS*. By changing the thermal equilibrium temperature in the room, the outdoor temperature can change the optimal heat distribution slightly. In the tested ranges and for this particular room, its effect on *RHDS* is more pronounced than changing the wall insulations.

5.3 Effects of geometry and thermal parameters

The geometry and thermal parameters of a room can clearly influence its optimal heat distribution and *RHDS*.

All three tested geometrical parameters affected the *RHDS* by at least 5%, two of which drastically changed the heat distribution itself for the mVH with a combination of floor and air volume heating.

The parameter that affected the *RHDS* the least is the WWR. It increased the *RHDS* by only 3.3% with a 500% variation in WWR, that is with windows 5 times larger than those in the reference case. However, the WWR did change the heat distribution for the mVH from only air volume heating to a combination of floor and air volume heating. Still, the air volume was the room element that was principally heated.

The parameter that affected the *RHDS* the most is the ceiling height. Not only did high ceilings distribute heat on both the floor and air volume for the mVH, but it also increased the *RHDS* by 4.8% with a variation in ceiling height of 240%. The ceiling height had nearly four times more effect than the WWR in increasing the *RHDS*.

When increasing the ceiling height, the window height was also increased as to maintain the WWR. The increase in window height provided an increased opportunity to heat the window far from the thermal comfort volume, thus increasing the potential inefficiency of the MVH. When the WWR was increased, this same effect took place as the window grew wider and taller. However, this did not have as much of an effect as a vertical increase because the window was still close to the thermal comfort volume. The result is consistent with the fact that radiant heating is most effective close to the source which it is intended to heat. Higher ceilings increase the chances of dispersing heat away from the objective, making the power consumption more sensitive to heat distribution.

Increasing the room depth led to the window having less of an effect on the thermal comfort and thus the *RHDS* was decreased. The room depth did not change the heat distribution. Proportionally, as the room increased in depth, the window heat loss represented less of the total power loss, thus its effect on the *RHDS* was diminished.

From the results, it is also evident that the thermal envelope of a room can also affect the optimal heat distributions and the *RHDS*. Window thermal resistance affected the *RHDS* the most, as followed by the outdoor temperature, air exchange rate, ceiling insulation, wall 1 insulation, floor insulation and wall 2-4 insulation.

With a single pane window, the worst $RHDS = 0.860$ was achieved; while with a triple pane window, the best $RHDS = 0.274$ was achieved.

The mVH for different thermal parameters heated the air volume with the exception of when high air exchange rates were involved. The air temperature is strongly tied to thermal comfort as a lower air temperature also lowers the indoor wall temperature, and consequently the mean radiant temperature. This can then double the effect of air temperature on thermal comfort as it changes both the air temperature and mean radiant temperature. In the particular case when heating the air becomes less efficient, floor heating was the next preferred method followed by ceiling heating. The floor and ceiling both have high insulation, higher than the other room surfaces, which led to these results. The floor being closer to the thermal comfort volume made floor heating the preferred method over the ceiling heating. The air volume heating always remained amongst the preferred methods even when floor and ceiling heating were involved.

Conversely, the MVH maximizes heat transfer by heating the room elements that retain their heat the least. The average view factor of a surface on the thermal comfort volume also plays an important role in optimal heat distribution. It is most efficient to heat surfaces that have a good view factor on the thermal comfort volume. The air temperature is directly linked to thermal comfort while the surface view factors are linked to the thermal comfort through the mean radiant temperature. This partially explains why air volume heating along with centered floor and ceiling heating were preferred. On the other hand, it also explains why MVH solutions had a window temperature profile where the upper extremities, surfaces with low view factors to the thermal comfort volume, were heated the most.

The importance of both the geometry and thermal parameters is highlighted. The window has heated, since it is the worst insulated element of the room, while the air volume, floor and

ceiling were heated because they are the most insulated elements of the room. Furthermore, when the window is placed far from the thermal comfort volume it becomes less efficient to heat it and the *RHDS* is also increased. The air volume became less attractive to heat in three cases: an increase in heat loss due to the window size; a reduction in the effectiveness of heating the thermal comfort volume when high ceilings are involved; and an increase in heat loss when the air exchange rate is increased.

From this comparison, it can be seen that the room parameters that are most involved in the heat loss process, i.e. the window, air exchange rate and outdoor temperature, are also those that affected the *RHDS* the most. This result is somewhat expected since the optimization for the virtual heaters, the total heat consumption is the objective function.

From the solutions of the mVH, it can be said that it is most efficient to heat the room elements that will minimize heat transfer and that it affects thermal comfort the most, whether due to high thermal resistance, air tightness or even geometry, all of which should be considered in an optimal heat distribution problem. For the tested cases, this generally meant heating the air volume. However, this result should be appreciated in the context that no air flow model was used in the optimization process. It is possible that local discomfort could be greater near the window as a consequence of a cold draft from a convection heat transfer from the window, an effect not modeled in this thesis.

As for the MVH, one should avoid heating the window. Common practice places the heater below the window, which could lead to heating this poorly insulated surface depending on the heating device. When looking at the *RHDS*, it is clear that having triple pane windows is preferred. Not only does it significantly reduce the energy consumption, it also reduces the *RHDS*, which is a measure of the risk of having poor heat distribution.

Another interesting finding is that the geometries that were most energy efficient where also the geometries with the lowest *RHDS*. This was true for all three tested geometrical parameters. The most energy efficient room that also resulting in having the lowest *RHDS* is thus a very deep room with small windows and a low ceiling. Its optimal heater would heat the air volume.

This is not to say that all rooms should be designed in this way as there are other design objectives to consider such as lighting and room use.

5.4 Conclusions

In summary, the effect of geometry and thermal parameters on optimal heat distribution was studied in this chapter. A total of 31 different rooms were compared to assess the effect of geometrical and thermal parameters on the heat distribution. The geometrical parameters tested include the window-to-wall ratio, the depth of the room, and the height of the room; while, the thermal parameters tested include wall 1 insulation, wall 2, 3 and 4 insulations, floor insulation, ceiling insulation, number of window panes, air exchange rate, and outdoor temperature.

The results of the geometrical parameter testing showed that the room height affected the *RHDS* the most while the WWR affected the *RHDS* the least for the mVH and MVH. However, both had a stronger influence on the mVH heat distribution than the room depth. For high ceiling rooms with high WWR, floor heating becomes an attractive alternative to air volume heating, air volume heating being most efficient for rooms with low ceilings and low WWR.

The MVH saw little change apart from variations in its window heat distribution. It is less efficient to heat the window where it has a globally low view factor on the thermal comfort volume. However, not all rooms necessarily behave in this way.

It was also found that energy efficiency and *RHDS* varied together when the room geometry was changed.

Investigating the thermal parameters showed that window R-value was the most sensitive parameter to affect the *RHDS* because it is poorly insulated and only has an effect on thermal comfort through radiation; therefore, it has less of an effect on the far end of the thermal comfort volume. The second most sensitive parameter was the outdoor air temperature, which affected the *RHDS* by changing the wall temperatures and the total heat transfer directly. The air exchange rate also had a significant impact on the *RHDS* and was the only thermal parame-

ter to drastically change the mVH heat distribution. When the air exchange rate was increased, floor heating became an attractive alternative to heating the air volume. As the air exchange rate increased and the floor achieved a maximum temperature, it then became attractive to heat the ceiling surface while still lowering the indoor air temperature.

Meanwhile, the indoor wall insulation and floor insulation, both exposed to the warm interior space, affected the heat distribution and the *RHDS* the least. This is likely because these surfaces are not the most insulated neither are they the least. There is also very little heat transfer going through these interior surfaces, thus less opportunity to change the total heat loss.

Overall, heating a poorly insulated element of the room far from the thermal comfort volume is inefficient, while heating the most insulated element of the room close to the thermal comfort volume is most efficient. Geometries that provide opportunities to heat far from the thermal comfort volume are then prone to inefficient heating. This is the case of rooms with high ceilings. Moreover, thermal reistance topologies with high variations in their resistance values are also sensitive to heat distribution.

This chapter also presented how virtual heaters can be applied to solve heating problems in a building environment. In this case, they were used to investigate how rooms of different dimensions and thermal resistance are sensitive to heat distribution. Geometry and insulation do have an effect on optimal heat distributions. Building designers should be aware of these effects when they endeavor to design energy efficient buildings.

CONCLUSION AND RECOMMENDATIONS

In an effort to study the energy efficiency of heating systems to achieve thermal comfort from the perspective of heat distribution, this thesis answered the following two questions:

- Do all electric heating systems consume the same amount of energy while providing an equal thermal comfort?
- What characterises an energy optimal indoor heat distribution constrained by thermal comfort?

To answer the first question, a bi-climatic chamber called Klimat, was built to experimentally compare heating systems in a controlled environment. This research tool incorporated some key innovations for a bi-climatic chamber. Its modular walls allows for a quick reconfiguration of the test room geometry, thermal resistance or wall type (door/window/insulated wall). Moreover, the custom LabView acquisition and control program for the Klimat allowed for the test room heaters to be controlled via a thermal comfort measure.

Using this new experimental tool, the energy consumption of three electric heating systems were compared to each other at equal thermal comfort. As such, this thesis views thermal comfort as a constraint that heating systems should achieved, i.e. thermal comfort is the primary objective of the heater, while the energy consumption of this system is a negative consequence that arises from achieving this thermal comfort. Of course, a colder environment would result in energy savings, but this is beside the point that an efficient system should achieve that level of comfort with less energy.

By controlling each heating systems with a thermal comfort controller, the energy consumption of the heaters were evaluated at four different cold room temperature levels ($-20°$C, $-10°$C, $0°$C, $10°$C). The results from the experiment showed that electric heating systems do not

all consume the same amount of energy to provide an equal thermal comfort. The convector consumed 4% to 11% less energy than the tested radiant heater. The baseboard consumed 4% to 6% more than the convector. This is significant as a simple change of the heat distributor can lead to energy efficiency. Installing each heater bellow a set of windows, the convector heated these windows less than the other two systems. The differences in heating efficiency are thus attributed to their heat distribution. Heating the window is inefficient, therefore should be avoided. This conclusion is however limited by its experimental parameters. The cases tested within the thesis are at equal predicted mean vote for a specific clothing factor and metabolic rate. Moreover, some factors such as radiant asymmetry was not considered in the thermal comfort calculation.

Comparing heaters in a bi-climate chamber is limited to answer the second research question. By comparing existing heaters, true optimal heat distribution characteristics cannot be found. In fact, papers published in literature have primaraly focused on a comparison approach. The comparison is limited to the heaters that are compared. There is no way to know if the best heat distribution found with the best heater is indeed the optimal heat distribution. The concept of virtual heaters, through an optimization problem, is introduced in this thesis to resolve this issue.

Virtual heaters are a set of two heat distributions. The minimum virtual heater (mVH) is the heat distribution that minimizes the heat loss of a room while it maintains thermal comfort within this room. On the other hand, the maximum virtual heater (MVH) is the one that maximizes the heat loss in that same room and maintains thermal comfort. As such, the virtual heaters have no bias toward any existing heating device. From the virtual heaters, the heat distribution performance of heating systems and room can also be assessed. Three performance indices were defined for this purpose.

The heat distribution effectiveness (ε_{AH}) measures how close a heating system is to the mVH as compared to the difference between the mVH and MVH. In this way, the heat distribution effectiveness can be used to assess the heat distribution performance of heating systems.

The room heat distribution sensitivity (*RHDS*) measures the magnitude of the difference between the mVH and MVH. The *RHDS* can be interpreted as the percentage increase in consumption of the MVH when compared to the mVH. It is a measure of the heat distribution performance of a room. Rooms with low *RHDS* have a high heat distribution performance as the consumption of heating system is insensitive to heat distribution. The energy consumption of rooms with high *RHDS* can be very sensitive to heat distribution. Greater care should be taken in these situations to design systems that have good heat distribution.

The maximum power savings (*MPS*) is the the maximum energy saving that can be achieved relative to the actual power of a real heating system.

To find the virtual heaters, a simplified heat transfer model and a thermal comfort model was introduced.

The thermal comfort model is twofold. First, the predicted mean vote (PMV) is used as a constraint on an occupied volume within the range of $-0.5 < PMV < 0.5$. Second, the average PMV over the volume is also used as a constraint.

The heat transfer model is also divided into two primary parts. The total heat loss calculated by simple 1-Dimensionnal conduction heat loss trough the walls, and air exchange heat loss between the indoor air volume and outdoor air volume forms the first part of the model. The second part of the model estimate the heat input of each element of the room. In this case, these elements might include a section of wall, window or the air volume. The wall sections are sub-divided into smaller wall sub-sections of $0.25\text{m} \times 0.25\text{m}$. A radiant heat transfer model, conduction heat transfer model and convective heat transfer model was applied to each of

these wall sections. The air volume is considered as one single volume to be heated (one-node model). A convective heat transfer and air exchange heat transfer model was applied to this node. The major assumption for the heat transfer model is that only one average air temperature is considered for the indoor air volume. The virtual heaters were then limited to a balance between radiant heat distributions on the walls and a heat input in the air volume.

Using these heat transfer and thermal comfort models, the virtual heaters were found for the test room of the Klimat. The maximum virtual heater concluded the same as the experimental results. Heating the windows is inefficient and should be avoided. The minimum virtual heater showed for the test room of the Klimat that heating the air volume is most efficient followed by floor heating. By comparing the heat distributions of the mVH and MVH, it was also concluded that two major driving factors influence optimal heating. The first is the thermal resistance of each room element. Low insulated elements of the room such as windows should not be heated. Instead, high thermal hesitance of the room such as the air volume and floor should be heated. The second is the influence that each of these elements have on the average thermal comfort in the occupied volume. The average air temperature has a high influence on thermal comfort thus should be kept high by the heater. Moreover, surfaces that are closer to the thermal comfort volume, i.e. have a high overall view factor on the thermal comfort volume, should be heated over those who are far from the occupied volume.

The Klimat test room is one example of a room. Optimal heat distribution can change when considering different rooms. As such, to properly characterise optimal heating, different rooms have been studied. Within the limitation of the model used to calculate virtual heaters, a parametric analysis of the effect of thermal parameters and geometry on optimal heat distribution was performed. The considered parameters were the window to wall ratio, the depth of the room, the height of the room, the wall 1 insulation, wall 2, 3 and 4 insulation, floor insulation, ceiling insulation, window pane number, air exchange rate, and outdoor temperature.

The results showed that the room height, window to wall ratio and air exchange rate all had an influence on the minimum virtual heater heat distribution. When either of the three parameters are increased, heating the air volume become less attractive while floor heating and ceiling heating progressively replace this heating load. These results are explained by the effects mentioned above. As the ceiling is higher, the ratio of the air volume to the thermal comfort volume increases. Heating the entire air volume then becomes less efficient to provide thermal comfort on the occupied volume. Furthermore, when the window size is increased, the air volume has an increased heat loss by convection to the window and become less efficient to heat. An increase in heat loss of the air volume is also associated with higher air exchanges. Second to the air volume, floor heating is also an efficient way to provide thermal comfort. The floor is well insulated and has the best overall view of the thermal comfort volume. The third best method of heating is then the ceiling because of its high thermal resistance. However, it is important to note that temperature stratification was not considered and could penalised the efficiency of heating the ceiling.

When observing the maximum virtual heaters, heating the windows on the corners far from the thermal comfort volume was consistently the worst method of heating. This had already been observed by others (Olesen *et al.*, 1980; Hannay *et al.*, 1978; Sevilgen & Kilic, 2011). It can then be said that heating the windows should always be avoided unless some other room element has an even poorer thermal resistance.

By comparing the tested cases, the optimal heat distribution is characterised by the two governing factors mentioned above. It is optimal to heat well insulated elements of a room that also have a strong effect on thermal comfort in the occupied volume. Conversely, it is least efficient to heat elements of the room that are poorly insulated and have small effects on thermal comfort.

From the parametric study, the *RHDS* of different rooms was also investigated. The window thermal resistance and air exchange rate where the two parameters that effected the *RHDS* the most. They are also the room elements that were heated for either the mVH or MVH. The *RHDS* is then most effected by the surfaces with extreme (low or high) thermal resistance. As the poorest insulated element of the room increases its thermal resistance, the *RHDS* is lowered. As the highest thermally resistant element of the room increases its thermal resistance, *RHDS* is increased. The spread between the best and worst thermal resistance is thus important measure along with the *RHDS* to assess how sensible a room is to heat distribution.

Virtual heaters are useful tools to evaluate the performance of a room and its heating system. It was found that the thermal envelope does, for some room elements, significantly influence the *RHDS* and in some cases the optimal heat distribution. Heat distribution sensitivities (*RHDS*) of up to 86% found in this work indicate that the heat distribution should not be neglected in design since poor heat distribution could lead to significantly inefficient heating.

More work should be done on optimal heat distribution using virtual heater and a heat transfer model that incorporates the air flow in the room. This would lead to having more accurate heat distribution results, specifically for the air volume, a limitation of this work. Such a model would allow for finding suggested locations of hot air outlets or even of convection heaters. Some expected road blocks to optimizing these models is the computation time, not only for the heat transfer model, but mostly for the optimization as the number of considered heat input variables grow.

Other future perspectives include an investigation of non-rectangular shape room such as an L-shape room. For these rooms, optimal heating might be different, since not all room surfaces can view the entire thermal comfort volume. Moreover, the inclusion of the sun irradiation for rooms that are mainly occupied during the day time could also change the optimal heat distributions.

Given that heating the air was found to be efficient for many rooms, future optimization works on convector outlet flow design to heat the air and not the window could lead to more efficient electric heating devices. In a similar effort to heat the air and avoid heating the window, different locations of an electric heating devices could be tested in a bi-climatic chamber.

Heat distribution is not to be neglected in design. The mVH, MVH and their associated performance indices as a function of room geometry and thermal parameters could help architects and engineers make better informed design decisions regarding heat distribution. The efficiency of a heating system is not only characterise by its method of heat production; but also the proper use of the heat which can lead to energy savings.

APPENDIX I

CALIBRATION OF THERMOCOUPLE WIRE

The calibration of thermocouple wire for the bi-climatic chamber was performed using the procedure outline in this appendix. The calibration is a single point calibration.

Thermocouples are connected to the thermocouple extension wire via a thermocouple connector. Using the Fluke 714B temperature calibrator, a temperature can be simulated. To calibrate the extension wire, the thermocouple is disconnected from its connector and the Fluke calibrator is connected to the extension wire, see Figure I-1.

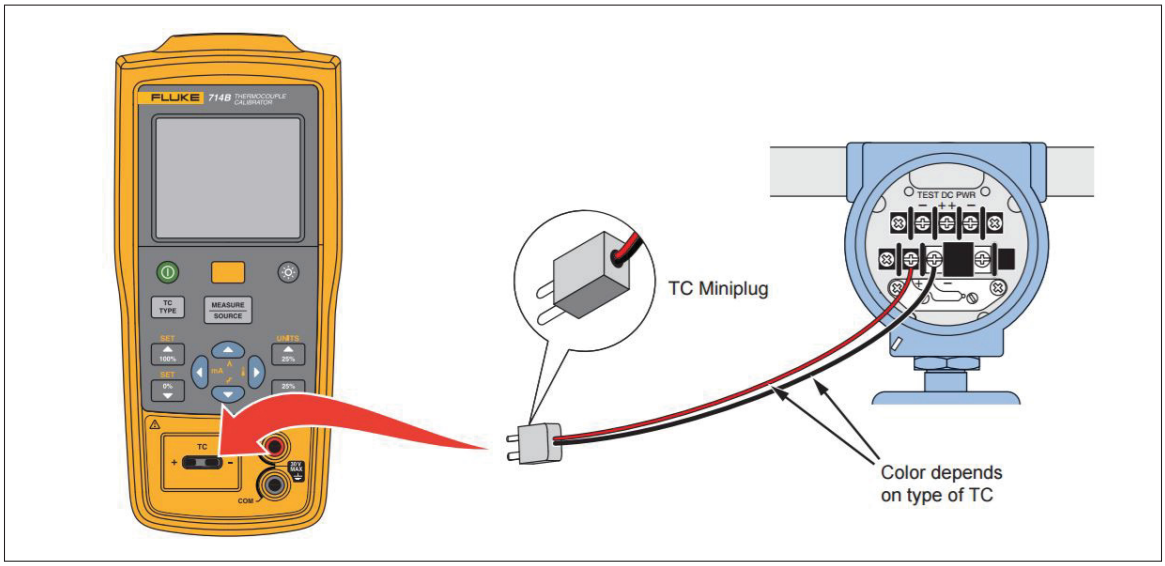

Figure-A I-1 Fluke 714B connection to extension wire. Source: (Fluke, 2017)

The Fluke calibrator is set to simulate a temperature of 0°C for the cold room thermocouples and 20°C for the warm room, the test room and the crawl space thermocouples. A difference in simulated temperature and measured temperature is observed. This value is used to calibrate the extension wire and acquisition module of the thermocouple.

Using a LabView data logging software, the measured temperature is logged for one minute in order to get repeated measurements. The data collected over one minute is then averaged. The

average gives the calibration value which must be subtracted to the actual measured value so to have an accurate temperature measurement.

To calibrate the thermocouple itself, a temperature simulator is used to measure temperature offset from impurities in metals. The thermocouple is placed inside the machine, which simulates a constant temperature, then measurements are logged for one minute. The average value of these measurements gives the calibration offset. Adding both offsets from the extension wire and the thermocouple gives the final calibration value. This value is then used to with the extension wire calibration to calibrate measurements and have a more accurate measure of temperature.

APPENDIX II

MEASURING THE INFILTRATIONS OF THE KLIMAT

Infiltrations through wall, ceiling and floor surfaces are the consequence of a small pressure differential across these surfaces that may be cause by wind pressure, ventilation pressure or natural pressure gradient caused by temperature gradients. For the Klimat chamber, most of the infiltration is caused by temperature gradients as no ventilation system is installed and there is minimal wind in the chamber. A small portion of infiltration is due to outdoor air flow (wind pressure), caused predominately by the refrigeration systems and recirculation fans which direct the flow parallel to the cold room surfaces.

To measure the infiltration of the Klimat, a blower door test was used. The blower door test is a common method to estimate the infiltration rates of indoor spaces. It measures leaks at a pressure of 50Pa from which infiltration can be estimated from eq. (A II-1) (Sherman, 1987; Younes *et al.*, 2011).

$$\dot{V}_{\text{ex}} = \frac{\dot{V}_{\text{ex,50Pa}}}{20} \tag{A II-1}$$

To setup a blower door test, a door blocking panel is installed on a door. This panel should be as air tight as possible to prevent adding more leaks to the room. A fan is installed on the blocking panel to pressurize or depressurize the room. For the case of the Klimat chamber, a pressurisation test is needed as pressure stabilization valve lets air go into the chamber. A depressurization test would add air leaks to the chamber. In a standard blower door test, two pressure measurements are installed: one to measure the pressure at the fan level, to later deduct flow rate; and the other, to measure pressure inside the room. Both pressure measurements are taken relative to the outside ambient pressure.

To perform the blower door test, the fan is turned to its ON position and controlled to achieve an indoor relative pressure of 50Pa. The flow rate and pressure is then measured once the

pressure has stabilized itself. This measure is apparently enough to estimate infiltration using eq.(A II-1); however, it is better to use the pressure/flow characteristic curve to characterise the leaks and have a better estimate of the leakage at 50Pa. The characteristic curve is found by setting the blower door to multiple pressure points then measuring pressure and flow. The pressure/flow relation is known to behave according to the following equation (Younes *et al.*, 2011):

$$\dot{V} = C(\Delta P)^n \tag{A II-2}$$

Plotting the curve on a log/log graph, constants n and C can easily be estimated (Conservatory, 2012). The value of C is an indicator of leakage surface area (Younes *et al.*, 2011; Chan *et al.*, 2005). The value of n gives a measure of flow regime, e.g. the proportion of laminar to turbulent flow (turbulent when $n = 0.5$). From the flow regime, the mean size of the orifice can be estimated (Sinnott & Dyer, 2012).

Using the Minneapolis blower door system, model 3, blower door tests were perform on the Klimat chamber. The series of carefully planned test allowed for measuring not only the total infiltration, but also an approximation of the infiltration between the test room and each adjacent room.

To find the exfiltration/infiltration between each room, it is important to write an expanded form of the flow rate:

$$\dot{V}_{\text{in}} = \sum_{\text{i}}^{3} \dot{V}_{\text{i}} \tag{A II-3}$$

where $\dot{V}_i$ denote different flow rates to the adjacent rooms and $\dot{V}_{in}$ is the total exfiltration flow rate at a given test room pressure. The Klimat chamber has 5 distinct spaces of interest: the test room, the cold room, the warm room, the crawl space and the exterior. In total there are 9 independent air exchanges taking place between each of these rooms. No air exchange takes place between the test room and the exterior space as they do not share a common wall, ceiling or floor surface. With the nine exchanges, there are 18 parameters that must be found to fully

describe the pressure/flow of the system, n and C for each air exchange. To better understand the problem the following graph representation of the different possible air flows is useful.

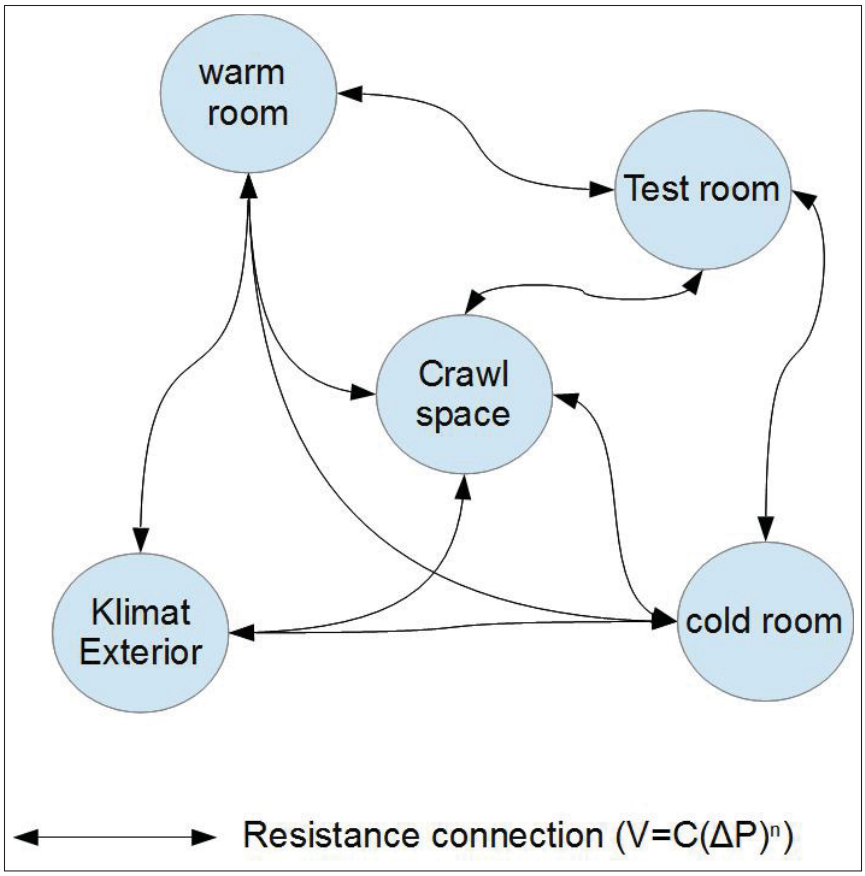

Figure-A II-1 Graph representation of flow in Klimat

In the graph, pressure/flow resistance are shown as lines. Since only the room surfaces adjacent to the test room are of interest, three pressure/flow relations are pertinent. The other flow equations of the system describe infiltration through unattractive parts of the system, e.g. the flow between the cold room, the crawl space, the warm room and the exterior. By opening/closing the cold room door and crawl space sections, the following 3 graphs representations describe useful test configurations for determining the infiltration through the sections of interest.

On Figure II-2a, a configuration with an open crawl space and open cold room is presented. Figure II-2b shows the configuration when only the cold room door is open, while Figure II-

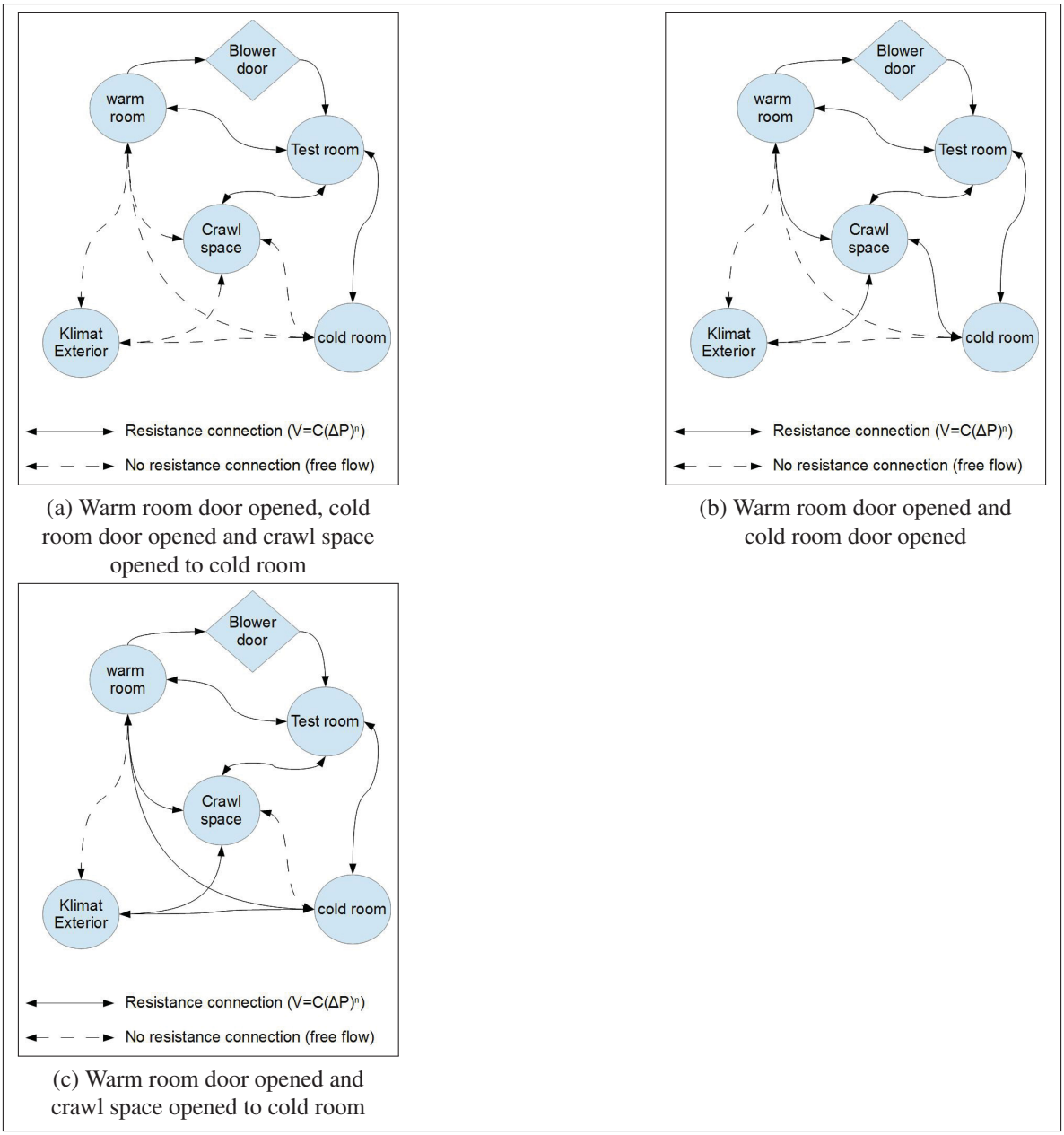

(a) Warm room door opened, cold room door opened and crawl space opened to cold room

(b) Warm room door opened and cold room door opened

(c) Warm room door opened and crawl space opened to cold room

Figure-A II-2 Graph representation of flow in Klimat for three configurations

2c represents the configuration where both the cold room door and access to crawl space are closed.

Using these configurations, the pressure of each room will vary in a different way. Notice that the blower door is installed on the access door between the test room and the warm room. The

warm room door to the exterior of the Klimat is always open. The configurations provide 3 independent equations that can be used to solve the 6 parameters of interest:

$$\dot{V}_{ex,1} = C_{warm}(\Delta P_{test})^{n_{warm}} + C_{crawl}(\Delta P_{test})^{n_{crawl}} + C_{cold}(\Delta P_{test})^{n_{cold}} \quad \text{(A II-4a)}$$

$$\dot{V}_{ex,2} = C_{warm}(\Delta P_{test})^{n_{warm}} + C_{crawl}(\Delta P_{crawl})^{n_{crawl}} + C_{cold}(\Delta P_{test})^{n_{cold}} \quad \text{(A II-4b)}$$

$$\dot{V}_{ex,3} = C_{warm}(\Delta P_{test})^{n_{warm}} + C_{crawl}(\Delta P_{cold})^{n_{crawl}} + C_{cold}(\Delta P_{cold})^{n_{cold}} \quad \text{(A II-4c)}$$

where ΔP_{test} is the difference in pressure between the test room and the warm room/exterior, ΔP_{crawl} is the pressure of the crawl space relative to the exterior, ΔP_{cold} is the pressure of the cold room relative to the exterior. Index warm is for walls separating the test room from the warm room, index cold is for the separations between the test room and the cold room and index crawl is for the separation between the test room and the crawl space.

By measuring and controlling a second pressure, it is possible to avoid finding all 18 parameters of the system and only find the 6 parameters of interest using the system of eq. (A II-4). For each configuration shown in Figure II-2, at least two test room pressure are tested. From these 6 equations or more, depending on the number of test room pressure tested, the system of equation with variables C_i, and n_i is constructed. The system can then be solved by least squares optimization to find the C_i, and n_i that best fits the measured data.

Using the configurations of Figure II-2, the following blower door test results were obtained:

The test room has a volume of 43.5m^3 (1536ft^3). The air change per hour (ACH) is 64.2ACH at 50Pa (see Figure II-3a). This is about six times the infiltration of a residential spaces dwelling tested in (Sinnott & Dyer, 2012). As it will be shown later, only 21% of the infiltration at 50Pa is in exchange with the cold room, room representing the outdoor environment. Even if considering only 21% of the air change, 13.5ACH at 50Pa would still be considered high when comparing to (Sinnott & Dyer, 2012). The Klimat, with its high infiltration rate, should not perform well with heater that heat primarily the air when compared to normal residential dwellings.

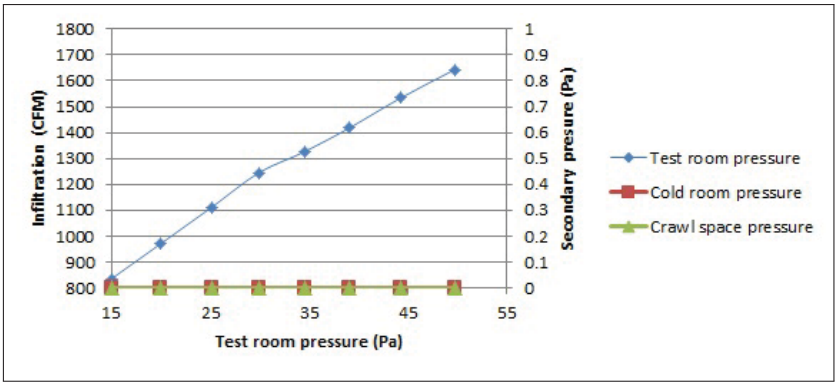

(a) Warm room door opened, cold room door opened and crawl space opened to cold room

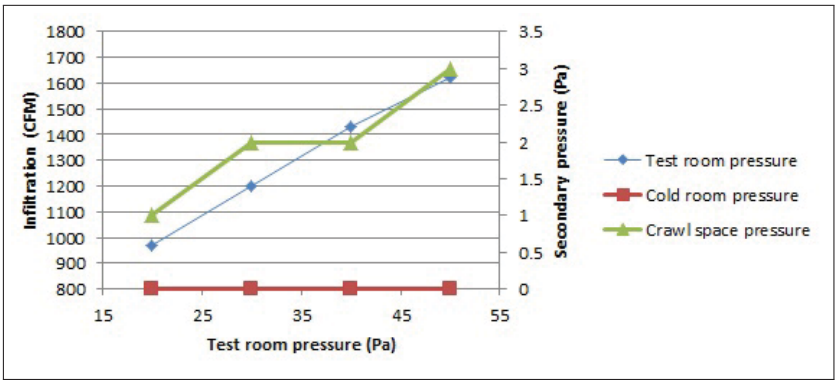

(b) Warm room door opened and cold room door opened

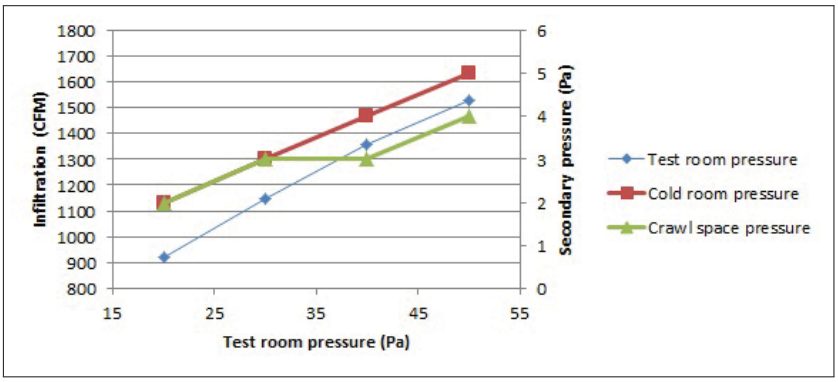

(c) Warm room door opened and crawl space opened to cold room

Figure-A II-3 Flow/pressur results for each tested configuration

From Figure II-3, and by opening/closing the crawl space and cold room to the outside environment, different secondary pressures can be observed. These pressures have an influence on the total infiltration rate of the test room. They may be used to estimate the infiltration between the test room and its adjacent rooms.

Using the results of Figure II-3, the parameters C_i and n_i describing the pressure/flow relations between each room were solved for in eqs.(A II-4a), (A II-4b) and (A II-4b) by using the GRG optimizer in Excel (Lasdon *et al.*, 1978). These results are shown in Table II-1. Estimated infiltration rates and equivalent leakage area for each room are shown in the Table II-2.

Table-A II-1 Infiltration constants

	C ($Pa^{-n}m^3/h$ ($Pa^{-n}CFM$))	n	Infiltration percent (%)
Warm room surfaces	246 (145)	0.5	65.7
Cold room surfaces	26 (30)	0.8	20.9
Crawl space surfaces	51 (26)	0.5	13.4
All surfaces (standard blower test)	306 (180)	0.6	100.0

Table-A II-2 Klimat leakage

	Flow at 50Pa (m^3/h (CFM))	Estimated infiltration (m^3/h (CFM))	Equivalent leakage area (cm^2)
Warm room surfaces	1736 (1021)	89 (51)	446
Cold room surfaces	652 (383)	33 (19)	142
Crawl space surfaces	362 (213)	18 (11)	91
All surfaces (standard blower test)	2791 (1643)	149 (82)	722

The surfaces adjacent to the warm room are responsible for most of the total infiltration. This is to be expected as no sealing tape is used to seal these surfaces. The modular construction of the walls also contributes to an increase in air exchange between these two rooms. With 20.9% of the total infiltration rate, the cold room surfaces lets more air through than a normal construction by a factor of at least 3 when comparing the ACH at 50Pa of modern homes(Sinnott & Dyer, 2012). The crawl space has the lowest infiltration rate. This is also expected as it has least surface area.

The calculated infiltration curves are shown along with the measured infiltration curve in Figure II-4

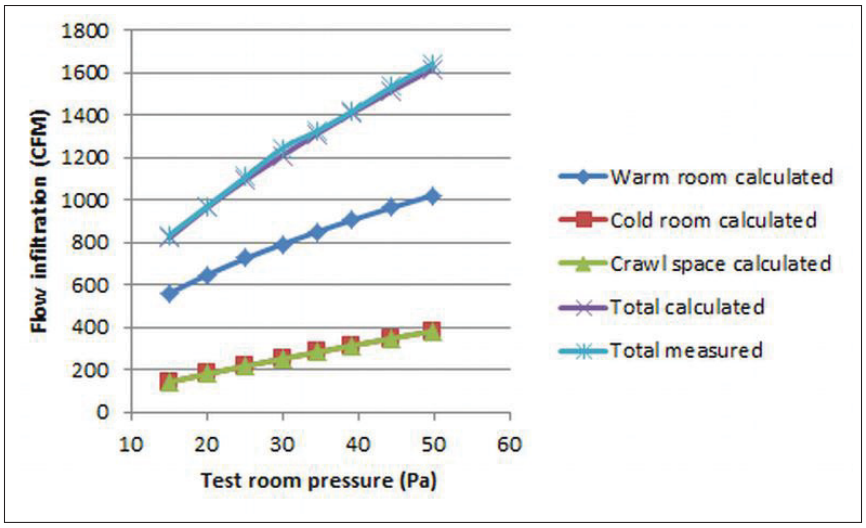

Figure-A II-4 Results of infiltration calculations

The total calculated infiltration using the standard blower door test (see eq. (A II-2)) and the one using parameters in Table II-1 along with eq. (A II-3) show good agreement with the experimental results. Figure II-4 also highlight that warm room infiltration is greater than cold room infiltration, which is also greater than the crawl space infiltration. This was to be expected as the crawl space only share the floor area with the test room and some attention to sealing the cold room walls helped reduce the infiltration through these surfaces.

As discussed in the first part of this section, most of the infiltration occurring in the Klimat is due to temperature gradients. If considering that the warm room and test room both have similar temperature gradients, as should be the case if they are both subjected to similar conditions, negligible infiltration should occur between the warm room and test room. A temperature gradient in the crawl space would however create a pressure differential between the test room and crawl space. The infiltration between these two cannot be neglected. As for the cold room to test room infiltration, the behaviour should be similar to an outdoor wall. Infiltration must then be considered.

In summary, multiple blower door tests were performed to evaluate the total and individual infiltration rates of each test room surface. By opening and closing doors, this allowed modulating the pressure map of the chamber rendering an over-defined system of independent equa-

tions. With optimal curve fitting, individual surface infiltration rates could then be calculated. Using calculated results in Table II-2, the infiltrations of the test room can be modeled as the sum of the crawl space and cold room infiltrations. As a global result, the infiltration/exfiltration of the Klimat is observed.

APPENDIX III

CALCULATING THE VIEW FACTORS

A view factor, also called shape, angle or configuration factor, is a measure of how one surface can see another. The general equation for the view factor is:

$$F_{12} = \frac{1}{\pi A_1} = \int_{A_1} \int_{A_2} \frac{\cos(\theta_1)\cos(\theta_2)}{||\mathbf{r}_{12}||^2} dA_2 dA_1 \qquad \text{(A III-1)}$$

for which no one has yet to have found a general analytical solution. In eq. (A III-1), the indexes denote surface number and $\mathbf{r}_{12}$ is the distance between two point on surface 1 and 2. Some special analytical solutions however, do exist, and one can also always compute the integral using a numerical approach. The problem with numerical methods is that they are computationally expensive, especially when a large number of surface are to be considered (Narayanaswamy, 2015).

A general solution to eq. (A III-1) for the case of two planar polygon surfaces has proposed by Schröder and Hanrahan (Schröder & Hanrahan, 1993). Narayanaswamy (Narayanaswamy, 2015) then improved on the numerical behaviour of this solution.

More commonly in engineering practice and for simple shapes, the exact solutions from the open source catalogue (Howell, 2016) created by Howell are used. This catalogue is a agglomeration of the different exact solutions to eq. (A III-1) found in literature for special surface shapes and configurations. From this catalogue, many view factors can be calculated. The use of the solutions within this catalogue was chosen as the preferred method of calculating view factors in this work since all shapes and configurations of surfaces are kept simple.

All surfaces modeled are kept parallel or perpendicular to each other. Furthermore, all surfaces in this thesis are rectangular in shape except for the thermal comfort point modeled as a differential sphere. These two mesh constraints allows the computation of all the view factors between surface with these equations:

Parallel rectangles (Howell, 2016)

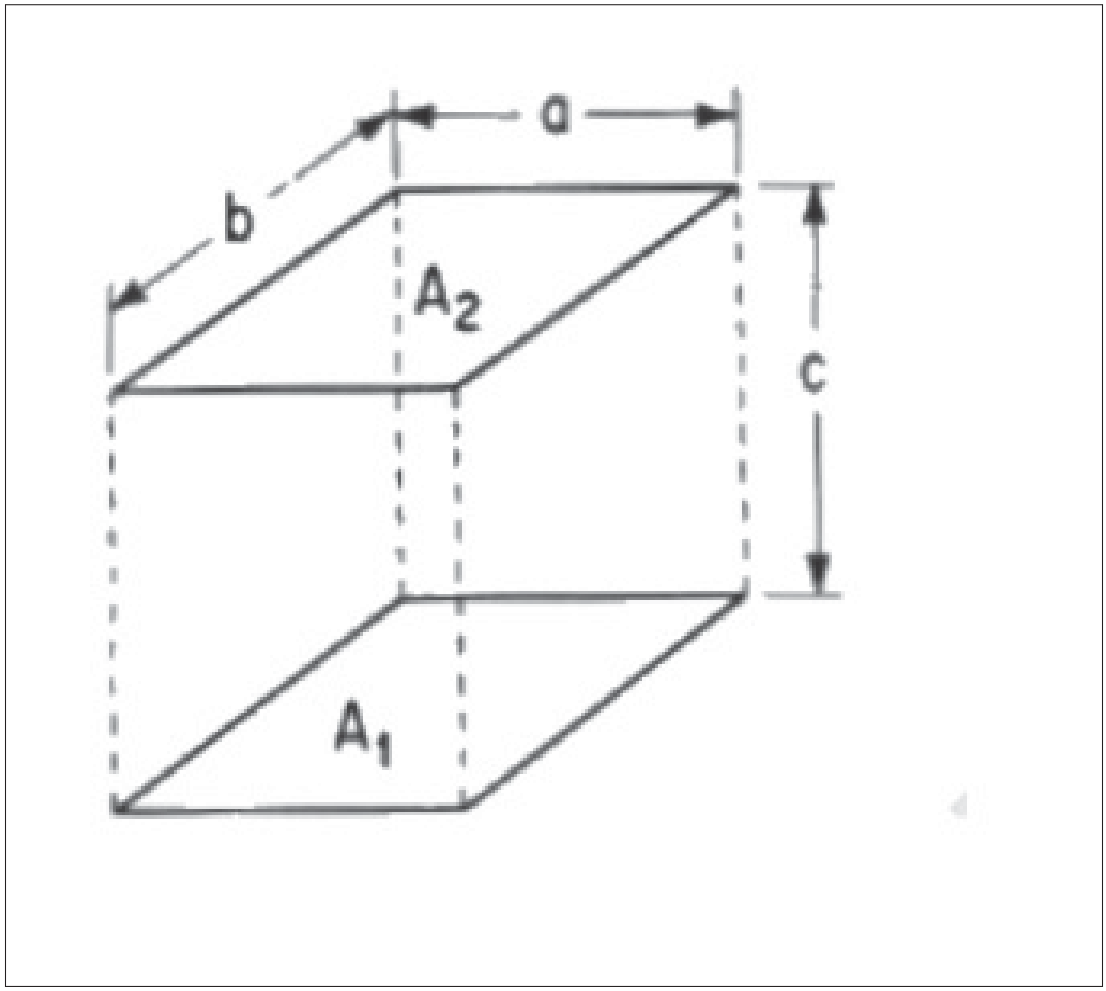

Figure-A III-1 View factor for parallel rectangles of same shape. Source: (Howell, 2016)

$$F_{12} = \frac{1}{XY\pi}\left\{\ln\left[\frac{(1+X^2)(1+Y^2)}{1+X^2+Y^2}\right] + X\sqrt{1+Y^2}\tan^{-1}\left(\frac{X}{\sqrt{1+Y^2}}\right)\right. \qquad \text{(A III-2a)}$$
$$\left. + Y\sqrt{1+X^2}\tan^{-1}\left(\frac{Y}{\sqrt{1+X^2}}\right) - X\tan^{-1}(X) - Y\tan^{-1}(Y)\right\}$$
$$X = \frac{a}{c}, \quad Y = \frac{b}{c}$$

Perpendicular rectangles (Howell, 2016)

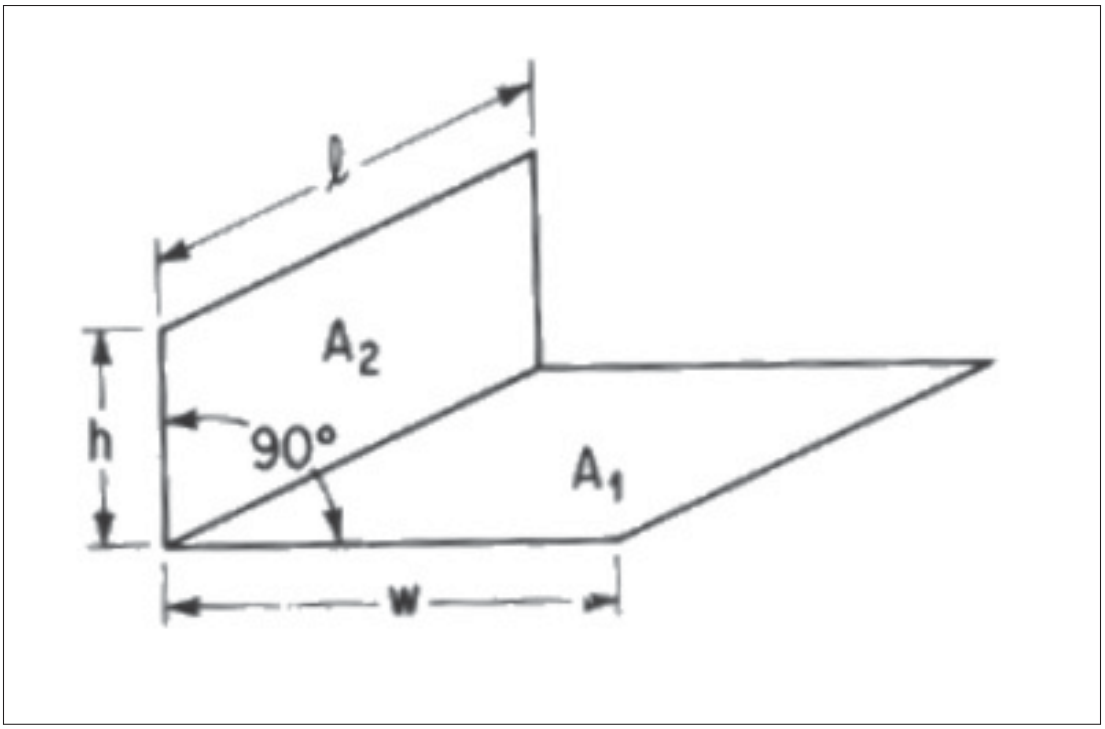

Figure-A III-2 View factor for perpendicular rectangles sharing a common edge. Source: (Howell, 2016)

$$F_{12} = \frac{1}{W\pi}\left(W\tan^{-1}\left(\frac{1}{W}\right) + H\tan^{-1}\left(\frac{1}{H}\right) \right. \tag{A III-3a}$$
$$- \sqrt{H^2+W^2}\tan^{-1}\left(\frac{1}{\sqrt{H^2+W^2}}\right) + \frac{1}{4}\ln\left\{ \frac{(1+W^2)(1+H^2)}{1+W^2+H^2} \right.$$
$$\left.\left[\frac{W^2(1+W^2+H^2)}{(1+W^2)(W^2+H^2)}\right]^{W^2} \left[\frac{H^2(1+H^2+W^2)}{(1+H^2)(H^2+W^2)}\right]^{H^2} \right\}\Bigg)$$
$$H = \frac{h}{l}, \quad W = \frac{w}{l}$$

and between a sphere with a rectangular surface (Howell, 2016):

$$F_{12} = \frac{1}{4\pi}\tan^{-1}\left(\frac{AB}{(1+A_1^2+B_2^2)^{1/2}}\right) \tag{A III-4a}$$
$$A = \frac{a}{c}, \quad B = \frac{b}{c}$$

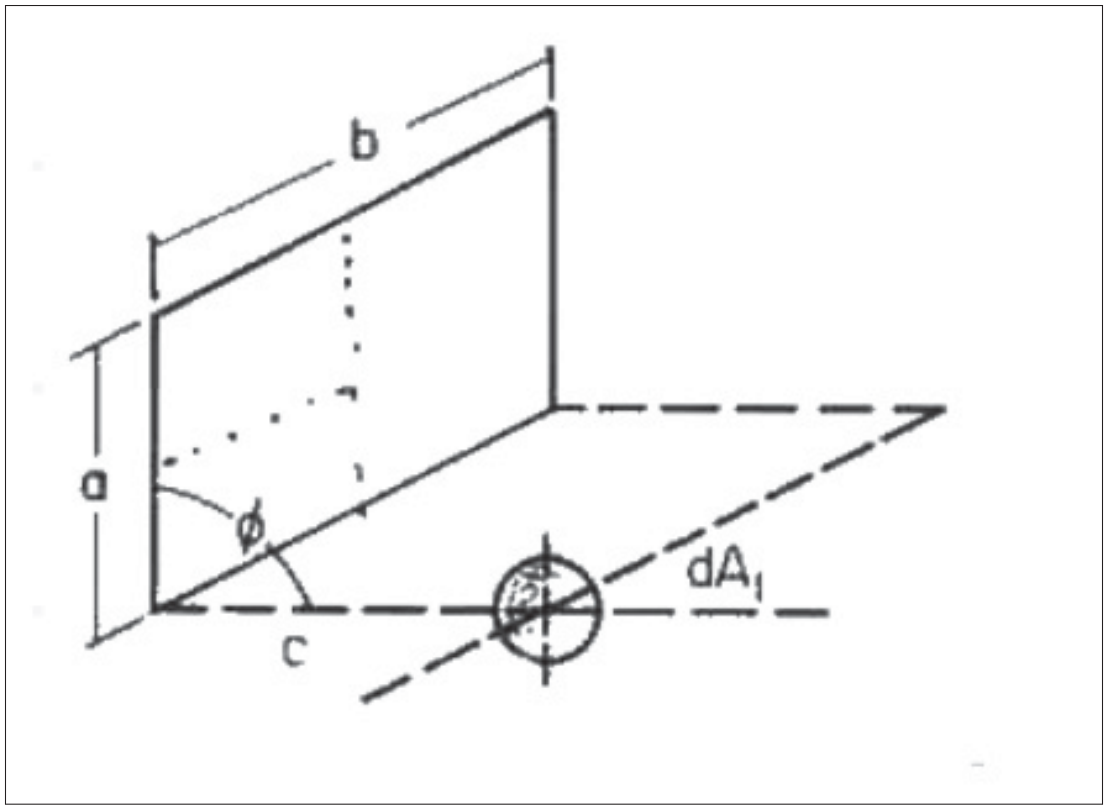

Figure-A III-3 View factor of a differential sphere to surface area ($\phi = \frac{\pi}{2}$). Source: (Howell, 2016)

Other pertinent relations relating to view factor are:

- Reciprocity

$$F_{ij}Ai = F_{ji}Aj \tag{A III-5}$$

- Superposition

$$F_{1(2+3)} = F_{12} + F_{13} \tag{A III-6}$$

- Sum of view factor for all n surfaces

$$\sum_{j=1}^{n} F_{ij} = 1 \quad \forall i \tag{A III-7}$$

A MatLab function using the four corners of the two rectangles as inputs was programmed. It first assesses which surface configuration is present and then choses the proper equation that is programmed from the catalogue. The code was tested against a numerical method for the different possible scenarios of the view factor that the analytical code can handle. The analytical results agreed with the numerical results. A second verification of the code was also performed. The tested sum of all view factors from one surface is equal to one. The details of the MatLab program are found in Appendix IV.

APPENDIX IV

MATLAB FUNCTIONS

1. Main code

```
% optimization of temperature distribution
% must run matlab as administrator

%%%%%%%%%%%%%%%%%%%%%%%%%%%%%%%% set parallel computations
clear all
clc
c=parcluster;
% delete(c.Jobs)
distcomp.feature( 'LocalUseMpiexec', false );
if c.NumWorkers~=8
    c.NumWorkers=4;
end
if matlabpool('size') == 0 %open pool of workers
    matlabpool open local 4
end
disp(c)
tic
%%%%%%%%%%%%%%%%%%%%%%%%%%%%%%%% geometry and view factor
% define key
parameters.geometry=define_geometry_mesh3(); % defines mesh
parameters.geometry=Find_VFs(parameters.geometry); %
    calculates surface areas and view factor for heat transfer

% points to calculate constraint
```

```
24 offset=1; % offset from wall
25 offset2=0.1; % offset from floor
26 offsetheight=1.8; % height of comfort volum from the floor
27 n=9; % number of point in x
28 m=9; % number of point in y
29 l=9; % number of point in z
30
31 positionx=offset:(parameters.geometry.wall1_W-2*offset)/(n-1):
       parameters.geometry.wall1_W-offset;
32 positiony=offset2:(offsetheight-offset2)/(m-1):offsetheight;
33 positionz=offset:(parameters.geometry.wall2_W-2*offset)/(l-1):
       parameters.geometry.wall2_W-offset;
34 % positionx=offset:(parameters.geometry.wall1_W-2*offset)/(n
       -1):parameters.geometry.wall1_W-offset;
35 % positiony=offset:(parameters.geometry.wall1_H-2*offset)/(m
       -1):parameters.geometry.wall1_H-offset;
36 % positionz=offset:(parameters.geometry.wall2_W-2*offset)/(l
       -1):parameters.geometry.wall2_W-offset;
37 % positionx=parameters.geometry.wall1_W/2;
38 % positiony=parameters.geometry.wall1_H/2;
39 % positionz=parameters.geometry.wall2_W/2;
40 [~, n]=size(positionx);
41 [~, m]=size(positiony);
42 [~, l]=size(positionz);
43
44 parameters.const_pts=zeros(3,n*m*l);
45 [~,si]=size(parameters.geometry.x);
46 parameters.const_pts_VF=zeros(si,n*m*l);
47 int=0;
```

```
48 % VF_point(parameters.const_pts(:,1),parameters.geometry); %
       view factor of point int
49
50 h = waitbar(0,'Initializing waitbar...');
51 for k=1:l
52     for j=1:m
53         for i=1:n
54             int=int+1;
55             parameters.const_pts(:,int)=[positionx(i);
                   positiony(j); positionz(k)]; % point int
56             parameters.const_pts_VF(:,int)=VF_point(parameters
                   .const_pts(:,int),parameters.geometry); % view
                   factor of point int
57             waitbar(int/(l*m*n),h,'calculating view factor for
                    each point')
58             %disp(int/(l*m*n)*100)
59         end
60     end
61 end
62 disp('view factor for surface calculated')
63 close(h)
64
65 disp('condition number of matrix F')
66 disp(cond(parameters.const_pts_VF,2))
67 % parameters.s_mrt=parameters.const_pts_VF*((parameters.
       const_pts_VF'*parameters.const_pts_VF)\ones(n*l*m,1));
68 % parameters.null_mrt=null(parameters.const_pts_VF'); % all
       solutions are found from T_wall^4=s_mrt*T_mrt^4+parameters.
       null_mrt*x
```

```
% [~,parameters.null_mrtsize]=size(parameters.null_mrt);

%%%%%%%%%%%%%%%%%%%%%%%%%%%%%%%%%% define window and special
    surface (not regular wall) (give index number for window
    surface)
% window 1 and window 2 are on xy plane
A=parameters.geometry.x([1; 2],1:parameters.geometry.size(1));
win1=find((A(1,:)>=parameters.geometry.win1_pose(1) & A(1,:)<
    parameters.geometry.win1_pose(1)+parameters.geometry.win_W)
     &...
     (A(2,:)>=parameters.geometry.win1_pose(2) & A(2,:)<
         parameters.geometry.win1_pose(2)+parameters.geometry.
         win_H)); % width then height
win2=find((A(1,:)>=parameters.geometry.win2_pose(1) & A(1,:)<
    parameters.geometry.win2_pose(1)+parameters.geometry.win_W)
     &...
     (A(2,:)>=parameters.geometry.win2_pose(2) & A(2,:)<
         parameters.geometry.win2_pose(2)+parameters.geometry.
         win_H));
[~,sizeA]=size(A);
wall1=ones(1,sizeA);
wall1([win1, win2])=[zeros(size(win1)), zeros(size(win2))];
wall1=find(wall1);
% window 3 and window 4 are on zy plane
A=parameters.geometry.x([3; 2],(sum(parameters.geometry.size
    (1:2))+1):sum(parameters.geometry.size(1:3)));
win3=sum(parameters.geometry.size(1:2))+find((A(1,:)>=
    parameters.geometry.win3_pose(1) & A(1,:)<parameters.
    geometry.win3_pose(1)+parameters.geometry.win_W) &...
```

```
85        (A(2,:)>=parameters.geometry.win3_pose(2) & A(2,:)<
              parameters.geometry.win3_pose(2)+parameters.geometry.
              win_H));
86  win4=sum(parameters.geometry.size(1:2))+find((A(1,:)>=
        parameters.geometry.win4_pose(1) & A(1,:)<parameters.
        geometry.win4_pose(1)+parameters.geometry.win_W) &...
87        (A(2,:)>=parameters.geometry.win4_pose(2) & A(2,:)<
              parameters.geometry.win4_pose(2)+parameters.geometry.
              win_H));
88  [~,sizeA]=size(A);
89  wall2=ones(1, sizeA);
90  wall2([win3, win4]-sum(parameters.geometry.size(1:2)))=[zeros(
        size(win3)), zeros(size(win4))];
91  wall2=sum(parameters.geometry.size(1:2))+find(wall2);
92  % door is on zy+ plane
93  A=parameters.geometry.x([3; 2],(sum(parameters.geometry.size
        (1:3))+1):sum(parameters.geometry.size(1:4)));
94  door=sum(parameters.geometry.size(1:3))+find((A(1,:)>=
        parameters.geometry.door_pose(1) & A(1,:)<parameters.
        geometry.door_pose(1)+parameters.geometry.door_W) &...
95        (A(2,:)>=parameters.geometry.door_pose(2) & A(2,:)<
              parameters.geometry.door_pose(2)+parameters.geometry.
              door_H));
96  [~,sizeA]=size(A);
97  wall4=ones(1, sizeA);
98  wall4(door-sum(parameters.geometry.size(1:3)))=zeros(size(door
        ));
99  wall4=sum(parameters.geometry.size(1:3))+find(wall4);
100
```

```
101 wall3=sum(parameters.geometry.size(1))+find(ones(size((sum(
        parameters.geometry.size(1))+1):sum(parameters.geometry.
        size(1:2)))));
102 floor=sum(parameters.geometry.size(1:4))+find(ones(size((sum(
        parameters.geometry.size(1:4))+1):sum(parameters.geometry.
        size(1:5)))));
103 plaf=sum(parameters.geometry.size(1:5))+find(ones(size((sum(
        parameters.geometry.size(1:5))+1):sum(parameters.geometry.
        size(1:6)))));
104
105 win1=win1';
106 win2=win2';
107 win3=win3';
108 win4=win4';
109 door=door';
110
111 %%%%%%%%%%%%%%%%%%%%%%%%%%%%%%%% Thermal properties and flow
112 % temperature parameters
113 parameters.wallout=[ones(parameters.geometry.size(1), 1)*(-20)
        ; ones(parameters.geometry.size(2), 1)*22; ...
114       ones(parameters.geometry.size(3), 1)*(-20); ones(
              parameters.geometry.size(4), 1)*(22);...
115       ones(parameters.geometry.size(5), 1)*22; ones(parameters.
              geometry.size(6), 1)*(-20)];% temperature of outside
              section of wall in deg C [Wxy; Wxy+; ...Wzy; Wzy+; ...
             Wxz; Wxz+]
116 parameters.wallout([win1; win2; win3; win4; door])=[-20*ones(
        size(win1)); -20*ones(size(win2)); -20*ones(size(win3));
```

```
    -20*ones(size(win4)); 22*ones(size(door))]; % set special
    feature temperature
117 parameters.airout=[-20; 22; -20; 22; 22; -20];% temperature of
     outside air in deg C [Wxy; Wxy+; Wzy; Wzy+; Wxz; Wxz+]
118
119 % emisivity of surfaces
120 parameters.epsilon=[ones(parameters.geometry.size(1), 1)*0.9;
    ones(parameters.geometry.size(2), 1)*0.9; ...
121     ones(parameters.geometry.size(3), 1)*0.9; ones(parameters.
        geometry.size(4), 1)*0.9;...
122     ones(parameters.geometry.size(5), 1)*0.9; ones(parameters.
        geometry.size(6), 1)*0.91];% emmisivity of wall [Wxy;
        Wxy+; ...Wzy; Wzy+; ...Wxz; Wxz+];
123 parameters.epsilon([win1; win2; win3; win4; door])=[0.93*ones(
    size(win1)); 0.93*ones(size(win2)); 0.93*ones(size(win3));
    0.93*ones(size(win4)); 0.93*ones(size(door))]; % set
    special feature emmisivity
124
125 % insulation of surface
126 parameters.insulation=[ones(parameters.geometry.size(1), 1)*3;
     ones(parameters.geometry.size(2), 1)*1; ...
127     ones(parameters.geometry.size(3), 1)*3; ones(parameters.
        geometry.size(4), 1)*1;...
128     ones(parameters.geometry.size(5), 1)*5.28; ones(parameters
        .geometry.size(6), 1)*7.16];% insulation of wall in RSI
         [Wxy; Wxy+; ...Wzy; Wzy+; ...Wxz; Wxz+];%
129 parameters.insulation([win1; win2; win3; win4; door])=[0.41*
    ones(size(win1)); 0.41*ones(size(win2)); 0.41*ones(size(
```

```
win3)); 0.41*ones(size(win4)); 0.8*ones(size(door))]; % set special feature insulation

% conductivity of surface (k*t) were t is the thicknes
parameters.conductivity=[ones(parameters.geometry.size(1), 1)*0.17*0.0095; ones(parameters.geometry.size(2), 1)*0.17*0.0095; ...
    ones(parameters.geometry.size(3), 1)*0.17*0.0095; ones(parameters.geometry.size(4), 1)*0.17*0.0095;...
    ones(parameters.geometry.size(5), 1)*0.17*0.0191; ones(parameters.geometry.size(6), 1)*0.17*0.0286];% insulation of wall in RSI [Wxy; Wxy+; ...Wzy; Wzy+; ...Wxz; Wxz+];%
parameters.conductivity([win1; win2; win3; win4; door])=[0.8*0.00635*ones(size(win1)); 0.8*0.00476*ones(size(win2)); 0.8*0.00476*ones(size(win3)); 0.8*0.00476*ones(size(win4)); 0.08*0.04*ones(size(door))]; % set special feature insulation

% air echange
parameters.air_exchange=1/2.5*[12.7;0;15.9;0;0;3]/3600;%in m^3/s 43.5/3600*[0.1;0.2;0.1;0.5;0.05;0.05];% air exchange in m^3/s [Wxy; Wxy+; ...Wzy; Wzy+; ...Wxz; Wxz+]; (set in vector ACH)

%%%%%%%%%%%%%%%%%%%%%%%%%%%%%%%%%%%%%%%%%%%%%%%%%%%%%%%%%%%%%%%%%%Define Heat transfer problem (associated matrices)
% convection factors
```

```
142 % parameters.h=[ones(parameters.geometry.size(1), 1)*1.14;
        ones(parameters.geometry.size(2), 1)*1.64; ...
143 %       ones(parameters.geometry.size(3), 1)*1.14; ones(
        parameters.geometry.size(4), 1)*1.64;...
144 %       ones(parameters.geometry.size(5), 1)*4.8; ones(
        parameters.geometry.size(6), 1)*6.61];% insulation of wall
        in RSI [Wxy; Wxy+; ...Wzy; Wzy+; ...Wxz; Wxz+];%
145 % parameters.h([win1; win2; win3; win4; door])=[8.67*ones(size
        (win1)); 8.67*ones(size(win2)); 8.67*ones(size(win3));
        8.67*ones(size(win4)); 1.64*ones(size(door))]; % set
        special feature insulation
146
147 parameters.h=2.5; % convection factor
148 parameters.cp=1005; % J/kgK heat capacity of air for -50 to 40
        degC
149 parameters.rho=1.293; % weight of air at 0 degC
150
151 opt_param=HT_matrices(parameters, parameters.wallout,
        parameters.airout); % define matrices
152 %PMV parameters
153 opt_param.PMV.v=0.02; % draft in m/s
154 opt_param.PMV.Pa=1/10; % 2.8755% water pressurin kPa taken at
        23degC
155 opt_param.PMV.I_cl=1; % clothing % see table in clo
156 opt_param.PMV.M=1*58.15; % Metabolic rate see table in W/m^2
        (1 met = 58.15W/m^2)
157 opt_param.const_pts_VF=parameters.const_pts_VF;
158
159
```

```
160 T_0=ones(sum(parameters.geometry.size)+1, 1)*0; % use a
      temperature point that has below expected loss (23.15)
161 % T_0=ones(sum(parameters.geometry.size)+1, 1)*20; % use a
      temperature point that has below expected loss (23.15)
162 % T_0(1241)=30;
163 %T_0([win1; win2; win3; win4; door])=[14.5*ones(size(win1));
      14.5*ones(size(win2)); 14.5*ones(size(win3)); 14.5*ones(
      size(win4)); 21.7*ones(size(door))]; % set special feature
      temperature
164 % initialise at T_0=23 for all
165 maxT=80*ones(size(T_0));
166 maxT(floor)=27*ones(size(floor));
167
168 %%%%%%%%%%%%%%%%%%%%%%%%%%%%%%%%%%%%%%%%%%%%%%%%%%%%%%%% Setup and solve
      optimization
169 % define objectif function and constraints
170 % A=[eye(si), zeros(si,1); zeros(1,si), 1];
171 % objective=@(x)objective_temp_dist((A*(x-0)),parameters,1); %
      flip x for ga
172 % constraints=@(x)constraint_temp_dist2((A*(x-0)),parameters);
173 disp('setup time')
174 toc
175 % set optimisation parameters and run optimisation
176 disp('start optimisation')
177 tic
178 h=figure('Name', 'wall temperature solution');
179 plot_mesh_data(parameters.geometry, T_0(1:si,1))
```

```
180 % optim.options = optimset('Algorithm', 'sqp', 'Display', 'off
    ', 'MaxFunEvals', 5000, 'Maxiter', 5000, 'TolFun', 1e-6, '
    TolCon', 1e-6, 'TolX', 1e-6);
181
182 % normal run (one run)
183 % options = optimset('UseParallel', 'always', 'Display','iter-
    detailed','Algorithm','sqp' ,'GradObj','on', 'GradConstr',
    'on',...
184 %     'LargeScale', 'on', 'TolX', 1e-10, 'TolCon', 1e-6, '
    TolFun', 1e-6, 'MaxFunEvals', 10^12, 'Maxiter', 500, '
    SubproblemAlgorithm', 'ldl-factorization', 'ScaleProblem',
    'obj-and-constr',...
185 %     'OutputFcn', @(x, optimValues, state)plot_solution_iter(
    x, optimValues, state, parameters, si, h));
186 % [T_sol, f_opt]=fmincon(@(x)obj_2017(x, opt_param),T_0
    ,[],[],[],[],[],[],@(x)const_2017(x, opt_param),options); %
     local optimisation (ver2017) use maxT for temperature
    limit
187 %[T_sol, f_opt]=fmincon(@(x)obj_2017(x, opt_param),T_0
    ,[],[],[],[],[],maxT,@(x)const_2017(x, opt_param),options);
     % local optimisation (ver2017) use maxT for temperature
    limit
188
189 % run updating convection factor
190 runs=8;
191 for i=1:runs
192 if i==runs
```

```
193     options = optimset('UseParallel', 'always', 'Display','
            iter-detailed','Algorithm','sqp' ,'GradObj','on', '
            GradConstr', 'on' ,...
194     'LargeScale',  'on', 'TolX', 1e-10, 'TolCon', 1e-6, '
            TolFun', 1e-6, 'MaxFunEvals', 1000, 'Maxiter', 500, '
            SubproblemAlgorithm', 'ldl-factorization', '
            ScaleProblem', 'obj-and-constr' ,...
195     'OutputFcn', @(x, optimValues, state)plot_solution_iter(x,
            optimValues, state, parameters, si, h));
196 else
197     options = optimset('UseParallel', 'always', 'Display','
            iter-detailed','Algorithm','sqp' ,'GradObj','on', '
            GradConstr', 'on' ,...
198     'LargeScale',  'on', 'TolX', 1e-10, 'TolCon', 1e-6, '
            TolFun', 1e-6, 'MaxFunEvals', 1000, 'Maxiter', 10, '
            SubproblemAlgorithm', 'ldl-factorization', '
            ScaleProblem', 'obj-and-constr' ,...
199     'OutputFcn', @(x, optimValues, state)plot_solution_iter(x,
            optimValues, state, parameters, si, h));
200 end
201 [T_sol, f_opt]=fmincon(@(x)obj_2017(x, opt_param),T_0
    ,[],[],[],[],[],[],@(x)const_2017(x, opt_param),options); %
     local optimisation (ver2017) use maxT for temperature
    limit
202 %[T_sol, f_opt]=fmincon(@(x)obj_2017(x, opt_param),T_0
    ,[],[],[],[],[],maxT,@(x)const_2017(x, opt_param),options);
     % local optimisation (ver2017) use maxT for temperature
    limit
203 parameter_update
```

```
204 end
205
206
207 %%%%%%%%%%%%%%%%%%%%%%%%%%%%%%%%%%%%%%%%%%%%%%%%%%%%%%%%%%% extract info and
        save
208 % [q, q_rad, q_conv_wall, q_cond, q_conv_air]=Virtual_heater(
      T_sol(1:si), T_sol(si+1),parameters.wallout, parameters.
      airout ,parameters.rad_transfer_const, parameters.
      conduction_transfer_const, parameters.
      convection_transfer_const);
209 % Energy=sum(q);
210 % [~, PMV]=const_2017(T_sol,opt_param);
211 optimisation.opt_param=opt_param;
212 optimisation.parameters=parameters;
213 optimisation.const=const_2017(T_sol,opt_param);
214 optimisation.T_0=T_0;
215 optimisation.T_sol=T_sol;
216 optimisation.f_opt=f_opt;
217 optimisation.objective=obj_2017(T_sol,opt_param);
218 % optimisation.Heat_transfer.q=q;
219 % optimisation.Heat_transfer.q_rad=q_rad;
220 % optimisation.Heat_transfer.q_conv_wall=q_conv_wall;
221 % optimisation.Heat_transfer.q_cond=q_cond;
222 % optimisation.Heat_transfer.q_conv_air=q_conv_air;
223 optimisation.index.wall1=wall1;
224 optimisation.index.wall2=wall2;
225 optimisation.index.wall3=wall3;
226 optimisation.index.wall4=wall4;
227 optimisation.index.floor=floor;
```

```
optimisation.index.plaf=plaf;
optimisation.index.win1=win1;
optimisation.index.win2=win2;
optimisation.index.win3=win3;
optimisation.index.win4=win4;
optimisation.index.door=door;

%%%%%%%%%%%%%%%%%%%%%%%%%%%%%%%%%%%%%%%%%%%%%%%%%%%%%%%%%%%%%%%%% display
    results
figure('Name', 'wall temperature solution')
plot_mesh_data(parameters.geometry, T_sol(1:si,1)) % initial
    guess

optimisation.stats.T_sol=all_stats(T_sol, optimisation.index);
   % orde [moy, minimum, index_min, maximum, index_max]

disp('Max T_sol:')
disp(max(T_sol))
disp('Min T_sol:')
disp(min(T_sol))
disp('Minimum')
disp(f_opt)
% disp('Energy')
% disp(Energy)
disp('optimisation time')
toc
%matlabpool close
```

2. Objective function

```
% objective function
function [f, df]=obj_2017(T,opt_param)
f=-(opt_param.sum_cc_mat*T+opt_param.sumb);
df=-opt_param.sum_cc_mat';
end
```

3. Constraint function

```
% constraint of optimisation
function [ ineq, eq, dineq, deq]=const_2017(T,opt_param)
% Thermal compfort constraints
[n,~]=size(T);
[~,m]=size(opt_param.const_pts_VF);
PMVi=ones(m,1);
%T_r=PMVi;
gradPMVi=zeros(m,n);
sp_vect=1:1:n;
parfor i=1:m % for each constraint point
    T_r=mean_rad_temp(opt_param.const_pts_VF(:,i), T(1:n-1));
      % mean radiant temperature
    [PMVi(i), gradPMV]=predicted_mean_vote_with_grad(T(n), T_r
      , opt_param.PMV.v, opt_param.PMV.Pa, opt_param.PMV.I_cl
      , opt_param.PMV.M); % predicted mean vote at position
    dtr_4_dT=4*opt_param.const_pts_VF(:,i)'*sparse(sp_vect(1:n
      -1),sp_vect(1:n-1),(T(1:n-1)+273.15).^3); % dt_r^4/dT
    dtr_dtr4=1/(4*(T_r+273.15)^(3)); % dtr^4/dtr=4*tr^3 donc
      1/(4*tr^3)=dtr/dtr^4
    gradPMVi(i,:)=[gradPMV(2)*dtr_dtr4*dtr_4_dT, gradPMV(1)];
      % grad of PMV at constraint point i
end
```

```
17 PMV_av=mean(PMVi); % average PMV on all points
18 dPMV_av=mean(gradPMVi,1); % gradiant of average PMV on all
       points
19 PMV_sq=PMVi.^2-0.5^2; % PMV range for each single point (use
       of square reduces by half the number of inequlity -0.5<PMV
       <0.5)
20 dPMV_sq=(2*diag(PMVi)*gradPMVi); % gradiant of PMV_sq
21
22 % virtual heater constraints
23 Q_vh=-(opt_param.cc_mat*T+opt_param.b+opt_param.rad_mat*(T
       +273.15).^4); % virtual heaters (conduction/convection part
        + radiation part)
24 dQ_vh=-(opt_param.cc_mat+opt_param.rad_mat*(sparse(sp_vect,
       sp_vect,4*(T+273.15).^3))); % gradiant of virtual heaters
25
26 % outputs
27 eq=PMV_av;
28 deq=dPMV_av';
29 ineq=[PMV_sq;Q_vh]';
30 dineq=[dPMV_sq;dQ_vh]';
31
32 % eq=PMV_av;
33 % deq=dPMV_av';
34 % ineq=PMV_sq';
35 % dineq=dPMV_sq';
36 end
```

4. Define mesh

```
1
```

```
function geometry=define_geometry_mesh3()
geometry.wall1_W=3.75;
geometry.wall2_W=5;% 5
geometry.wall1_H=2.5;

geometry.win_W=0.75;
geometry.win_H=1;
geometry.win1_pose=[0.5; 1];
geometry.win2_pose=[1.5; 1];
geometry.win3_pose=[1.5; 1];
geometry.win4_pose=[2.5; 1];

geometry.door_W=1;
geometry.door_H=2;
geometry.door_pose=[4; 0];


%%%%%%%%%%%%%%%%%%%%%%%%%%%%%%%%%%%%%%%%%%%%%%%%%%%%%%%%define mesh grid
% div=8;% number of divisions
% divx=div;
% divy=div;
% divz=div;
step=0.25;%0.25; % steps with
dx=step;
dy=step;
dz=step;
% dx=geometry.wall1_W/divx;
% dy=geometry.wall1_H/divy;
% dz=geometry.wall2_W/divz;
```

```
distx=geometry.wall1_W;
disty=geometry.wall1_H;
distz=geometry.wall2_W;
x=0:dx:distx; % meshing points in x
% x=0:distx:distx;
x=x';
[n,~]=size(x);
y=0:dy:disty; % meshing points in y
%y=0:disty:disty;
y=y';
[m,~]=size(y);
z=0:dz:distz; % meshing points in z
%z=0:distz:distz;
z=z';
[l,~]=size(z);

%%%%%%%%%%%%%%%%%%%%%%%%%%%%%%%%%%%%%%%%

%%%%%%%%%%%%%%%%%%%%%%%%%%%%%%%%%%%%%%%% define surfaces in
    mesh
% xy plane (z=0)
meshxy.x=zeros(3,(n-1)*(m-1));
meshxy.v1=zeros(3,(n-1)*(m-1));
meshxy.v2=zeros(3,(n-1)*(m-1));
[~,nm]=size(meshxy.x);
neighbors_xy=zeros(4,nm);
inc=0;
for j=1:m-1
    for i=1:n-1
```

```
59            inc=inc+1;
60            meshxy.x(:,inc)=[x(i); y(j); 0];
61            meshxy.v1(:,inc)=[x(i+1)-x(i); 0; 0];
62            meshxy.v2(:,inc)=[0; y(j+1)-y(j); 0];
63            if i==1
64                neighbors_xy(1:2,inc)=[nan; inc+1];
65            elseif i==n-1
66                neighbors_xy(1:2,inc)=[inc-1; nan];
67            else
68                neighbors_xy(1:2,inc)=[inc-1; inc+1];
69            end
70            if j==1
71                neighbors_xy(3:4,inc)=[nan; inc+n-1];
72            elseif j==m-1
73                neighbors_xy(3:4,inc)=[inc-(n-1); nan];
74            else
75                neighbors_xy(3:4,inc)=[inc-(n-1); inc+n-1];
76            end
77        end
78    end
79
80    % zy plane (x=0)
81    meshzy.x=zeros(3,(l-1)*(m-1));
82    meshzy.v1=zeros(3,(l-1)*(m-1));
83    meshzy.v2=zeros(3,(l-1)*(m-1));
84    [~,lm]=size(meshzy.x);
85    neighbors_zy=zeros(4,nm);
86    inc=0;
87    for j=1:m-1
```

```
88      for k=1:l-1
89          inc=inc+1;
90          meshzy.x(:,inc)=[0; y(j); z(k)];
91          meshzy.v1(:,inc)=[0; 0; z(k+1)-z(k)];
92          meshzy.v2(:,inc)=[0; y(j+1)-y(j); 0];
93          if k==1
94              neighbors_zy(1:2,inc)=[nan; inc+1];
95          elseif k==n-1
96              neighbors_zy(1:2,inc)=[inc-1; nan];
97          else
98              neighbors_zy(1:2,inc)=[inc-1; inc+1];
99          end
100         if j==1
101             neighbors_zy(3:4,inc)=[nan; inc+l-1];
102         elseif j==m-1
103             neighbors_zy(3:4,inc)=[inc-(l-1); nan];
104         else
105             neighbors_zy(3:4,inc)=[inc-(l-1); inc+l-1];
106         end
107     end
108 end
109
110 % xz plane (y=0)
111 meshxz.x=zeros(3,(n-1)*(l-1));
112 meshxz.v1=zeros(3,(n-1)*(l-1));
113 meshxz.v2=zeros(3,(n-1)*(l-1));
114 [~,nl]=size(meshxz.x);
115 neighbors_xz=zeros(4,nm);
116 inc=0;
```

```
for k=1:l-1
    for i=1:n-1
        inc=inc+1;
        meshxz.x(:,inc)=[x(i); 0; z(k)];
        meshxz.v1(:,inc)=[x(i+1)-x(i); 0; 0];
        meshxz.v2(:,inc)=[0; 0; z(k+1)-z(k)];
        if i==1
            neighbors_xz(1:2,inc)=[nan; inc+1];
        elseif i==n-1
            neighbors_xz(1:2,inc)=[inc-1; nan];
        else
            neighbors_xz(1:2,inc)=[inc-1; inc+1];
        end
        if k==1
            neighbors_xz(3:4,inc)=[nan; inc+n-1];
        elseif k==l-1
            neighbors_xz(3:4,inc)=[inc-(n-1); nan];
        else
            neighbors_xz(3:4,inc)=[inc-(n-1); inc+n-1];
        end
    end
end
%%%%%%%%%%%%%%%%%%%%%%%%%%%%%%%%%%%%%%%%%%%%%%%%%%%%%store
    mesh in geometry
% geometry follows the folowing rule [xy(z=0)surface, xy(z=
    opposite wall)surface, zy(x=0)surface, zy(x=opposite wall)
    surface, xz(y=0)surface, xz(y=opposite wall)surface]
geometry.size=[nm, nm, lm, lm, nl, nl]; % is the number of
    element per wall
```

```
142 geometry.dims=[n-1,m-1,l-1];
143 geometry.x=[meshxy.x, meshxy.x+[zeros(1,nm);zeros(1,nm);distz*
    ones(1,nm)], ...
144     meshzy.x, meshzy.x+[distx*ones(1,lm);zeros(1,lm);zeros(1,
        lm)], ...
145     meshxz.x, meshxz.x+[zeros(1,nl);disty*ones(1,nl);zeros(1,
        nl)]]; % surface origine
146 geometry.v1=[meshxy.v1, meshxy.v1, meshzy.v1, meshzy.v1,
    meshxz.v1, meshxz.v1]; % surface vector 1
147 geometry.v2=[meshxy.v2, meshxy.v2, meshzy.v2, meshzy.v2,
    meshxz.v2, meshxz.v2]; % surface vector 2
148 geometry.neighbors=[neighbors_xy, neighbors_xy+nm, ...
149     neighbors_zy+2*nm, neighbors_zy+2*nm+lm,...
150     neighbors_xz+2*nm+2*lm, neighbors_xz+2*nm+2*lm+nl];
151 disp('number of surfaces')
152 disp(2*(nm+nl+lm))
153 disp('number of surfaces VF')
154 disp((2*(nm+nl+lm))^2/2)
155 end
```

5. View factors

5.1 View factors between surfaces

```
1 % function to extract view factor information from geometry
    and calculate
2 % surface area also
3 % geometry follows the folowing rule [xy(z=0)surface, xy(z=
    opposite wall)surface, zy(x=0)surface, zy(x=opposite wall)
    surface, xz(y=0)surface, xz(y=opposite wall)surface]
```

```
4  % For each surface they are numbered allready from 1 to n
       where n is the total number of surfaces. To save
       computations a
5  % global numbering scheme is use here to be able to manage F21
       =A1/A2*F12 (only F12 must be found)
6  function geometry=Find_VFs(geometry)
7  [~, n]=size(geometry.x);% number of mesh surface
8
9  % initialisation
10 VF=zeros(n,n);
11 Ai=zeros(n,1);
12 x=geometry.x;
13 v1=geometry.v1;
14 v2=geometry.v2;
15 parfor i=1:n
16     Ai(i)=norm(v1(:,i))*norm(v2(:,i)); % get surface info
17 end
18 disp('view factor for surface progress')
19 parfor_progress(n);
20 parfor i=1:n
21 %     xi=x(:,i);
22 %     v1i=v1(:,i);
23 %     v2i=v2(:,i);
24 VFj=zeros(1,n);
25     for j=i:n % only sweep half of matrix
26         if i==j
27             VFj(1,j)=0;
28         else
```

```
29                P1=[x(:,i), x(:,i)+v1(:,i), x(:,i)+v1(:,i)+v2(:,i)
                      , x(:,i)+v2(:,i)];
30                P2=[x(:,j), x(:,j)+v1(:,j), x(:,j)+v1(:,j)+v2(:,j)
                      , x(:,j)+v2(:,j)]; % warning ignored the full
                      vector is needed
31                VFj(1,j)=rect_view_factor(P1,P2); % analytical
                      method used here (numerical uses viewfactor(P1
                      ',P2',4);)
32            end
33        end
34        VF(i,:)=VFj;
35        parfor_progress;% update progress
36    end
37     parfor_progress(0);
38
39    for i=1:n
40    %       VFi=VF(i,:);
41        for j=i:n % fill other half
42                VF(j,i)=Ai(i)/Ai(j)*VF(i,j); % warning ignored the
                      full vector is needed
43        end
44    end
45    geometry.Ai=Ai;
46    geometry.VF=VF;
47    % output is Ai and VF through geometry structure
48    end
```

```
1  % this function is to calculate the view factor between two
       rectangular
```

```
% surface either parrallel or perpendicular. Furthermore, the surfaces
% cannot partialy intersect so as hat they are either totaly over each
% other or are not

function VF=rect_view_factor(P1,P2)
% define some key vectors
V1=zeros(3,4);
V2=V1;
for i=1:4
    j=mod(i,4)+1; % permute index
    V1(:,i)=P1(:,i)-P1(:,j);
    V2(:,i)=P2(:,i)-P2(:,j);
end
e1=cross(V2(:,1),V2(:,2));
e1=e1/norm(e1);
e2=cross(V1(:,1),V1(:,2));
e2=e2/norm(e2);


% check if parrallel or perpendicular
if dot(e1,e2)==0 % squ2 is perendicular to e1
    % get proper orientaation of e1 and e2
    if dot(e1,P1(:,1)-P2(:,2))==0
        e1=e1*sign(dot(e1,P1(:,3)-P2(:,2)));
    else
        e1=e1*sign(dot(e1,P1(:,1)-P2(:,2)));
    end
```

```
29      if dot(e2,P2(:,1)-P1(:,2))==0
30          e2=e2*sign(dot(e2,P2(:,3)-P1(:,2)));
31      else
32          e2=e2*sign(dot(e2,P2(:,1)-P1(:,2)));
33      end
34      e3=cross(e1,e2); % define axe direction
35      E=[e1'; e2'; e3'];
36      eta1=zeros(3,4);
37      eta2=eta1;
38      for i=1:4
39          eta1(:,i)=E*(P1(:,i)-P1(:,1));
40          eta2(:,i)=E*(P2(:,i)-P1(:,1));
41      end
42      axealigned(1,:)=eta2(2,:)==0; % evaluate from squ1
43      axealigned(2,:)=eta1(1,:)-ones(1,4)*eta2(1,1)==0; %
            evaluate from squ2
44
45      aligned_mat(1,:)=eta2(3,:)==0; % points on line 1
46      aligned_mat(2,:)=eta2(3,:)-ones(1,4)*eta1(3,3)==0; %
            points on line 3
47      online=[sum(aligned_mat(1,:)); sum(aligned_mat(2,:))]/2;
48      number_online=sum(online);
49      % view factor
50      VF=perpendicular_VF(eta1, eta2, axealigned, number_online)
            ;
51
52  else % must be parrallel if not perpendicular
53      % e3 is the normal direction
54      e1=V1(:,1)/norm(V1(:,1));
```

```
55      e2=V1(:,2)/norm(V1(:,2));
56      e3=cross(e1,e2);
57      norm_dist=abs(dot(e3,P1(:,1)-P2(:,1)));
58      if norm_dist==0
59          VF=0; % if the normal duistance is zero, the surface
                do not seee each other
60      else
61          % define new ref systeme and work in 2D
62          E=[e1'; e2'];
63          eta1=zeros(2,4);
64          eta2=eta1;
65          for i=1:4
66              eta1(:,i)=E*(P1(:,i)-P1(:,1));
67              eta2(:,i)=E*(P2(:,i)-P1(:,1));
68          end
69          aligned_mat=zeros(4,4);
70          aligned_mat(1,:)= eta2(2,:)==0; % line 1 to 2
71          aligned_mat(2,:)= eta2(1,:)-ones(1, 4)*eta1(1,3)==0; %
                line 2 to 3
72          aligned_mat(3,:)= eta2(2,:)-ones(1, 4)*eta1(2,3)==0; %
                line 3 to 4
73          aligned_mat(4,:)= eta2(1,:)==0; % line 4 to 1
74          number_aligned=sum(sum(aligned_mat))/2;
75          % Function to find case and calculate VF
76          VF=parallel_VF(eta1, eta2, norm_dist, number_aligned,
                aligned_mat);
77      end
78  end
79  end
```

```
% this function finds the case for perpendicular view factor
    then computes the
% VF depending on the case

function F=perpendicular_VF(eta1, eta2, axealigned,
    number_online)
squaxe=[sum(axealigned(1,:)); sum(axealigned(2,:))]/2;
number_aligned_axe=sum(squaxe);
a=max([abs(eta1(3,1)-eta1(3,2)), abs(eta1(3,2)-eta1(3,3))]);
b=max([abs(eta1(1,1)-eta1(1,2)), abs(eta1(1,2)-eta1(1,3))]);
c=max([abs(eta2(3,1)-eta2(3,2)), abs(eta2(3,2)-eta2(3,3))]);
d=max([abs(eta2(2,1)-eta2(2,2)), abs(eta2(2,2)-eta2(2,3))]);
e=min([abs(eta1(3,1)-eta2(3,1)), abs(eta1(3,1)-eta2(3,3)), ...
    abs(eta1(3,3)-eta2(3,1)), abs(eta1(3,3)-eta2(3,3))]); %
       min distance between squ1 and squ2 in direction 3
switch number_aligned_axe
    case 2 % 2 axes are aligned
        F=VF_2axe(a,b,c,d,e, number_online);
    case 1 % 1 axe is aligned (cases 9 to 11)
        % determine which axe is aligned
        % recal this function with no axes aligned
        if squaxe(1)==0 % squ 1 aligned
            d1=min([abs(eta2(2, 1)), abs(eta2(2, 2)), abs(eta2
                (2, 3))]); % distance of sq2 from axes
            F=VF_1axe_all(a, b, c, d, e, d1, number_online);
        else % squ2 must then be aligned
            d1=min([abs(eta1(1, 1)-eta2(1, 1)), abs(eta1(1, 2)
                -eta2(1, 1)), abs(eta1(1, 3)-eta2(1, 1))]); %
                distance of sq1 from axes
```

```
24                F21=VF_1axe_all(c, d, a, b, e, d1, number_online);
25                A1=a*b;
26                A2=c*d;
27                F=A2/A1*F21;
28            end
29        case 0 % No axes are aligned (case 12)
30            d1=min([abs(eta1(1, 1)-eta2(1, 1)), abs(eta1(1, 2)-
                  eta2(1, 1)), abs(eta1(1, 3)-eta2(1, 1))]); %
                  distance of sq1 from axes
31            d2=min([abs(eta2(2, 1)), abs(eta2(2, 2)), abs(eta2(2,
                  3))]); % distance of sq2 from axes
32            F=VF_0axe_all(a, b, c, d, e, d1, d2, number_online);
33    end
34    end

1   % this function finds the case for parrallel view factor then
        computes the
2   % VF depending on the case
3
4   function VF=parallel_VF(eta1, eta2, norm_dist, number_aligned,
        aligned_mat)
5   switch number_aligned
6       case 4 % base case #1
7           % parameters
8           a=norm(eta1(:,2));
9           b=norm(eta1(:,4));
10          c=norm_dist;
11          % view factor
12          VF=VFcase1(a, b, c);
```

```
13          %disp('case 1 base')
14      case 3 % case #2
15          mat_score_squ1=sum(aligned_mat,2); % lines
16          mat_score_squ2=sum(aligned_mat); % points
17          % find point on squ2 sitting on connected line
18          point_on_line=  [find(mat_score_squ2==2), find(
                mat_score_squ2~=2)]; % [points conected, point not
                connected]
19          % find line that is not alligned
20          line_not_aligned= find(mat_score_squ1==0); % line not
                aligned
21          % parameters
22          a=norm(eta1(:,line_not_aligned)-eta1(:,mod(
                line_not_aligned,4)+1)); % find distance on squ1
                point not aligned
23          b=norm(eta1(:,mod(line_not_aligned,4)+1)-eta1(:,mod(
                mod(line_not_aligned,4)+1,4)+1)); % find lenght of
                next line (next to not aligned)
24          c=min(norm(eta2(:,point_on_line(1))-eta2(:,
                point_on_line(3))), norm(eta2(:,point_on_line(1))-
                eta2(:,point_on_line(4)))); % compare on point on
                connected two the two points not connected
25          d=norm_dist;
26          % view factor
27          VF=VFcase2(a,b,c,d);
28          %disp('case 2')
29      case 2 % case 3a or 3b
30          max_pt_al=max(sum(aligned_mat));
31          if max_pt_al==2 % case 3a
```

```
32              % find lines that are alligned
33              mat_score_squ1=sum(aligned_mat,2); % lines
34              line_aligned= find(mat_score_squ1==2); % two for
                    one aligned
35              % define some useful vectors
36              % for squ1
37              v1=eta1(:,line_aligned(1))-eta1(:,mod(line_aligned
                    (1),4)+1);
38              e1=v1/norm(v1);
39              v2=eta1(:,line_aligned(2))-eta1(:,mod(line_aligned
                    (2),4)+1);
40              e2=v2/norm(v2);
41              % for squ2
42              v12=eta2(:,2)-eta2(:,1);
43              v14=eta2(:,4)-eta2(:,1);
44              % parameters
45              a=norm(v1);
46              b=norm(v2);
47              c=max(abs(dot(e1,v12)), abs(dot(e1,v14)));
48              d=max(abs(dot(e2,v12)), abs(dot(e2,v14)));
49              e=norm_dist;
50              % vie factor
51              VF=VFcase3a(a,b,c,d,e);
52              %disp('case 3a')
53          else %  case 3b
54              mat_score_squ1=sum(aligned_mat,2); % lines
55              line_aligned= find(mat_score_squ1==2); % two for
                    one aligned
56
```

```
57              v1=eta1(:,line_aligned(1))-eta1(:,mod(line_aligned
                    (1),4)+1);
58              v2=eta1(:,mod(line_aligned(1),4)+1)-eta1(:,mod(mod
                    (line_aligned(1),4)+1,4)+1);
59              e1=v1/norm(v1);
60              % parameters
61              a=norm(v2);
62              b=norm(v1);
63              c=max([abs(dot(e1,eta2(:,2)-eta2(:,1))),abs(dot(e1
                    ,eta2(:,4)-eta2(:,1)))]); % finds c and find if
                     use 1 to 2 or 1 to 4 in direction of e1
64              d=min([abs(dot(e1, eta1(:,1)-eta2(:,1))), abs(dot(
                    e1, eta1(:,1)-eta2(:,3))),...
65                   abs(dot(e1, eta1(:,3)-eta2(:,1))), abs(dot(e1,
                         eta1(:,3)-eta2(:,3)))]);% need close
                        points.
66              e=norm_dist;
67              % view factor
68              VF=VFcase3b(a,b,c,d,e);
69              %disp('case 3b')
70          end
71      case 1 % case 4
72          mat_score_squ1=sum(aligned_mat,2); % lines
73          line_aligned= find(mat_score_squ1==2); % two for one
                aligned
74          v1=eta1(:,line_aligned)-eta1(:,mod(line_aligned,4)+1);
75          v2=eta1(:,mod(line_aligned(1),4)+1)-eta1(:,mod(mod(
                line_aligned(1),4)+1,4)+1);
76          e1=v1/norm(v1);
```

```
77          e1=e1*sign(dot(e1,eta2(:,1)-eta1(:,1))); % make e1
                point from squ1 to squ2
78          e2=v2/norm(v2);
79          % parameters
80          a=norm(v1);
81          b=norm(v2);
82          c=max([abs(dot(e1,eta2(:,2)-eta2(:,1))),abs(dot(e1,
                eta2(:,4)-eta2(:,1)))]);
83          d=max([abs(dot(e2,eta2(:,2)-eta2(:,1))),abs(dot(e2,
                eta2(:,4)-eta2(:,1)))]);
84          [~,pt1]=min([norm(eta1(:,1)-eta2(:,1)), norm(eta1(:,2)
                -eta2(:,1)), norm(eta1(:,3)-eta2(:,1)), norm(eta1
                (:,4)-eta2(:,1))]);
85          e=min([norm(eta1(:,pt1)-eta2(:,1)), norm(eta1(:,pt1)-
                eta2(:,2)), norm(eta1(:,pt1)-eta2(:,3)), norm(eta1
                (:,pt1)-eta2(:,4))]); % need close points
86          f=norm_dist;
87          % view factor
88          VF=VFcase4(a,b,c,d,e,f);
89          %disp('case4')
90      case 0 % case 5
91          v1=eta1(:,2)-eta1(:,1);
92          v2=eta1(:,3)-eta1(:,2);
93          v12=eta2(:,2)-eta2(:,1);
94          v14=eta2(:,4)-eta2(:,1);
95          e1=v1/norm(v1);
96          e1=e1*sign(dot(e1,eta2(:,1)-eta1(:,1))); % make e1
                point from squ1 to squ2
97          e2=v2/norm(v2);
```

```
98          e2=e2*sign(dot(e2,eta2(:,1)-eta1(:,1))); % make e2
               point from squ1 to squ2
99          % parameters
100         a=norm(v1);
101         b=norm(v2);
102         [c, index1]=max([abs(dot(e1,v12)),abs(dot(e1,v14))]);
103         [d, index2]=max([abs(dot(e2,v12)),abs(dot(e2,v14))]);
104 %           v1x=eta2(:,2*index1)-eta2(:,1);
105 %           v1y=eta2(:,2*index2)-eta2(:,1);
106 %           e=abs(dot(e1,eta2(:,1)))+max([dot(-e1,v1x),0])-(abs(
    dot(e1,eta1(:,1)))+max([dot(e1,v1),0])); % need close
    points. add v only if far point. the far point is determine
     by the sign of the dot product when comparing to 0
107 %           f=abs(dot(e2,eta2(:,1)))+max([dot(-e2,v1y),0])-(abs(
    dot(e2,eta1(:,1)))+max([dot(e2,v2),0])); % need close
    points. add v only if far point. the far point is determine
     by the sign of the dot product when comparing to 0
108         [~, pt1]=min([norm(eta1(:,1)-eta2(:,1)), norm(eta1
               (:,2)-eta2(:,1)), norm(eta1(:,3)-eta2(:,1)), norm(
               eta1(:,4)-eta2(:,1))]);
109         [~, pt2]=min([norm(eta1(:,pt1)-eta2(:,1)), norm(eta1
               (:,pt1)-eta2(:,2)), norm(eta1(:,pt1)-eta2(:,3)),
               norm(eta1(:,pt1)-eta2(:,4))]); % need close points
110         ptp=eta1(:,pt1)-eta2(:,pt2);
111         e=abs(dot(e1, ptp));
112         f=abs(dot(e2, ptp));
113         g=norm_dist;
114         % view factor
115         VF=VFcase5(a,b,c,d,e,f,g);
```

```
116         %disp('case5')
117     otherwise
118         disp('error in parallel switch case (case was not
                identified)')
119 end
120 end
```

```
1 % VF for perdepicular 2 axes are not aligned
2 % a=width of squ1 (axe direction)
3 % b= depth of squ1
4 % c= width of squ2
5 % d= depth of squ2
6 % e= distance between squ1 and squ2
7 function F=VF_0axe_all(a, b, c, d, e, d1, d2, number_online)
8 % surfaces
9 A1=a*b;
10 A3=a*(b+d1);
11 A5=a*d1;
12 % sub VF
13 F34=VF_2axe(a,b+d1,c,d+d2,e, number_online);
14 F56=VF_2axe(a,d1,c,d2,e, number_online);
15 F36=VF_2axe(a,b+d1,c,d2,e, number_online);
16 F54=VF_2axe(a,d1,c,d+d2,e, number_online);
17 % view factor
18 F=A3/A1*(F34-F36)+A5/A1*(F56-F54);
19 end
```

```
1 % VF for perdepicular when squ1 is aligned on axes
2 % a=width of squ1 (axe direction)
3 % b= depth of squ1
```

```
% c= width of squ2
% d= depth of squ2
% e= distance between squ1 and squ2
function F=VF_1axe_all(a, b, c, d, e, d1, number_online)
% sub VF
F13=VF_2axe(a, b, c, d+d1, e, number_online);
F14=VF_2axe(a, b, c, d1, e, number_online);
% view factor
F=F13-F14;
end
```

```
% VF for perdepicular when squ1 is aligned on axes
% a=width of squ1 (axe direction)
% b= depth of squ1
% c= width of squ2
% d= depth of squ2
% e= distance between squ1 and squ2
function F=VF_2axe(a,b,c,d,e, number_online)
switch number_online
    case 2 % 2 lines are aligned (base case (case 6))
        %disp('case 6')
        F=VFcase6(a, b, d);
    case 1 % 1 line is aligned (case 7)
        %disp('case 7')
        F=VFcase7(a, b, c, d);
    case 0 % no line are aligned (case 8)
        %disp('case 8')
        F=VFcase8(a,b,c,d,e);
end
```

```
19 end

1 % finds the view factor between two aligned facing surfaces of
      same dimenssions
2 % a is the width
3 % b is the depth
4 % c is the height seperating the plates
5
6 function F=VFcase1(a, b, c)
7 X=a/c;
8 Y=b/c;
9 F=2/(pi*X*Y)*(log(sqrt((1+X^2)*(1+Y^2)/(1+X^2+Y^2))) ...
10      +X*sqrt(1+Y^2)*atan(X/sqrt(1+Y^2)) ...
11      +Y*sqrt(1+X^2)*atan(Y/sqrt(1+X^2)) ...
12      -X*atan(X)-Y*atan(Y));
13 end

1 % side to side view factor
2 % a= common lenght
3 % b= depth of squ 1
4 % c= depth of squ 2
5 % d= normal distance from surfaces
6
7 function F=VFcase2(a,b,c,d)
8 % surfaces
9 A1=a*b;
10 A3=a*(b+c);
11 A5=a*c;
12 % sub VF
13 F34=VFcase1(a,b+c,d);
```

```
F16=VFcase1(a,b,d);
F52=VFcase1(a,c,d);
% view factor
F=1/2*(A3/A1*F34-F16-A5/A1*F52);
end
```

```
% stagered view factor for non symetric case (depth are not
    the same so as to have F12!=F65 thus not symetric)
% a=width of squ1
% b=depth of squ1
% c=width of squ2
% d=depth of squ2
% e=noraml distance from squ1 to sq2

function F=VFcase3a(a,b,c,d,e)
if b==d % symetric case
    F=VFcase3a_sym(a,b,c,d,e);
elseif b<d % can use VFnonsym_case directly
    funct=@(d1)VFcase3a_sym(a,d1,c,d1,e);
    funct56=@(d1)VFcase4_sym(d1,a,d1,c,2*b,e);
    F=VFnon_sym_case(b, d, a, funct, funct56);
else % must use VFnonsym_case from 2 to 1
    A1=a*b;
    A2=c*d;
    funct=@(d1)VFcase3a_sym(c,d1,a,d1,e);
    funct56=@(d1)VFcase4_sym(d1,c,d1,a,2*d,e);
    F21=VFnon_sym_case(d, b, c, funct, funct56);
    F=A2/A1*F21;
end
```

```
23 end

1 % stagered view factor symetric case (depth are the same so as
      to have F12=F65 by symetry)
2 % a=width of squ1
3 % b=depth of squ1
4 % c=width of squ2
5 % d=depth of squ2
6 % e=noraml distance from squ1 to squ2
7
8 function F=VFcase3a_sym(a,b,c,d,e)
9 % surfaces
10 A1=a*b;
11 A3=(a+c)*b;
12 A5=c*b;
13 % sub VF
14 F34=VFcase2(a+c,b,d,e);
15 F16=VFcase2(a,b,d,e);
16 F52=VFcase2(c,b,d,e);
17 % view factor
18 F=1/2*(A3/A1*F34-F16-A5/A1*F52);
19 end

1 % side to side spaced view factor (case 3b)
2 % a=common distance(width)
3 % b=depth of squ1
4 % c=depth of squ2
5 % d=distance seperating squ1 from squ2
6 % e= normal distance
7
```

```
function F=VFcase3b(a,b,c,d,e)
% sub VF
F13=VFcase2(a,b,c+d,e);
F14=VFcase2(a,b,d,e);
% view factor
F=F13-F14;
end

% view factor for only one aligned line and non symetric case(
    case 4)
% a=length of squ1 on aligned edge
% b=length of squ1 not on aligned edge
% c=length of squ2 on aligned edge
% d=length of squ2 not on aligned edge
% e=plane distance from squ1 to squ2
% f= normal distance from squ1 to squ2

function F=VFcase4(a,b,c,d,e,f)
if a==c % symetric case
    F=VFcase4_sym(a,b,c,d,e,f);
elseif a<c % can use VFnonsym_case directly
    funct=@(d1)VFcase4_sym(d1,b,d1,d,e,f);
    funct56=@(d1)VFcase4_sym(d1,b,d1,d,2*a+e,f);
    F=VFnon_sym_case(a, c, b, funct, funct56);
else % must use VFnonsym_case from 2 to 1
    A1=a*b;
    A2=c*d;
    funct=@(d1)VFcase4_sym(d1,d,d1,b,e,f);
    funct56=@(d1)VFcase4_sym(d1,d,d1,b,2*c+e,f);
```

```
21      F21=VFnon_sym_case(c, a, d, funct, funct56);
22      F=A2/A1*F21;
23  end
24  end
```

```
1  % view factor for only one aligned line and symetric case(case
       4)
2  % a=length of squ1 on aligned edge
3  % b=length of squ1 not on aligned edge
4  % c=length of squ2 on aligned edge
5  % d=length of squ2 not on aligned edge
6  % e=plane distance from squ1 to squ2
7  % f= normal distance from squ1 to squ2
8
9  function F=VFcase4_sym(a,b,c,d,e,f)
10 % surfaces
11 A1=a*b;
12 A3=a*(b+d);
13 A5=a*d;
14 % sub VF
15 F34=VFcase3b(b+d,a,c,e,f);
16 F16=VFcase3b(b,a,c,e,f);
17 F52=VFcase3b(d,a,c,e,f);
18 % view factor
19 F=1/2*(A3/A1*F34-F16-A5/A1*F52);
20 end
```

```
1  % view factor when no edges aligned (case 5)
2  % a= width of squ1
3  % b= depth of squ1
```

```
% c= width of squ2
% d= depth of squ2
% e= distance between squ1 and squ2 along the width dimenssion
% f= distance between squ1 and squ2 along the depth dimenssion
% g= normal distance between squ1 and squ2

function F=VFcase5(a,b,c,d,e,f,g)
% sub VF
F13=VFcase3a(a,b,c+e,d+f,g);
F14=VFcase3a(a,b,e,f,g);
F15=VFcase4(a,b,c,f,e,g);
F16=VFcase4(b,a,d,e,f,g);
% view factor
F=F13-F14-F15-F16;
end
```

```
% finds the view factor between two perpendicular surfaces of
    same length
% connected by one of its edges
% l is the width
% h is the depth of the top plate (squ2)
% w is the depth of the bottom plate (squ1)

function F=VFcase6(l, w, h)
H=h/l;
W=w/l;
F=1/(pi*W)*(W*atan(1/W)+H*atan(1/H)-sqrt(H^2+W^2)*atan(1/sqrt(
    H^2+W^2))...
      +1/4*log(((1+W^2)*(1+H^2)/(1+W^2+H^2))...
```

```
12        *(W^2*(1+W^2+H^2)/((1+W^2)*(W^2+H^2)))^(W^2)...
13        *(H^2*(1+W^2+H^2)/((1+H^2)*(W^2+H^2)))^(H^2)));
14  end
```

```
1  % View factor for one line aligned when axes are aligned and
       non symetric case
2  % a=width of squ1 (axe direction)
3  % b= depth of squ1
4  % c= width of squ2
5  % d= depth of squ2
6  function F=VFcase7(a, b, c, d)
7  if b==d % symetric case
8       F=VFcase7_sym(a, b, c, d);
9  elseif b<d % can use VFnonsym_case directly
10      funct=@(d1)VFcase7_sym(a, d1, c, d1);
11      funct56=@(d1)F56_nonsym_case7(a, d1, c, b);
12      F=VFnon_sym_case(b, d, a, funct, funct56);
13 else % must use VFnonsym_case from 2 to 1
14      A1=a*b;
15      A2=c*d;
16      funct=@(d1)VFcase7_sym(c, d1, a, d1);
17      funct56=@(d1)F56_nonsym_case7(c, d1, a, d);
18      F21=VFnon_sym_case(d, b, c, funct, funct56);
19      F=A2/A1*F21;
20 end
21 end
```

```
1  % View factor for one line aligned when axes are aligned and
       symetric case
2  % (meaning: b=d)
```

```
% a=width of squ1 (axe direction)
% b= depth of squ1
% c= width of squ2
% d= depth of squ2
function F=VFcase7_sym(a, b, c, d)
% surfaces
A1=a*b;
A3=(a+c)*b;
A5=c*b;
% sub VF
F34=VFcase6(a+c, b, d);
F16=VFcase6(a, b, d);
F52=VFcase6(c, b, d);
% view factor
F=1/2*(A3/A1*F34-F16-A5/A1*F52);
end
```

```
% view factor axes aligned but no line aligned
% a=width of squ1 (axe direction)
% b= depth of squ1
% c= width of squ2
% d= depth of squ2
% e= distance between squ1 and squ2

function F=VFcase8(a,b,c,d,e)
F13=VFcase7(a, b, c+e, d);
F14=VFcase7(a, b, e, d);
F=F13-F14;
end
```

```
% this function is built to find view factor when a symetry condition is
% not present. This function is general as long as: depth squ1 < depth squ2
% param= structur of parameters of the function (symetric function)
% funct(depth1)= the symetric function to be used
% funct56 is the function use to calculate VF from 5 to 6, it may be the
% same as funct but not for all cases (for example when 12, 14, 32 have 2 common edge but 56 does not)
% d1=depth of squ1
% d2=depth of squ2
% a=width of squ1

function F=VFnon_sym_case(d1, d2, a, funct, funct56)
% surfaces
A1=a*d1;
A3=a*d2;
A5=a*(d2-d1);
% sub VF
F32=funct(d2);
F14=funct(d1);
F56=funct56(d2-d1);
% view factor
F=1/2*(A3/A1*F32+F14-A5/A1*F56);
end
```

```
% VF 5 to6 for non symetric case 7
```

```
% a=width of squ1 (axe direction)
% b= depth of squ1
% c= width of squ2
% d= depth of squ2
function F=F56_nonsym_case7(a, b, c, d1)
% surface
A5=a*b;
A9=(a+c)*b;
A7=c*b;
% sub VF
F910=VF_0axe_all(a+c, b, a+c, b, 0, d1, d1, 2);
F58=VF_0axe_all(a, b, a, b, 0, d1, d1, 2);
F76=VF_0axe_all(c, b, c, b, 0, d1, d1, 2);
% view factor
F=1/2*(A9/A5*F910-F58-A7/A5*F76);
end
```

5.2 View factor for the mean radiant temperature

```
% view factors for each wall
% x is the vector pointing to the point where T_r is measured
    in frame
% Master

% x is the point of T_r measurement
% geometry are geometrical parameters describing the test room
% VF are the view outputed factors
function VF=VF_point(x,geometry)

x0=geometry.x;
```

```
11 v1=geometry.v1;
12 v2=geometry.v2;
13
14 [~,n]=size(x0);
15 VF=zeros(n,1);
16 %disp('VF for thermal comfort points progress')
17 % parfor_progress(n)
18 parfor i=1:n
19     a=norm(v1(:,i));
20     b=norm(v2(:,i));
21     ex=v1(:,i)/a;
22     ey=v2(:,i)/b;
23     ez=cross(ex,ey);
24     ez=ez/norm(ez);
25     dx=[ex'; ey']*(x-x0(:,i));
26     c=abs(dot(ez,x-x0(:,i)));
27
28     VF(i)=VF_wall_section2(a, b, dx, c);
29 %       disp('VF point percentage')
30 %       disp(i/n*100)
31 end
32 % parfor_progress(0);
33 %sum(VF)
34 end
```

```
1 % this function computes the view factor of a of a surface
      from a point
2
3 function VF=VF_wall_section2(a,b,dx,c)
```

```
4  if dx(1)==0 && dx(2)==0% case on origine, origine
5      VF=VF_diff_sphere_corner_wall(a,b,c);
6  elseif dx(1)==0 && dx(2)>b % case on origine, passed second
       line
7      F1=VF_diff_sphere_corner_wall(a,dx(2),c);
8      F2=VF_diff_sphere_corner_wall(a,dx(2)-b,c);
9      VF=F1-F2;
10 elseif dx(1)==0 && dx(2)<0 % case on origine, case neg
11     F1=VF_diff_sphere_corner_wall(a,-dx(2)+b,c);
12     F2=VF_diff_sphere_corner_wall(a,-dx(2),c);
13     VF=F1-F2;
14 elseif dx(1)==0 % case on origine, case inside
15     F1=VF_diff_sphere_corner_wall(a,dx(2),c);
16     F2=VF_diff_sphere_corner_wall(a,b-dx(2),c);
17     VF=F1+F2;
18 elseif dx(1)>a && dx(2)==0% case passed second line, origine
19     F1=VF_diff_sphere_corner_wall(dx(1),b,c);
20     F2=VF_diff_sphere_corner_wall(dx(1)-a,b,c);
21     VF=F1-F2;
22 % elseif dx(1)>a && dx(2)==b % case on opposite corner, passed
       second line
23 %     F1=VF_diff_sphere_corner_wall(a,b,c);
24 %     F2=VF_diff_sphere_corner_wall(a,b,c);
25 %     VF=0;F1-F2;
26 elseif dx(1)>a && dx(2)>b % case passed second line, passed
       second line
27     F1=VF_diff_sphere_corner_wall(dx(1),dx(2),c);
28     F2=VF_diff_sphere_corner_wall(dx(1)-a,dx(2)-b,c);
29     F3=VF_diff_sphere_corner_wall(dx(1)-a,dx(2),c);
```

```
30      F4=VF_diff_sphere_corner_wall(dx(1),dx(2)-b,c);
31      VF=F1-F3-F4+F2;
32  elseif dx(1)>a && dx(2)<0 % case passed second line, neg
33      F1=VF_diff_sphere_corner_wall(dx(1),-dx(2)+b,c);
34      F2=VF_diff_sphere_corner_wall(dx(1)-a,-dx(2),c);
35      F3=VF_diff_sphere_corner_wall(dx(1),-dx(2),c);
36      F4=VF_diff_sphere_corner_wall(dx(1)-a,-dx(2)+b,c);
37      VF=F1-F3-F4+F2;
38  elseif dx(1)>a % case passed second line, inside
39      F1=VF_diff_sphere_corner_wall(dx(1),dx(2),c);
40      F2=VF_diff_sphere_corner_wall(dx(1),b-dx(2),c);
41      F3=VF_diff_sphere_corner_wall(dx(1)-a,dx(2),c);
42      F4=VF_diff_sphere_corner_wall(dx(1)-a,b-dx(2),c);
43      VF=F1+F2-F3-F4;
44  elseif dx(1)<0 && dx(2)==0 % case negative, origine
45      F1=VF_diff_sphere_corner_wall(-dx(1)+a,b,c);
46      F2=VF_diff_sphere_corner_wall(-dx(1),b,c);
47      VF=F1-F2;
48  elseif dx(1)<0 && dx(2)>b % case negative, passed second line
49      F1=VF_diff_sphere_corner_wall(-dx(1)+a,dx(2),c);
50      F2=VF_diff_sphere_corner_wall(-dx(1),dx(2)-b,c);
51      F3=VF_diff_sphere_corner_wall(-dx(1)+a,dx(2)-b,c);
52      F4=VF_diff_sphere_corner_wall(-dx(1),dx(2),c);
53      VF=F1-F3-F4+F2;
54  elseif dx(1)<0 && dx(2)<0 % case negative, neg
55      F1=VF_diff_sphere_corner_wall(-dx(1)+a,-dx(2)+b,c);
56      F2=VF_diff_sphere_corner_wall(-dx(1),-dx(2),c);
57      F3=VF_diff_sphere_corner_wall(-dx(1)+a,-dx(2),c);
58      F4=VF_diff_sphere_corner_wall(-dx(1),-dx(2)+b,c);
```

```
59      VF=F1-F3-F4+F2;
60  elseif dx(1)<0 % case negative, inside
61      F1=VF_diff_sphere_corner_wall(-dx(1)+a,dx(2),c);
62      F2=VF_diff_sphere_corner_wall(-dx(1)+a,b-dx(2),c);
63      F3=VF_diff_sphere_corner_wall(-dx(1),dx(2),c);
64      F4=VF_diff_sphere_corner_wall(-dx(1),b-dx(2),c);
65      VF=F1+F2-F3-F4;
66  elseif dx(2)==0 % case inside, origine
67      F1=VF_diff_sphere_corner_wall(dx(1),b,c);
68      F2=VF_diff_sphere_corner_wall(a-dx(1),b,c);
69      VF=F1+F2;
70  elseif dx(2)>b % case inside, passed second line
71      F1=VF_diff_sphere_corner_wall(dx(1),dx(2),c);
72      F2=VF_diff_sphere_corner_wall(a-dx(1),dx(2),c);
73      F3=VF_diff_sphere_corner_wall(dx(1),dx(2)-b,c);
74      F4=VF_diff_sphere_corner_wall(a-dx(1),dx(2)-b,c);
75      VF=F1+F2-F3-F4;
76  elseif dx(2)<0 % case inside, neg
77      F1=VF_diff_sphere_corner_wall(dx(1),-dx(2)+b,c);
78      F2=VF_diff_sphere_corner_wall(a-dx(1),-dx(2)+b,c);
79      F3=VF_diff_sphere_corner_wall(dx(1),-dx(2),c);
80      F4=VF_diff_sphere_corner_wall(a-dx(1),-dx(2),c);
81      VF=F1+F2-F3-F4;
82  else % case inside, inside
83      F1=VF_diff_sphere_corner_wall(dx(1),dx(2),c);
84      F2=VF_diff_sphere_corner_wall(a-dx(1),dx(2),c);
85      F3=VF_diff_sphere_corner_wall(dx(1),b-dx(2),c);
86      F4=VF_diff_sphere_corner_wall(a-dx(1),b-dx(2),c);
87      VF=F1+F2+F3+F4;
```

```
88 end
89 end
```

```
1 % View factor between differencial point sphere and wall at
      distance c,
2 % vector c being normal to the wall and joinning the sphere
      and corner of
3 % the wall
4
5 % c is the distance to the wall
6 % a is the width of the wall
7 % b is the height of the wall
8
9 function F=VF_diff_sphere_corner_wall(a,b,c)
10 A=a/c;
11 B=b/c;
12 F=1/(4*pi)*atan((A*B)/sqrt(1+B^2+A^2));
13 end
```

6. Thermal comfort

```
1 % function that calulates the predicted mean vote (PMV) as a
      function of
2 % its six parameter:
3 % T_a is the air temperature
4 % T_r is the mean radiant temperature
5 % v is the draft velocity
6 % Pa is the water vapor presure
7 % I_cl is the clothing insulation level
8 % M is the work done
```

```
9  % the function also caculates intermediate heat transfer
       values and stores
10 % them in heat_transfers, its also outputs clothing
       temperature
11
12 function [PMV, gradPMV]=predicted_mean_vote_with_grad(T_a, T_r
       , v, Pa, I_cl, M)
13 %%%%%%%%%%%%%% find PMV
14 eta=0;% eta is effiency of mechanical energy conversion
15
16 % find the clothing temperature and asssociated heat transfers
17 T_0=skin_temperature(M, eta);
18 [T_cl, heat_transfers.R, heat_transfers.C]=
       clothing_temperature(T_0-1, I_cl, v, M, T_r, T_a, eta);
19
20 % find heat blance L and associated heat transfers
21 heat_transfers.H=internal_heat(M, eta);
22 heat_transfers.E_d=water_diffusion_loss(M, eta, Pa);
23 heat_transfers.E_sw=sweat_loss(M, eta);
24 heat_transfers.E_re=latent_respiration_loss(M, Pa);
25 heat_transfers.E_dr=dry_respiration_loss(M, T_a);
26
27 heat_transfers.L=heat_transfers.H+heat_transfers.E_d+
       heat_transfers.E_sw+heat_transfers.E_re+heat_transfers.E_dr
       -heat_transfers.R-heat_transfers.C;
28
29 % find PMV
30 PMV=(0.303*exp(-0.036*M)+0.028)*heat_transfers.L;
31 %%%%%%%%%%%%%% find grad PMV
```

```
A=0.303*exp(-0.036*M)+0.028; % multiplying value for PMV
% with respect to T_a
heat_transfers_derivatives.dE_dr_dT_a=partial_E_dr_T_a(M);
heat_transfers_derivatives.dR_dT_a=partial_R_T_a(I_cl, v, T_cl
    , T_a);
heat_transfers_derivatives.dC_dT_a=partial_C_T_a(I_cl, v, T_cl
    , T_a);
gradPMV(1,1)=A*(-heat_transfers_derivatives.dE_dr_dT_a-
    heat_transfers_derivatives.dR_dT_a-
    heat_transfers_derivatives.dC_dT_a);

% with respect to T_r
heat_transfers_derivatives.dR_dT_r=partial_R_T_r(I_cl, v, T_cl
    , T_a, T_r);
heat_transfers_derivatives.dC_dT_r=partial_C_T_r(I_cl, v, T_cl
    , T_a, T_r);
gradPMV(2,1)=A*(-heat_transfers_derivatives.dR_dT_r-
    heat_transfers_derivatives.dC_dT_r);
end
```

```
% normal skin temperature

function T_skin=skin_temperature(M, eta)
T_skin=35.7-0.0275*M*(1-eta);
end
```

```
% function to calculate the clothing temperature and
    associated Radiative
% and convective heat transfer

```

```
% the fixed point method is used here
% T_0 is the inital guess
% toll is the convegence criterion as the variation in T_cl
    from two
% iteration
function [T_cl, R, C]=clothing_temperature(T_0, I_cl, v, M,
    T_r, T_a, eta)
%toll=0.01; % set tolerance
fun=@(T_cl)T_cl-skin_temperature(M, eta)+0.155*I_cl*(
    radiation_loss(I_cl, T_r, T_cl)+convective_loss(I_cl, v,
    T_cl, T_a));
options=optimset('Display', 'off');
T_cl=fsolve(fun,T_0,options); % clothing temperature

R=radiation_loss(I_cl, T_r, T_cl); % radiative heat loss
C=convective_loss(I_cl, v, T_cl, T_a); % convective heat loss
end
```

```
% calculates internal heat production based on mechanial
    convesion
% efficienty, Units in W/m^2
% eta is effiency of mechanical energy conversion
% M is the work done
function H=internal_heat(M, eta)
H=M*(1-eta);
end
```

```
% heat loss by water diffusion through skin
% units of W/m^2
% eta is effiency of mechanical energy conversion
```

```
% M is the work done
% Pa is the water vapor presure
function E_d=water_diffusion_loss(M, eta, Pa)
E_d=-3.05*(5.7662-0.00704*M*(1-eta)-Pa);
end
```

```
% evoparive heat loss from sweat from the skin
% Units in W/m^2
% eta is effiency of mechanical energy conversion
% M is the work done
function E_sw=sweat_loss(M, eta)
E_sw=-0.42*(M*(1-eta)-58.15);
end
```

```
% latent heat respiration heat loss
% units W/m^2
% M is the work done
% Pa is the water vapor presure
function E_re=latent_respiration_loss(M, Pa)
E_re=-0.0172*M*(5.867-Pa);
end
```

```
% Dry respiration heat loss (note that parson uses L as the
    variable wheras here E_dr is used)
% units W/m^2
% M is the work done
% T_a is the air temperature
function E_dr=dry_respiration_loss(M, T_a)
E_dr=-0.0014*M*(34-T_a);
end
```

```
% convective heat loss to the enviroment
% units W/m^2
% f_cl is the clothing factor
% I_cl is the clothing insulation level
% h_c is the convective heat transfer coeficient to the
    environment
% T_cl is the clothing temperature
% T_a is the air temperature
% v is the draft velocity

function C=convective_loss(I_cl, v, T_cl, T_a)
f_cl=clothing_factor(I_cl);
h_c=convective_HT_coefficient(T_cl, T_a, v);
C=f_cl*h_c*(T_cl-T_a);
end
```

```
% radiation heat loss to the environment
% units W/m^2
% T_cl is the clothing temperature
% T_r is the mean radiant temperature
% f_cl is the clothing factor
% I_cl is the clothing insulation level
function R=radiation_loss(I_cl, T_r, T_cl)
f_cl=clothing_factor(I_cl);
R=3.96*10^(-8)*f_cl*((T_cl+273.15)^4-(T_r+273.15)^4);
end
```

```
% clothing factor
% I_cl is the clothing insulation level
function f_cl=clothing_factor(I_cl)
```

```
4 if I_cl<=0.5
5     f_cl=1+0.2*I_cl;
6 else
7     f_cl=1.05+0.1*I_cl;
8 end
9 end

1 % Convective heat transfer coeficient to the environment
2
3 function h_c=convective_HT_coefficient(T_cl, T_a, v)
4 if 2.38*(abs(T_cl-T_a))^(1/4)>=12.1*sqrt(v)
5     h_c=2.38*(abs(T_cl-T_a))^(1/4);
6 else
7     h_c=12.1*sqrt(v);
8 end
9 end

1 % partial derivative of E_dr wrt T_a
2
3 function dE_dr_dT_a=partial_E_dr_T_a(M)
4 dE_dr_dT_a=0.0014*M;
5 end

1 % partial derivative of R wrt T_a
2
3 function dR_dT_a=partial_R_T_a(I_cl, v, T_cl, T_a)
4 f_cl=clothing_factor(I_cl);
5 h_c=convective_HT_coefficient(T_cl, T_a, v);
6 A=(-2.4552*10^(-8)*I_cl*f_cl*(T_cl+273.15)^(3))
      /(1+2.4552*10^(-8)*I_cl*f_cl*(T_cl+273.15)^(3));
7 if 2.38*(T_cl-T_a)^(1/4)>=12.1*sqrt(v)
```

```
        dR_dT_a=(-1.25*f_cl*h_c*A)/(1+0.19375*f_cl*h_c*I_cl*(1+A))
            ;
    else
        dR_dT_a=(-f_cl*h_c*A)/(1+0.155*f_cl*h_c*I_cl*(1+A));
    end
    end

% partial derivative of C wrt T_a

function dC_dT_a=partial_C_T_a(I_cl, v, T_cl, T_a)
f_cl=clothing_factor(I_cl);
h_c=convective_HT_coefficient(T_cl, T_a, v);
A=(-2.4552*10^(-8)*I_cl*f_cl*(T_cl+273.15)^(3))
    /(1+2.4552*10^(-8)*I_cl*f_cl*(T_cl+273.15)^(3));
if 2.38*(T_cl-T_a)^(1/4)>=12.1*sqrt(v)
        dC_dT_a=(-1.25*f_cl*h_c)/(1+0.19375*f_cl*h_c*I_cl*(1+A));
else
        dC_dT_a=(-f_cl*h_c)/(1+0.155*f_cl*h_c*I_cl*(1+A));
end
end

% partial derivative of R wrt T_r

function dR_dT_r=partial_R_T_r(I_cl, v, T_cl, T_a, T_r)
f_cl=clothing_factor(I_cl);
h_c=convective_HT_coefficient(T_cl, T_a, v);
if 2.38*(T_cl-T_a)^(1/4)>=12.1*sqrt(v)
        B=(-0.19375*f_cl*h_c*I_cl)/(1+0.19375*f_cl*h_c*I_cl);
        dR_dT_r=(-15.84*10^(-8)*f_cl*(T_r+273.15)^3)
            /(1+2.4552*10^(-8)*f_cl*I_cl*(T_cl+273.15)^3*(B+1));
```

```
else
    C_1=(-0.155*f_cl*h_c*I_cl)/(1+0.155*f_cl*h_c*I_cl);
    dR_dT_r=(-15.84*10^(-8)*f_cl*(T_r+273.15)^3)
        /(1+2.4552*10^(-8)*f_cl*I_cl*(T_cl+273.15)^3*(C_1+1));
end
end
```

```
% partial derivative of C wrt T_r

function dC_dT_r=partial_C_T_r(I_cl, v, T_cl, T_a, T_r)
f_cl=clothing_factor(I_cl);
h_c=convective_HT_coefficient(T_cl, T_a, v);
if 2.38*(T_cl-T_a)^(1/4)>=12.1*sqrt(v)
    B=(-0.19375*f_cl*h_c*I_cl)/(1+0.19375*f_cl*h_c*I_cl);
    dC_dT_r=(-15.84*10^(-8)*f_cl*(T_r+273.15)^3*B)
        /(1+2.4552*10^(-8)*f_cl*I_cl*(T_cl+273.15)^3*(B+1));
else
    C_1=(-0.155*f_cl*h_c*I_cl)/(1+0.155*f_cl*h_c*I_cl);
    dC_dT_r=(-15.84*10^(-8)*f_cl*(T_r+273.15)^3*C_1)
        /(1+2.4552*10^(-8)*f_cl*I_cl*(T_cl+273.15)^3*(C_1+1));
end
end
```

7. Define heat transfer problem

```
% code for matrix construction for optimization problem
function opt_param=HT_matrices(parameters, T_out_wall,
    T_out_air)

```

```
% use sparse matrix for convection/conduction problem (matrix
    is tridiagonal/arrowhead)
% use full matrix for radiative exchange problem
% use vector for gradiant of f and computation of f (f=A*T+b
    where A is a vector and b=A*const_temps, A is grad_f)

%%%%%%%%%%%%%%%%%%%%%% Conduction part
% include conduction to outside + conduction to adjacent walls
[n,~]=size(parameters.geometry.Ai);
A_ins=parameters.geometry.Ai./parameters.insulation;
k=parameters.conductivity;
v1=parameters.geometry.v1;
v2=parameters.geometry.v2;
neighbors=parameters.geometry.neighbors;
cond_mat=zeros(n+1,n+1);
for i=1:n
    cond_mat(i,i)=A_ins(i);
    for j=1:4
        if isnan(neighbors(j,i))
        else% not(isempty(neighbors(neighbors(:,i)==j))) %
            identify if j is neighbors of element i
            %neighbors_ind=neighbors(:,i)==j;
            neighbors_val=neighbors(j,i);
            if j==1 || j==2 %neighbors_ind(1)==1 ||
                neighbors_ind(2)==1
                resistance=norm(v2(:,i))*1/((norm(v1(:,i))/2)/
                    k(i)+(norm(v1(:,neighbors_val))/2)/k(
                    neighbors_val)); % note that (k defined as
```

```
                    k*t) width X ((k/ length)^-1 + (k/lenght)
                    ^-1)^-1 (weight average)
26              else
27                  resistance=norm(v1(:,i))*1/((norm(v2(:,i))/2)/
                    k(i)+(norm(v2(:,neighbors_val))/2)/k(
                    neighbors_val)); % width X kav / length
28              end
29              cond_mat(i,neighbors_val)=-resistance;
30 %              cond_mat(j,i)=-resistance;
31              cond_mat(i,i)=cond_mat(i,i)+resistance;
32          end % all other cases are zero
33      end
34 end
35 b_cond=[-diag(A_ins)*T_out_wall;0]; % include conduction to
    outside (known precalculations)
36
37
38 %%%%%%%%%%%%%%%%%%%%%% Convection part
39 hAi=parameters.h.*parameters.geometry.Ai;
40 Heatmass_air_exchange=parameters.cp*parameters.rho*parameters.
    air_exchange;
41 conv_mat=[diag(hAi), -hAi; -hAi', sum(Heatmass_air_exchange)+
    sum(hAi)]; % Include convection wall/air and air exchange
    from air to outside
42 b_conv=[zeros(n,1); -(Heatmass_air_exchange)'*T_out_air]; %
    include convection to outside (known precalculations)
43
44 %%%%%%%%%%%%%%%%%%%% Combining Conduction and convection (both
    are linea rin this model)
```

```
45 cc_mat=sparse(cond_mat+conv_mat); % this matrix is the
       conduction and convection part that goes along with vector
       b (sparse matrix for faster multiplication)
46 sum_cc_mat=full(sum(cc_mat,1)); % this is the gradiant of f,
       it will be used in the objective function (vector form is
       faster here)
47 b=b_cond+b_conv; % this is the known part of convection/
       conduction (premultiplication is done)
48 sumb=sum(b); % for use in the objectif function (sumb is a
       constant)
49
50 %%%%%%%%%%%%%%%%%% Radiation part
51 aF=zeros(n,n);
52 for i=1:n
53     for j=1:n
54         if i==j
55             aF(i,j)=aF(i,i)+0;
56         else
57             aF(i,i)=aF(i,i)+parameters.geometry.Ai(i)*
                   parameters.geometry.VF(i,j);
58             aF(i,j)=-parameters.geometry.Ai(i)*parameters.
                   geometry.VF(i,j);
59         end
60     end
61 end
62 aeps_mat=diag(parameters.geometry.Ai.*parameters.epsilon(i)
       ./(1-parameters.epsilon)); % Ak*e_k/(1-ek)
63 eb_mat=5.670367*10^(-8)*eye(n); % eb=eb_mat*T^p4 (eb_mat=sigma
       *eye)
```

```
64 A_rad=eb_mat\(aeps_mat\aF+eye(n)); % A_radJ=T^p4
65 rad_mat=[aeps_mat*(eb_mat-A_rad\eye(n)), zeros(n,1); zeros(1,n
       ), 0]; % E_rad=rad_mat*T^p4
66
67 %%%%%%%%%%%%%%%%%% Outputs
68 % for use in objective function and gradiant
69 opt_param.sum_cc_mat=sum_cc_mat;
70 opt_param.sumb=sumb;
71 % for use in constrints and constrain gradiant
72 opt_param.rad_mat=rad_mat;
73 opt_param.cc_mat=cc_mat;
74 opt_param.b=b;
75 end
```

8. Other functions

```
1 % this function plots the data in data for one wall surface
      specified by
2 % wall
3 % geometry contains point and vector defining each grid point
4 % data is a vector of value to be color ploted
5
6 function plot_mesh_data(geometry, data)
7 % geometry.x
8 % data
9 scatter3(geometry.x(1,:)+0.5*geometry.v1(1,:)+0.5*geometry.v2
      (1,:),...
10      geometry.x(3,:)+0.5*geometry.v1(3,:)+0.5*geometry.v2(3,:)
            ,...
```

```
11      geometry.x(2,:)+0.5*geometry.v1(2,:)+0.5*geometry.v2(2,:)
            ,...
12      100,data,'filled')
13  % caxis([0 10])
14  xlabel('Wall 1')
15  ylabel('Wall 2')
16  zlabel('Height')
17  end
```

```
1   % This function makes the VH plots from the saved properties
2   function make_plots(optimisation)
3   parameters=optimisation.parameters;
4   opt_param=optimisation.opt_param;
5   T_sol=optimisation.T_sol;
6   [n,~]=size(T_sol);
7
8   figure('Name', 'All wall convection factors')
9   plot_mesh_data(parameters.geometry, optimisation.parameters.h)
10  disp('Convection factors')
11  disp('average T')
12  disp(mean(optimisation.parameters.h))
13  disp('maximum T')
14  disp(max(optimisation.parameters.h))
15  disp('minimum T')
16  disp(min(optimisation.parameters.h))
17  disp('-----------------------------------')
18
19  figure('Name', 'All wall temperature solution')
20  plot_mesh_data(parameters.geometry, T_sol(1:n-1,1))
```

```
21 disp('Air temperature')
22 disp(T_sol(n,1))
23 disp('average T')
24 disp(mean(T_sol))
25 disp('maximum T')
26 disp(max(T_sol))
27 disp('minimum T')
28 disp(min(T_sol))
29 disp('----------------------------------------')
30
31
32 Q_vh=(opt_param.cc_mat*T_sol+opt_param.b+opt_param.rad_mat*(
       T_sol+273.15).^4);
33 figure('Name', 'All wall VH solution')
34 plot_mesh_data(parameters.geometry, Q_vh(1:n-1,1))
35 disp('average Q_vh')
36 disp(mean(Q_vh))
37 disp('maximum Q_vh')
38 disp(max(Q_vh))
39 disp('minimum Q_vh')
40 disp(min(Q_vh))
41 disp('----------------------------------------')
42
43 % Assemble surf plots
44 sx=parameters.geometry.dims(1);
45 sy=parameters.geometry.dims(2);
46 sz=parameters.geometry.dims(3);
47
48 T_sol_wall1=T_sol(1:parameters.geometry.size(1));
```

```
49 T_sol_wall1w=T_sol_wall1;
50 T_sol_win_12=T_sol([optimisation.index.win1, optimisation.
       index.win2]);
51 T_sol_wall1([optimisation.index.win1, optimisation.index.win2
       ])=nan;
52 T_sol_wall2=T_sol(optimisation.index.wall2);
53 T_sol_win_34=T_sol([optimisation.index.win3, optimisation.
       index.win4]);
54 % T_sol_wall2([optimisation.index.win3, optimisation.index.
       win3])=nan;
55 T_sol_wall3=T_sol(optimisation.index.wall3);
56 T_sol_wall4=T_sol(sum(parameters.geometry.size(1:3)):sum(
       parameters.geometry.size(1:4)));
57 T_sol_wall4w=T_sol_wall4;
58 T_sol_wall4(optimisation.index.door)=nan;
59 T_sol_door=T_sol(optimisation.index.door);
60 Q_vh_wall1=Q_vh(1:parameters.geometry.size(1))./parameters.
       geometry.Ai(1:parameters.geometry.size(1));
61 Q_vh_wall1w=Q_vh_wall1;
62 Q_vh_wall1([optimisation.index.win1, optimisation.index.win2])
       =nan;
63 T_sol_plaf=T_sol(optimisation.index.plaf);
64 T_sol_floor=T_sol(optimisation.index.floor);
65 Q_vh_plaf=Q_vh(optimisation.index.plaf)./parameters.geometry.
       Ai(optimisation.index.plaf);
66 Q_vh_floor=Q_vh(optimisation.index.floor)./parameters.geometry
       .Ai(optimisation.index.floor);
67
```

```
68 x=0:parameters.geometry.wall1_W/sx:parameters.geometry.wall1_W
       -parameters.geometry.wall1_W/sx;
69 y=0:parameters.geometry.wall1_H/sy:parameters.geometry.wall1_H
       -parameters.geometry.wall1_H/sy;
70 z=0:parameters.geometry.wall2_W/sz:parameters.geometry.wall2_W
       -parameters.geometry.wall2_W/sz;
71 x=x+(parameters.geometry.wall1_W/sx)/2;
72 y=y+(parameters.geometry.wall1_H/sy)/2;
73 z=z+(parameters.geometry.wall2_W/sz)/2;
74
75 T_sol_win=zeros(sx,sy)*nan;
76 T_sol_matw1=zeros(sx,sy);
77 Q_vh_matw1=zeros(sx,sy);
78 T_sol_matw1w=zeros(sx,sy);
79 Q_vh_matw1w=zeros(sx,sy);
80 T_sol_matplaf=zeros(sx,sz);
81 Q_vh_matplaf=zeros(sx,sz);
82 T_sol_matfloor=zeros(sx,sz);
83 Q_vh_matfloor=zeros(sx,sz);
84 for j=1:sy
85     for i=1:sx
86         T_sol_matw1(i,j)=T_sol_wall1(i+(j-1)*sx);
87         Q_vh_matw1(i,j)=Q_vh_wall1(i+(j-1)*sx);
88         T_sol_matw1w(i,j)=T_sol_wall1w(i+(j-1)*sx);
89         Q_vh_matw1w(i,j)=Q_vh_wall1w(i+(j-1)*sx);
90         if isnan(T_sol_matw1(i,j))
91             T_sol_win(i,j)=T_sol_matw1w(i,j);
92         end
93     end
```

```
94  end
95  T_sol_matw4=zeros(sz,sy);
96  T_sol_matw4w=zeros(sz,sy);
97  T_sol_door=zeros(sz,sy)*nan;
98  for j=1:sy
99      for i=1:sz
100         T_sol_matw4(i,j)=T_sol_wall4(i+(j-1)*sz);
101         T_sol_matw4w(i,j)=T_sol_wall4w(i+(j-1)*sz);
102         if isnan(T_sol_matw4(i,j))
103             T_sol_door(i,j)=T_sol_matw4w(i,j);
104         end
105     end
106 end
107 for j=1:sz
108     for i=1:sx
109         T_sol_matplaf(i,j)=T_sol_plaf(i+(j-1)*sx);
110         Q_vh_matplaf(i,j)=Q_vh_plaf(i+(j-1)*sx);
111
112         T_sol_matfloor(i,j)=T_sol_floor(i+(j-1)*sx);
113         Q_vh_matfloor(i,j)=Q_vh_floor(i+(j-1)*sx);
114     end
115 end
116
117 figure('Name', 'Wall 1 temperature solution')
118 surf(x,y,T_sol_matw1')
119 figure('Name', 'Wall 1 temperature solution 2D')
120 hold on
121 plot([0.5, 1.25, nan, 1.5, 2.25], [1, 1, nan, 1, 1], 'color',
    'k')
```

```
122 plot([0.5, 1.25, nan, 1.5, 2.25], [2, 2, nan, 2, 2], 'color',
      'k')
123 plot([0.5, 0.5, nan, 1.25, 1.25], [1, 2, nan, 1, 2], 'color',
      'k')
124 plot([1.5, 1.5, nan, 2.25, 2.25], [1, 2, nan, 1, 2], 'color',
      'k')
125 contour(x,y,T_sol_win', 'ShowText','on')
126 contour(x,y,T_sol_matw1', 'ShowText','on')
127 caxis([min(min(T_sol_matw1w)), max(max(T_sol_matw1w))])
128 xlabel('Wall 1 length (m)')
129 ylabel('Height (m)')
130 axis([0, parameters.geometry.wall1_W, 0, parameters.geometry.
      wall1_H])
131 disp('average T on wall 1')
132 disp(nanmean(nanmean(T_sol_matw1)))
133 disp('maximum T on wall 1')
134 disp(max(max(T_sol_matw1)))
135 disp('minimum T on wall 1')
136 disp(min(min(T_sol_matw1)))
137 disp('-----------------------------------')
138
139 disp('average T on wall 2')
140 disp(nanmean(nanmean(T_sol_wall2)))
141 disp('maximum T on wall 2')
142 disp(max(max(T_sol_wall2)))
143 disp('minimum T on wall 2')
144 disp(min(min(T_sol_wall2)))
145 disp('-----------------------------------')
146
```

```
147 disp('average T on wall 3')
148 disp(nanmean(nanmean(T_sol_wall3)))
149 disp('maximum T on wall 3')
150 disp(max(max(T_sol_wall3)))
151 disp('minimum T on wall 3')
152 disp(min(min(T_sol_wall3)))
153 disp('-------------------------------------')
154
155 disp('average T on win 1 2')
156 disp(nanmean(nanmean(T_sol_win_12)))
157 disp('maximum T on win 1 2')
158 disp(max(max(T_sol_win_12)))
159 disp('minimum T on win 1 2')
160 disp(min(min(T_sol_win_12)))
161 disp('-------------------------------------')
162
163 disp('average T on win 3 4')
164 disp(nanmean(nanmean(T_sol_win_34)))
165 disp('maximum T on win 3 4')
166 disp(max(max(T_sol_win_34)))
167 disp('minimum T on win 3 4')
168 disp(min(min(T_sol_win_34)))
169 disp('-------------------------------------')
170
171 disp('average T on door')
172 disp(nanmean(nanmean(T_sol_door)))
173 disp('maximum T on door')
174 disp(max(max(T_sol_door)))
175 disp('minimum T on door')
```

```
176 disp(min(min(T_sol_door)))
177 disp('-----------------------------------')
178
179 figure('Name', 'Wall 4 temperature solution')
180 surf(z,y,T_sol_matw4')
181 figure('Name', 'Wall 4 temperature solution 2D')
182 hold on
183 plot([3.75, 3.75, nan, 4.75, 4.75], [0, 2, nan, 0, 2], 'color'
    , 'k')
184 plot([3.75, 4.75, nan, 3.75, 4.75], [0, 0, nan, 2, 2], 'color'
    , 'k')
185 contour(z,y,T_sol_door', 'ShowText','on')
186 contour(z,y,T_sol_matw4', 'ShowText','on')
187 caxis([min(min(T_sol_matw4w)), max(max(T_sol_matw4w))])
188 xlabel('Wall 4 length (m)')
189 ylabel('Height (m)')
190 axis([0, parameters.geometry.wall2_W, 0, parameters.geometry.
    wall1_H])
191 disp('average T on wall 4')
192 disp(nanmean(nanmean(T_sol_matw4)))
193 disp('maximum T on wall 4')
194 disp(max(max(T_sol_matw4)))
195 disp('minimum T on wall 4')
196 disp(min(min(T_sol_matw4)))
197 disp('-----------------------------------')
198
199
200 figure('Name', 'Ceiling temperature solution')
201 surf(x,z,T_sol_matplaf')
```

```
202 figure('Name', 'Ceiling temperature solution 2D')
203 hold on
204 v=[21:2:25, 49, 59]';
205 contour(x,z,T_sol_matplaf',v, 'ShowText','on')
206 v=(21:2:59)';
207 contour(x,z,T_sol_matplaf',v)
208 xlabel('Wall 1 length (m)')
209 ylabel('Wall 2 length (m)')
210 axis([0, parameters.geometry.wall1_W, 0, parameters.geometry.
      wall2_W])
211 disp('average T on ceiling')
212 disp(nanmean(nanmean(T_sol_matplaf)))
213 disp('maximum T on ceiling')
214 disp(max(max(T_sol_matplaf)))
215 disp('minimum T on ceiling')
216 disp(min(min(T_sol_matplaf)))
217 disp('-----------------------------------')
218
219 figure('Name', 'Floor temperature solution 2D')
220 hold on
221 v=[23.5:1:25.5]';
222 contour(x,z,T_sol_matfloor',v, 'ShowText','on')
223 v=(23.5:0.5:25.5)';
224 contour(x,z,T_sol_matfloor',v)
225 xlabel('Wall 1 length (m)')
226 ylabel('Wall 2 length (m)')
227 axis([0, parameters.geometry.wall1_W, 0, parameters.geometry.
      wall2_W])
228 disp('average T on floor')
```

```
229 disp(nanmean(nanmean(T_sol_matfloor)))
230 disp('maximum T on floor')
231 disp(max(max(T_sol_matfloor)))
232 disp('minimum T on floor')
233 disp(min(min(T_sol_matfloor)))
234 disp('-----------------------------------')
235
236 figure('Name', 'Wall 1 virtual heater solution')
237 surf(x,y,Q_vh_matw1')
238 disp('average Q_vh on wall 1')
239 disp(nanmean(nanmean(Q_vh_matw1)))
240 disp('maximum Q_vh on wall 1')
241 disp(max(max(Q_vh_matw1)))
242 disp('minimum Q_vh on wall 1')
243 disp(min(min(Q_vh_matw1)))
244 disp('-----------------------------------')
245
246 figure('Name', 'Ceiling virtual heater solution')
247 surf(x,z,Q_vh_matplaf')
248 figure('Name', 'Ceiling virtual heater solution 2D')
249 hold on
250 v=[0, 150, 300]';
251 contour(x,z,Q_vh_matplaf',v,'ShowText','on')
252 v=(0:50:300)';
253 contour(x,z,Q_vh_matplaf',v)
254 xlabel('Wall 1 length (m)')
255 ylabel('Wall 2 length (m)')
256 axis([0, parameters.geometry.wall1_W, 0, parameters.geometry.
      wall2_W])
```

```
257 disp('average Q_vh on ceiling')
258 disp(nanmean(nanmean(Q_vh_matplaf)))
259 disp('maximum Q_vh on ceiling')
260 disp(max(max(Q_vh_matplaf)))
261 disp('minimum Q_vh on ceiling')
262 disp(min(min(Q_vh_matplaf)))
263 disp('-----------------------------------')
264
265
266 % thermal comfort and radiant temperature
267 [~,m]=size(opt_param.const_pts_VF);
268 PMVi=ones(m,1);
269 T_r=PMVi;
270 for i=1:m % for each constraint point
271     T_r(i)=mean_rad_temp(opt_param.const_pts_VF(:,i), T_sol(1:
          n-1)); % mean radiant temperature
272     [PMVi(i), ~]=predicted_mean_vote_with_grad(T_sol(n), T_r(i
          ), opt_param.PMV.v, opt_param.PMV.Pa, opt_param.PMV.
          I_cl, opt_param.PMV.M); % predicted mean vote at
          position
273 end
274 PMV_cart=ones(round(m^(1/3)), round(m^(1/3)), round(m^(1/3)));
275 x_conf=zeros(9,1);
276 y_conf=zeros(9,1);
277 z_conf=zeros(9,1);
278 for i=1:round(m^(1/3))
279     for j=1:round(m^(1/3))
280         for k=1:round(m^(1/3))
281             PMV_cart(i,j,k)=PMVi(i+9*(j-1)+81*(k-1));
```

```
282                 if i==1 && j==1
283                     z_conf(k)=parameters.const_pts(3,1+(k-1)*81);
284                 end
285             end
286             if i==1
287                 y_conf(j)=parameters.const_pts(2,1+(j-1)*9);
288             end
289         end
290         x_conf(i)=parameters.const_pts(1,i);
291 end
292
293 figure('Name', 'PMV')
294 plot_mesh_data2(parameters.const_pts, PMVi)
295 figure('Name', ['Slice z=', num2str(z_conf(1))])
296 contour(x_conf, y_conf, PMV_cart(:,:,1)', 'ShowText','on')
297 xlabel('Wall 1 length (m)')
298 ylabel('Height (m)')
299 figure('Name', ['Slice z=', num2str(z_conf(4))])
300 contour(x_conf, y_conf, PMV_cart(:,:,4)', 'ShowText','on')
301 xlabel('Wall 1 length (m)')
302 ylabel('Height (m)')
303 figure('Name', ['Slice z=', num2str(z_conf(9))])
304 contour(x_conf, y_conf, PMV_cart(:,:,9)', 'ShowText','on')
305 xlabel('Wall 1 length (m)')
306 ylabel('Height (m)')
307 disp('average PMV')
308 disp(mean(PMVi))
309 disp('maximum PMV')
310 disp(max(PMVi))
```

```
311 disp('minimum PMV')
312 disp(min(PMVi))
313 disp('------------------------------------')
314
315 figure('Name', 'Mean radiant temperature')
316 plot_mesh_data2(parameters.const_pts, T_r)
317 disp('average MRT')
318 disp(mean(T_r))
319 disp('maximum MRT')
320 disp(max(T_r))
321 disp('minimum MRT')
322 disp(min(T_r))
323 disp('------------------------------------')
324
325 disp('Total heating on wall 1')
326 disp(sum(Q_vh(optimisation.index.wall1)))
327 disp('Total heating on win 1 and 2')
328 disp(sum(Q_vh([optimisation.index.win1,optimisation.index.win2
    ])))
329 disp('Total heating on wall 2')
330 disp(sum(Q_vh(optimisation.index.wall2)))
331 disp('Total heating on win 3 and 4')
332 disp(sum(Q_vh([optimisation.index.win3,optimisation.index.win4
    ])))
333 disp('Total heating on wall 3')
334 disp(sum(Q_vh(optimisation.index.wall3)))
335 disp('Total heating on wall 4')
336 disp(sum(Q_vh(optimisation.index.wall4)))
337 disp('Total heating on door')
```

```
disp(sum(Q_vh(optimisation.index.door)))
disp('Total heating on wall ceiling')
disp(sum(Q_vh(optimisation.index.plaf)))
disp('Total heating on wall floor')
disp(sum(Q_vh(optimisation.index.floor)))
disp('Total heating of air')
disp(Q_vh(n))
disp('Total heat loss')
disp(sum(Q_vh))
end
```

```
% function to calculate the mean radiant temperature
% epsilon(i) is the emmisivity of surface i
% VF are the view factors
% T are the surface temperature
function T_r=mean_rad_temp(VF, T)
%disp('sum of VF')
%disp(sum(VF))
T_r=VF(:,1)'*(T(:,1)+273.15).^4;
T_r=T_r^(1/4)-273.15;
end
```

APPENDIX V

ARTICLES IN CONFERENCES

1. Des instruments de mesure pour la thermique du bâtiment: la Klimat

Authors: J. Léger, D.R. Rousse, K. Le Borgne, F. Coulombe

Abstract: La réduction de la consommation énergétique du chauffage résidentiel est un objectif qui peut avoir d'importantes contributions sur l'efficacité énergétique au Canada. La problématique de développer un système de chauffage électrique efficace, du point de vue de la distribution de chaleur, est donc intéressante à étudier. Pour étudier le chauffage électrique, une chambre bi-climatique (Klimat) a été construite. Cette chambre a été conçue pour lui conférer des caractéristiques particulières qui lui permettent d'être modulaire, d'être capable de changer sa configuration et son type de pièce test. De plus, le côté froid de la chambre est capable d'atteindre une température s'étendant de $-37.5°C$ à $35°C$. Dans cet article, l'innovation de cette chambre ainsi que son potentiel en recherche expérimental sont décrits. Les auteurs présentent cette communication technique afin de pouvoir démarrer de nouveaux partenariats en utilisant cette nouvelle chambre climatique au Canada.

2. Comparaison exprérimentale de la distribution de chaleur engendrée par des appareil de chauffage électrique

Authors: J. Léger, D.R. Rousse, K. Le Borgne, S. Lassue

Abstract: Le chauffage électrique est aujourd'hui très utilisé dans les habitations nord-américaines. Dans un effort de modernisation d'anciens immeubles qui sont chauffés avec des systèmes électriques, il est certainement intéressant d'étudier le potentiel de réduction de la charge de chauffage en distribuant mieux la chaleur dans une pièce, soit par un simple changement d'appareil. Dans ce travail, une chambre bi-climatique, basée sur la norme CSA828-13, est utilisée pour comparer de façon expérimentale une plinthe électrique à des convecteurs électriques. Dans cette étude préliminaire, le couple appareil de chauffage et thermostat est com-

paré pour trois cas distincts. Les résultats montrent que le système thermostat mécanique avec plinthe consomme plus d'énergie que les systèmes avec convecteurs. Cela va à l'encontre de la croyance que tous les appareils de chauffage électrique ont une même efficacité énergétique car ils convertissent tous leur puissance en chaleur de la même façon.

3. The use of virtual heaters in assessing the effect of window glazing and air exchange rate on optimal indoor heat distribution

Authors: J. Léger, D.R. Rousse

Abstract: Indoor heating is a significant source of total residential power consumption in northern countries such as Canada. It is also known that heat distribution can affect the performance of a heating system and thus should be considered in the design process. There has been some interest into achieving optimal heat distributions, but most works have focused on existing heaters. Recently, a new approach to the optimal indoor heat distribution problem was introduced. The main idea is to find the optimal heat distribution, via constrained optimization, by varying the temperature distribution in a room with a heat transfer model to optimize the power consumption while making sure that thermal comfort is maintained. Using the maximum and minimum heat consumption, i.e. the virtual heaters, the total energy consumption sensibility to heat distribution can be assessed. It has been determined that window glazing and air exchange rate were the most significant parameters to affect the room heat distribution sensibility. In the complete paper, the virtual heaters are used to explore how the power consumption sensibility to the heat distribution of a room might change with respect to the window glazing and the air exchange rate for different room types. This is achieved by first finding the virtual heaters for the specific cases, then calculating the room heat distribution sensibility. The sensibilities are then compared with each other and the most sensible and least sensible rooms to heat distribution are found.

APPENDIX VI

ARTICLES IN JOURNALS

1. Comparing electric heating systems at equal thermal comfort: An experimental investigation

Authors: J. Léger, D.R. Rousse, K. Le Borgne, S. Lassue

Abstract: Electric heaters are still widely used for residential heating. It is often believed that electric systems all perform equally; however, this is not the case as diffusors distribute heat in different ways. In this study, an experimental investigation of electric heating systems shows that heat distribution can indeed influence the effectiveness of the equipment to maintain thermal comfort. A baseboard heater, a convector and a radiant heater are compared at equal thermal comfort conditions in a bi-climatic chamber at different cold room temperatures. To demonstrate the repeatability of the results, a statistical analysis is presented. Results show that the convector consumes less energy than the baseboard and radiant heaters despite achieving similar thermal comfort. Though only small differences were observed, the investigation shows that electric heating systems are not all equal in energy efficiency. There is thus an opportunity to improve the heating effectiveness by improving the heat distribution of the equipment.

2. Optimal indoor heat distribution: the virtual heaters

Authors: J. Léger, D.R. Rousse, S. Lassue

Abstract: It is well known that indoor heat distribution can affect energy consumption in relation with thermal comfort of the occupants. While most work on this topic has focused on specific heaters and how they distribute heat, this paper's intention is to generalize the concept of optimal indoor heat distribution. A new concept termed virtual heaters is proposed. Virtual heaters are a set of optimal heat distributor that maximise and minimise the energy consumption inside a room while maintaining the same thermal comfort. To find the "virtual heaters", a simplified heat transfer model considering a quartic in temperature radiation model and a linear

in temperature conduction and convection model is programmed. A volumetric thermal comfort model using predicted mean vote (*PMV*) is also discussed and used. The simplified heat transfer model with the thermal comfort constraint is then optimized via a sequential quadratic programming (SQP) algorithm. The proposed method is applied to heating a room, similar to the one in a bi-climatic chamber, subject to an outdoor temperature of $-20°$C. The minimum and maximum virtual heaters can then be compared to the real heater tested in the room at constant thermal comfort. Results show here that the maximum virtual heater consumes approximately 35% more energy than the minimum virtual heater. These differences are purely caused by distinct heat distributions. Through this heating example, it is clear that the concept of optimal heat distribution could help engineers design better heat distributors for indoor spaces. It should also allow engineers to: assess the heat distribution performance of heaters; and, to assess the room sensibility of energy consumption to heat distribution.

3. The effect of geometry on optimal heat distribution for indoor spaces using virtual heaters

Authors: J. Léger, D.R. Rousse, S. Lassue

Abstract: Optimizing indoor space heating systems for energy efficiency remains an important topic of investigation since heating comprises a significant part of the total energy consumption of a building in a cold climate. It is known that heat distribution inside a room may affect the thermal comfort and consequently the energy consumption of the heating system. Recently, the geometry of rooms, and how this may affect energy consumption was been a topic of investigation. In this paper, it is shown how optimal heat distribution may be effected by the room geometry. This is accomplished by comparing the optimal heat distributions and the room heat distribution sensibility (*RHDS*) of different room geometries. To find the optimal heat distribution, the concept of virtual heaters, a set of maximum and minimum consuming heaters, is used in this work. The results show that the room height and the window to wall ratio could significantly change the minimum energy consumption heat distribution whereas the room depth had no significant effects on the distribution. As for the *RHDS*, it was affected

by all three geometrical parameter. The window to wall ratio and room height increase the sensibility while the room depth decreased the sensibility. The differences in *RHDS* and in the heat distribution are interesting and should be considered in the design process of buildings as energy saving can be made from understanding the optimal heat distributions.

4. Building thermal envelope effects on the optimal indoor heat distribution and heat consumption of rooms using virtual heaters

Authors: J. Léger, D.R. Rousse, S. Lassue

Abstract: The thermal envelope is no doubt one of the major considerations in energy efficient building design. It is well known that increasing the insulation of any surface will undoubtedly reduce heat loss toward the outdoor environment. What is less well known is how this thermal envelope changes the optimal heat distribution. Is it better to heat the floor directly or the air volume? This is an unanswered question that has no exact answers as it depends on the thermal envelope of a room. This work attempts to answer this type of questions with regard to the thermal envelope. To evaluate the effect of the insulation and air-tightness parameters on optimal heating, the concept of virtual heaters is used. This recently formulated concept tries to optimise the energy consumption via the heat distribution while maintaining thermal comfort. From which, the best and worst heaters are found and can then be used to assess the room heat distribution performance. This paper investigates these heat distributions and how the thermal envelope affects them from two points of view. The first is the sensibility of the energy consumption to the heat distribution and the second is the heat distribution itself and how it changes. Results show that the window, air exchange rate and outdoor temperatures all have significant effects. The window mostly affects the room heat distribution sensibility while the air exchange rate can drastically affect the heat distribution. The results from this study could potentially help building designers make more informed energy efficiency choices in the built environment by having a better understanding of optimal heat distribution and how the thermal envelope might affect it.

BIBLIOGRAPHY

12567, E. S. E. I. (2010). *Thermal performance of windows and doors - Determination of thermal transmittance by the hot-box method*.

Aditya, L., Mahlia, T. M. I., Rismanchi, B., Hasan, M. H., Metselaar, H. S. C., Muraza, O. & Aditiya, H. B. (2017). A review on insulation materials for energy conservation in buildings. *Renewable and Sustainable Energy Reviews*, 73, 1352-1365.

Ahmed, A. Q., Gao, S. & Kareem, A. K. (2016). A numerical study on the effects of exhaust locations on energy consumption and thermal environment in office room served by displacement ventilation. *Energy Conversion and Management*, 117, 74-85.

Ahmed, A. Q., Gao, S. & Kareem, A. K. (2017). Energy saving and indoor thermal comfort evaluation using a novel local exhaust ventilation system for office rooms. *Applied Thermal Engineering*, 110, 821-834.

Amai, H., Tanabe, S., Akimoto, T. & Genma, T. (2007). Thermal sensation and comfort with different task conditioning systems. *Building and Environment*, 42, 3955-3964.

Angeles, J., Anderson, K. & Gosselin, C. (1990). Constrained design optimization using orthogonal decomposition. *Journal of Mechanical Design*, 112, 255-256.

ASHRAE. (2009). *ASHRAE handbook fundamentals*. American Society of Heating, Refrigeration and Air-Conditioning Engineers.

ASHRAE-55. (2013). *Thermal Environment Conditions for Human Occupancy*.

Atthajariyakul, S. & Leephakpreeda, T. (2004). Real-time determination of optimal indoor-air condition for thermal comfort, air quality and efficient energy usage. *Energy and Buildings*, 36, 720-733.

Babiak, J., Olesen, B. W. & Petras, D. (2007). *Low temperature heating and high temperature cooling: REHVA Guidebook No 7*. REHVA.

Bedford, T. (1936). The warmth factor in comfort at work. Aphysiological study of heating and ventilation. *Industrial Health Research Board Report. Medical research council*, 4, 102.

Bertsekas, D. P. (2014). *Constrained optimization and lagrange multiplier methods*. Academic press.

Bischof, W., Lund Madsen, T., Clausen, J., Lund Madsen, P. & Wildschiodtz, G. (1993). Sleep and the temperature of the bed. *Journal of Thermal Biology*, 18, 393-398.

Bottou, L., Curtis, F. E. & Nocedal, J. (2016). Optimization methods for large-scale machine learning. *CoRR, abs/1606.04838*.

Bouden, C. & Ghrab, N. (2005). An adaptive thermal comfort model for the Tunisian context: a field study results. *Energy and Buildings*, 37, 952-963.

Brager, G., Zhang, H. & Arens, E. (2015). Evolving opportunities for providing thermal comfort. *Building Research and Information*, 43, 274-287.

BS-EN-15251. (2007). *Indoor environmental input parameters for design and assessment of energy performance of buildings addressing indoor air quality, thermal environment, lighting and acoustics*.

building, A. & energy research group. (2011). *Salford energy house: An overview*.

Buratti, C. & Paola, R. (2009). Adaptive analysis of thermal comfort in university classrooms: Correlation between expermimental data and mathematical models. *Building and Environment*, 44, 674-687.

Cabrera, D. M. (2016). Evolutionary algorithms for large-scale global optimisation: a snapshot, trends and challenges. *Progress in Artificial Intelligence*, 5, 85-89.

Canada, N. R. (2016). Energy fact book.

Cao, G., Awbi, H., Yao, R., Fan, Y., Sirén, K., Kosonen, R. & Zhang, J. (2014). A review of the performance of different ventilation and airflow distribution systems in buildings. *Building and Environment*, 73, 171-186.

Castilla, M., Álvarez, J. D., Berenguel, M., Pérez, M., Rodríguez, F. & Guzmán, J. L. (2010). Técnicas de Control del Confort en Edificios. *Revista Iberoamericana de Automática e Informática Industrial RIAI*, 7, 5-24.

Castilla, M., Álvarez, J. D., Berenguel, M., Rodríguez, F., Guzmán, J. L. & Pérez, M. (2011). A comparison of thermal comfort predictive control strategies. *Energy and Buildings*, 43, 2737-2746.

Castilla, M., Álvarez, J. D., Normey-Rico, J. E. & Rodriguez, F. (2012, July 3-6). A nonlinear model based predictive control strategy to maintain thermal comfort inside a bioclimatic building. *Proc. of the 20th Mediterrranean Conference on Control and Automation (MED)*.

Castilla, M., Álvarez, J. D., Ortega, M. G. & Arahal, M. R. (2013). Neural network and polynomial approximated thermal comfort models for HVAC systems. *Building and Environment*, 59, 107-115.

Catalina, T., Virgone, J. & Kuznik, F. (2009). Evaluation of thermal comfort using combined CFD and experimentation study in a test room equipped with a cooling ceiling. *Building and Environment*, 44, 1740-1750.

Causone, F., Corgnati, S. P., Filippi, M. & Olesen, B. W. (2009). Experimental evaluation of heat transfer coefficients between radiant ceiling and room. *Energy and Buildings*, 41, 622-628.

Causone, F., Baldin, F., Olesen, B. W. & Corgnati, S. P. (2010). Floor heating and cooling combined with displacement ventilation: Possibilities and limitations. *Energy and Buildings*, 42, 2338-2352.

Çengel, Y. A. & Boles, M. A. (2008). *Thermodynamics: An Engineering Approach, 6th edition*. McGraw-Hill.

Chan, Q., Peng, X. & van Paassen, A. H. C. (1995). Prediction of room thermal response by CFD technique with conjugate heat transfer and radiation models. *American Society of Heating, Refrigerating and Air-Conditioning Engineers*.

Chan, W. R., Nazaroff, W. W., Price, P. N., Sohn, M. D. & Gadgil, A. J. (2005). Analyzing a database of residential air leakage in the United States. *Atmospheric Environment*, 39, 3445-3455.

Chen, Q. (2009). Ventilation performance prediction for buildings: A method overview and recent applications. *Building and Environment*, 44, 848-858.

Choudhury, D. (1993). *Introduction to the renormalization group method and turbulance modeling*.

Chun, C., Kwok, A., Mitamura, T., N., M. & Tamura, A. (2008). Thermal diary: Connecting temperature history to indor comfort. *Building and Environment*, 43, 877-885.

Chung, T. M. & Tong, W. C. (1990). Thermal comfort study of young chinese people in Hong Kong. *Building and Environment*, 25, 317-328.

Chwieduk, D. A. (2017). Towards modern options of energy conservation in buildings. *Renewable and Sustainable Enrgy Reviews*, 101, 1194-1202.

Cigler, J., Prívara, S., Váňa, Z., Žáčeková, E. & Ferkl, L. (2012). Optimization of Predicted Mean Vote index within Model Predictive Control framework: Computationally tractable solution. *Energy and Buildings*, 52, 39-49.

Conservatory, T. E. (2012). *Minneapolis blower door operation manual for model 3 and model 4 systems*.

Corgnati, S. P., Fabrizio, E. & Filippi, M. (2008). The impact of indoor thermal conditions, system controls and building types on the building energy demand. *Energy and Buildings*, 40, 627-636.

CSA. (2013). *C828-13 Performance requiements for thermostats used with individual room electric space heating devices*.

Cvetković, D. & Bojić, M. (2014). Optimization of thermal insulation of a house heated by using radiant panels. *Energy and Buildings*, 85, 329-336.

de Dear, R. (2004). Thermal comfort in practice. *Indoor Air*, 14, 32-39.

de Dear, R. & Brager, G. S. (2001). The adaptive model of thermal comfort and energy conservation in the built environment. *Journal of Biometeorology*, 45, 100-108.

de Dear, R. J. & Brager, G. S. (1998). Developing an adaptive model of thermal comfort and preference. *ASHRAE Transaction*, 104, 145-167.

Djongyang, N., Tchinda, R. & Njomo, D. (2010). Thermal comfort: A review paper. *Renewable and Sustainable Energy Reviews*, 14, 2626-2640.

Doherty, T. & Arens, E. A. (1988). Evaluation of the physiological bases of thermal comfort models. *ASHRAE Transactions*, 94, 1371-1383.

Donaisky, E., Oliveira, G. H. C., Freire, R. Z. & Mendes, N. (2007). PMV-based predictive algorithms for controlling thermal comfort in building plants. *IEEE International Conference on Control Applications*.

Dounis, A. I. & Caraiscos, C. (2009). Advanced control systems engineering for energy and comfort management in a building environment—A review. *Renewable and Sustainable Energy Reviews*, 13, 1246-1261.

Fanger, P. O. (1970). *Thermal Comfort. Analysis and Applications in Environmental Engineering*. New York: McGraw-Hill.

Fanger, P. O. & Toftum, J. (2002). Extension of the PMV model to non-air-conditioned buildings in warm climates. *Energy and Buildings*, 34, 533-536.

Fazio, P., Athientis, A. K., Marsh, C. & Rao, J. (1997). Enviromental chamber for investigation of building envelope performance. *Architectural Engineering*, 3, 97-102.

Fernández-Gutiérrez, A., González-Prieto, I., Parras, L., Cejudo-López, C. & del Pino, C. (2015). Experimental and numerical study of a small-scale and low-velocity indoor diffuser coupled with radiant floor cooling. *International Journal of Heat and Mass Transfer*, 87, 71-78.

Fiala, D. & Havenith, G. (2015a). *Modeling Human Heat Transfer and Temperature Regulation*. Berlin: Springer.

Fiala, D. & Havenith, G. (2015b). *Modelling Human Heat Transfer and Temperature Regulation*. Springer.

Fiala, D., Lomas, K. J. & Stohrer, M. (2007, August 19-24). Dynamic simulation of human heat transfer and thermal comfort. *Proc. International Conference on Environmental Ergonomics*.

Fiala, D., Psikuta, A., Jendritzky, G., Paulke, S., Nelson, D. A. & van Marken Lichtenbelt, W. D. (2010). Physiological modeling for technical, clinical and research applications. *Frontiers in Bioscience*, 2, 939-968.

Fiala, D., Havenith, G., Bröde, P., Kampmann, B. & Jendritzky, G. (2012). UTCI-Fiala multi-node model of human heat transfer and temperature regulation. *International Journal of Biometeorology*, 56, 429-441.

Fluke. (2017). *Fluke 714B user manual*.

Fong, M. L., Hanby, V., Greenough, R., Lin, Z. & Cheng, Y. (2015). Acceptance of thermal conditions and energy use of three ventilation strategies with six exhaust configurations for the classroom. *Building and Environment*, 94, 606-619.

Fountain, M., Brager, G. & de Dear, R. (1996). Expectations of indoor climate control. *Energy and Buildings*, 24, 179-182.

Gagge, A. P. & Gonzalez, R. R. (1972, September 13-15). Standard effective temperature - a single temperature index of temperature sensation and thermal discomfort. *Proc. of the CIB commission (human requirements)*.

Gagge, A. P., Fobelets, A. P. & Berglund, L. G. (1986, June 22). A standard predictive index of human response to the thermal environment. *Proc. ASHRAE annual meeting)*.

Gan, G. (1995). Evaluation of room air distribution systems using computational fluid dynamics. *Energy and Buildings*, 23, 83-93.

Gao, J., Wang, Y. & Wargocki, P. (2015). Comparative analysis of modified PMV models and SET models to predict human thermal sensation in naturally ventilated buildings. *Building and Environment*, 92, 200-208.

Ghaddar, N., Salam, M. & Ghali, K. (2006). Steady thermal comfort by radiant heat transfer: The impact of the heater position. *Heat transfer Engineering*, 27, 29-40.

Goia, F. (2016). Search for the optimal window-to-wall ratio in offece buildings in different European climates and the implications on total energy saving potential. *Solar Energy*, 132, 467-492.

Gosselin, L., Tye-Gingras, M. & Mathieu-Potvin, F. (2009). Review of utilization of genetic algorithms in heat transfer problems. *International Journal of Heat and Mass Transfer*, 52, 2169-2188.

group, C. (2017). Modular walk-in chambers.

Halawa, E., van Hoof, J. & Soebarto, V. (2014). The impacts of the thermal radiation field on thermal comfort, energy consumption and control—A critical overview. *Renewable and Sustainable Energy Reviews*, 37, 907-918.

Han, Y., Li, Z. & Xu, P. (2014). Comparative study on energy consumption of gas-fired infrared radiant and convection heating. *Advanced Materials Research*, 953, 849-853.

Hannay, J., Laret, L., Lebrun, J., Marret, D. & Nusgens, P. (1978). Thermal comfort and energy consumption in winter conditions. A new experimental approach. *ASHRAE transactions*, 84, 150-175.

Hirch, J. (2015). Building Energy use and Cost Analysis Software.

Hoffmann, S. & Boudier, K. (2016). A new approach to provide thermal comfort in office buildings - a field study with heated and cooled chairs. *Proc. 9th International Conference on Indoor Air Quality Ventilation and Energy Conservation in Buildings*.

Holz, R., Hourigan, A., Sloop, R., Monkman, P. & Krarti, M. (1997). Effects of standard energy conserving measures on thermal comfort. *Building an Environment*, 32, 31-43.

Horikiri, K., Yao, Y. & Yao, J. (2014). Modelling conjugate flow and heat transfer in a ventilated room for indoor thermal comfort assessment. *Building and Environment*, 77, 135-147.

Horikiri, K., Yao, Y. & Yao, J. (2015). Numerical optimisation of thermal comfort improvement for indoor environment with occupants and furniture. *Energy and Buildings*, 88, 303-315.

Howell, J. R. (2016). A catalog of radiation heat transfer configuration factors.

Huang, C. & Wang, X. (2009). Discussion of design method and optimization on airflow distribution in a large0-space building with stratified air-conditioning system. *ASHRAE Transactions*.

Huang, C., Zou, Z., Li, M., Wang, X., Li, W., Huang, W., Yang, J. & Xiao, X. (2007). Measurments of indoor thermal environment and energy analysis in a large space building in typical seasons. *Building and Environment*, 42, 1869-1877.

Huimei, C., Yufeng, Z., Jinyong, W. & Qinglin, M. (2010). Thermal comfort study in hot-humid area of china. *Proc. of Adapting to Change: New Thinking on Comfort*.

Humphreys, M. (1978). Outdoor temperature and comfort indoors. *Building Research and Practice*, 6, 92.

Humphreys, M., Nicol, F. & Roaf, S. (2015). *Adaptive Thermal Comfort: Foundations and Analysis*. New York: Routledge.

Humphreys, M. A. & Nicol, J. F. (2002). The validity of ISO-PMV for predicting comfort votes in every-day thermal environments. *Energy and Buildings*, 34, 667-684.

Inard, C., Bouia, H. & Dalicieux, P. (1996). Prediction of air temperature distribution in buildings with a zonal model. *Energy and Buildings*, 24, 125-132.

Inard, C., Meslem, A. & Depecker, P. (1998). Energy consumption and thermal comfort in dwelling-cells: A zonal-model approach. *Building and Environment*, 33, 279-291.

Inc., C. (2017). Produit convectair.

Incropera, F. P. & DeWitt, D. P. (2011). *Fundamentals of Heat and Mass Transfer, 7th Edition*. Wiley.

ISO-7730. (2005). *Ergonomics of thermal environment-Analytical determination and interpretation of thermal comfort using calculation of the PMV and PPD indices and local thermal comfort criteria*.

Jahantigh, N., Keshavarz, A. & Mizaei, M. (2015). Hybrid heating systems optimization of residential environment to have thermal comfort conditions by numerical conditions. *IJournal of Environmental Health Science and Engineering*, 13.

Kalmár, F. & Kalmár, T. (2012). Interrelation between mean radiant tmeperature and room geometry. *Energy and Buildings*, 55, 414-421.

Karmann, C., Stefano, S. & Bauman, F. (2017). Thermal comfort in buildings using radiant vs. all-air systems: A critical literature review. *Building and Environment*, 111, 123-131.

Katabira, K., Zhao, H., Nakagawa, Y. & Shibasaki, R. (2008). Real-time monitoring of people flows and indoor temperature distribution for advanced air-conditioning control. *Proc. 11th International Conference on Intelligent Transportation Systems*.

Kim, T., Kato, S. & Murakami, S. (2001). Indoor cooling/heating load analysis based on coupled simulation of convection, radiation and HVAC control. *Building and Enviornemnt*, 36, 901-908.

Krajčik, M., Kudiváni, L. & Mahdavi, A. (2016). Energy saving potential of personalized ventilation applied in an open space office under winter conditions. *Applied Mechanics and Materials*, 861, 417-424.

Kuehn, L. A., Stubbs, R. A. & Weaver, R. S. (1970). Theory of the globe thermometer. *Journal of Applied Physiology*, 29, 750-757.

Kuzuhara, K. & Nishi, H. (2013). Accurate indoor condition control based on PMV prediction in BEMS environments. *39th IEEE Conference of the Industrial Electronics Society*.

Kwong, Q. J., Adam, N. M. & Sahari, B. B. (2014). Thermal comfort assessment and potential for energy efficiency enhancement in modern tropical buildings: A review. *Energy and Buildings*, 68, 547-557.

Lasdon, L. S., Waren, A. D., Jain, A. & Ratner, M. (1978). Design and testing of a generalized reduced gradient code for nonlinear programming. *ACM Transaction on Mathematical Software*, 4, 34-50.

LaTorre, A., Muelas, S. & Peña, J. (2015). A comprehensive comparison of large scale global optimizers. *Information Sciences*, 316, 517-549.

Le Dréau, J. & Heiselberg, P. (2014). Sensitivity analysis of the thermal performance of radiant and convective terminals for cooling buildings. *Energy and Buildings*, 82, 482-491.

Le Dréau, J., Heiselberg, P. & Jensen, R. L. (2015). A full-scale experimental set-up for assessing the energy performance of radiant wall and active chilled beam for cooling buildings. *Building Simulation*, 8, 39-50.

Léger, J., Rousse, D. R., Le Borgne, K. & Coulombe, F. (2017, May 22-24). Des instruments de mesure pour la thermique du bâtiment: La Klimat. *Colloque Interuniversitaire Franco-Québecois sur la Thermique des Systèmes*.

Léger, J., Rousse, D., Le Borgne, K. & Lassue, S. (2018). Comparing electric heating systems at equal thermal comfort: An experimental investigation. *Building and Environment*, 128, 161-169.

Léger, J., Rousse, D. R. & Lassue, S. (2019). Optimal indoor heat distribution: the virtual heaters. *Submitted to Applied Energy*, -, -.

Linden, W. V. D., Loomans, M. & Hensen, J. (2008, August 17-22). Adaptive thermal comfort explained by PMV. *Proc. of the 11th International Conference on indoor air quality and climate*.

Lu, W., Howarth, A. T. & Jeary, A. (1997). Prediction of airflow and temperature field in a room with convective heat source. *Building and Environment*, 32, 541-550.

Luo, M., de Dear, R., Ji, W., Bin, C., Lin, B., Ouyang, Q. & Zhu, Y. (2016). The dynamics of thermal comfort expectations: The problem, challenge and implication. *Building and Environment*, 95, 322-329.

Machairas, V., Tsangrassoulis, A. & Axarli, K. (2014). Algorithms for optimization of building design: A review. *Renewable and Sustainable Energy Reviews*, 31, 101-112.

Martín, R. H., Martínez, F. J. & Gómez, E. V. (2008). Thermal comfort analysis of a low temperature waste energy recovery system: SIECHP. *Energy and Buildings*, 40, 561-572.

MATLAB. (2017). Choosing the algorithm.

Megri, A. C. & Haghighat, F. (2007). Zonal modeling for simulating indoor environment of buildings: Review, recent developments, and applications. *HVAC&R Research*, 13, 887-905.

Megri, A. C. & Yu, Y. (2015). New calibrated zonal model ($POMA^{+}$) for temperature and airflow predictions. *Building and Environment*, 94, 109-121.

Merriam-Webster. (2015). *Merriam-Webster's Collegiate Dictionary, Eleventh Edition*. Encyclopedia Britanica.

Michailidis, I. T., Baldi, S., Kosmatopoulos, E. B., Pichler, M. F. & Santiago, J. R. (2015). Control Theory: Perspectives, Applications and Developments (ch. Improving energy savings and thermal comfort in large-scale buildings via adaptive optimization). Nova Science.

Mohamed, S. & Srinavin, K. (2005). Forecasting labor productivity changes in construction using the PMV index. *International Journal of Industrial Ergonomics*, 35, 345-351.

Mohammad, T., Tenpierik, M., Kurvers, S. & van den Dobbelsteen, A. (2013). A review into thermal comfort in buildings. *Renewable and Sustainable Energy Reviews*, 26, 201-215.

Mui, K. W. H. & Chan, W. T. D. (2003). Adaptive comfort temperature model of air-conditioned building in Hong Kong. *Building and Environment*, 38, 837-852.

Musy, M., Wurtz, E., Winkelmann, F. & Allard, F. (2001). Generation of a zonal model to simulate natural convection in a room with a radiative/convective heater. *Building and Environment*, 36, 589-596.

Myhren, J. A. & Holmberg, S. (2006). Comfort temperature and operative temperatures in an office with different heaating methods. *Proc. of the Healthy Buildings*, 2.

Myhren, J. A. & Holmberg, S. (2008). Flow patterns and thermal comfort in a room with panel, floor and wall heating. *Energy and Buildings*, 40, 524-536.

Myhren, J. A. & Holmberg, S. (2009). Design considerations with ventilation-radiators: Comparisons to traditional two-panel radiators. *Energy and Buildings*, 41, 92-100.

Nagarathinam, S., Doddi, H., Vasan, A., Sarangan, V., Ramakrishna, P. V. & Sivasubramaniam, A. (2017). Energy efficient thermal comfort in open-plan office buildings. *Energy and Buildings*, 139, 476-486.

Nägele, F., Kasper, T. & Girod, B. (2017). Turning up the heat on obsolete thermostats: A simulation-based comparison of intelligent control approaches for residential heating systems. *Renewable and Sustainable Energy Reviews*, 75, 1254-1268.

Narayanaswamy, A. (2015). An analytic expression for radiatio view factor between two arbitrarily oriented planar polygons. *International Journal of Heat and Mass Transfer*, 91, 841-847.

Nguyen, A. T., Reiter, S. & Rigo, P. (2014). A review on simulation-based optimization methods applied to builing perfomrance analysis. *Applied Energy*, 113, 1043-1058.

Nicol, F., Humphreys, M. & Roaf, S. (2012). *Adaptive Thermal Comfort: Principles and Practice*. New York: Routledge.

Nishi, Y. & Gagge, A. P. (1977). Effective temperature scale for hypo- and hyperbaric environment. *Aviation, Space and Environmental Medicine*, 48, 97-107.

Nocedal, J. & Wright, S. J. (1999). *Numerical Optimization*. Springer.

Nordic, K. (2017). Construction component chambers.

Ochoa, C. E., Aries, M. B. C., van Loenen, E. J. & Hensen, J. L. M. (2012). Considerations on design optimization criteria for windows providing low energy consumption and high visual comfort. *Applied Energy*, 95, 238-245.

Olesen, B. W. (2007). Radiant floor heating in theory and practice. *ASHRAE Journal*, 44, 19-26.

Olesen, B. W., Mortensen, E., Thorshauge, J. & Berg-Munch, B. (1980). Thermal comfort in a room heated by different methods. *ASHRAE transactions*, 86, 34-48.

Oosthuizen, P. & Lightstone, M. (2010). Use of CFD in the analysis of heat transfer related problems that arise in building energy studies. *Proc. 14th International Heat Transfer Conference IHTC14*.

Ovchinnikov, P., Borodinecs, A. & Strelets, K. (2017). Utilization potential of low temperature hydronic space heating systems: A comparative review. *Building and Environment*, 112, 88-98.

Ozel, M. (2014). Effect of insulation location on dynamic heat-transfer characteristics of building extrenal walls and optimization of insulation thickness. *Energy and Buildings*, 72, 288-295.

Özkan, D. B. & Onan, C. (2011). Optimization of insulation thickness for different glazing areas in buildings for various climatic regions in Turkey. *Applied Energy*, 88, 1331-1342.

Parekh, A., Roux, L. & Gallant, P. (2007). Thermal and Air Leakage Characterisitics of Canadian Housing. *11th Canadian Conference on Building Science and Thechnology*, Banff, Alberta.

Parsons, K. (2010). Materials for energy efficiency and thermal comfort in buildings (ch. Thermal comfort in buildings). Woodhead.

Parsons, K. (2014). *Human thermal environments*. Boca Raton: Crc Press.

Parsons, K. C. (2002). The effects of gender, acclimation state, the opportunity to adjust clothing and physical disability on requirements for thermal comfort. *Energy and Buildings*, 34, 593-599.

Patankar, S. V. (1980). *Numerical heat transfer and fluid flow*. CRC Press.

Peeters, L., Beausoleil-Morrison, I. & Novoselac, A. (2011). Internal convective heat transfer modeling: Critical review and discussion of experimentally derived correlations. *Energy and Buildings*, 43, 2227-2239.

Petráš, D. & Kalús, S. (2000). Effect of thermal comfort/discomfort due to infrared heaters installed at workplaces in industrial buildings. *Indoor Built Environment*, 9, 148-156.

Pikas, E., Thalfeldt, M. & Kurnitski, J. (2014). Cost optimal and nearly zero energy building solutions for office buildings. *Energy and Buildings*, 74, 30-42.

Products, W. (2017). Heating solutions.

Raji, B., Tenpierik, M. J. & van der Dobbelsteen, A. (2017). Early-stage design considerations for the energy-efficiency of high-rise office buildings. *Sustainability*, 9, 623.

Randelovic, D., Bogdanovic, V. & Vasov, M. (2014, June 20-22). Influence of floor plan geomerty and organization in aim to improve designed buildings. *Proc. of the* 4th *International Scientific Conference on Geometry and Graphics*, 1.

Rees, S. & Haves, P. (2013). An experimental study of air flow and temperature distribution in a room with displacement ventilation and a chilled ceiling. *Building and Environment*, 59, 358-368.

Ren, Z. & Stewart, J. (2003). Simulating air flow and temperature distribution inside buildings using a modified version of COMIS with sub-zonal divisions. *Energy and Buildings*, 35, 257-271.

Rhee, K. N. & Kim, K. W. (2015). A 50 year review of basic and applied research in radiant heating and cooling systems for the built environment. *Building and Environment*, 91, 166-190.

Rhee, K. N., Olesen, B. W. & Kim, K. W. (2017). Ten question about radiant heating and cooling systems. *Building and Environment*, 112, 367-381.

Rijal, H. B., Humphreys, M. & Nicol, F. (2015). Adaptive thermal comfort in Japanese houses during the summer season: Behavioral adaptation and the effect of humidity. *Buildings*, 5, 1037-1054.

Ruparathna, R., Hewage, K. & Rehan, S. (2016). Improving the energy efficiency of the existing building stock: A critical review of commercial and institutional buildings. *Renewable and Sustainable Enrgy Reviews*, 53, 1032-1045.

Rupp, R. F., Vásquez, N. G. & Lamberts, R. (2015). A review of human thermal comfort in the built environment. *Energy and Buildings*, 105, 178-205.

Ryan, T. P. (2007). *Modern engineering statistics*. John Wiley & Sons.

Schiavon, S., Bauman, F., Tully, B. & Rimmer, J. (2012). Room air stritification in combined chilled ceiling and displacement ventilation systems. *HVAC&R Research*, 18, 147-159.

Schröder, P. & Hanrahan, P. (1993). A closed form expression for the form factor between two polygons. *Princeton University*.

Schweiker, M. & Wagner, A. (2015). A framework for an adaptive thermal heat balance model (ATHB). *Building and Environment*, 94, 252-262.

Sevilgen, G. & Kilic, M. (2011). Numerical analysis of air flow, heat transfer, moisture transport and thermal comfort in a room heated by two-panel radiators. *Energy and Buildings*, 43, 137-146.

Sherman, M. H. (1987). Estimation of infiltration from leakage and climate indicators. *Energy and Buildings*, 10, 81-86.

Sinnott, D. & Dyer, M. (2012). Air-tightness field data for dwellings in Ireland. *Building and Environment*, 51, 269-275.

Snider, B. (2006). Home heating and the environment. *Canadian Social Trends*, 11, 15-19.

Stolwijk, J. A. & Hardy, J. D. (1977). Control of body temperature. *Comprehensive Physiology*.

Susorova, I., Tabibzadeh, M., Rahman, A. & Clack, H. L. (2013). The effect of geometry factors on fenestration energy performance and energy savings in office buildings. *Energy and Buildings*, 57, 6-13.

Teodosiu, R. (2013). Integrated moisture (including condensation) – Energy–airflow model within enclosures. Experimental validation. *Building and Environment*, 61, 197-209.

Tham, K. W. (2016). Indoor air quality and its effects on human-A review of challenges and developments in the past 30 years. *Energy and Buildings*, 130, 637-650.

Toe, D. H. C. & Kubota, T. (2013). Development of an adaptive thermal comfort equation for naturally ventillated buildings in hot-humid climates using ASHRAE RP-884 database. *Frontiers of Architectural Research*, 2, 278-291.

Tye-Gingras, M. & Gosselin, L. (2012). Comfort and energy consumption of hydronic heating radiant ceilings and walls based on CFD analysis. *Building and Environment*, 54, 1-13.

Tzempelikos, A., Athienitis, A. K. & Panagiota, K. (2007). Simulation of façade and envelope design options for a new institutional building. *Solar Energy*, 81, 1088-1103.

Valančius, K., Motuzienė, V. & Paulauskaitė, S. (2015). Redeveloping industrial buildings for residential use: Energy and thermal comfort aspects. *Enery for Sustainable Development*, 29, 38-46.

van Breemen, A. J. N. & de Vries, T. J. A. (2001). Design and implementation of room thermostat using an agent-based approach. *Control Engineering Practice*, 9, 233-248.

Van Hoof, J. (2008). Forty years of Fanger's model of thermal comfort: comfort for all? *Indoor Air*, 18, 182-201.

Wan, J. W., Yang, K., Zhang, W. J. & Zhang, J. L. (2009). A new method of determination of indoor temperature and relative humidity wth consideration of human thermal comfort. *Building and Environment*, 44, 411-417.

Wang, Y., Wong, K. K. L., Du, W., Qing, J. & Tu, J. (2014). Design configuration for higher efficiency air conditioning system in large space building. *Energy and Buildings*, 72, 167-176.

Wang, Y., Zewei, M., Zhou, Y., Zhu, H., Huang, Y. & Yang, Y. (2016). Experimental investigation on the airflow characteristics of an attachment-based personalized ventilation method. *Building Services Engineering Research and Technology*, 37, 710-729.

Werner, J. (1990, October). Properties of the human thermostat: results from mathematical and experimental analysis. *Proc. International Conference on Environmental Ergonomics*.

Wissler, E. H. (1961). Steady-state temperature distribution in man. *Journal of Applied Physiology*, 16, 734-740.

Wray, W. (1980). A simple procedure for assessing thermal comfort in passive solar heated buildings. *Solar Energy*, 25, 327-333.

Wurtz, E., Mora, L. & Inard, C. (2006). An equation-based simulation environment to investigate fast building simulation. *Building and Environment*, 41, 1571-1583.

Yang, I. H., Yeo, M. S. & Kim, K. W. (2003). Application of artificial neural network to predict the optimal start time for heating system in building. *Energy Conservation and Management*, 44, 2791-2809.

Yang, K. H. & Su, C. H. (1997). An approach to building energy savings using the PMV index. *Building and Environment*, 32, 25-30.

Yang, L., Yan, H. & Lam, J. C. (2014). Thermal comfort and building energy consumption implications - A review. *Applied Energy*, 115, 164-173.

Yang, Y., Baizhan, L., Liu, H., Tan, M. & Yao, R. (2015). A study of adaptive thermal comfort in a well controlled climate chamber. *Applied Thermal Engineering*, 76, 283-291.

Yao, R., Li, B. & Liu, J. (2009). A theoretical adaptive model of thermal comfort - Adaptive Predicted Mean Vote (aPMV). *Building and Environment*, 44, 2089-2096.

Yau, Y. H. & Chew, B. T. (2014). A review on predicted mean vote and adaptive thermal comfort models. *Building Services Engineering Research and Technology*, 35, 23-35.

Yongchao, Z., Yufeng, Z., Qinglin, M., Huimei, C. & Jinyong, W. (2014). Gender differences in thermal comfort. *Proc. 13th Indoor Air*.

Younes, C., Shdid, C. A. & Bitsuamlak, G. (2011). Air infiltration through building envelopes: A review. *Building Physics*, 35, 267-302.

Zhao, M., Künzel, H. M. & Antretter, F. (2015). Parameters influencing the energy performance of residential buildings in different Chinese climate zones. *Energy and Buildings*, 96, 64-75.

Zuo, W. & Chen, Q. (2009). Real-time or faster-than-real-time simulation of airflow in buildings. *Indoor Air*, 19, 33-44.